A LOW COST INTEGRATED WATER QUALITY MONITORING SYSTEM

TOWARDS AN INTEGRATED WATER QUALITY MONITORING SYSTEM USING LOW COST ELECTROCHEMICAL SENSORS

By

ARIF UL ALAM

B. SC. ISLAMIC UNIVERSITY OF TECHNOLOGY, 2008
M. A. SC. MCMASTER UNIVERSITY, 2013

A Thesis Submitted to the School of Graduate Studies in Partial Fulfilment of the
Requirements for the Degree of Doctor of Philosophy

i

McMaster University   Doctor of Philosophy (2019)

Hamilton, Ontario   (Electrical and Computer Engineering)

TITLE: Towards an integrated water quality monitoring system using

                            low cost electrochemical sensors

AUTHOR: Arif Ul Alam,

                            B. Sc. Islamic University of Technology, Gazipur,

                            Bangladesh

                            M. A. Sc. McMaster University, Hamilton, Canada

SUPERVISOR: Dr. Matiar M. R. Howlader

                            Dr. M. Jamal Deen (Co-supervisor)

NUMBER OF PAGES: xxxi, 216

Lay Abstract

Low-cost, easy-to-use, and sensitive monitoring system for pharmaceuticals, heavy metal, pH and free chlorine in drinking water is crucial for public health safety. In this thesis, we develop solution-based synthesis of multi-walled carbon nanotubes modified by β-cyclodextrin for electrochemical sensing of pharmaceuticals and heavy metal. The modification approaches are compared and characterized to analyze their electrochemical behavior and sensing performances. The developed sensors are highly sensitive toward the detection of acetaminophen (a widely used pain-killer) and estrogen hormone in drinking water. We also develop a modified spin-coating technique to deposit palladium/palladium oxide films for potentiometric pH sensor, a calibration-free free chlorine sensor based on modified carbon electrode, and a resistive temperature sensor. The developed pH, free chlorine and temperature sensors are highly sensitive, and stable with fast response time. All the sensors are integrated and interfaced with a custom-made and smartphone-controlled electronic readout system for accurate and on-site drinking water quality monitoring at low cost.

Abstract

The monitoring of pharmaceuticals, heavy metal, pH and free chlorine concentration in drinking water is important for public health and the environment. However, conventional laboratory-based analytical methods are labor-intensive, expensive, and time consuming. This thesis focuses on developing an integrated, highly sensitive, easy-to-use, and low-cost pharmaceuticals, heavy metal, pH and free chlorine sensing system for drinking water quality monitoring.

A low-temperature, solution-processed modification of multi-walled carbon nanotubes (MWCNT) with β-cyclodextrin (βCD) on glassy carbon electrode is developed for detecting low levels of acetaminophen. The adsorption properties of βCD are combined with the high surface area of carbon nanotubes towards enhanced electrochemical sensing of acetaminophen with a limit of detection of 11 nM and linear range from 0.05-300 μM. Also, a systematic investigation is carried out using four types of modified MWCNT-βCD. A novel, one-step approach called Steglich esterification modified MWCNT-βCD results in large effective surface area, and fast electron transfer towards sensitive detection of acetaminophen and 17β-estradiol (E2, primary female sex hormone) in the range of 0.005–20 and 0.01–15 μM, with low detection limits of 3.3 and 2.5 nM, respectively. The similar MWCNT-βCD modified electrodes can also detect heavy metal ion (lead, Pb^{2+}) with a limit of detection of <10 ppb. Low frequency noise behavior of these sensors are studied.

A spin-coated Pd/PdO based pH sensor, and amine-modified carbon electrode-based free chlorine sensor are fabricated on a common substrate together with the pharmaceuticals and heavy metal sensors. A Wheatstone-bridge temperature sensor is fabricated based on silicon and PEDOT:PSS on another substrate. All the sensors are connected to an Arduino microcontroller based data acquisition system with a smartphone application interface. The integrated sensing system is easy-to-use, low-cost, and can provide accurate monitoring data with real drinking water samples.

Acknowledgements

I would like to express my gratitude to Dr. Matiar M. R. Howlader for providing me the opportunity to study as an M.A.Sc and a Ph.D. student at McMaster University. As my supervisor, he built a good research team for me with talented researchers such as Yiheng Qin, Taufique Z. Redhwan, Md. Maksud Alam, Fangfang Zhang, and Rishad Arfin. I truly appreciate his efforts in building and maintaining the unique and advanced Micro and Nano Systems Laboratory, where my research work was carried out. Also, his door is always open for me for technical supports and valuable discussions. I am grateful for his continuous guidance and support on my research.

I would like to express my profound appreciation and acknowledgements to my co-supervisor Dr. M. Jamal Deen for giving me this exciting and challenging project to work on, and also for his help, encouragement, guidance and insightful discussions throughout this research work. I would like to express my special appreciation to Dr. Deen for his efforts in arranging me to work at Xerox Research Centre of Canada (XRCC) as a visiting scientist, and maintaining the collaboration with XRCC. I would like to thank Dr. Deen for the training he provided to me in all aspects of research, including critical thinking, experiment planning, problem solving, data analysis, technical writing, and presentation to people with different disciplines and research backgrounds. In addition, I truly appreciate the extra opportunities Dr. Deen gave me to communicate and interact with top water researchers from Canada and India under the umbrella of RES'EAU WaterNET and IC-IMPACTS projects. It is also a great pleasure to work in Dr. Deen's water research team with Dr. Hyuck-Jin Kwon, and Si Pan.

I would also like to thank my other committee members Dr. Yaser M. Haddara and Dr. Ravi Selvaganapathy for their advice on my research and for taking the time to review my thesis.

Table of Contents

Lists of Figures

Appendix Figures

List of Tables

List of Appendices

List of Abbreviations

AA	Ascorbic acid
ADC	Analogue-to-digital converter
AFM	Atomic force microscopy
Ag	Silver
AgCl	Silver chloride
APAP	Acetaminophen
APTES	3-triethoxysilylpropylamine
Ar	Argon
ASV	Anodic stripping voltammetry
Au	Gold
BJT	Bipolar junction transistor
CA	Chronoamperometry
CaCl$_2$	Calcium chloride
CC	Click chemistry
CEC	Contaminants of emerging concerns
Cl$^-$	Chloride ion
CNT	Carbon nanotube
-COOH	Carboxyl group
CV	Cyclic voltammetry
DA	Dopamine
DBU	1,8-diazabicyclo[5.4.0]undec-7-ene
DI	Deionized
DMAP	4-(dimethylamino)pyridine
DMF	N,N-dimethylformamide
DPASV	Differential pulse anodic stripping voltammetry
DPD	N,N-diethyl-p-phenylenediamine
DPV	Differential pulse voltammetry
DSA	Dynamic signal analyzer
EPA	Environmental protection agency
FFT	Fast Fourier transform
FIWQMS	Fully integrated water quality monitoring system
FTIR	Fourier transform infrared

GCE	Glassy carbon electrode
H_3BO_3	Boric acid
H_3O^+	Hydronium ion
H_3PO_4	Phosphoric acid
HOCl	Hypochlorous acid
HPLC	High-performance liquid chromatography
HPLC-MS	High-performance liquid chromatography coupled mass spectroscopy
HRTEM	High resolution transmission electron microscopy
ICP	Inductively coupled plasma
IPA	Isopropanol
K_2SO_4	Potassium sulfate
KCl	Potassium chloride
KI	potassium iodide
KNO_3	Potassium nitrate
LCMS	Liquid chromatography coupled mass spectrometry
LFN	Low frequency noise
LPF	Low pass filter
LSV	Linear sweep voltammetry
MIP	Molecularly imprinted polymer
MWCNT	Multi-walled carbon nanotube
N_2	Nitrogen
Na_2HPO_4	Sodium phosphate dibasic
NaCl	Sodium chloride
NaOAc	Sodium acetate
NaOCl	Sodium hypochlorite
NaOH	Sodium hydroxide
NIRS	Near infrared spectroscopy
NMP	N-methylpyrrolidone
NMR	Nuclear magnetic resonance
NP	Nanoparticle
O_2	Oxygen
OCl^-	Hypochlorite ion
OD	Outer diameter
OH^-	Hydroxide ion
-OH	Hydroxyl group

Pb	Lead
$Pb(NO_3)_2$	Lead nitrate
PBS	Phosphate buffered saline
Pd	Palladium
PdO	Palladium(II) oxide
PEC	Predicted environmental concentration
PEDOT:PSS	Poly(3,4-ethylenedioxythiophene) doped with poly(styrenesulfonate)
PI	Polyimide
PNEC	Predicted no effect concentration
ppm	Parts per million
PSD	Power spectral density
Pt	Platinum
RPM	Revolution per minute
RSD	Relative standard deviation
RTD	Resistance temperature detector
SE	Steglich esterification
SEM	Scanning electron microscopy
Si	Silicon
SWCNT	Single-walled carbon nanotube
SWV	Square wave voltammetry
TCR	Temperature coefficient of resistance
TE	Thionyl chloride mediated esterification
TG	Thermogravimetric
TGA	Thermogravimetric analysis
TIA	Transimpedance amplifier
UV	Ultraviolet
WHO	World Health Organization
WQM	Water quality monitor
WWTW	Wastewater treatment works
XPS	X-ray photoelectron spectroscopy
βCD	β-cyclodextrin

List of Symbols

T	Absolute temperature
k	Boltzmann constant
E	Cell potential
E^0	Standard cell potential
z	Valence of ion
K_a	Dissociation constant
E_{pulse}	Pulses with a constant amplitude
E_{pc}	Cathodic peak potential
E_{pa}	Anodic peak potential
I_{pc}	Cathodic peak current
I_{pa}	Anodic peak current
ΔR	Change of resistance
A	Effective surface area
D	Diffusion coefficient
v	Scan rate
N	Number of electrons transferred
α	Charge transfer coefficient
k_s	Heterogeneous electron transfer rate constant
R^2	Regression coefficient
n_α	Electron transfer number
f	Frequency
$S(f)$	Spectral density
K_F	Flicker noise coefficient
α	Flicker noise frequency exponent
C	Concentration
C_{OCl^-}	Concentration of hypochlorite ion
C_{HOCl}	Concentration of hypochlorous acid
$C_{total\ free\ chlorine}$	Concentration of the total free chlorine
F	Faraday constant
R	Gas constant
pK_a	Logarithmic dissociation constant of hypochlorous acid
R_0	Measured initial resistance
E_{meas}	Measured output voltage of a pH sensor
ΔR	Measured resistance difference

T_{meas}	Measured temperature of a water sample
V	Output voltage of the signal conditioning circuit for a free chlorine sensor
V_{out}	Output voltage of the temperature sensor
E_{ref}	Potential of reference electrode
E_{cal}	Recorded voltage when the sensor is in a pH = 7 calibration solution
T_{REF}	Reference temperature
R_{Si}	Resistance of the diced silicon wafer
$R_{\text{PEDOT:PSS}}$	Resistance of the drop-casted PEDOT:PSS film

Declaration of Academic Achievement

This thesis was written by Arif Ul Alam under the supervision of Dr. Matiar M. R. Howlader, and Dr. M. Jamal Deen from McMaster University. The research described in Chapter 2 to 4, and 6 (pharmaceuticals, heavy metal, and pH sensor part) was carried out in collaboration with Xerox Research Centre of Canada (XRCC). The research presented in Chapter 6 (free chlorine sensor part) was carried out in collaboration with Department of Chemical Engineering, McMaster University.

- Chapter 1: I conducted the literature review and summarized the research results.
- Chapter 2: I designed the devices and experiments. Yiheng Qin recorded the scanning electron microscopy images. I conducted all other experiments. Dr. Nan-Xing Hu (XRCC) assisted in data analysis.
- Chapter 3: I designed the devices and experiments. Massimo Catalano, Luhua Wang and Moon J. Kim recorded the scanning electron microscopy, and tunneling electron microscopy images. I conducted all other experiments. Dr. Nan-Xing Hu (XRCC) supported in data analysis.
- Chapter 4: I designed the devices and experiments and conducted all experiments. Dr. Nan-Xing Hu (XRCC) assisted in the data analysis.
- Chapter 5: Dr. Ognian Marinov (McMaster) helped me in designing the devices and experiments. I conducted all the experiments and analysis. Dr. Ognian Marinov and Sumit Majumder (McMaster) assisted in data analysis.
- Chapter 6: I designed the sensors, integrated devices and experiments. Si Pan (McMaster) assisted in the fabrication of free chlorine sensors. Dr. Hao Jin (Zhejiang University) designed the WQM circuit board. Dennis Clyne (McMaster) designed the potentiostat board and the Smartphone (Android) app. I did all other experiments and data analysis.

Chapter 1

Introduction*

1.1. Importance of water quality monitoring

Access to safe drinking water is fundamental to human development and well-being. Safe water is considered as one of the most effective instruments towards promoting health and reducing poverty, yet only 71% of the world population have access to safe drinking water, and 2 billion people use drinking water sources contaminated with faeces [1], making it one of the major public health crisis in many developing and underdeveloped countries. Key contaminants in untreated/source water include microorganisms such as viruses and bacteria; inorganic compounds such as salts and metals; and organic chemical contaminants such as pharmaceuticals, pesticides and industrial effluents. Most of the traditional treatment technologies cannot fully eliminate the organic contaminants in the finished/ drinking water. In fact, with ever increasing ageing population worldwide and associated intake and improper disposal of medications, the presence of pharmaceuticals in drinking water is becoming an emerging water problem [2]. Therefore, monitoring of these pharmaceuticals in drinking water is of critical importance to ensure safety and well-being of public health.

Another two important drinking water parameters are pH and free chlorine concentration which can indicate the quality of the water. A certain concentration of free chlorine is used in drinking water to disinfect the microorganisms and monitoring the free chlorine concentration also depends on the pH of water. Presence of heavy metals is another drinking water hazard in some parts of the world. Therefore, continuous and real-time

---

* Part of this work will be submitted for consideration for publication as: A. U. Alam, M. M. R. Howlader, N.-X. Hu, M. J. Deen, Carbon nanomaterials based electrochemical sensors for pharmaceuticals monitoring, April 2019. (in preparation)

monitoring of the level of pH and free chlorine concentration along with regular monitoring of pharmaceuticals and heavy metal in drinking, recreational, and food processing water can provide an improved public health safety. However, conventional analytical instruments such as bulky pH electrodes, expensive free chlorine meters and labour-intensive heavy metal and pharmaceutical sensing techniques suffer from slow response, complex operation, susceptibility to human error, frequent maintenance costs. In contrast, electrochemical sensors are cheaper, smaller in size, and highly sensitive. Therefore, electrochemical sensors are desirable for on-demand and online monitoring of pharmaceuticals, heavy metals, pH and free chlorine in drinking water.

In this chapter, we introduce the importance and conventional methods of pharmaceuticals, heavy metals, pH and free chlorine sensing for drinking water quality monitoring. Next, we discuss different electrochemical sensing techniques for the aforementioned parameters. These techniques include voltammetry-based sensors for electrochemical pharmaceuticals and heavy metals sensing; and potentiometry- and amperometry-based sensors for electrochemical pH and free chlorine sensing. We provided a brief summary and comparison of the sensor structures, operation conditions, sensing mechanisms, relevant materials, and some key performance parameters such as sensitivity, sensing range, response time and stability of each type of sensor. Then, the motivation of this research is provided along with the specifications of the proposed system and each sensor utilized in the system. Finally, the research contribution and thesis organization is presented.

1.2. Research background

Drinking water quality is evaluated by its bio-physico-chemical parameters. These parameters include, but not limited to pH, free chlorine concentration, turbidity, dissolved oxygen (O_2), conductivity, organic carbon, and a few varieties of microorganisms [3]. In recent years, "contaminants of emerging concern (CECs)" such as pharmaceuticals and organic micropollutants have drawn immense scientific and public health attentions. Painkillers, hormones and antibiotics are only some of the pharmaceuticals that have been

found in drinking water. Although, the pH and free chlorine concentration provides significant information about the water quality and efficacy of disinfection processes, the presence of trace pharmaceuticals poses a long-term public health risks. Also, the pH of water has influence on the presence of heavy metals in drinking water through metal pipes corrosion. Therefore, sensing of pharmaceuticals, heavy metals together with the pH and free chlorine concentration can provide a more comprehensive information about drinking water quality to ensure better public health safety.
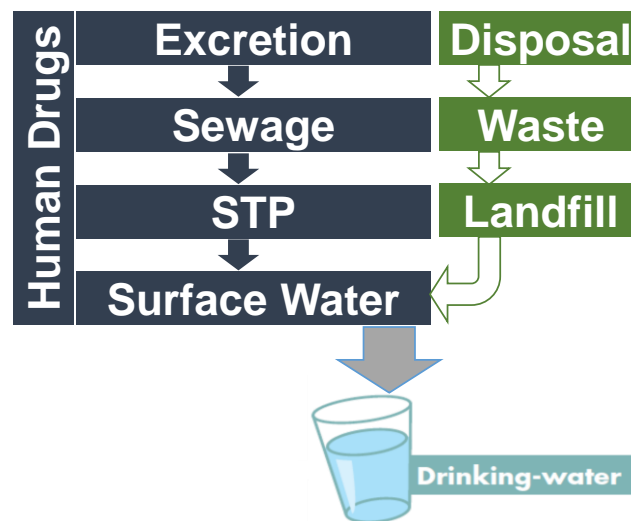
Figure 1-1. Fate and transport of pharmaceuticals in the environment and drinking water (adapted from [2]).

1.2.1. Sensing of water quality parameters

Pharmaceuticals sensing

Pharmaceuticals have been found in the aquatic environment for the last few decades [4,5]. Their presence began to stir widespread attention in the scientific community in the early 2000s. Numerous studies identified more than 80 different compounds [6] in wastewater treatment effluents, rivers, lakes and drinking water [7–9] across Europe and in North and South America with concentrations in the ng−µg l^{-1} range. Current concentration range is well below the acute toxicity level to humans, however, low level chronic exposure may be of concern due to two of the most severe suspected consequences being lower sperm counts and antibiotic resistance [10–13]. Also, the effect and chronic toxicity of the

mixtures of pharmaceutically active compounds due to their long-term exposure towards aquatic ecosystem is also not fully understood.

Potential sources of pharmaceutical contaminants include landfill sites with leaching from household waste containing disposed of drugs, effluents from industrial pharmaceutical production, run-off from agricultural land, and wastewater treatment works (WWTWs) being the main route [7,13–17]. A significant part of the medication does not get absorbed into human body and, therefore, gets excreted into the sewage system along with the unused drugs improperly disposed of via the drains, as shown in Figure 1-1 [18]. Studies have shown that many WWTWs cannot fully remove pharmaceuticals [9,19–21]. For example, Environment Agency in the UK found unusually high levels of some pharmaceuticals in WWTW effluent, with ibuprofen up to 27 µg l^{-1} [9]. Removal efficiencies of 65% for ibuprofen and 45% for naproxen was reported in a study at WWTWs in Spain [19].

More than 200 different pharmaceuticals have been reported in surface waters globally including painkillers (analgesics), hormone, antibiotics, antidepressants and β-clockers. A wide range of inorganic and organic contaminants in surface waters are traditionally controlled and legislated by the European Commission that are considered as industrial or agricultural chemicals [22]. A greater number of CECs is expected to be included into the legislation in a recent proposal [23]. A number of CECs showed single compound acute toxicity testing results with median effective concentrations to be < 1 µg l^{-1} [24–34], classifying them as potentially very toxic to aquatic organisms [35,36].

Two of the most common CEC pharmaceuticals are acetaminophen (APAP), also known as paracetamol, and 17β-estradiol (E2). The predicted environmental concentration (PEC) and predicted no effect concentration (PNEC) of APAP was estimated to be 65.4 and 136 µg l^{-1}, respectively, according to standard D. magna test organism [37]. The PNEC of 17β-estradiol (E2) was estimated to be 2 ng l^{-1} using species sensitivity distribution (SSD) methodology [38]. The more concerning aspects of the presence of these CEC pharmaceuticals in the environment are that they do not appear individually, rather in a complex mixture, which may lead to undesirable synergistic effects. Thus, the ubiquitous nature of these potentially toxic CEC pharmaceuticals in the environment reinforces the

necessity to better understand their occurrence, fate and ecological impact through low-cost, easy-to-use and highly sensitive monitoring tools.

pH, free chlorine and heavy metal sensing

The pH value and free chlorine concentration of drinking water are highly critical to the well-being of the natural environment and human health. The pH of an aqueous solution is defined as the negative common logarithm of the molar concentration of hydronium ions (H_3O^+), by the following equation:

$$pH = -\log\left[H_3O^+\right],\tag{1-1}$$

The pH values normally range from 0 to 14, where pH = 7 signifies neutral value, pH < 7 indicates acidic, and pH > 7 means a basic solution [39].

The recommended optimum pH level for drinking water is in the range of 6.5 to 9.5, according to the World Health Organization (WHO) [40]. The Health Canada guideline recommended a narrower range of 6.5 to 8.5 [41]. Any pH value of water outside the recommended range in the distribution system indicates potential problems in the water treatment processes that may eventually affect public health safety. For example, lower pH values may indicate leaching and nitrification of water [42]; the pH may indicate the presence of microorganisms in water due to the production of acidic or basic metabolites [43]; pH values outside the range of 4 to 10 may occur due to accidental spills of disinfecting chemicals which can result in the breakdown of the treatment system [44]. Other effects of unregulated pH include gastrointestinal irritation [45], corrosion of metal pipes [46], and inefficient disinfection of drinking water [47]. Therefore, pH needs to be regularly monitored at all stages of drinking water treatment and distribution system [48].

Chlorine (Cl) can bond with and destroy the outer surfaces of water-borne-diseases-causing bacteria and viruses such as Escherichia coli O157:H7, Salmonella, Salmonella typhi, Shigella, Campylobacter, Vibrio cholera and Pseudomonas, making it an ideal candidate for disinfection in water treatment system [49]. However, a controlled use of chlorine is necessary to ensure safe and effective disinfection of drinking water. The WHO

recommended concentration of chlorine in drinking water is 2 to 3 parts per million (ppm) for an effective disinfection and acceptable residual concentration [50]. The U.S. standard for the maximum residual chlorine concentration in drinking water is 2 ppm [51]. Moreover, the suggested concentration for free chlorine in swimming pool and food processing is 1.5−2 ppm and 50−200 ppm, respectively [51–53]. Low chlorine concentration may cause incomplete disinfection, whereas high concentration may increase the level of trihalomethane-based carcinogens in the treated water [54]. Thus, the free chlorine concentration in drinking water is a critical parameter requiring routine monitoring.

Heavy metals, such as lead (Pb), are toxic materials that accumulates in water causing adverse effects on human health [55]. Pb causes neurodevelopmental and behavioral disorders in children, and increased blood pressure and renal dysfunction in adults with concentrations range which were previously considered as safe [56–60]. Also, Pb can also cause cancer in kidneys, lung, or brain when exposed for long period of time [57]. WHO recommended guideline for safe limit for Pb in drinking water is 10 µg/L (or, 10 ppb) [57]. Thus, careful monitoring of its levels in tap water is required.

1.2.2. Conventional ways of water quality monitoring

Pharmaceuticals sensing

Conventional analytical techniques for pharmaceuticals stemmed from the investigation of bulk pharmaceutical/drug materials as well as their intermediates, products, formulations, impurities and degradations, and biological samples containing the drugs and their metabolites. The analysis/assay methods include titrimetry [61], spectrometry [62], chromatography [63], and capillary electrophoresis [64]. The conventional analysis techniques of pharmaceuticals and its metabolite can be either quantitative or qualitative and they are more extensively applied in the pharmacokinetic studies compared to that of water quality monitoring.

Titrimetric method of analysis was originally used somewhere in the middle of the 18th century. Gay–Lussac invented the volumetric method in 1835 which consequently led to the origin of term titration. Despite being very old method, it is still being modernized by incorporating potentiometric end point detection thereby improving the precision of the method. Establishing reaction rates in kinetic measurements was possible with the development of functional group analysis in titrimetric methods. Advantages of these methods include reduction of time and labor, high precision and no requirement for reference standards. Titrimetric methods were used for the determination of captopril, albendozole and gabapentin in commercial dosage forms [65]. Non-aqueous titration method was used for the determination of sparfloxacin [66]. Titrimetry has also been used for the estimation of degradation products of the pharmaceuticals in addition to its application in drug estimation [67].

Spectrophotometric methods found an important place in pharmacopoeias which is based on natural UV absorption and chemical reactions [68]. In this method, the reflection or transmission properties of a material is quantitatively measured as a function of wavelength. The advantages include low measurement time and labor consumption along with high precision. Spectrophotometric methods include UV–Visible spectrophotometry, derivative spectroscopy, near infrared spectroscopy (NIRS), and nuclear magnetic resonance spectroscopy (NMR). UV–Visible spectrophotometry have been extensively applied in the analysis of pharmaceutical dosage form [69–71]. These colorimetric methods generally utilize the following three aspects: (1) complex-formation reaction, (2) oxidation-reduction process, and (3) a catalytic effect.

Derivative spectroscopy is used for qualitative investigation and estimation which uses first or upper derivatives of absorbance with respect to wavelength, reported as early as in the 1950s. However, this technique received little attention due to the computational complexity of generating derivative spectra using early UV–Visible spectrophotometers, and gradually caught attention with the introduction of microcomputers in the late 1970s. NIRS allows a rapid and non-destructive procedure that provides multi component analysis of almost any matrix. The advantages include easy sample preparation without any pre-

treatments, the use of fiber optic probes, and the use of a single spectrum for the extraction of chemical and physical sample parameters. NMR was first reported in 1996 for screening drug molecule [72], after which a number of state-of-the-art approaches were established in both pharmaceutical and academic research [73].
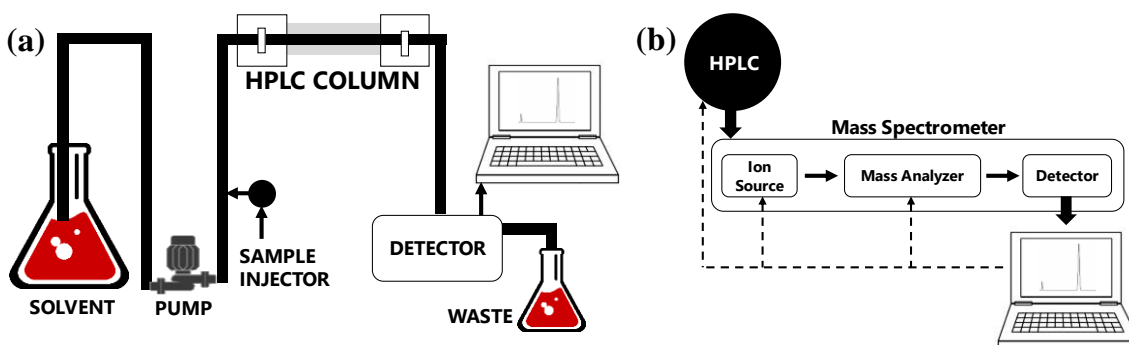
Figure 1-2. Schematic diagram of (a) High Performance Liquid Chromatography (HPLC) system, and (b) HPLC coupled Mass Spectroscopy (HPLC-MS) system for pharmaceutical analysis.

Common chromatography techniques include thin layer chromatography [74], high performance thin layer chromatography [63], high-performance liquid chromatography (HPLC) [75], and gas chromatography [76]. Among these techniques, HPLC has been the most widely used system. HPLC is a form of column chromatography that pumps an analyte in a solvent, known as the mobile phase, at high pressure through a column with chromatographic packing/adsorbing material, known as stationary phase, as shown in Figure 1-2(a). The sample mixture is then carried by a moving carrier gas stream of helium or nitrogen percolating through the column. The components of the sample move through the column at different velocities. These velocities are a function of specific physical interactions with the adsorbent or the stationary phase. The velocity of each component is determined by its chemical nature, the nature of the stationary phase or column and on the composition of the mobile phase. The time at which a specific analyte is eluted or emerged from the column is defined as its retention time. The retention time measured in particular conditions provides an identifying characteristic of a given analyte. HPLC can separate, and identify compounds that can be dissolved in a liquid in trace concentrations as low as parts per trillion in pharmaceutical formulations [75].

Although HPLC provides a major solution in the analysis of pharmaceuticals, the limitations include price of columns, solvents and a lack of long term reproducibility of the analysis due to the proprietary nature of stationary phase column packing. Liquid chromatography combined with mass spectrometry (LC–MS) is, however, considered as one of the most important techniques of the last decade of the 20th century [77]. Recently HPLC-MS has been used for the assay of pharmaceutical compounds [78–80]. Mass spectrometry (MS) is a process of ionizing atoms or molecules to facilitate their separation and detection in accordance with their molecular masses and charges, also known as mass to charge ratio. In HPLC-MS technique, the mixtures are separated in accordance with their physical and chemical properties, followed by identification of the components within each peak and their detection based on their mass spectrum, as schematically shown in Figure 1-2(b).

Heavy metals sensing

The U.S. Environmental Protection Agency (EPA) has two approved analytical methods, known as (1) Method 200.8 Rev. 5.4 and (2) Method 200.9 Rev. 2.2, for the analysis of lead in drinking water [57]. A number of methods developed by standard organizations and a commercial manufacturer with consensus are also approved by the U.S. EPA: Standard Method (SM) 3113B (APHA et al., 2005); D3559-96 and D3559-03 (ASTM, 1996, 2003); and Palintest method 1001 (U.S. EPA, 1994c, 2009a, 2014) [57]. These methods utilize inductively coupled plasma (ICP) followed by gas chromatography–mass spectrometry (GC-MS), graphite furnace atomic absorption spectroscopy (GFAAS) or differential pulse anodic stripping voltammetry (ASV) to analyze lead.

pH sensing

Conventional pH sensing technologies for water quality monitoring mainly utilizes glass electrode-based pH meters, which was invented by Arnold Beckman in 1934 and commercialized in 1936 [81]. The first pH meter comprised of a glass-indicating electrode developed by F. Haber and Z. Klemensiewicz in 1909 and integrated with a vacuum tube

amplifier [82]. Different types of pH sensors emerged in the following several decades, which could be categorized into three main types: (1) chemo-mechanical sensors, (2) electrochemical sensors, and (3) optical sensors [48]. Until these days, glass-membrane-based electrochemical electrodes are still the most commonly used pH sensors.

A glass electrode usually contains a bulb made of a specific glass (for example, a glass containing lithium or sodium ions), an internal solution (typically 0.1 M hydrochloride acid or buffered chloride solution), an internal electrode (typically silver/silver chloride, Ag/AgCl, or saturated calomel electrode), and a glass or plastic electrode body [83]. When any pH measurement is done, the outer surface of the bulb becomes hydrated by forming a silicate skeleton layer that is only selectively permeable to H_3O^+. Correspondingly, a hydrated layer is created on the inner side of the bulb with an accumulated charge proportional to the amount of permeated H_3O^+ at the outer side. Thus, the accumulated charge in the inner side of the bulb relates to the concentration of H_3O^+ in the external solution. The potential difference across the glass bulb membrane (E) is given by the famous Nernst equation [23]:

$$E = E^0 + \frac{2.303RT}{zF}\log\left[H_3O^+\right],\qquad(1-2)$$

where E^0 is the standard cell potential, which is a function of the standard potential of the internal reference electrode (relative to standard hydrogen electrode) and the resistivity of the internal solution, R is the gas constant (8.314 J/K·mol), T is the absolute temperature, z is the valence of the ion (1 for H_3O^+), F is the Faraday's constant (9.649 × 10^4 C/mol), and [H_3O^+] is the ion activity corresponding to the molar concentration of H_3O^+. At 25 °C, the electrode potential as a function of solution pH is found to be:

$$E = E^0 - 0.05916\text{pH},$$

$$(1-3)$$

which expresses the ideal pH sensitivity of the glass electrode as 59.16 mV/pH. This value is known as the Nernstian slope in the pH vs voltage relationship. Thereafter, Nernstian slope has been treated as the reference value in the development of emerging pH sensors.

Free chlorine sensing

Free chlorine in water comprises of hypochlorous acid (HOCl) and hypochlorite ion (OCl^-). Chlorine gas introduced into water for disinfection produces HOCl as follows [24]:

$$Cl_2 + H_2O \rightarrow HOCl + HCl, \tag{1-4}$$

where HOCl is a weak acid and partially get dissociated into H^+ and OCl^- in water:

$$HOCl \leftrightarrow H^+ + OCl^-, \tag{1-5}$$

In a particular temperature, the percentage distribution of HOCl and OCl^- is a function of the concentration of H^+ (H_3O^+) (which is the pH of the solution), and can be generally expressed by:

$$\log \frac{\left[OCl^-\right]}{\left[HOCl\right]} = \log K_a + pH, \tag{1-6}$$

where $[OCl^-]$ and $[HOCl]$ are the equilibrium concentrations of OCl^- and HOCl, respectively, and K_a is the dissociation constant of HOCl (around $10^{-7.53}$ at 25 °C) [25]. To obtain the level of free chlorine concentration, one needs to measure the solution pH together with the concentration of either HOCl or OCl^-. There are two major analytical methods to monitor free chlorine, such as colorimetric and electrochemical analysis, including: absorptiometry methods using *N,N*-diethyl-p-phenylenediamine (DPD) [84], *o*-tolidine [85] or other chemicals [86–88]; iodometric titration [89]; chromatography [90]; chemiluminescence [91]; and amperometric methods [92,93].

The DPD-based absorptiometry method has been widely used because of its high sensitivity. Free chlorine oxidizes DPD to form a colored magenta compound at solution pH value of around 7 [84]. The color is then photometrically read out to determine the amount/concentration of free chlorine. The detection range of this method for free chlorine sensing is from 0 to 5 ppm with an accuracy of 0.04 ppm. The United States Environmental Protection Agency declared it as a standard analytical approach and approved for online monitoring of free chlorine [93].

Temperature sensing

The temperature of water affects most of the bio-physico-chemical parameters in water. Therefore, temperature of water sample should be measured to monitor the drinking water quality with high accuracy. According to the Nernst equation (equation (1.2)), the sensitivity of a glass-electrode-based pH sensor depends on the water temperature. Also, in free chlorine monitoring, the dissociation constant of HOCl changes with the water temperature [94].

Typical temperature sensors can be categorized as resistance temperature detectors (RTD, including thermistors), thermocouples, and junction semiconductor sensors. RTD uses a pure metal, such as platinum (Pt), whose resistance increases linearly with the increase of temperature, making it a positive temperature coefficient of resistance (TCR) material [95]. The Pt-based RTD normally has a wide sensing range of −270 °C to +850 °C with a sensitivity of 0.00385 Ω/°C and an accuracy of ~0.25 °C (between 0 °C and 100 °C). An RTD can also be fabricated by a semiconductor material (such as silicon) that exhibits large changes in resistance for a small change in temperature, also known as thermistor [96]. The thermistor device has a negative TCR, signifying the decrease of resistance with the increase of temperature. Such device has an accuracy of 0.1 °C to 0.2 °C in the range of 0 °C to 100 °C. The major advantages of RTD are its small footprint and low cost.

In a thermocouple, two dissimilar metals are connected at their two ends which produces a thermoelectric potential when the two metal-metal junctions are exposed to two different temperatures (Seebeck effect) [97]. The value of the thermoelectric potential can be determined by the nature of the two metals and the temperature difference between the junctions. A thermocouple can sense up to 2000 °C depending on the metals used [96]. However, thermocouples have lower accuracy (~1 °C) than that of RTDs.

A p-n junction diode and bipolar junction transistor (BJT) shows strong temperature dependent electrical characteristics. For example, when a diode or a BJT is biased by a constant current, the forward biased voltage will change depending on the temperature

change [98]. The junction semiconductor sensors have a sensing range up to ~500 °C, and with sensitivity greater than 1 mV/°C.

1.2.3. Future water quality monitoring sensors

Conventional drinking water quality monitoring approaches require multiple steps, such as sampling of water, sample transportation to laboratories, and laboratory analysis by trained personnel [99]. These approaches are expensive, time-consuming, and laboratory-intensive. Moreover, the results may easily be interfered from human activities as well as long-term storage of the water samples [100,101]. For example, the operation of the low-cost multi-parameter water quality test kits costs 85 CAD for a 15-parameter test kit, and are based on the colorimetric method. The color of different reagents alters when they react with the analytes. These test kits provide qualitative results with low measurement accuracy, and can only be used for a limited number of times from 2−5 times. Conventional chromatography techniques for pharmaceuticals heavy metals sensing suffer from bulky instruments size, requirement for trained laboratory personnel. Glass pH electrodes suffer from fragility, large size, slow response time, high cost, and require regular maintenance such as calibration and refilling of the reference buffer solution [102]. For free chlorine monitoring, the DPD analyzers can provide high sensitivity and accurate results in a limited detection range only if they are frequently calibrated. However, such analyzers need expensive optical instruments, produce environmentally hazardous chemicals, and are difficult to scale down the sizes [103,104]. Therefore, alternative sensing technologies are essential to address these challenges.

Alternatively, sensors with high accuracy, easy operation, and small-footprint with low fabrication costs are receiving increased consideration. Specially, recent developments in electrochemical sensing technologies are going to facilitate the realization of such sensors. The advantages of the electrochemical sensing technologies include precision control in material structures (such as surface area), the ability to tailor material properties (such as electron transfer coefficient), and the use of small volume of materials. Also, sensors made of nanomaterials and functionalized nanomaterials can be integrated with microfabricated and microelectronic readout circuitry with easy sample preparation, signal processing and

transmission components to construct functional integrated systems for operation with minimum human intervention [105,106].

Several studies reported hydrogel-based sensors using micro chemical-mechanical transducers for the measurement of water quality parameters [107–110]. However, these sensors suffer from difficulty in implementation due to their delicate structures and very long response time in the range of hundreds of minutes. Contrarily, micro-optical sensors are highly accurate and sensitive, but they have limited sensing range and poor linearity. Also, the components for optical sensors such as lasers and detectors are costly [111–114], and typically, the sensors require chemical reagents to run the measurement [115]. Therefore, continuous, low-cost and easy-to-use water quality monitoring is difficult to achieve in chemo-mechanical and optical sensors. The advantages of the electrochemical sensors over other types of sensors and analytical methods include:

- Better ability to be easily mass-fabricated with current microfabrication technologies.
- Simpler integration with microelectronic components for automatic operation.
- Wider sensing range and faster response with similar sensitivity.
- Higher structural compatibility with existing water distribution systems due to smaller dimensions.
- Better compatibility with additive manufacturing technologies.
- Lower materials and fabrication cost to be installed more widely.

1.2.4. Research challenges

Challenges in pharmaceuticals and heavy metal sensing

Electrochemical sensing of pharmaceuticals and heavy metals have been extensively reported in the last few years. Electrochemical sensing strategies was employed together with biosensing, immunosensing, genosensing and nanomaterials based sensing techniques. However, biosensing, immunosensing, genosensing have some major challenges including the following:

- Handling of different biomolecules, and biological compounds such as antibody, enzyme, and DNA requires specific temperature and environmental conditions, which limits their long term use in ubiquitous water quality monitoring applications.

- Most of the biomolecules degrades over time, therefore, limits the long-term stability and reliability of these sensors.

- Some of the biomolecules may not be suitable for handing by non-trained personnel, which also makes their use limited.

- The fabrication of these sensors requires tedious chemical and biochemical reactions which cannot be done in a general chemistry or chemical laboratory, rather they require special apparatus and separate biochemical laboratory with suitable health and safety checks procedures.

Among the different electrochemical sensing techniques, nanomaterials based sensing is advantageous due to their simpler fabrication processes and tools, easy sample preparation, and long term stability. However, they suffer from reduced sensitivity as compared to that of the biosensors. Therefore, research efforts are desirable in improving the sensitivity of the nanomaterials based sensors while maintaining their simpler fabrication capability and long-term stability. For example, improving the sensitivity of an electrochemical sensor can be achieved by appropriate choice of nanomaterials and their optimized tailoring. The sensitivity can be improved in two ways: (1) reducing noise, and (2) increasing response current due to redox reactions. The current in the working electrode of the sensor can be tuned in a way so that less noise is observed. When the noise level is low, then the limit of detection (LoD) of the sensor can be increased. Similarly, the sensitivity of a sensor can be increased when a larger response current is measured once the analyte interacts with the working electrode. In this regard, carbon nanomaterials can be both advantageous in tuning the LoD and sensitivity due to their large surface areas and high conductivity.

A larger electrode surface area of carbon nanomaterials facilitates an increased current response for an analyte in solution due to the presence of increased reactive sites in the same geometric surface area. This process is favourable for sensing small analyte concentrations. However, this increased current response can be offset by an increase in the

background current [116]. The increased background current can ultimately limit the sensitivity and in turn increase the LoD. This effect occurs when a large degree of pure carbon is present in the carbon nanomaterials. The pure carbon undergoes extensive electrochemical reduction during the sensing process leading to an increased background current. To address this challenge, carbon nanomaterials are normally functionalized with the attachments of other molecules or compounds such as oxides, metal NPs, organics, etc., so that enhanced and reproducible sensitivity can be accomplished. By the functionalization or modification of the carbon nanomaterials, the sensitivity and LoD can be improved through increased electron transfer between the analyte and the sensing electrode.

There are different approaches for the functionalization of carbon nanomaterials towards enhanced electrochemical performance. Choice of the functionalization procedure with appropriate agent is also another research challenge. Some functionalization processes require multiple chemical reaction steps and handling of air and moisture sensitive chemicals. Also, some processes require the use of organic solvents which may not be good for health and the environment. Therefore, research is needed to develop functionalization process with less number of chemical reaction steps for simplicity, with the use of environmentally benign reagents. Another challenge is to achieve multiple functionality with less complex material structure. For example, some organic/inorganic compounds can work both as functionalization agent for carbon nanomaterials and preconcentration agent for attracting more analytes into the electrode surface towards high sensitivity. Finally, reducing the size and cost of the potentiostat circuit used for the electrochemical sensing measurement is another important research challenge. In this regard, research should be done to develop open-source, low-cost and high-precision potentiostat circuit with wireless connectivity feature for portable water quality monitoring applications.

Challenges in pH and free chlorine sensing

Electrochemical pH sensors are widely reported. However, several challenges still remain. A major challenge is associated with the sensing performance of the sensors. For example, some sensors show sub-Nernstian pH response, while others exhibit near-Nernstian or

super-Nernstian response. Research should focus on improving the sensitivity of the sensors with sub-Nernstian response. On the other hand, stability and repeatability are the major issues related to sensors with near-Nernstian or super-Nernstian response. The instability and poor repeatability of the sensors with near-Nernstian or super-Nernstian response are most likely related to the following phenomena:

- Physical degradation of the sensing materials: sensor surface is impacted by water flow
- Chemical degradation of the sensing materials: irreversible reactions between the sensing material and H_3O^+ altering the chemical composition of the sensing material
- Interference from the test solution: adsorption of other ions or from bio-fouling that deteriorates the functionality of the sensors by blocking the redox reaction
- Instability of the electronic components: in transistor configurations with organic semiconductors, the electrical properties of the semiconductors change with time

Another challenge is related to the fabrication technologies that determine the cost of the sensors. The fabrication cost of the sensors should be inexpensive and consume small amount of materials. Therefore, fabrication processes at high temperatures and in vacuum environment should be avoided. In this regard, solution-based, low-cost and large-area processing is promising. However, the quality of the deposited materials often depends on post-treatment in high temperature. Thus, a trade-off between performance and cost of sensors can provide stimulus for further research into this problem. For example, the drawbacks of glass based pH electrodes in terms of their size and cost stimulated researches in the field of solid-state electrochemical pH sensors. Further research is still needed to develop new materials and processing techniques with their optimized compatibility for low-cost and high-performance pH sensors.

Research and development on electrochemical free chlorine sensors are not well focused compared to that of pH sensors. The major drawback is the lack of sensing materials with reversible reaction capability with HOCl or OCl⁻. An ideal electrochemical sensing material should either reversibly react with free chlorine, or selectively transport HOCl or OCl⁻ to the target electrode. In conventional DPD based optical detection technique, the chemical reaction of the reagents with free chlorine is an irreversible process. Another alternative is

the use of an ion-selective transport membrane. The ion-selective membrane technique exists for most of the ions, but very few were found for HOCl or OCl⁻ because of their oxidizing nature. Therefore, developing advanced sensing materials for free chlorine sensing is critically important.

The chemical reactivity of the free chlorine leaves us with limited electrochemical sensing options, such as the use of amperometric sensing electrodes. In this case, cyclic voltammetry measurement needs to be done to determine the bias voltage suitable for the amperometric measurement. The use of a bias voltage also increases the complexity in using the sensors. Furthermore, dissolved O_2 may also provide interference and reduce the sensing accuracy since dissolved O_2 becomes electroactive in voltage range between $+1$ and -1 V. Finally, amperometric sensor requires the use of a potentiostat which also increases additional complexity and cost of the sensor system. Hence, the sensor configurations need to be modified or redesigned with a suitable sensing material. Addressing these challenges can offer free chlorine sensor configurations and conditions similar to those for pH sensors with improved reliability and reduced fabrication costs.

1.3. Electrochemical sensors for water quality monitoring

1.3.1. Pharmaceuticals and heavy metals sensors

Electrochemical sensing techniques, often termed as electroanalytical techniques, offer a powerful strategy that are superior to different traditional analytical methods due to the advantages of instrumental simplicity, moderate cost, smaller footprint and portability [117]. A number of electroanalytical techniques have been employed for the development of electrochemical sensors to accurately detect and quantify a wide range of biomarkers, minerals, and pharmaceuticals and heavy metals in environmental and biological samples [118,119]. The design of an efficient, reliable, stable, and innovative sensing device requires highly efficient active electrocatalysts [120]. Many electrochemical sensor platforms have been developed for the detection and quantification of active pharmaceutical ingredients such as acetaminophen, and 17β-estradiol [121,122], and heavy

metals [123]. In addition, recent developments in the field of nanotechnology and synthesis of advanced functional materials have facilitated new strategies for the tailoring of novel materials with desired morphologies and exceptional physicochemical properties [124].

Electrochemical measurement techniques

Electrochemical measurement techniques utilize three electrodes, a Working Electrode (WE), a Reference Electrode (RE) and a Counter Electrode (CE), which are operated by a potentiostat circuit. A potentiostat is a three terminal analog feedback control circuit that maintains a pre-determined voltage between the WE and RE by obtaining current from the CE. Figure 1-3 shows a rough schematic of a potentiostat, where A1 and A2 are two amplifiers.
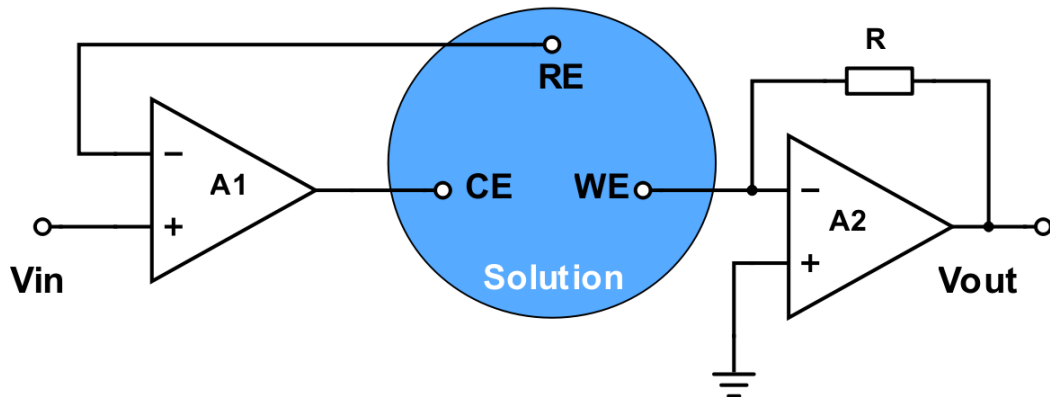
Figure 1-3. The potentiostat circuit diagram for electrochemical sensing measurement.

Available techniques for electroanalysis include, but not limited to, cyclic voltammetry (CV), differential pulse voltammetry (DPV), square wave voltammetry (SWV), and chronoamperometry (CA). CV is a potentiodynamic electrochemical measurement in which a cyclic potential scan is performed between two peak potentials E_{pc} and E_{pa}, as shown in Figure 1-4(a). The scan may start (E_{start}) at one of these peak potentials or anywhere in between. The scan is not fully linear, rather a combination of small potential steps (E_{step}). The current is measured or sampled during the second half of each step. So the number of points per scan of the current versus potential curve is $2 \times (E_{end} - E_{begin})/(E_{step}$

+1). The scan rate is specified by V/s, which determines the time between two steps and hence the sampling time. The interval time is calculated as (scan rate)/E_{step}. The current at the WE (μA) is plotted versus the applied voltage (V vs Ag/AgCl) (potential of WE) to give the CV trace, as shown in Figure 1-4(b).
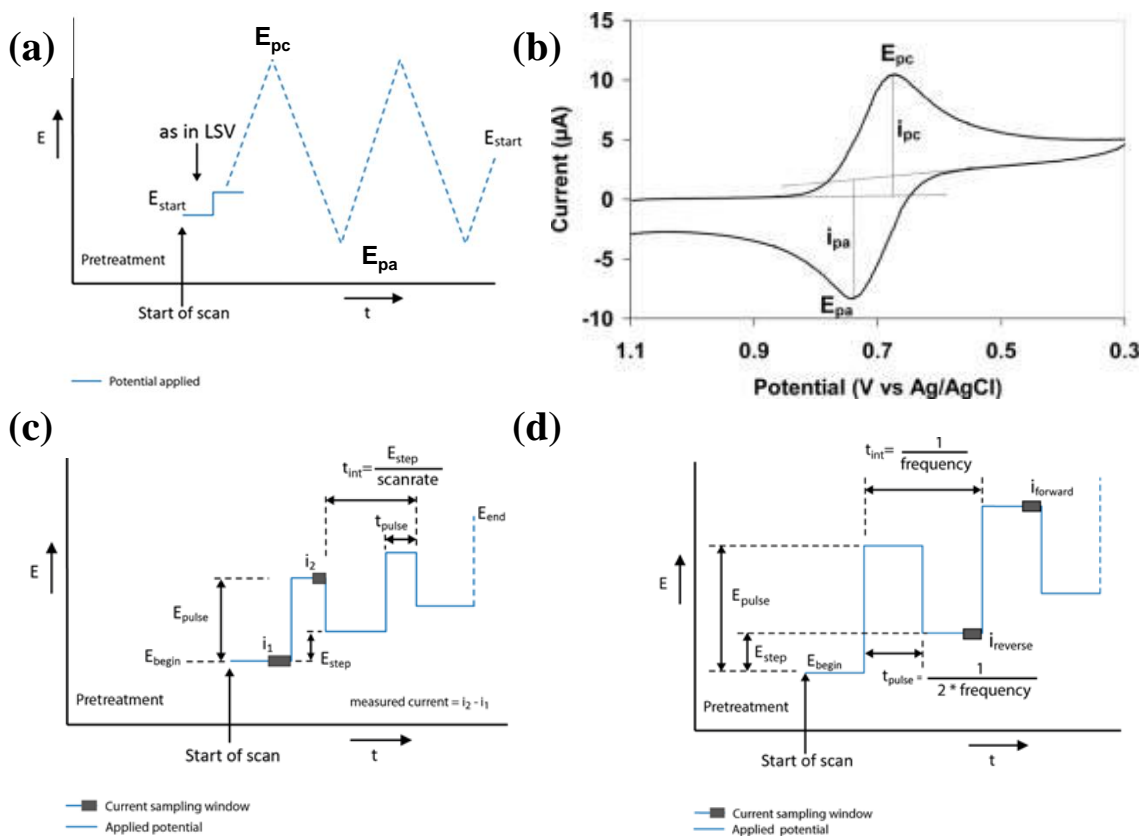
Figure 1-4. (a) Potential applied during Cyclic Voltammetry (CV) [125], and (b) Typical CV plot for a free diffusing redox species, where i_{pc} and i_{pa} show the peak cathodic and anodic current, respectively, (c) (a) Potential applied during Differential Pulse Voltammetry (DPV), (d) (a) Potential applied during Square Wave Voltammetry (SWV).

CV is commonly used to study the electrochemical properties of an analyte (analyte that is sensed) in solution or of a molecule that is adsorbed onto the electrode. On the other hand, DPV is used for both quantitative chemical analysis and to study the mechanism, kinetics, and thermodynamics of chemical reactions. In DPV technique, a potential scan is made using pulses with a constant amplitude (E_{pulse}) superimposed on a dc-potential (Figure 1-4(c)). SWV is a special version of DPV when t_{pulse} is equal $t_{interval}/2$, as shown in Figure 1-4(d). DPV and SWV are used to study the redox properties of extremely small amounts

of analytes because of the two major characteristics: (1) high sensitivity can be achieved by minimizing the effect of the charging current, and (2) a more precise electrode reaction can be analyzed due to the extraction of only the faradaic current. The most simple electrochemical measurement technique is chronoamperometry (CA). In CA techniques, a constant dc potential is applied and the current is measured with a constant interval time. The obtained current is then divided by the calibration factor to calculate the concentration of a specific analyte in the sample. However, CA technique is more prone to noise and fluctuations and, therefore, suffer from low accuracy in detecting analytes at very low concentrations.

Electrochemical sensing strategies

The versatility of the electrochemical sensing method lies in the wide range of ways in which the working electrodes (WEs) may be modified to enhance their functions and applications. Depending on the modification strategies, there are two broad categories: (1) biomolecules-based sensing (also known as biosensing), and (2) nanomaterials-based sensing, as shown in Figure 1-5.

Biosensors

In biosensing approach, the modifications of the WEs include immobilization of analyte-specific biomolecules, such as, enzymes (biosensors), antibodies (immunosensors), and nucleic acids (genosensors). These biomolecules function as the sensing element of the system. Enzyme-based biosensors combine the high specificity of the enzyme binding with the great sensitivity of the electrochemical transducers [126]. A thin layer of the desired enzyme is immobilized on the WE surface to obtain high selectivity to the compounds of interest. Common enzymes for biosensing include cytochrome P450 (CYP450) [127], horseradish peroxidase (HRP) [128], Tyrosinase (Tyr) [129], acetylcholinesterase [130], and butyrylcholinesterase [131]. For example, HRP was immobilized in carbon nanotubes-polyethyleneimine or polypyrrole nanocomposite film for the detection of acetaminophen using carbon based-screen printed electrodes (SPEs) and glassy carbon electrodes (GCEs)

WEs [126]. In another study, carbon nanodiamonds and potato starch film were immobilized with Tyr to detect phenolic compounds such as catechols [129].
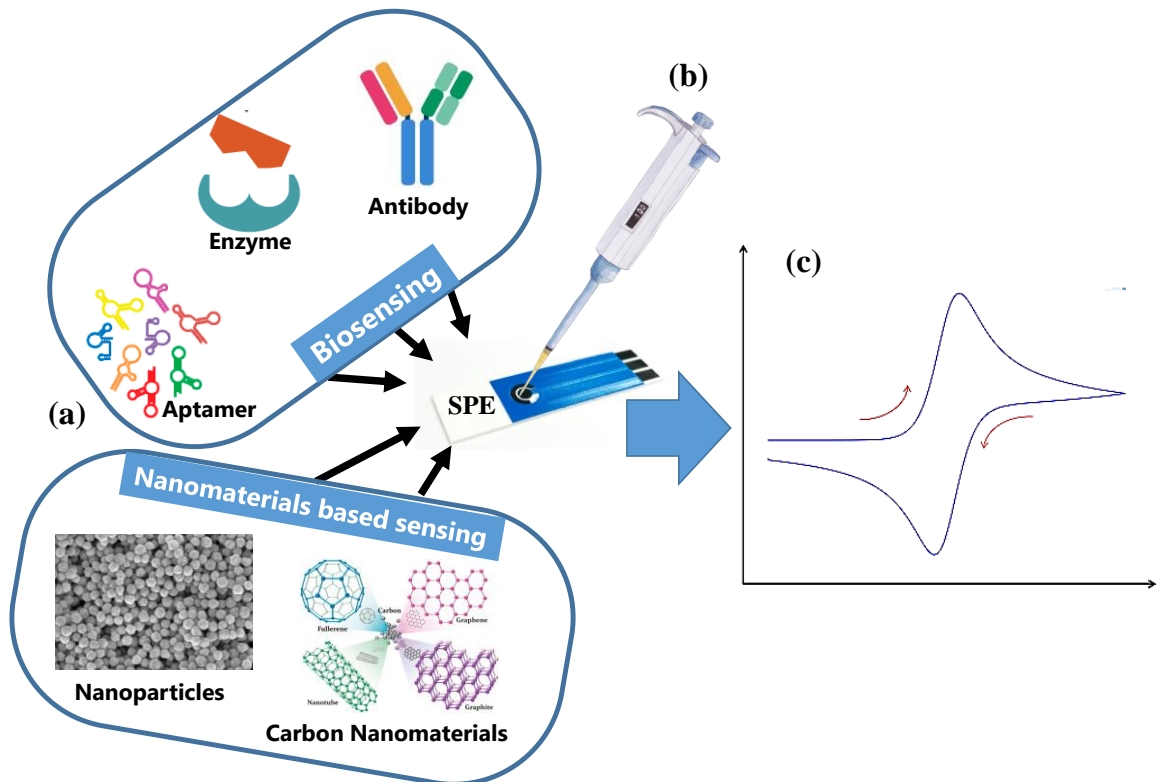
Figure 1-5. Fabrication and application of modified electrochemical sensing electrodes. (a) Modification of the electrode surface; (b) analysis of a drop of a sample; (c) electrochemical measurement of the pharmaceuticals or heavy metal.

Antibodies-modified biosensors, also known as electrochemical immunosensors, have gained much attention in the past few years. In this sensing approach, a specific antigen-antibody interaction facilitates the recognition and binding of the analyte molecule by the WE surface which is readily detected by the catalysed chemical reaction [120]. Immunosensors are extreme selective and sensitive to the analyte of interest having excellent limits of detection through the use of small volumes of samples. A key parameter in evaluating and optimizing immunosensor is the interaction or the binding mechanism between the analyte and the electrode surface that determines the specificity, sensitivity and stability of the immunosensor. In one study, an electrochemical immunosensor was

fabricated by immobilizing rabbit anti-mouse IgG and monoclonal mouse anti-estradiol passive adsorption on SPE surface for the detection of the hormone estradiol [132].

Nucleic acids-based biosensors, or genosensors, rely on the aptamer-based recognition together with the promising attributes of electrochemical sensors. Aptamers are short DNA or RNA fragments which are immobilized onto the surface of the WE as recognition probes. In this approach, the aptamer (i.e., a specific oligonucleic acid sequence) recognizes specific ligands and binds to many target molecules with high affinity and specificity, including proteins and pharmaceuticals. Aptamers were first reported in 1990 by three groups independently and are now attracting immense interest in the areas of therapeutics, diagnostics, analytical chemistry, and pharmaceuticals analysis [133]. For example, a single stranded DNA (ssDNA) aptamer was immobilized by self-assembled monolayers (SAMs) on WE through strong gold-sulphur (Au–S) bonds for the detection of endocrine disrupting chemical progesterone [134].

Nanomaterials based sensors

Nanomaterial-based electrochemical sensors represent a dominant element towards the adoption and implementation of electrochemical methods due to their functional tunability, ability to self-assemble, and novel electrical, and catalytic properties that occur at this scale. The direct outcomes of these properties are tremendous gains in terms of sensitivity, selectivity and versatility. The nanomaterials can be grouped into: (1) carbon based nanomaterials, (2) metal and metal oxide based nanomaterials, (3) nanocomposites, and (4) other nanostructures (e.g., molecularly imprinted polymers (MIPs)).

Carbon-based nanomaterials have a unique position in nanotechnology owing to their distinctive electrical, thermal, chemical, and mechanical properties. Carbon nanotubes (CNTs), graphene, fullerenes (C_{60}), mesoporous carbons, and carbon quantum dots are different types of carbon nanomaterials [135]. The metallic or semiconductor properties of carbon nanostructures can induce catalytic properties by participating in charge transfer processes during electrochemical sensing. Improved sensitivity, electrocatalytic properties, and resistance to fouling and reduced interference can be achieved by adding carbon

nanostructures into a carbon paste or depositing onto the electrode surface as modifiers [136]. For example, CNTs showed enhanced electrocatalytic activity, inhibited adsorption of chemical-reaction products, antifouling properties and induced topological defects [137,138]. These basal plane and edge-plane-like defect sites showed reversible electrochemistry with low redox potential [139]. Graphene, two-dimensional (2-D) nanomaterial with a hexagonal lattice of sp^2 carbon atoms, has also attracted attention in recent years due to its excellent mechanical strength, high specific surface area, high thermal and electrical conductivity at low cost. The enhanced electron transfer of graphene is due to its subtle electronic properties [140].

Metallic nanomaterials, such as gold, platinum, and silver nanoparticles (NPs), possess high catalytic activities for different chemical reactions. When these NPs are incorporated to modify WEs, enhanced electrocatalysis can be observed in many electrochemical processes which can be explained by both thermodynamic and kinetic properties. From thermodynamic point of view, quantum confinement effect of these NPs enables electrooxidization or electroreduction of pharmaceuticals at lower or less negative potentials, respectively [141]. From a kinetic point of view, these NPs accelerate electron transfer due to enhancement in the effective surface area of the electrode [69]. Appropriate selection of the metal NPs is critical to achieve high sensitivity in electrooxidation or electroreduction of a pharmaceutical since direct electron transfer process is related to the type of metal NPs, and different metals NPs perform electrodic processes at different rate. Metal oxide NPs show direct, mediated, or a combinatory electron transfer processes. Noble metal oxide NPs enhance the kinetics through direct electron transfer in drugs. Transition metal oxide NPs (TMONPs), however, possess multiple valences of metal ions that can flip-flop between these valence states. Also, TMNOPs can cause electrooxidation/ electroreduction of organics due to their strong electrocatalysis with high/low valence states [142].

Nanocomposites or hybrid nanomaterials are specifically custom-made to provide desirable properties or to exclude any undesirable ones in various applications, including electrochemical sensing. Nanocomposites may exhibit properties which are linear

combinations of individual properties of each component, or entirely new properties not apparent in any material found in their unmodified form. Some of the composite nanomaterials which have been utilized for the analysis of pharmaceuticals include combinations of multiwalled carbon nanotubes (MWCNT), graphene (GR), and platinum (Pt), with alumina-coated silica (ACS), zinc oxide (ZnO), and titanium dioxide (TiO_2) [124].

Molecularly imprinted polymer (MIP), a molecular imprinting technique which leaves cavities in the polymer matrix with an affinity for a chosen "template" molecule, has recently gained attention due to its very high selectivity and ability to be combined with other nanomaterials [143]. In the MIP-based sensing technique, the representative fragment of the target molecule is anchored into the surface of the polymer matrix and then chemically removed to create imprints of that target molecule fragment, which facilitates selective capture and recognition of the target. Two methods for the preparation of MIPs are bulk and surface imprinting [144,145]. Bulk imprinting of MIPs has shown successes with low-molecular-weight compounds. However, bulk imprinting is not suitable for large macromolecules because of their hindered mobility in the highly reticulated polymer network. In general, epitope approach is used where a representative fragment of the target molecule is prepared as a template for the MIP layer [146]. Binding capacity of surface imprinted polymers can also be maximized by increasing the effective surface area of the electrode surface using additional nanomaterials, such as CNTs and graphene, which are deposited before the formation of the MIPs. In addition, a self-assembled anchor layer can also be formed on top of CNTs to increase the homogeneity of the binding sites [147].

1.3.2. pH and free chlorine sensors

pH sensing

Working principles of solid-state electrochemical pH sensors have been explained in more than seven different mechanisms [148–150]. For example, H_3O^+ ion exchange occurs in a membrane rich in hydroxyl groups (−OH) for conventional glass electrodes. Other

mechanisms include: redox equilibrium involving H_3O^+ ions between a metal and its oxides; redox equilibrium involving H_3O^+ ions between metal oxides with different metal valences; redox equilibrium involving a solid-phase material and H_3O^+ ions where hydrogen content is changed by applying an electrical current; steady-state corrosion of the electrode material by H_3O^+ ions; change of surface potential of a solid-state material due to the pH change of the contacting solution based on the site-dissociation and double-layer models at the solid-liquid interface; and variation of electrical properties (such as resistivity) of a material with changes in the pH of the solution.
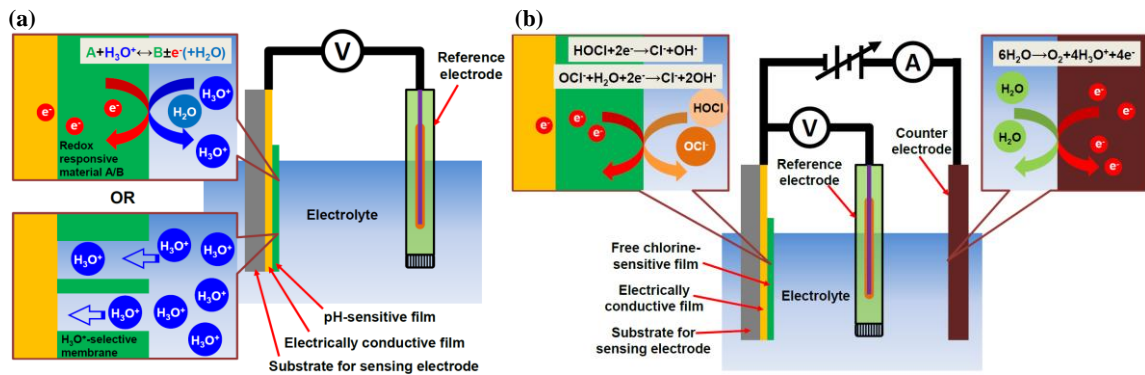
Figure 1-6. Schematic of (a) a potentiometric pH sensor and its possible sensing mechanisms, (b) an amperometric free chlorine sensor and its sensing mechanism [54].

Different configurations of pH sensors were developed based on the above transduction mechanisms. However, we will focus on the most widely reported pH sensors known as potentiometric electrodes. A typical potentiometric sensor is a two-electrode structure. One of the electrodes is called the sensing electrode and the other is called the reference electrode. The most commonly used reference electrode material in potentiometric pH sensor is Ag/AgCl [151,152]. When the two electrodes are in contact with the solution, an electrical potential difference is generated between them which is measured to determine the H_3O^+ concentration, as shown in Figure 1-6(a).

Two possible mechanisms have been proposed for potentiometric pH sensors, such as redox reactions and ion-selective permeation. According to redox reaction mechanisms, the material on the sensing electrode undergoes redox reactions with H_3O^+, generating a potential difference by the free energy change and a reversible chemical reactions

approaches their equilibrium conditions [54]. In ion-selective permeation mechanism, the sensing material acts as an ion-selective membrane, generating a potential difference due to the concentration gradient of ions across the membrane. In both cases, the generated potential can be quantitatively determined by the Nernst equation, as discussed previously in section 1.1. In an ideal scenario from equation (1−3), the change of 1 pH unit will result in 59.16 mV change in the potential difference at 25 °C between the sensing and the reference electrodes. The advantages of potentiometric configuration include: requirement of only two electrodes and no power supply; smaller dimensions of potentiometric sensors; compatibility with inexpensive and commercially available voltmeters for the read out of the potential difference between the sensing and reference electrodes, which is normally in the range of hundreds of millivolts. Thus, newly developed pH sensitive materials are being extensively developed with the help of potentiometric sensor configurations.

Free chlorine sensing

Amperometric free chlorine sensing is based on three-electrode potentiometric principle. In this method, a constant potential is applied between the working and the reference electrodes, when the current is monitored between the working and counter electrodes, as shown in Figure 1-6(b) [54]. The value of the constant potential is determined from the position of the redox peaks potential in the cyclic voltammetry curve of the corresponding analyte (i.e., free chlorine). The redox reaction of free chlorine takes place at the selected constant potential without the interference of other chemical groups. The amplitude of the measured current is proportional to the free chlorine concentration in the solution. The working electrode is commonly made of noble metals such as Au and Pt with an optional coated membrane for selectivity to hypochlorite ions. Free chlorine is electrochemically reduced at the working electrode by the applied constant potential with respect to the reference electrode [153]. The electrochemical reactions at the working electrode can be written as the follows:

$$HOCl + 2e^- + Cl^- + OH^-, \qquad (1-7)$$

$$OCl^- + H_2O + 2e^- \rightarrow Cl^- + 2OH^-, \qquad (1-8)$$
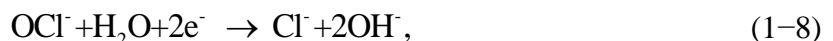
The above chemical reactions cause the transfer of electrons which generates a current that is proportional to the concentration of free chlorine. It should be noted that an accurate measurement of free chlorine also needs careful control and precise measurement the pH, temperature, flow rate and pressure of the solution.

1.3.3. Noise

The noise of an electrochemical sensor determines the fidelity of the sensing signals generated by the sensor, which also affect the limit of detection. However, experimental study of noise is rarely addressed in literature in the field of electrochemical sensing electrodes. The parameters that may contribute to noise in electrochemical sensors include, but not limited to, type of electrode materials, type of the solutions, electrode biasing conditions, and external circuitry. The noise behavior of the electrochemical sensing electrodes can provide insight into the optimization of sensor performance. While the theory and modelling of noise is well defined in solid-state electrical and electronic devices, noise in solid-liquid interface devices are not well-studied. Common classes of noises include thermal noise, shot noise and flicker noise. The noises may also depend on frequency and temperature. The most common frequency dependent noise is termed as flicker noise or $1/f$ noise, which is virtually present in all natural phenomena. Therefore, research should be done in optimizing noise performance of electrochemical sensors towards developing highly sensitive water quality monitoring system.

1.4. Research motivation

Many research has been carried out to develop advanced pharmaceuticals, heavy metals, pH and free chlorine sensors. However, very few of them were readily applicable for field applications. This research is devoted to developing an integrated drinking water quality monitoring system that is capable of on-demand measurement of pharmaceuticals and heavy metals, and continuous monitoring of the pH, free chlorine concentration, and

temperature of water samples accurately. Such an integrated drinking water quality monitoring system should realise the following objectives:

- **High accuracy**: The system should be comprised of sensors that have high sensitivity, reversibility, stability, and selectivity.

- **Real-time response**: The sensors in the system should respond fast to obtain results on-site towards the detection of the target analyte.

- **Easy operation**: The system should be designed for users with no comprehensive technical training. Also, the sensor output should be easily understandable by the users.

- **Low-cost**: A low-cost integrated system can be afforded by people living in developing and underdeveloped regions and can also be distributed over a wide geographical area.

Table 1-1: Proposed specifications of the integrated water quality monitoring sensors.

Parameters	APAP/E2 sensor	Heavy Metal sensor	pH sensor	Free Cl sensor	T sensor
Sensitivity	$2-12$ µA/µM	~0.1 µA/ppb	59.5 mV/pH	186 nA/ppm	~1% $\Delta R/^{o}C$
Resolution	-	-	0.1 pH	0.16 ppm	0.1 ℃
Sensing range	$0.01 - 15$ µM	$3.3 - 103$ ppb	pH = $6 - 10$	$0.2 - 8$ ppm	$0 - 50$ ℃
Accuracy/LoD	< 10 nM (LoD)	< 10 ppb (LoD)	± 0.1 pH	±0.035 ppm	± 0.05 ℃
Response time	~600 s	~600 s	< 1 min	< 1 min	< 1 min
Stability	One-time use	Multiple use	~1 month	~1 month	~1 months
Size	< 10 cm³	< 10 cm³	< 1 cm³	<1 cm³	< 15 cm³
Cost	< \$1	< \$1	< \$1	< \$1	< \$1
Operation temperature	$0 - 40$ ℃	$0 - 40$ ℃	$0 - 40$ ℃	$0 - 40$ ℃	$0 - 40$ ℃

To accomplish the abovementioned objectives, this research focuses on the development of an integrated water quality monitoring system with pharmaceuticals, heavy metal, pH, free chlorine, and temperature sensors. The proposed specifications of these sensors are listed in Table 1-1. For the pharmaceutical sensor, we are targeting two of the most commonly found pharmaceutical contaminants in sources of drinking water, such as acetaminophen or APAP (pain-killer), and 17β-estradiol or E2 (female sex hormone). There is no national or international standards yet for monitoring pharmaceuticals in

drinking water. However, we are targeting the sensitivity that is close to the predicted no effect concentrations (PNEC) of APAP and E2. The PNEC of APAP and E2 was reported to be 136 µg l^{-1} (0.9 µM) and 2 ng l^{-1} (0.007 nM), respectively [37,38]. For heavy metal sensor, we are targeting the most commonly found heavy metal (i.e., lead (Pb) in drinking water). For Pb sensor, we are aiming at the sensitivity close to WHO recommended guideline for safe limit of Pb in drinking water, which is 10 µg/L (or, 10 ppb) [57].

For the pH sensor, we are aiming at the sensitivity close to a commercial pH meter (59 mV/pH), which can provide a resolution of 0.1 pH. The sensor should function in common water samples, such as drinking, recreation, and food processing water. The ability to distinguish between safe and unsafe water can be achieved by the accuracy of ±0.1 pH. For the free chlorine sensor, the sensor should be able to accurately monitor drinking water with accuracy better than ±0.1 ppm. For the temperature sensor, an accuracy of ±2.5 °C is necessary to guarantee an accurate readout for the pH and free chlorine sensors. In addition, all five sensors should have short response time, small footprint, high stability of around one month, low-cost fabrication capability, operation temperature between 0 to 40 °C, and simple storage conditions.

The design goal for the APAP/E2 and Pb sensor are realized by using a single three-electrode voltammetric configuration. The base sensing material is a screen-printed carbon electrode (SPE), where the working and counter electrodes are made of carbon and the reference electrode is made of Ag/AgCl. The working (i.e., sensing) electrode is then modified by carbon nanomaterials. The main advantage of this carbon nanomaterials modified SPE electrode is that the same electrode can be used for sensing both the pharmaceuticals and heavy metal, thereby, simplifying the sensor configuration, reducing overall fabrication cost and having a smaller footprint. However, this electrode can only be used once for pharmaceutical sensing, and several times for heavy metal sensing through regeneration process. Yet, the sensor provides a low-cost and highly sensitive platform for monitoring pharmaceuticals and heavy metal since the SPE can easily be cleaned with common alcohols and re-frabciated by drop-casting and drying only few microliters of carbon nanomaterials solution onto the surface SPE electrode.

The design goals for the pH sensor are realized by utilizing a simple two-electrode potentiometric configuration. The sensing electrode uses metal/metal oxide because of its wide sensing range, high sensitivity, and high stability. An Ag/AgCl reference electrode provides stable reference voltage, which is insensitive to pH and other common ions. The potentiometric pH sensor is fabricated by developing a low temperature, solution-based processing at low cost, without the use of cleanroom environment and high vacuum equipment.

The free chlorine sensor is implemented by simplifying an amperometric free chlorine sensor developed by our group. The performance of the simplified free chlorine sensor is studied in the integrated drinking water quality monitoring system. The temperature sensor uses a Wheatstone bridge circuit to accomplish high sensitivity. The thermistors in the circuit are fabricated by using low cost materials.

Finally, this research aims to demonstrate a fully integrated drinking water quality monitoring system using the five types of sensors. The integration process is developed to fabricate the sensors on only two substrates. An electronic data acquisition system is designed and programmed to sample and process the sensor signals, followed by displaying the water quality parameters on a smartphone application (app) interface.

1.5. Research contributions

The research work conducted in this thesis focuses on developing an integrated, easy-to-use, and accurate water quality monitoring system using low-cost electrochemical sensors. The major contributions of this work are summarized as follows.

- **The development of pharmaceutical-contaminant (APAP) sensing electrode using multi-walled carbon nanotubes (MWCNT) and β-cyclodextrin (βCD).** A low temperature solution based processing was developed to realize a well-dispersed MWCNT-βCD solution, which was then drop-casted on glassy carbon electrode (GCE) surface and dried. The electrochemical sensing performance of the electrode was

characterized in terms of their effective surface area, scan-rate and pH of the solution. A linear APAP sensing response in the range of 0.05−300 μM with a limit of detection of 11 nM was obtained.

- **Tailoring MWCNT and βCD for improved detection of pharmaceutical contaminants, (APAP and E2).** A simple, one-step chemical synthesis approach was developed to realize a chemically modified MWCNT-βCD solution, which was then drop-casted on GCE electrode surface and dried. The electrochemical sensing performance of the electrode was characterized in terms of the type of MWCNT-βCD modifications, their effective surface area, scan-rate and pH of the solution. Linear APAP and E2 sensing response in the ranges of 0.005−20 μM and 0.01−15 μM with limits of detection of 3.3 nM and 2.5 nM were obtained, respectively.

- **The development of heavy metal (Pb) sensor using multi-walled carbon nanotubes (MWCNT) and β-cyclodextrin (βCD).** The synthesis approaches of MWCNT-βCD developed in pharmaceutical sensing were compared and analyzed for the detection of Pb in drinking water. The electrochemical sensing performance of the electrode was characterized in terms of the modification approaches of MWCNT-βCD. A linear Pb sensing response in the range of 3−103 ppb with a limit of detection of 0.9 ppb was achieved.

- **Noises in electrochemical sensors were studied.** The noise in pharmaceutical sensors were studied with a potentiostatic configuration similar to the electrochemical sensing approach. The effect of bias voltages, type of electrolytes and electrode materials on the noise power spectra density (PSD) was studied. Similarly, noises in the pH and free chlorine sensors were studied in potentiometric and amperometric configurations, respectively. The noise in the temperature sensor was also studied.

- **A fully-integrated water quality monitoring system was developed by using Arduino Uno microcontroller along with wireless connectivity to a smartphone application to sample, process, and display the signals from an integrated sensors array.** The integrated sensors array consisted of a MWCNT-βCD modified screen-printed electrode (SPE) as APAP/E2/Pb sensor; a spin-coated pH sensor; a carbon-

based amperometric free chlorine sensor; and a low-cost, custom-designed temperature sensor, on two glass substrates. Linear sensing responses with limits of detection of 17 nM, 11 nM and 2.3 ppb was achieved for APAP/E2/Pb, respectively. A linear pH response with sensitivity of ~57.5 mV/pH was obtained for pH between 4 and 10. A sensitivity of ~186 nA/ppm was obtained for monitoring of free chlorine. The sensitivity of the temperature sensor was ~16.95 mV/°C.

Publications:

- (Invited) M. J. Deen, A. U. Alam, Low Frequency Noise in Electrochemical Sensors for Water Quality Monitoring, 25th International Conference on Noise and Fluctuations – ICNF 2019, Neuchâtel, Switzerland, accepted, Jun 2019.

- (Keynote) M. J. Deen, A. U. Alam, Flexible Sensors – Materials, Interfaces and Surfaces, IEEE 6th International Workshop on Low Temperature Bonding for 3D Integration (LTB-3D), Kanazawa, Japan, accepted, May 2019.

- (Invited) M. M. Alam, A. U. Alam, M. M. R. Howlader, Sweat Glucose Sensing by Directly Bonded Films, IEEE 6th International Workshop on Low Temperature Bonding for 3D Integration (LTB-3D), Kanazawa, Japan, accepted, May 2019.

- A. U. Alam, Y. Qin, M. M. R. Howlader, N.-X. Hu, M. J. Deen, Electrochemical Sensing of Lead in Drinking Water Using β-Cyclodextrin-Modified MWCNTs, *Sens. Actuators B: Chem.*, 2019, under revision (manuscript ID: SNB-D-19-01084).

- T. Z. Redhwan, A. U. Alam, Y. Qin, M. M. R. Howlader, Y. M. Haddara, Fully-integrated Sensor based on Surface Activated Copper/Polymer Bonding for Sub-parts-per-billion-level Lead Detection, *Sens. Actuators B: Chem.*, 2019, under revision (manuscript ID: SNB-D-18-06094).

- A. U. Alam, Y. Qin, M. Catalano, L. Wang, M. J. Kim, M. M. R. Howlader, N.-X. Hu, M. J. Deen, "Tailoring MWCNTs and β-Cyclodextrin for Sensitive Detection of Acetaminophen and Estrogen," *ACS Applied Materials and Interfaces*, vol. 10(25), pp. 21411–21427, Jun. 2018.

- A. U. Alam, Y. Qin, S. Nambiar, J. T. Yeow, M. M. R. Howlader, N.-X. Hu, M. J. Deen, "Polymers and organic materials-based pH sensors for healthcare applications," *Progress in Materials Science*, vol. 96, pp. 174–216, Jul. 2018.

- T. Z. Redhwan, A. U. Alam, M. Catalano, L. Wang, M. J. Kim, Y. M. Haddara, M. M. R. Howlader, "Direct bonding of copper and liquid crystal polymer," *Materials Letters*, vol. 212, pp. 214–217, Feb. 2018.

- Y. Qin, A. U. Alam, S. Pan, M. M. R. Howlader, R. Ghosh, N.-X. Hu, H. Jin, S. Dong, C.-H. Chen, M. J. Deen, "Integrated water quality monitoring system with pH, free chlorine, and temperature sensors," *Sensors and Actuators B: Chemical*, vol. 255, pp. 781-790, Feb 2018.

- T. Z. Redhwan, A. U. Alam, Y. M. Haddara, M. M. R. Howlader, "Copper and liquid crystal polymer bonding towards lead sensing," *Japanese Journal of Applied Physics*, vol. 57 (2S1), pp. 02BB03, Jan. 2018.

- A. U. Alam, Y. Qin, M. M. R. Howlader, N.-X. Hu, M. J. Deen, "Electrochemical sensing of acetaminophen using multi-walled carbon nanotube and β-cyclodextrin", *Sensors and Actuators B: Chemical*, vol. 254, pp. 896-909, Jan 2018.

- H. Jin, Y. Qin, S. Pan, A. U. Alam, S. Dong, R. Ghosh, M. J. Deen, "Open-Source Low-Cost Wireless Potentiometric Instrument for pH Determination Experiments", *Journal of Chemical Education*, vol. 95, pp. 326-330, Nov 2017.

- Y. Qin, A. U. Alam, M. M. R. Howlader, N.-X. Hu, M. J. Deen, "Morphology and electrical properties of inkjet-printed palladium/palladium oxide," *Journal of Materials Chemistry C*, vol. 5(8), pp. 1893-1902, Jan 2017.

- Y. Qin, A. U. Alam, M. M. R. Howlader, N.-X. Hu, M. J. Deen, "Inkjet Printing of a Highly Loaded Palladium Ink for Integrated, Low-Cost pH Sensors," *Advanced Functional Materials*, vol. 26(27), pp. 4923-4933, Jan 2017.

- A. U. Alam, Y. Qin, M. M. R. Howlader, M. J. Deen, "Direct bonding of liquid crystal polymer to glass," *RSC Advances*, vol. 6, pp. 107200-107207, Nov 2016.

▪ Y. Qin, A. U. Alam, M. M. R. Howlader, N.-X. Hu, M. J. Deen, "Low-temperature solution processing of palladium/palladium oxide films and their pH sensing performance," *Talanta*, vol. 146, pp. 517-524, Jan 2016.

▪ M. M. R. Howlader, A. U. Alam, R. P. Sharma, M. J. Deen, "Materials Analyses and Electrochemical Impedance of Implantable Metal Electrodes," *Physical Chemistry Chemical Physics*, vol. 17(15), pp. 10135-10145, Mar 2015.

▪ A. U. Alam, N.-X. Hu, M. M. R. Howlader, M. J. Deen, "Pharmaceutical Contaminants and pH Sensing using MWCNTs based Electrodes," *2017 International Conference on Solid State Devices and Materials (SSDM 2017)*, Sendai, Sep 2017.

▪ T. Z. Redhwan, A. U. Alam, Y. M. Haddara, M. M. R. Howlader, "Bonding mechanism and electrochemical impedance of directly bonded liquid crystal polymer and copper," *IEEE 2017 5th International Workshop on Low Temperature Bonding for 3D Integration (LTB-3D)*, Tokyo, pp. 40, May 2017.

1.6. Thesis organization

In Chapter 1, an introduction to the importance of water quality monitoring is presented. The recent research activities in electrochemical pharmaceuticals, heavy metal, pH and free chlorine sensors are discussed and compared with conventional sensing techniques. Then, the motivation of developing simple, low-cost, and highly sensitive integrated water quality monitoring systems is presented. Finally, a brief summary of the main contributions of this research and the structure of this thesis are described.

In Chapter 2, a low-temperature, solution-processed modification of multi-walled carbon nanotubes (MWCNT) with β-cyclodextrin (βCD) on glassy carbon electrode for detecting low levels of acetaminophen in water is presented. Detailed fabrication approaches, material characterization methods, and sensor characterization set-ups used in this research are given. In particular, efforts are devoted to studying the sensing mechanisms, and to characterize the sensor performance in terms of effective surface area, scan-rate, pH of the solution, and sensing performance with common interfering ions. This process combines

the adsorption properties of βCD with high surface area of carbon nanotubes to achieve a low limit of detection of 11 nM and with linear response from 50 nM to 300 μM.

In Chapter 3, a systematic investigation of four types of modifications of multi-walled carbon nanotubes (MWCNTs) and β-cyclodextrin (βCD): physical mixing, "click reaction", thionyl chloride esterification, and Steglich esterification to fabricate electrochemical sensors are reported for improved sensitivity and accurate determination of two emerging pharmaceutical contaminants in water such as acetaminophen and estrogen. The electrochemical behavior and sensing performances of the four types of MWCNT-βCD modified electrodes were compared and a novel one-step synthesis approach was developed which provided the highest sensitivity to APAP and E2 detection with limits of detection of 3.3 and 2.5 nM, respectively. Accurate sensing performances were also obtained with APAP- and E2-spiked urine and drinking water samples.

In Chapter 4, a low-temperature, solution-processed modification of multi-walled carbon nanotubes (MWCNT) with β-cyclodextrin (βCD) on scree-printed carbon electrode (SPE) for the detection of heavy metal (lead, Pb) in drinking water is presented. The fabrication approaches, material characterization methods, measurement set-up, and sensor performances analyzed in this research are given. Efforts are devoted to studying the sensing mechanisms, and to characterize the sensor performance in terms of the MWCNT-βCD modification approaches, low-cost nature of the sensing electrodes, and sensing performance with common interfering ions.

In Chapter 5, noises in electrochemical sensors are studied. The noise in pharmaceuticals and heavy metal sensors are studied with a potentiostatic configuration similar to the electrochemical sensing approach. The noise power spectra density (PSD) are studied with respect to the bias voltages, type of electrolytes and electrode modification materials. Similarly, noises in the pH and free chlorine sensors are studied in potentiometric and

amperometric configurations, respectively. The noise in the temperature sensor was also studied where the thermistors are connected in Wheatstone bridge configuration.

In Chapter 6, a fully integrated water quality monitoring system is presented. Such a system includes a MWCNT-βCD modified SPE electrode for the detection of APAP/E2/Pb as discussed in Chapter 3 and Chapter 4, a spin-coated pH sensor, a Wheatstone-bridge-based temperature sensor fabricated by silicon and PEDOT:PSS, and a free chlorine sensor. The free chlorine sensor is a simplified version of an amperometric sensor with an amine-modified carbon electrode as the sensing electrode. The sensors are fabricated on two glass substrates and their sensing performance is characterized. An Arduino Uno microcontroller shield, two shields for sensor data acquisition (potentiostat shield: APAP/E2/Pb; WQM shield: pH/free chlorine/temperature), and a smartphone application with Bluetooth wireless shield were programmed as the user interface to sample, process, and display the sensor signals.

In Chapter 7, this thesis is concluded with a summary of the research and several recommendations for future improvements for pharmaceutical, heavy metal, pH, free chlorine, temperature sensors, and the integrated sensing system for water quality monitoring.

Chapter 2

Electrochemical sensing of acetaminophen using MWCNT and β-cyclodextrin[*]

Acetaminophen (APAP) is one of the most commonly and widely used painkillers worldwide. Because of its increased use in the past several decades, APAP is now present at higher concentrations in source water, thus necessitating its monitoring. In this work, we report a low-temperature, solution-processed modification of multi-walled carbon nanotubes (MWCNT) with β-cyclodextrin (βCD) on glassy carbon electrode for detecting low levels of acetaminophen in water. This process combines the adsorption properties of βCD with high surface area of carbon nanotubes. An improved dispersion of MWCNT was observed due to the hydrophilicity of βCD. A surface-limited process involving equal number of protons and electrons controlled the electrochemical reaction of acetaminophen with the sensor. The sensor's limit of detection was 11.5 nM and its linear response was from 50 nM to 300 μM. The sensors exhibited a reproducible and stable response over four weeks and negligible interference from commonly present chemicals in urine, such as dopamine and ascorbic acid. These promising results could facilitate the development of simple and low-cost electrochemical sensors for monitoring of APAP in water.

---

[*] Adapted with permission from A. U. Alam, Y. Qin, M. M. R. Howlader, N.-X. Hu, and M. J. Deen, Electrochemical sensing of acetaminophen using multi-walled carbon nanotube and β-cyclodextrin, Sensors and Actuators B: Chemical, 254, 2018: 896-909. Copyright (2018) Elsevier (Appendix C).

2.1. Background

Over the last fifty years, the quality of human health has improved mostly due to better medicines, education, and lifestyle [154]. In parallel, we have witnessed increasing use of pharmaceuticals to prolong life as well as to prevent and cure illnesses and diseases [155]. One of the most commonly used pharmaceuticals is painkillers. Among painkillers, acetaminophen (APAP) (N-acetyl-P-aminophenol or paracetamol) is widely used for fever and pain relief [156]. Because of its increasing use, excreted APAP plus its disposal in effluents from manufacturing industries increase its presence in source water systems [157]. The presence of APAP with concentration ranges in few hundreds to several thousands of $ng \cdot l^{-1}$ has been reported [23,158–162], thus making it a fast-growing, emerging water problem worldwide [163–165]. Further, increasing amounts of APAP in drinking water may cause increased mortality, and heart, gastro-intestine, and kidney diseases [166]. Also, overdose and toxic-dose of APAP cause not only hepato- and nephro-toxic effects on health [167], but also contaminate water. To address these challenges, monitoring of APAP in water is important. However, monitoring is limited by the sensing resources and data, and it requires standard sampling with the current analytical techniques.

Existing analytical techniques to determine APAP in pharmaceutical tablets and biological fluids include titrametry [168], spectrophotometry [169], high performance liquid chromatography [170], gas chromatography [171], and chemiluminescence [172] which require extraction processes before detection. While these methods offer high sensitivity, selectivity and precision, their difficulty in use, complicated operation and high cost limit their widespread application. In contrast, electrochemical sensing techniques are promising because of the fabrication simplicity and small foot print of the sensors, high selectivity and sensitivity, fast response, wide linear range, and simple sample preparation [173–175].

In electrochemical sensing, redox compounds at the sensing electrode, such as carbon nanostructures, metallic nanoparticles [176], conductive polymers [177] or their combinations [178], facilitate the conversion of irreversible oxidation processes into reversible one due to the rapid electron transfer rates [121]. Among these compounds,

carbon nanostructures, especially single-walled carbon nanotubes (SWCNTs), graphene and multi-walled carbon nanotubes (MWCNTs) have been extensively utilized for electrochemical sensing [179–182]. For example, CNTs can be functionalized/modified with different chemical groups such as -COOH [183], or organic molecules such as chitosan or ethylenediamine [184], to enhance sensing performance for the detection of APAP through adsorption-controlled and quasi-reversible redox reactions [185–187]. However, the functionalization of CNTs is complex and requires many chemical reaction steps. Also, CNTs functionalization with polymers mostly requires the use of electropolymerization processes, and the handling of monomers and reagents that are sensitive to oxygen and moisture [184]. Furthermore, MWCNT cannot be highly dispersed in a solution without surfactant, which is important to achieve a uniform thin layer [188]. These disadvantages limit the development of simple and low-cost sensors for APAP.

To overcome these disadvantages, large effective surface area and strong electrochemical interaction (e.g., redox capability) of MWCNTs can be combined with the host-guest interaction capabilities of β-cyclodextrin (βCD) [116,189,190]. This method does not require any chemical modification because it mixes unmodified MWCNTs and βCD. The βCD is a 7-membered cyclic oligosaccharides material that adsorbs APAP contaminations [191],[192], which is commonly used in food, pharmaceutical, drug delivery, and chemical industries [193],[194]. However, the sensing potential of physically mixed MWCNT with βCD for detection of APAP has not yet been investigated. In fact, physical mixing of the unmodified MWCNTs with porous βCD molecules enabled us to realize a simple, low cost and drop-casted electrode for sensing APAP.

In this paper, we develop a simple, rapid, and low-cost electrochemical APAP sensor based on MWCNT and βCD modified glassy carbon electrode (GCE). The composite was prepared through physical-mixing of MWCNT and βCD in deionized water. The MWCNT-βCD composite was then drop-casted on the GCE electrode surface to create the electrochemical sensor.

This chapter is organized as follows. The experimental details are given in Section 2.2. Then, in section 2.3.1, we describe the characterization of the thermal weight loss profile and surface morphologies of the composite. In section 2.3.2, we provide a comparison of the sensing performance of MWCNT/GCE with MWCNT-βCD/GCE using cyclic voltammetry method as well as the optimized sensing conditions to achieve better sensor performance. In section 2.3.3, the sensors' limit of detection and linear range using differential pulse voltammetry is discussed. Finally, in section 2.3.4, we describe the sensor's aging performance and stability with chemical interferers and its use to detect APAP in urine.

2.2. Experimental set-up

2.2.1. Reagents and Materials

Acetaminophen, β-cyclodextrin, dopamine, ascorbic acid and phosphate buffer solution (PBS) tablets (P4417) were purchased from Sigma Aldrich Canada. All chemicals were of analytical grade and used without further purification. All the aqueous solutions were prepared with deionized (DI) water ($\geq$ 18 MΩ cm). MWCNT (diameters 8-15 nm and length 10-50 μm, $\geq$95 wt% purity) was purchased from Cheap Tubes. The 0.01 M phosphate buffer solutions (PBS) with 0.0027 M potassium chloride and 0.137 M sodium chloride at pH 7.4 were prepared by dissolving one PBS tablet into 200 ml DI water. The 0.01 M phosphate buffer solutions with 0.0027 M potassium chloride (KCl) and 0.137 M sodium chloride (NaCl) at different pH were prepared by dissolving appropriate amount of Na_2HPO_4, NaH_2PO_4, KCl and NaCl into ultrapure water. Tylenol® regular strength and Tylenol® Extra Strength tablets were purchased from a drugstore.

2.2.2. Apparatus

All electrochemical measurements were carried out with an electrochemical workstation in a conventional three-electrode cell at room temperature. PalmSens EmStat 3 potentiostat (purchased from PalmSens.com) was connected to a three-electrode cell connected to a

computer (Intel Core i5, 2400 MHz) and with PSTrace 4.8 software. The three-electrode cell assembly consisted of a platinum wire as an auxiliary electrode and an Ag/AgCl electrode as a reference electrode. The working electrode was either an unmodified GCE or a GCE modified with MWCNT and MWCNT-βCD composite materials with an exposed area of 0.070 cm^2. All the electrodes were purchased from CHI instruments. Additionally, the GCEs modified with MWCNT and MWCNT-βCD was measured in 5 mM $K_3[Fe(CN)_6]$ with 0.1 M KCl solution to obtain the cyclic voltammetry (CV) curves and calculate for the electrochemically active surface area. All measurements were performed at 25±2 ℃. The surface morphologies of the composites were investigated using scanning electron microscopy (SEM, JEOL 7100F). Thermogravimetric analysis (TGA) of the MWCNT and MWCNT-βCD composite was done by using a TGA equipment Q5000 from TA Instruments. The chemical composition at the electrode surfaces were characterized by using X-ray Photoelectron Spectroscopy (XPS) (XPS, JPS-9200, JEOL, Mg-α source, 10 keV, 15 mA).

2.2.3. Preparation of the MWCNT-βCD modified electrode

Two milligrams of MWCNTs was dispersed by using an ultrasonic preprocessor in 20 ml of βCD solution (2 wt.%) to give a 2 mg/ml black suspension. The surface of the GCE electrodes were polished on fine emery paper and chamois leather containing alumina (Al_2O_3) with 1.0, 0.3, and 0.05 μm alumina powder (purchased from CHI Instruments), respectively, rinsed thoroughly with DI water between each polishing step, and then sonicated in DI water and dried with purified compressed air. An aliquot of 8 μL of 2 mg/ml MWCNT suspension in βCD solution was drop-casted on the GCE, which was dried in air for 20 minutes at 80 ℃ in an oven. A schematic overview of the electrode modification steps is shown in Figure 2-1.
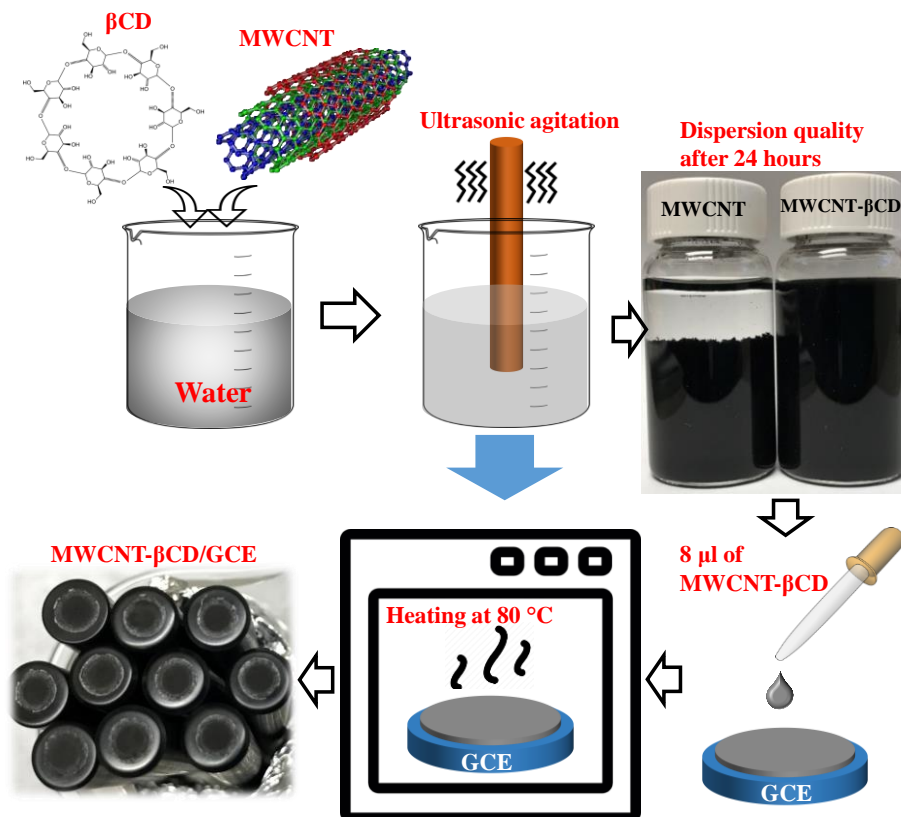
Figure 2-1. Process flow for the modification of glassy carbon electrode (GCE) with MWCNT-βCD composites.

2.2.4. Preparation of drinking water and urine samples

The tablet solution was prepared by completely grinding and homogenizing one tablet of Tylenol® Regular Strength or Tylenol® Extra Strength, labeled 325 mg and 500 mg per tablet, respectively. Then, each grinded tablet was dissolved into ultrapure water by magnetic stirring for 60 min. The solution was filtered by a 0.45 μm pore-diameter syringe filter membrane, and then the filtrate was diluted in PBS solution with pH value of 7.4 to make 0.1 mM stock solution of APAP from the tablet. Urine samples were diluted four times with PBS (pH 7.4) without any further treatment. The diluted urine sample was spiked with different amounts of APAP. The recovery tests were carried out using differential pulse voltammetry (DPV) for the determination of APAP in APAP tablet containing water and human urine.

2.3. Results and discussions

2.3.1. Characterization of the MWCNT-βCD/GCE electrode

TGA analysis of MWCNT and MWCNT-βCD

The amount of MWCNT and βCD compositions suspended in deionized water (DIW) was quantified using thermogravimetric analyzer (TGA). Figure 2-2 shows the normalized TGA weight-loss profile for the MWCNTs with and without βCD. The weight of the dry MWCNT was ~99.8% at 400 °C. This result indicates the MWCNT was very pure and had almost no impurities. In the case of MWCNT-βCD, the weight loss started at around 300 °C, and became ~15.8% at ~400 °C mainly due to the thermal decomposition of βCD [195]. This loss corresponds to 84.2 wt. % of βCD in the MWCNT solid, or ~0.18 wt% of βCD in the water suspension, which is close to 0.2 wt% of βCD in the MWCNT-βCD that was originally prepared. The slight mismatch in the TGA weight loss profile may be due to the strong adsorption of βCD with MWCNT [196] preventing its complete decomposition.
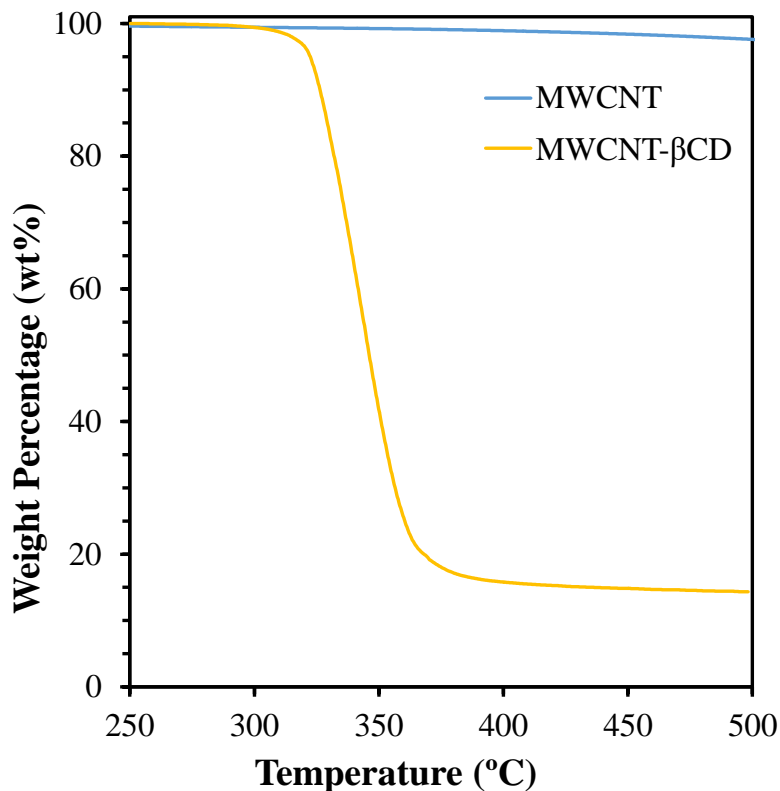
Figure 2-2. TGA plot of MWCNT and MWCNT-βCD acquired under nitrogen. The temperature profile involved a ramp of 30 °C per minute from room temperature to 500 °C.

Surface Morphology of MWCNT-βCD/GCE

Surface morphology controls electrochemical sensing performance through electrolytic participation and ionic transport [197]. Hence, the MWCNT/GCE and MWCNT-βCD/GCE surfaces were examined with microscopic imaging analysis. Figure 2-3 shows the scanning electron microscope (SEM) images at different magnifications. The MWCNT/GCE surface showed inhomogeneous coverage which were possibly due to the effect of heat distribution as well as the surface tensions associated with the droplet [198]. These inhomogeneous distributions could also be due to the coagulation of the carbon nanotubes during heating [199]. Adhesion of MWCNT with GCE could be another parameter which could influence on their coagulation [200]. In contrast, when the MWCNT was dispersed with βCD, the morphology became smooth. In fact, the hydrophilic outer shell of the βCD molecules resulted in better dispersion of MWCNT-βCD in DIW, which may be responsible for the better electrochemical sensing performance [201] for the detection of APAP as discussed in the section 3.3.
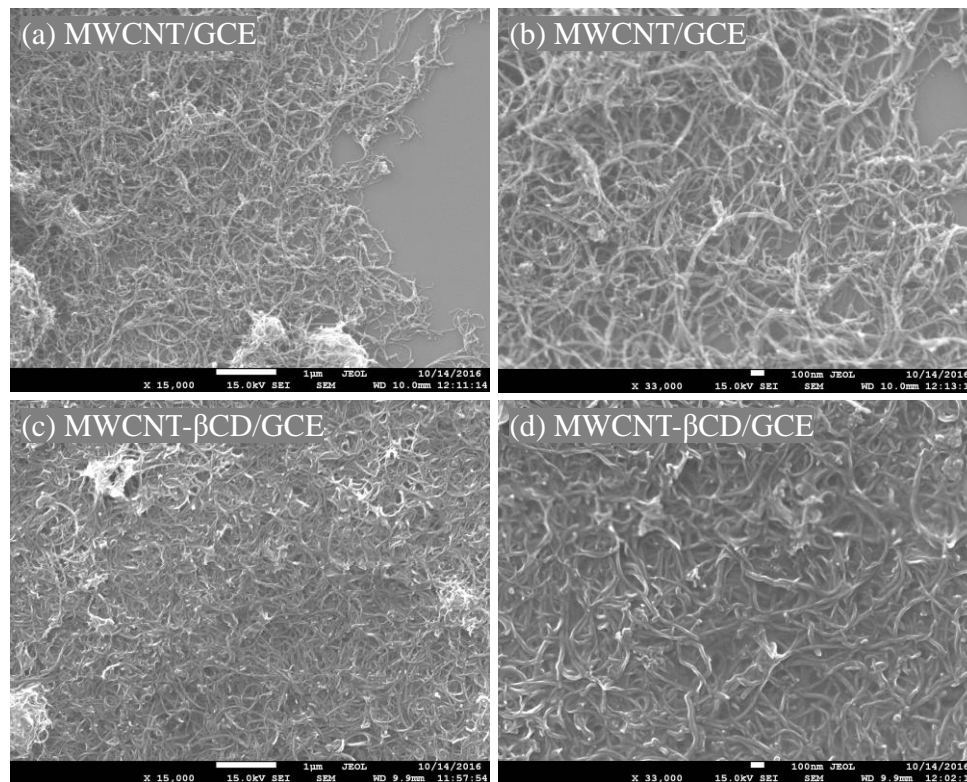
Figure 2-3. SEM images of MWCNT/GCE surfaces (a, b) and MWCNT-βCD/GCE surfaces (c, d). The images on the left and right hand sides are in low and high magnifications, respectively.
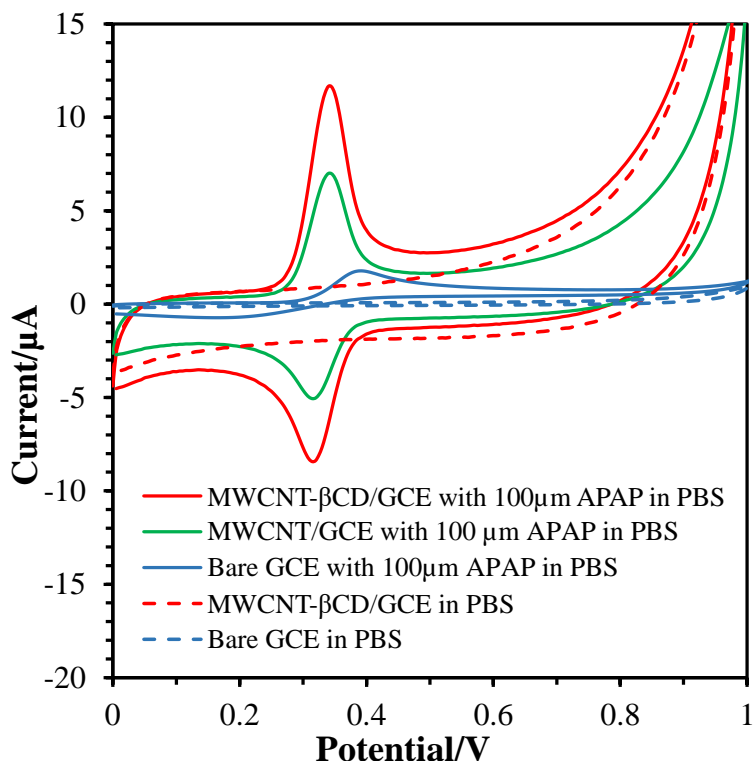
Figure 2-4. CVs of bare GCE (blue curves), MWCNT/GCE (green curves), and MWCNT-βCD/GCE (red curves) recorded in 0.01 M PBS (pH 7.4) in the absence (dashed lines) and in the presence of 100 μM APAP (solid lines) in 0.01 M PBS at a scan rate of 20 mV/s.

2.3.2. Performance optimization of the MWCNT-βCD/GCE electrode

Electrochemical performance of MWCNT-βCD/GCE

The role of MWCNT and β-cyclodextrin

The electrochemical sensing performance of a modified composite electrode depends on the redox activity of the sensing electrode with the target analyte (APAP). When high surface area of MWCNTs [202] is combined with the capturing ability of βCD [203] in the composite, the sensing performance using cyclic voltammetry (CV) method can be enhanced. Figure 2-4 shows the CV results of the MWCNT-βCD/GCE and bare GCE with and without APAP in PBS. A low scan rate of 10 mV/s was chosen to identify low-intensity redox peaks. No oxidation or reduction peaks were observed for both the bare GCE (blue-dashed curve) and the MWCNT-βCD/GCE (red-dashed curve) in the PBS at the applied potential range. However, the area of the CV curves of MWCNT-βCD/GCE was

significantly increased as compared to that of the GCE due to the increase in the double-layer capacitance. In the presence of APAP, a broad peak appeared in the bare GCE (blue-solid curve) at around +0.4 V, which may be attributed to the electrochemical oxidation of APAP. However, the reduction peak was not significant, indicating a slow rate of electron transfer occurring at the bare GCE due to an irreversible oxidation process.

In contrast, for the MWCNT-βCD/GCE (red-solid curve), a pair of strong and well-defined redox peaks were observed at anodic peak potential (E_{pa}) at 340 mV and cathodic peak potential (E_{pc}) at 320 mV. It was, therefore, observed that the APAP oxidation peak current of MWCNT/GCE was improved by 4 times compared to that of bare GCE, while for MWCNT-βCD/GCE, it was improved by approximately 7 times. Also, the APAP oxidation peak potential of MWCNT-βCD/GCE was shifted by -8 mV relative to that of the bare GCE. Hence, the modified MWCNT-βCD/GCE effectively boosted the oxidation of APAP. This improvement can be attributed to three major factors. First, carbon nanotubes themselves provide an enhanced electrocatalytic activity towards the oxidation of APAP due to their inherent materials properties such as, high conductivity and electron transfer capability [204]. Second, the high surface-to-volume ratio of the MWCNT provides a more favorable pathway towards oxidation of APAP [205]. Third, the presence of βCD with MWCNT facilitates a synergistic effect by introducing even higher surface area of the sensor as well as a closer contact of APAP molecule due to the porous structure of βCD, which will be discussed more in the subsequent paragraph [206]. The intensities and positions of these peaks signify that the fabricated MWCNT-βCD/GCE favors the reversible electrochemical reaction, as illustrated in the scheme below:
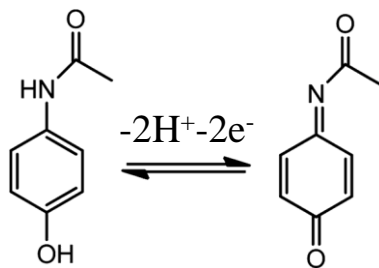
where the oxidation and reduction processes involve two electrons and two protons. The substantial increase in the peak currents and the presence of well-defined redox peaks

demonstrate that the MWCNT-βCD/GCE not only possesses a high electrochemically active surface area, but also has excellent redox activity, which are desirable attributes for the development of electrochemical sensors for pharmaceuticals.

The improved current response in the oxidation of APAP in the presence of βCD has two main aspects. Firstly, on pure MWCNT, APAP results in a single-layer adsorption. In the case of MWCNT-βCD, βCD provides a hydrophilic outer surface with its hydrophobic inner core covering the MWCNT. This multilayer surface structure adsorbed more APAP on the electrode surface compared to the single layer adsorption in MWCNT, resulting in higher detection sensitivity of APAP. Secondly, the introduction βCD onto the surface of MWCNT may enhance detection sensitivity of APAP through the formation of supramolecular host-guest complexes between βCD and APAP [207]. Therefore, the combined effect of βCD and MWCNT provided an increased sensing surface for enhanced detection of APAP.

The host-guest interaction of βCD and APAP can be experimentally investigated using X-ray Photoelectron Spectroscopy (XPS) of MWCNT/GCE and MWCNT-βCD/GCE surfaces before and after APAP detection, as shown in Figure 2-5. Acetaminophen (APAP) contains C-N, C-O and C=O bonds, βCD contains C-C and C-O bonds, and MWCNT contains C-C bond. The C-C and C-O bonds may be present in all these materials due to their chemical nature. Therefore, it is reasonable to focus on C=O and C-N peaks to quantify APAP on the sensor surfaces [208–210]. The comparative narrow scan spectra identify the elemental species and the influence of APAP adsorption (Figure 2-5(a-d)). It is shown in Figure 2-5(c) and Figure 2-5(d) that MWCNT-βCD has stronger C=O and C-N peaks than that of the MWCNT. The stronger C=O and C-N peaks indicate enhanced adsorption of APAP onto the surface of MWCNT-βCD/GCE than that of the MWCNT/GCE during the electrochemical sensing of APAP.
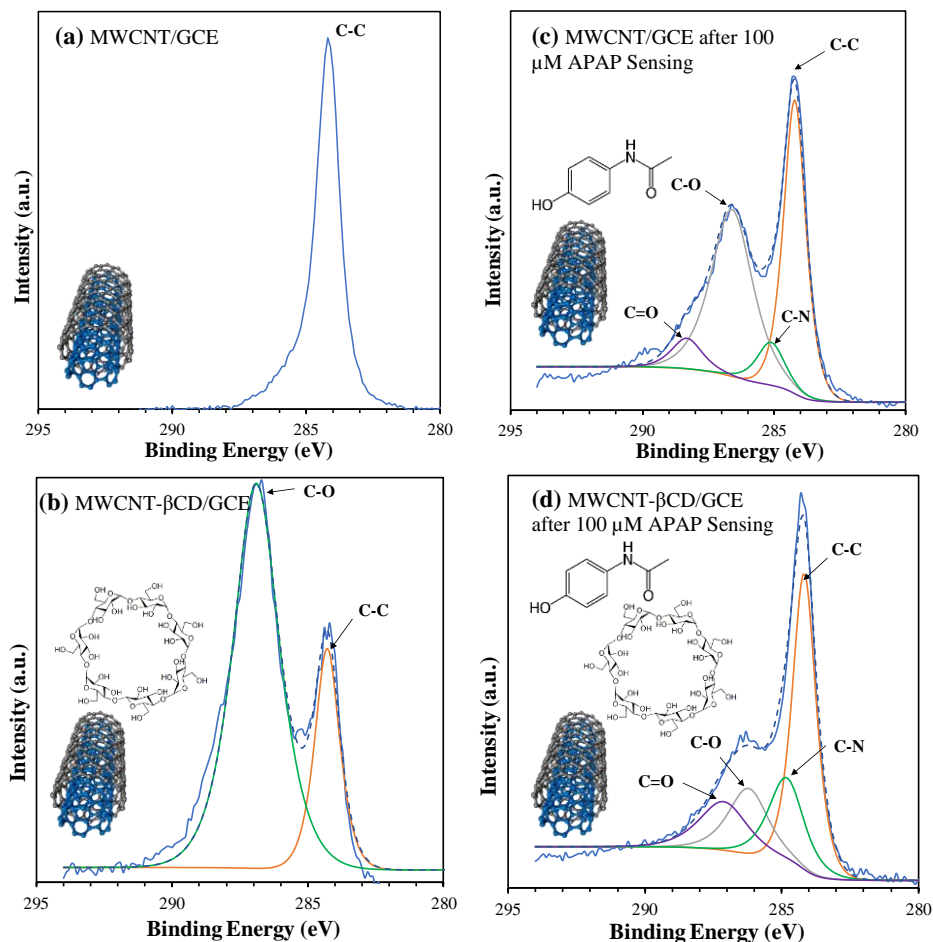
Figure 2-5. XPS narrow scan spectra of the surfaces of (a) MWCNT/GCE electrode, (b) MWCNT-βCD/GCE electrode, (c) MWCNT/GCE electrode after sensing of 100 µM APAP, and (d) MWCNT-βCD/GCE electrode after sensing of 100 µM APAP. Each figure shows the corresponding chemical structures.

The role of surface area

To understand the role of surface area on the electrochemical behaviors of the electrodes, we investigated its redox behavior in standard solution of $K_3[Fe(CN)_6]$, which is usually being used as a redox probe. Figure 2-6(a) shows the CVs of a bare GCE, MWCNT/GCE and MWCNT-βCD/GCE electrodes in an aqueous solution of 5.0 mM $K_3[Fe(CN_6)]$ containing 0.1 M KCl at a scan rate of 60 mV/s. The bare GCE electrode showed two well-defined redox peaks with peak-to-peak separation (ΔE_p) of 339 mV. An increase in peak current (I_p) and a decrease in ΔE_p were observed for the MWCNT/GCE and MWCNT-βCD/GCE, indicating relatively faster electron transfer at the modified electrodes compared to that of the bare GCE. This effect is attributed to the excellent electrical

conductivity and the large surface area of MWCNT and MWCNT-βCD on the electrode surface. The effective surface area of the modified electrode was calculated using the Randles–Sevcik equation, for a reversible process monitored by CV using $K_3[Fe(CN_6)]$, as shown in Figure 2-6(b) [211].

$$I_p = 2.69 \times 10^5 AD^{1/2}n^{3/2}v^{1/2}C \,, \qquad (2\text{-}1)$$

where A is the effective surface area, C is the bulk concentration of $K_3[Fe(CN_6)]$, n is the number of electrons transferred ($n = 2$), D is the diffusion coefficient of $K_3[Fe(CN_6)]$ (6.67×10^{-6} cm^2 s^{-1}), and v is the scan rate. The square root of scan-rate vs peak current relationship is shown in the inset of Figure 2-6(b). The slope of the I_p-$v^{1/2}$ curve was used in equation (2-1) to calculate the effective surface area. In this work, the effective surface area of MWCNT-βCD/GCE was calculated to be 0.189 cm^2. The area of the bare glassy carbon electrode and MWCNT/GCE were 0.070 cm^2, and 0.102 cm^2, which were largely amplified by the MWCNT-βCD modification. Although, the effective surface area of the electrode increases with the inclusion of βCD due to its porous structure, the conductivity of the electrode surface may be affected since βCD is an insulating polymer. Further research is needed to optimize βCD and its role to the sensing performance of the electrodes.
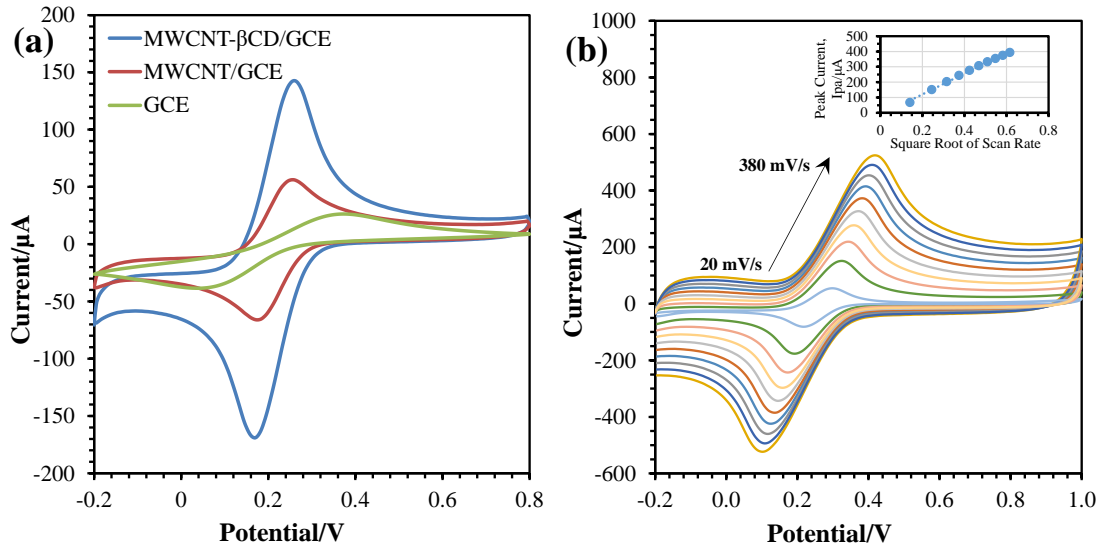
Figure 2-6. (a) CV curves of different electrodes: bare GCE, MWCNT/GCE, and MWCNT-βCD/GCE in an aqueous solution of 5.0 mM $K_3[Fe(CN_6)]$ containing 0.1 M KCl at a scan rate of 60 mV/s. (b) CV curves MWCNT-βCD/GCE at different scan rate (20, 60, 100, 140, 180, 220, 260, 300, 340, and 380 mV/s) with the same solution.
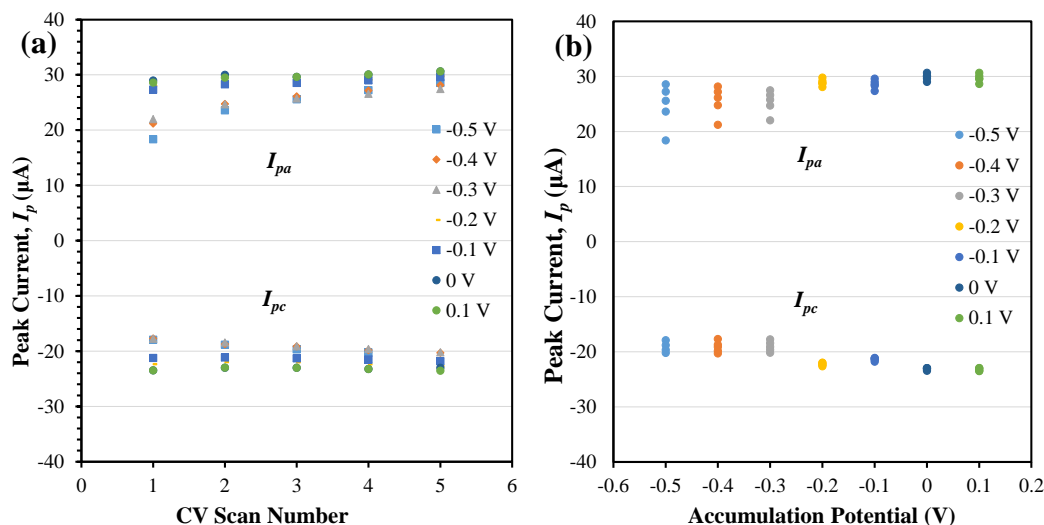
Figure 2-7. Peak current from the CV of MWCNT-βCD/GCE in 0.1 mM APAP (a) scatter plot at different accumulation time and CV scan cycle, and (b) scatter plot at different accumulation time. Scan Rate: 60 mV/s. Supporting electrolyte: 0.01 M PBS. Accumulation potential: 0 V.
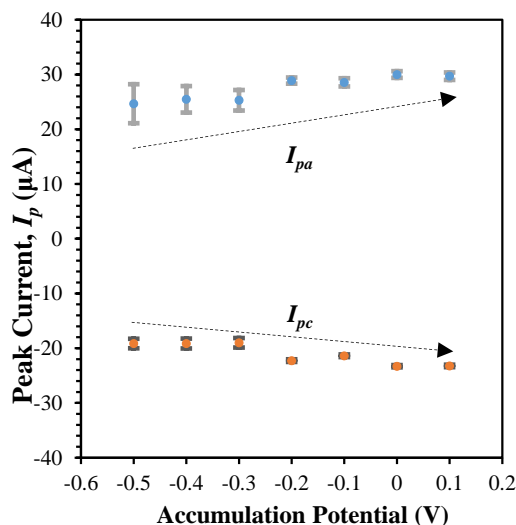
Figure 2-8. Peak current from the CV of MWCNT-βCD/GCE in 0.1 mM APAP with average/standard-deviation plot at different accumulation potential. Scan Rate: 60 mV/s. Supporting electrolyte: 0.01 M PBS. Accumulation time: 120 s.

Effect of accumulation potential and accumulation time

The optimization of accumulation potential and accumulation time is important to identify the best condition for the host-guest interaction to achieve better redox sensitivity [212]. Figure 2-7 and Figure 2-8 shows the effect of accumulation potential on oxidation peak current of APAP on the MWCNT-βCD/GCE electrode. There was no significant increase

in oxidation peak current due to increase of accumulation potential. However, when the accumulation potential was varied from −0.6 to 0.1 V, the oxidation peak current of APAP reached to a more stable maximum value at 0 V. After that, the oxidation peak current was saturated with the increase of the accumulation potential. Thus, 0 V was chosen as the optimal accumulation potential for all the electrochemical measurements. On the other hand, Figure 2-9 and Figure 2-10 shows the relationship between accumulation time and oxidation peak current of APAP. Similar to accumulation potential, the oxidation peak current reached to a more stable maximum value with the increase of the accumulation time up to 120 s, and then levels off for more than 120 s. It indicates that an accumulation time of 120 s was essential to achieve saturated adsorption of APAP on the MWCNT-βCD/GCE surface. Therefore, 120 s was chosen as the optimal accumulation time. Accumulation potential of 0 V was also reported in a previous study [213] of square wave anodic stripping voltammetry detection of APAP and ciprofloxacin using graphene oxide and nickel oxide nanoparticles modified electrodes. In our study, similar anodic peak currents were observed regardless of the accumulation potential. Since APAP is charge-neutral and it does not have any bias towards anodic/cathodic stripping at any positive/negative potential, the accumulation of APAP could be governed by physical adsorption at 0 V accumulation potential [214].
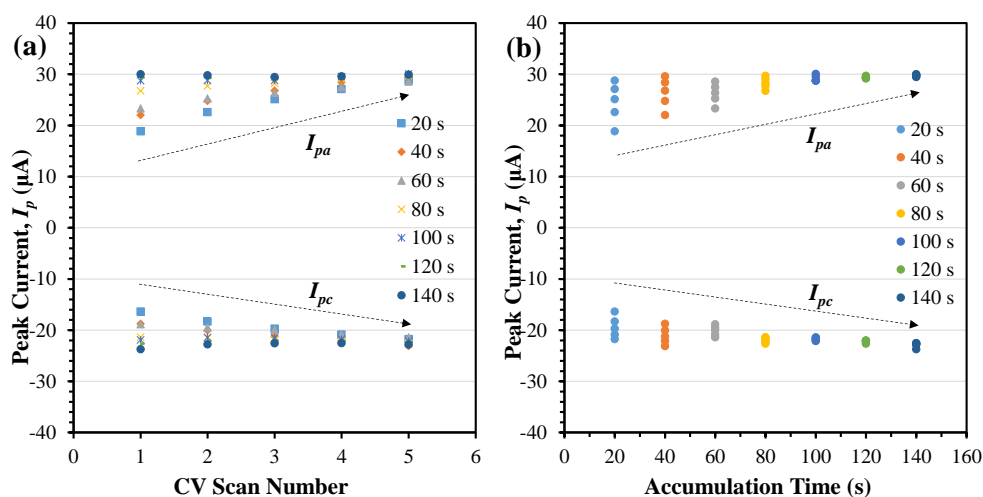
Figure 2-9. Peak current from the CV of MWCNT-βCD/GCE in 0.1 mM APAP (a) scatter plot at different accumulation potential and CV scan cycle, and (b) scatter plot at different accumulation potential. Scan Rate: 60 mV/s. Supporting electrolyte: 0.01 M PBS. Accumulation time: 120 s.
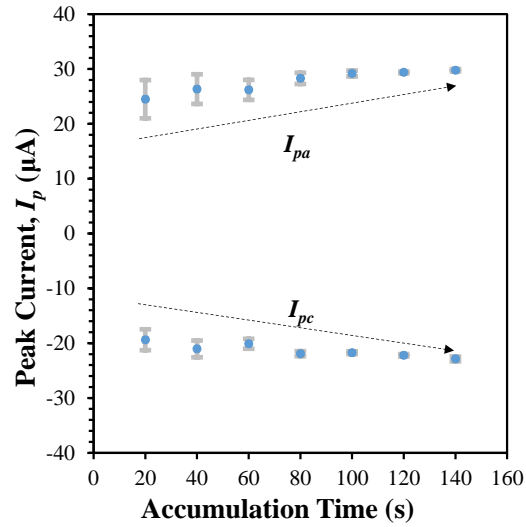
Figure 2-10. Peak current from the CV of MWCNT-βCD/GCE in 0.1 mM APAP with average/standard-deviation plot at different accumulation time. Scan Rate: 60 mV/s. Supporting electrolyte: 0.01 M PBS. Accumulation potential: 0 V.

Effect of scan rate

Another performance indicator of the sensing electrode is the charge transfer ability. This can be understood by analyzing scan rate (v) dependent redox peak currents and peak potentials. Figure 2-11(a) shows the CVs of the MWCNT-βCD/GCE in the presence of APAP for different scan rates from 20 to 400 mV/s. The increase of the scan rate increased the redox peak currents, as indicated by the Randles-Sevcik equation (equation 2-1). Figure 2-11(b) shows that both the oxidation and reduction peak currents were proportional to the scan rates. The fitted regression equations can be expressed as follows:

$$I_{pa} \ (\mu A) = -13.236 + 0.6171v \ (v: mV/s, R^2 = 0.9989), \tag{2-2}$$

$$I_{pc} \ (\mu A) = 11.994 - 0.4242v \ (v: mV/s, R^2 = 0.9976). \tag{2-3}$$

The linear relationship of the peak currents (I_{pa} and I_{pc}) with the scan rate (v) indicates that the electrochemical reaction of APAP at MWCNT-βCD/GCE is a surface-controlled process [35]. The effect of scan rate on the peak potential was also studied. Figure 2-11(c) shows the relationship between the peak potentials and the logarithmic values of the scan rates (log v). The oxidation peak potential shifted positively and the reduction peak potential shifted negatively with the increase of the scan rate. This behavior may be due to

the quasi-reversible nature of the redox of APAP where the rate of electron transfer becomes comparable to the mass transport rate [215]. At higher scan rates from 200 to 400 mV/s, the E_{pa} and E_{pc} were proportional with the log v with the linear regression equations as follows:

$$E_{pa} \text{ (V)} = 0.117 + 0.1252 \log v \text{ } (v: \text{mV/s}, R^2 = 0.9915), \tag{2-4}$$

$$E_{pc} \text{ (V)} = 0.4838 - 0.0715 \log v \text{ } (v: \text{mV/s}, R^2 = 0.9421). \tag{2-5}$$
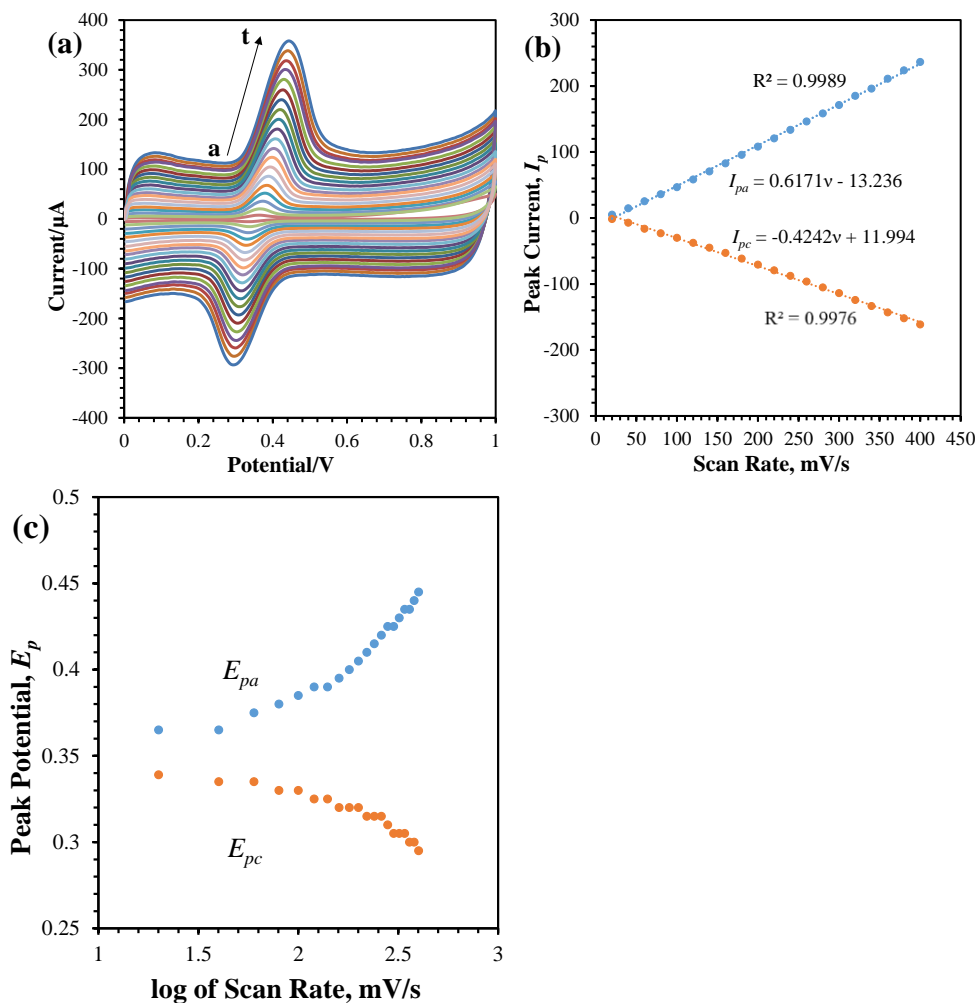
Figure 2-11. (a) CVs of MWCNT-βCD/GCE in 0.01 M PBS (pH 7.4) with 0.1 mM APAP at different scan rates (a–t: 20, 40, 60, 80, 100, 120, 140, 160, 180, 200, 220, 240, 260, 280, 300, 320, 340, 360, 380, 400 mV/s). (b) The relationship between the redox peak currents of APAP and the scan rates. (c) The dependence of the redox peak potentials of APAP on log v.

According to Laviron's theory [216], the slopes of the lines were equal to $2.3RT/(1-\alpha)n\text{F}$ and $-2.3R\text{T}/\alpha n\text{F}$ for the anodic and cathodic peaks, respectively. Here, R is the ideal gas constant (joules per kelvin per mole), T is the temperature in kelvins and F is the Faraday's constant. The charge transfer coefficient, α, was then calculated to be 0.36 based on the slopes of the two straight lines using the following equation:

$$\log \frac{k_a}{k_c} = \log \frac{\alpha}{1-\alpha} \quad \text{or} \quad \frac{k_a}{k_c} = \frac{\alpha}{1-\alpha} \, , \tag{2-6}$$

where k_a and k_c are the slopes of the straight lines for E_{pa} vs. log v and E_{pc} vs. log v, respectively. In addition, the apparent heterogeneous electron transfer rate constant, k_s, can be calculated based on the following equation [216]:

$$\log k_s = \alpha \log (1-\alpha) + (1-\alpha) \log \alpha - \log \frac{RT}{nFv} - \frac{\alpha(1-\alpha)nF\Delta E_p}{2.3RT} , \tag{2-7}$$

where n is the number of electrons involved in the reaction, ΔE_p is the peak-to-peak potential separation, α is the charge transfer coefficient, v is the scan rate, and other symbols have their usual meaning. The number of electrons involved in the reaction of APAP is 2, thus, the value of k_s was determined to be 1.659 s^{-1}. The high value of k_s indicates that the MWCNT-βCD/GCE composite film can effectively promote the electron transfer between the solution and the electrode [217].

Effect of pH of solution on the electrochemical behavior of APAP
The pH of a solution usually influences the electrochemical reaction by shifting the redox potential towards more positive or negative directions with varying redox peak currents, which could be due to the variation of acid dissociation of APAP [215]. Therefore, an optimum pH is required to maximize the intensity of the redox peak currents at low peak potentials. Figure 2-12(a) shows the effect of pH on the redox reaction of APAP with the MWCNT-βCD/GCE electrode in the pH range of 4.2–8.5. The CVs of the MWCNT-βCD/GCE showed a strong dependence on the pH values of solutions. The peak currents increased significantly when pH values increased from 4.2 to 7.4, and then decreased when the pH exceeded 7.4. These responses might be due to the structural changes in the –OH

and –NHCOCH$_3$ groups of APAP with respect to pH [218],[219]. At pH 7.4, charge neutrality of APAP may be responsible for the best response. Thus, the PBS of pH 7.4 was selected as the electrolyte pH in the following experiments. In addition, Figure 2-12(b) shows the relationship between the peak potentials and the pH of electrolytes. Figure 2-12(c) shows that both the oxidation (E_{pa}) and reduction (E_{pc}) peak potentials shifted negatively with the increase of pH, indicating that protons participate in the electrochemical redox process of APAP. Also, the E_{pa} and E_{pc} were proportional with the pH values in the pH range, and the linear regression equations were expressed as:

$$E_{pa} \text{ (V)} = -0.0598 \text{ pH} + 0.799 \text{ (}R^2 = 0.9972\text{)}, \tag{2-8}$$

$$E_{pc} \text{ (V)} = -0.0549 \text{ pH} + 0.7435 \text{ (}R^2 = 0.9955\text{)}, \tag{2-9}$$
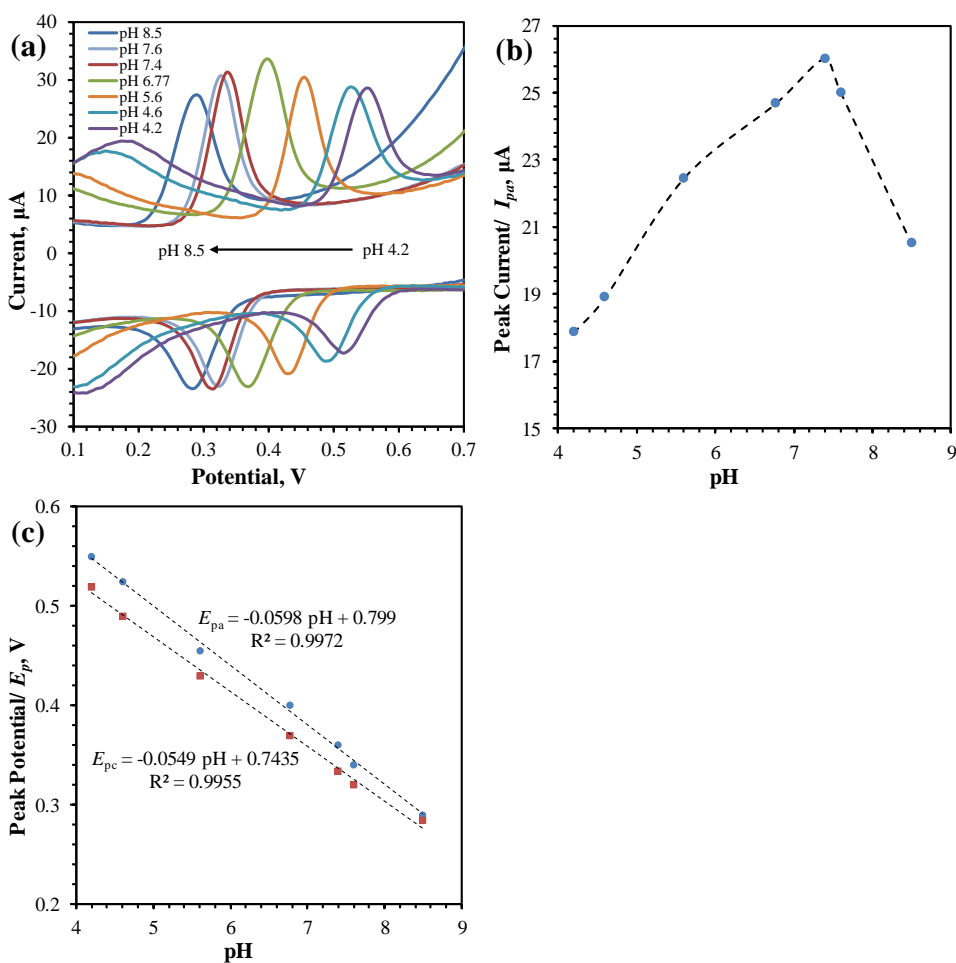
Figure 2-12. (a) CVs of MWCNT-βCD/GCE in 0.01 M PBS with different pH values (4.2, 4.6, 5.6, 6.77, 7.6, 8.5) in the presence of 0.1 mM APAP. Scan rate: 60 mV/s. (b) Plots of the anodic peak currents of APAP against the pH values. (c) Plots of the peak potentials of APAP against the pH values.

Now we can use the slope of the equations (2-8) and (2-9) to determine the ratio of proton and electron involved in the redox reactions according to the following equation [220]:

$$\frac{dE_P}{d\text{pH}} = 2.303 \frac{m\text{RT}}{n\text{F}} \, , \tag{2-10}$$

where m is the number of protons, and n is the number of electron. The m/n ratios were calculated to be 1.011 and 0.92 for the oxidation and the reduction process, respectively. It indicates that the numbers of protons and electrons involved in the redox processes of APAP were almost equal. Therefore, the redox reaction of APAP is likely to undergo a two-electron and a two-proton process [221],[222].
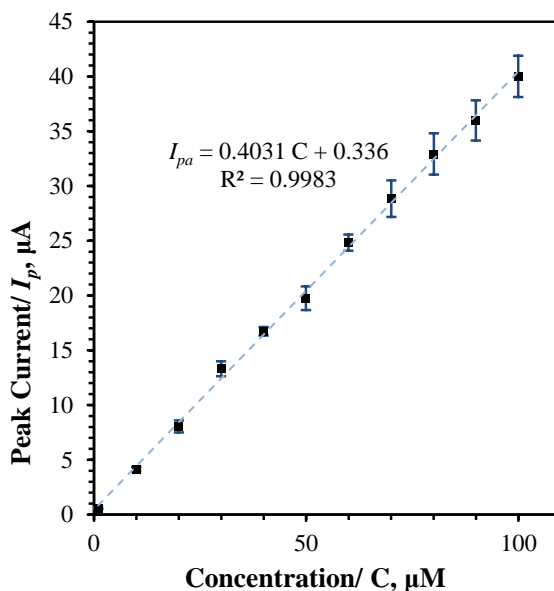
Figure 2-13. Determination of Acetaminophen (APA) from the peak currents of CV of MWCNT-βCD/GCE in 1-100 μM APAP. Scan Rate: 60mV/s. Supporting electrolyte: 0.01M PBS. Accumulation Potential: 0V. Accumulation time: 120s.

2.3.3. Voltammetric determination of APAP

It is worth noting that one of the main focuses in this study is the development of the sensing electrode to detect low concentration of APAP. However, the choice of sensing method itself often limits the outcome in the sensing performance. For the detection of low concentration of analytes, differential pulse voltammetry (DPV) method is preferable because of its higher sensitivity compared to that of CV. The better performance in DPV is

due to the reduced background currents, which are unrelated to the redox reactions [223]. For comparison, CV results for APAP detection is shown in Figure 2-13. In fact, the optimization parameters obtained by CV in the subsection 3.2 are applicable to DPV [224]. Figure 2-14(a) and Figure 2-14(c) depict the DPV curves for the concentration ranges of 0.05-1 μM and 1-300 μM, respectively. Similarly, Figure 2-14(b) and Figure 2-14(d) show the calibration curves for the concentration (C) ranges of 0.05-1 μM and 1-300 μM, respectively. The linear regression equations can be expressed as follows:

$$I_p \ (\mu A) = 2.6043C + 0.0236 \ (\mu M) \ (R^2 = 0.998), \ [0.05\text{-}1 \ \mu M, \ \text{Figure 2-14(b)}], \qquad (2\text{-}11)$$

$$I_p \ (\mu A) = 0.8646C + 3.7481 \ (\mu M) \ (R^2 = 0.9974), \ [1\text{-}300 \ \mu M, \ \text{Figure 2-14(d)}]. \qquad (2\text{-}12)$$
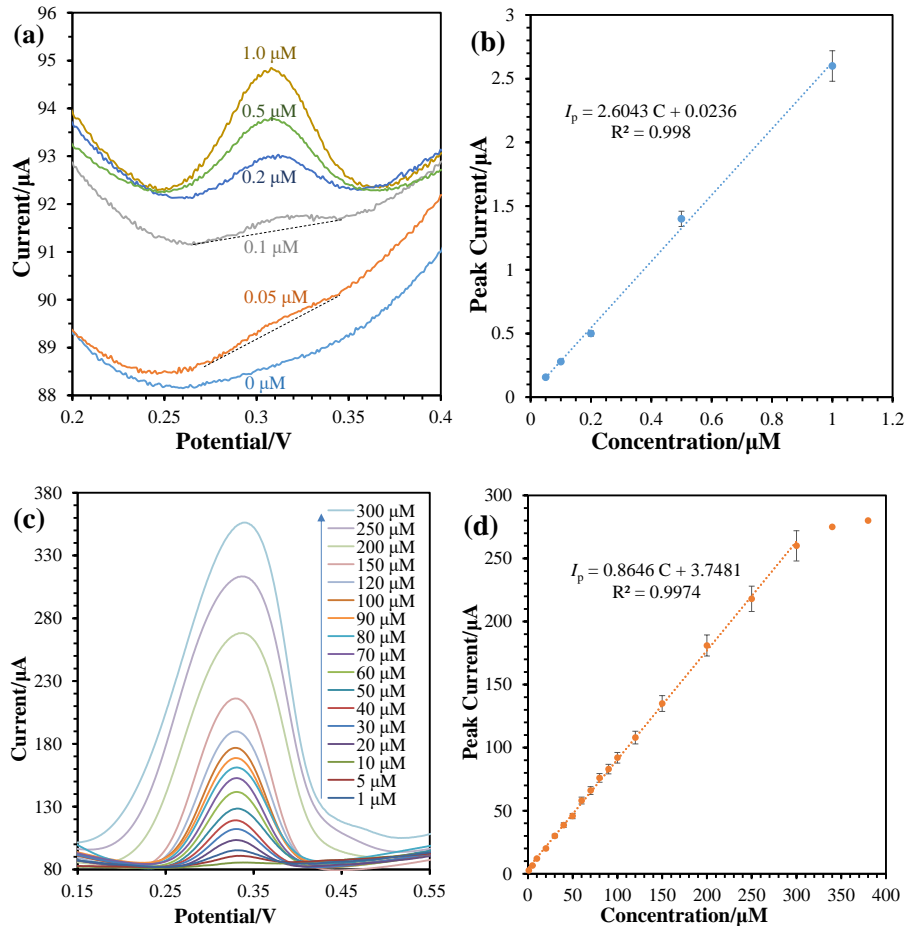
Figure 2-14. (a) DPVs of MWCNT-βCD/GCE in 0.01 M PBS (pH 7.4) in the presence of 0.05−1 μM APAP. (b) Calibration curve (i.e., peak current vs APAP concentration) from graph (a). (c) DPVs of MWCNT-βCD/GCE in 0.01 M PBS (pH 7.4) in the presence of 1−300 μM APAP. (b) Calibration curve (i.e., peak current vs APAP concentration) from graph (c).

Table 2-1: Comparison of the CNT-based electrochemical sensors for acetaminophen.

Type of Sensor Modification	Configuration	Detection method	Limit of detection, LoD (μM)	Linear Range (μM)	Reference
Unmodified CNT based sensors	SWCNT/CCE	DPV	0.05	0.08-200	[225]
	MWCNT-PDDA-PSS/GE	CA	0.5	25-400	[226]
	N-DHPB/MWCNT/CPE	DPV	10	15-270	[227]
	PtNP-MWCNT/CPE	DPV	0.17	0.4-60	[228]
	EF-NiO/MWCNT/CPE	SWV	0.5	0.8-600	[229]
	SWCNT-GNS/GCE	SWV	0.038	0.05-64.5	[205]
	MWCNTs-GNS/GCE	DPV	0.1	0.8-110	[230]
	MWCNT/BPPGE	AdsSV	0.01	0.01-2/2-20	[231]
Chemically modified CNT based sensors	fMWCNT/GCE	DPV	0.6	3-300	[183]
	ED-CMWCNT/GCE	DPV	0.092	1-200	[184]
	Chitosan/MWCNT/GCE	DPV	0.17	1-145/4-200	[232]
	fCNT-PMG-CE	CA	9.3	0-200	[233]
	AuNP-PGA-SWCNT/PET	DPV	1.18	8.3-145.6	[234]
	MWCNT-βCD/GCE	**DPV**	**0.0115**	**0.05-1/ 1-300**	**This Work**

Acronyms:
SWCNT/CCE = Single-wall carbon nanotubes modified carbon ceramic electrode.
MWCNT/GCE = multi-wall carbon nanotube modified GCE.
MWCNT-PDDA-PSS/GE = MWCNT on poly(diallyldimetheylammonium chloride)/poly styrene sulfonate modified graphite electrode.
N-DHPB/MWCNT/CPE = N-(3,4-dihydroxyphenethyl)-3,5-dinitrobenzamide-MWCNT modified carbon paste electrode.
PtNP-MWCNT/CPE = Pt nanoparticles - MWCNT modified CPE.
EF-NiO/MWCNT/CPE = ethynylferrocene and NiO - MWCNT modified CPE.
SWCNT-GNS/GCE = SWCNT graphene nanosheets modified GCE.
MWCNTs-GNS/GCE = MWCNT-graphene nanosheets nanocomposite modified GCE.
MWCNT/BPPGE = MWCNT/basal plane pyrolytic graphite electrode.
fMWCNT/GCE = functionalized MWCNT modified GCE.
ED-CMWCNT/GCE = ethylenediamine carboxylic acid functionalized MWCNT modified GCE.
Chitosan/MWCNT/GCE = Chitosan and MWCNT modified GCE.
fCNT-PMG-CE = functionalized CNT polymer poly(methylene green) composite electrode.
AuNP-PGA-SWCNT/PET = Au nanoparticles-polyglutamicacid-SWCNT-polyethyleneterephthalatesubstrate.
AdsSV = Adsorptive stripping voltammetry, DPV = differential pulse voltammetry.
SWV = square wave voltammetry; CA = chronoamperometry; LoD = limit of detection.

The decrease in sensitivity (slope) of the latter linear segment might be due to the saturation of the kinetic behavior of the electrode system [235],[236]. We observed that the I_P-C curve started to deviate from its linear behavior and became saturated after 300 μM concentration of APAP. The limit of detection (LoD), defined as LoD = $3s/m$ (where, s is the standard deviation of the blank solution (0.01 μA), and m is the slope of the calibration curve), was estimated to be 11 nM using the first linear segment [237]. These values are compared with the values reported by other research groups for the detection of APAP at the surfaces of physically and chemically modified electrodes based on CNT, as shown in Table 2-1. It is

observed that the MWCNT-βCD/GCE sensor has achieved wider linear range and lower limit of detection (LoD) for the detection of APAP. The better performance of the MWCNT-βCD/GCE sensor is attributed to the high effective surface area and enhanced host-guest interaction of the sensor, as discussed in the subsection 3.2.

2.3.4. Performance and stability of the MWCNT-βCD/GCE electrode

Selectivity and interference

The selectivity of the fabricated sensor for the detection of APAP was evaluated using interfering species under the optimized conditions. In biological samples, APAP usually coexists with ascorbic acid (AA) and dopamine (DA). Thus, DPV was performed to test the selectivity of this sensing platform with interferences from AA and DA. Figure 2-15 shows that APAP (0.1 mM) exhibited a well-defined anodic peak with good separations from AA (0.1 mM) and DA (0.1 mM). The peak potential of APAP shifted to a more positive value. This shift was because of the reduction of the pH value (from 7.4 to 6) due to the presence of ascorbic acid, which is shown in Figure 2-12(c). Therefore, it can be considered that this modified electrode showed satisfactory selectivity for the detection of APAP in the presence of AA and DA.

Reproducibility and stability

The reproducibility and stability of the MWCNT-βCD/GCE sensor were investigated utilizing the DPV technique. Five different MWCNT-βCD/GCE were prepared under the same conditions, and tested for the electrochemical detection of 0.1 mM APAP in 0.01 M PBS (pH 7.4). A relative standard deviation (RSD) of 4.6% was observed with the five different electrodes, confirming that the preparation of the MWCNT-βCD/GCE had considerable reproducibility. In addition, one of the five MWCNT-βCD/GCE was selected for the long-term stability tests over a 4-week period. The DPV was carried out once a week. The MWCNT-βCD/GCE was stored in a dry place at room temperature (25 °C). A relative standard deviation (RSD) of 5.5% was observed, showing the considerable stability of the MWCNT-βCD/GCE for the detection of APAP. Also, another electrode among the five MWCNT-βCD/GCE showed that the current response of the modified electrode lost

only 5% of the initial response after storage at room temperature for 4 weeks. These results indicate that the MWCNT-βCD/GCE has good reproducibility and stability for the APAP determination.
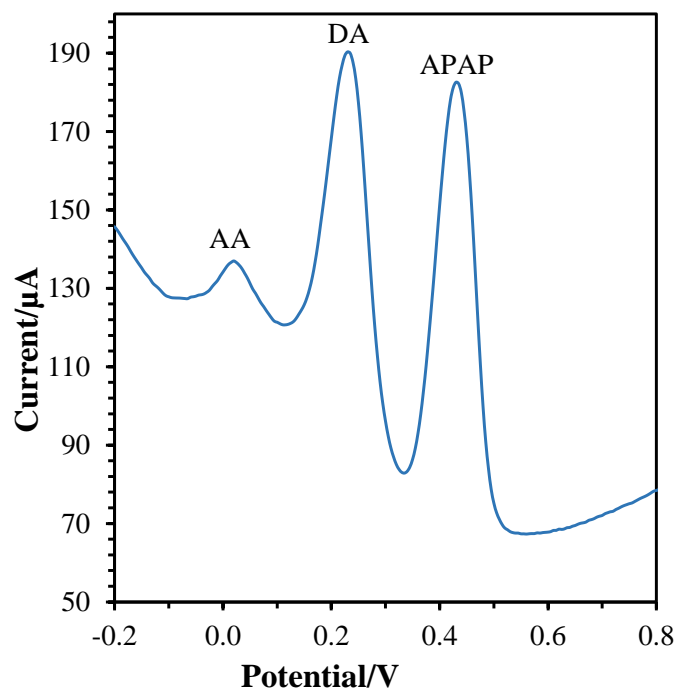
Figure 2-15. DPV on MWCNT-βCD/GCE with 0.1 mM acetaminophen (APAP), 0.1 mM dopamine (DA) and 0.1 mM ascorbic acid (AA) in 0.01 M PBS (pH = 7.4).

Table 2-2: Determination results of APAP in Tylenol® tablets by DPV.

Sample	Labeled Content	Prepared Concentration (μM)	Found (μM)[†]	Recovery
1[a]	325 mg	0.5	0.49	98%
		10	9.85	98.5%
		50	48.60	97.2%
		100	96.10	96.1%
2[b]	500 mg	0.5	0.48	96%
		10	9.81	98.1%
		50	51.70	103.4%
		100	102.60	102.6%

[a] Tylenol® Regular Strength tablets (Acetaminophen: 325 mg).
[b] Tylenol® Cold Extra Strength tablets (Acetaminophen: 500 mg, dextromethorphan hydrobromide: 10 mg, phenylephrine hydrochloride: 5 mg).
[†] Average values calculated from three determinations.

Table 2-3: Determination results of APAP in urine by DPV.

Sample	Added (μM)	Found (μM)[†]	Recovery
1	0.5	0.52	104%
	10	9.75	97.5%
	50	51.4	102.8%
	100	98.20	98.2%
2	0.5	0.50	100%
	10	9.82	98.2%
	50	49.21	98.4%
	100	103.60	103.6%

[†]Average values calculated from three determinations.

Determination of APAP in Water and Urine Samples

The practical application of the MWCNT-βCD/GCE sensor was validated by determining the concentration of APAP within a real sample such as APAP tablets and human urine. The recovery tests of APAP were carried out using DPV under optimized parameters through the standard addition method. In this method, the 0.1 mM stock solution made from the APAP tablets were added to 0.01 M PBS solution (pH 7.4) to make certain concentrations of APAP (e.g., 0.5 μM, 10 μM, 50 μM, and 100 μM). Table 2-2 shows that the sensor exhibited an excellent recovery from 96% to 103.4%. Similarly, standard addition method was also applied to the determination of APAP in urine samples. In this method, certain concentrations of APAP (e.g., 0.5 μM, 10 μM, 50 μM, and 100 μM) were added to the urine sample diluted by 0.01 M PBS solution. Table 2-3 shows that a recovery of the experimental results was obtained from 97.5% to 104%. These results clearly indicate that the developed sensor can detect APAP containing water and urine samples.

2.4. Conclusions

We fabricated a simple, rapid, and low-cost electrochemical sensor for precise sensing of acetaminophen based on MWCNT-βCD modification of glassy carbon electrode. The sensor demonstrated excellent redox activity towards acetaminophen sensing with limit of detection of 11 nM. Also, in contrast to most of the MWCNT based electrochemical

sensors, a wide two-step linear detection ranges from 0.05–1 μM and 1–300 μM was observed. The sensor exhibited high stability, good reproducibility and exclusive selectivity for the detection of acetaminophen in the presence of interfering species. We investigated the sensing performance of the sensor using commercially available acetaminophen tablets and human urine. A recovery of more than 95% was observed. Therefore, the developed sensor may find applications in the sensing of acetaminophen in water.

Chapter 3

Tailoring MWCNT and β-Cyclodextrin for Improved Detection of Acetaminophen and Estrogen[*]

Monitoring of trace amount of acetaminophen and estrogen in drinking water is of great importance because of their potential links to gastrointestinal diseases, and breast and prostate cancers. The sensitive and accurate detection of acetaminophen and estrogen requires the development of advanced sensing materials that possess appropriate number of analyte capturing sites and suitable signal conduction path. This can be achieved by implementing appropriate chemical attachment of multi-walled carbon nanotubes (MWCNTs) and β-cyclodextrin (βCD). Here, we report a systematic investigation of four types of modified MWCNT-βCD: (1) physical mixing, (2) "click reaction", (3) thionyl chloride esterification, and (4) Steglich esterification. The Steglich esterification is a one-step approach with shorter reaction-time, lower reaction-temperature, and eliminates handling of air/moisture-sensitive reagents. The MWCNT-βCD prepared by Steglich esterification possessed moderate βCD loading (5-10 wt%), large effective-surface-area, and fast electron transfer. The host-guest interaction of βCD and redox properties of MWCNT enabled sensitive detection of acetaminophen and 17β-estradiol (E2 is a primary female sex hormone) in the range of 0.005-20 µM and 0.01-15 µM, respectively, with low detection limits of 3.3 nM and 2.5 nM, respectively. We demonstrated accurate detection results of pharmaceutical compositions in water and urine samples. These results indicate

---

[*] Adapted with permission from A. U. Alam, Y. Qin, M. Catalano, L. Wang, M. J. Kim, M. M. R. Howlader, N.-X. Hu, and M. J. Deen, Tailoring MWCNTs and β-Cyclodextrin for Sensitive Detection of Acetaminophen and Estrogen, ACS Applied Materials & Interfaces, 10(25), 2018: 21411-21427. Copyright (2018) American Chemical Society (Appendix C).

that Steglich esterification method may be applied in fabricating pharmaceutical contaminants sensors for health and environmental applications.

3.1. Background

The increased presence of pharmaceutical contaminants in source and drinking water systems is due to the increased human excretion and improper disposal. These contaminants are threatening human health conditions due to their unknown toxicity, teratogenicity and carcinogenicity profiles, hence it is important to have monitoring so proper control measures can be implemented [154,155]. The lack of monitoring data also gives rise to ambiguous conclusions on their chronic effects on human physiology. The concentration of pharmaceutical contaminants such as acetaminophen (APAP, a painkiller) (N-acetyl-P-aminophenol or paracetamol) and estrogen (e.g., 17β-estradiol or E2, a primary female sex hormone) was reported to be up to several $\mu g \cdot L^{-1}$ [157]. Long-term exposure of individuals to APAP was associated with increased mortality [166]; heart, gastro-intestinal, and kidney diseases [166]; and hepato-nephro-toxicity [167]. Endogenous and exogenous estrogens of up to 17 $ng \cdot L^{-1}$ have also been detected in the source water of drinking water treatment plant [238].

Toxic levels of endogenous estrogens have been found to be linked with breast cancer in women and prostate cancer in men [239]. Exogenous estrogens have also perturbed fish physiology and affected the reproductive systems of both domestic and wild animals [239]. Although the available studies on exogenous estrogens reach dissimilar conclusions on potential effects on human health, there is no scientific agreement on the concentration limit which likely has no toxic effect, particularly for aquatic ecosystems [238]. Therefore, monitoring of APAP and estrogen in water cycles is important to estimate their adverse effects on human and environment. However, current technologies for monitoring of pharmaceutical contaminants are limited by the requirement of standard sampling procedure in conventional analytical techniques [170]; and the lack of simple, low-cost and easy-to-use sensors.

Conventional analytical techniques to determine pharmaceuticals in water and biological fluids include titrametry [168], spectrophotometry [169], and high-performance liquid chromatography (HPLC) [170]. These techniques provide high sensitivity, selectivity and precision. However, they are time-consuming, require several sample pre-treatment steps including derivatization, hydrolysis, and is carried out by specially trained personnel. To address these technical challenges, electrochemical sensing techniques were developed based on the electroactive nature of the pharmaceuticals in which the pharmaceutical contaminants provide electrical signal output through their oxidation- or reduction-conversion ability.

The advantages of electrochemical sensing techniques include low cost, high sensitivity, fast response, wide linear range, easy operation, simple fabrication, small foot print of the sensors, and ease-of-use [116]. Biosensors based on electrochemical detection mechanisms have achieved high selectivity and sensitivity by using antibody-antigen interaction [240], enzyme-substrate interaction [241], DNA aptamer hybridization [242], and molecularly imprinted polymer (MIP) [243]. Although these biosensing techniques have achieved very high sensitivity, they require biochemical reagents such as antibody, enzyme, DNA aptamer, and the target analyte itself to fabricate the imprint for MIP-based sensors. These reagents are expensive, unstable, temperature sensitive and unreliable in diverse sensing environment.

Carbon nanotubes (CNTs) and modified CNTs are excellent candidates to realize simple and easy-to-use electrochemical sensors because of their exceptional electrochemical properties, ease of chemical modification and low cost fabrication [244,245]. In particular, functionalized/modified CNT with β-cyclodextrin (βCD) showed enhanced sensitivity for the detection of pharmaceuticals and organic micro-pollutants such as rutin and bisphenol A [246,247]. CNTs with high aspect ratio (>3000) provide a large effective surface area and strong redox capability, whereas βCD facilitates enhanced host-guest interaction capabilities [116,189–191,248]. To prepare the CNT-βCD based sensing material in electrochemical sensors, two methods are generally used: physical/non-covalent and chemical/covalent methods.

The physical/non-covalent modification of CNT-βCD is a simple method, but the resulting material was unstable due to the solubility of βCD in water [249]. Also, the non-covalently modified CNT with βCD lacks direct electron transfer path, which limits its sensitivity in electrochemical sensing applications [250]. On the other hand, the chemical/covalent functionalized CNTs with βCD produces composites with enhanced host-guest interaction capabilities with pharmaceutical and/or organic molecules. These functionalized CNTs can then be used to realize sensors with high sensitivity [250].

Different routes for chemical functionalization of CNTs with βCD have been reported for applications such as electrochemical sensing [250], filtration of organic micro-pollutants [196], and waste-water treatment [251,252]. For example, "click chemistry" (CC) based modifications of CNT-βCD showed fully functionalized CNTs with βCD from the sidewalls for waste-water treatment and filtration of organic micro-pollutants [251]. However, the CC approach requires complex and multi-step chemical reaction processes. On the other hand, thionyl chloride mediated esterification (TE) of CNT-βCD has shown moderate amount of βCD attachment (~10 wt%) through the carboxylic acid groups located at the edges of the CNTs. Despite the limited βCD attachment, TE modified CNT-βCD showed ~30% enhancement in electrochemical sensing signal for the detection of 10 µM bisphenol A compared to that of physically modified CNT-βCD [250].

The TE approach requires handling of air and moisture-sensitive reagents. Also, it is still unknown how the amount and the molecular orientation of βCD attachment on the side-walls or the edges of the CNTs affects the electrochemical sensing performance. Thus, a chemical functionalization of CNT with βCD is necessary to achieve both simple sensor fabrication and enhanced sensing performance. Therefore, a systematic and comparative analysis of physical and chemical functionalization of CNT-βCD is a crucial step to realize simple and reliable synthesis of sensing materials for electrochemical sensing of APAP and E2.

In this research, a systematic study of the modifications of MWCNT-βCD through four physical and chemical approaches is accomplished: **(1)** physical mixing (Phys), **(2)** "click reaction" based four-step synthesis (CC), **(3)** thionyl chloride mediated two-step

esterification (TE), and **(4)** Steglich esterification (SE) based one-step synthesis. Among the four modification methods, SE is reported for the first time. The four MWCNT-βCD modification approaches were compared to gain insights into their effects on the electrochemical sensing of APAP and E2. In the developed SE synthesis approach, βCD is covalently attached onto MWCNT through direct esterification of the carboxyl groups. Physical and chemical characterizations of each reaction steps were done to confirm the successful functionalization of MWCNT with βCD. After that, we used these four types of MWCNT-βCD composites to fabricate sensing electrodes by drop-casting the water-dispersed MWCNT-βCD onto glassy carbon electrode (GCE). Finally, their electrochemical sensing performances of APAP and E2 were characterized.

The CC method showed the highest amount of βCD functionalization with MWCNT, resulting in lowest electrochemical sensitivity, probably due to excessive sidewall functionalization of MWCNT. The TE and SE based MWCNT-βCD/GCE electrodes showed high effective surface area, electron transfer rate and sensing peak currents compared to that of pure MWCNT/GCE and physically modified MWCNT-βCD/GCE. Also, the SE based MWCNT-βCD/GCE showed higher sensitivity, lower limit-of-detection, faster response, and better stability compared to that of pure MWCNT and physically modified MWCNT-βCD/GCE, in measuring real water samples containing APAP and E2. These simple and easy-to-fabricate MWCNT-βCD (SE)/GCE based sensors have the potential to be implemented in future portable electrochemical sensing systems for water quality monitoring.

3.2. Sample preparations and measurement system

3.2.1. Chemicals and reagents

MWCNT (>95%, OD: 5-15 nm, Length: ~50 µm, electrical conductivity: >100 S/cm) (Figure 3-1(A)) and COOH functionalized MWCNT (MWCNT-COOH, >95%, OD: 5-15 nm, Length: ~50 µm, electrical conductivity: >100 S/cm) were purchased from US Research Nanomaterials Inc. Sodium hydroxide (NaOH) pellets (>97%), hydrochloric acid

was purchased from Caledon Laboratories Ltd. β-cyclodextrin (βCD, ≥97%) (Figure 3-1 (B) and Figure 3-1(C)), toluenesulfonyl chloride (TsCl, ≥98%), sodium azide (NaN$_3$, ≥99.5%), 4-ethynylaniline (97%), isopentyl nitrite (96%), thonyl chloride (SOCl$_2$, 97%), N,N-Dimethylformamide (DMF) (>99.9%), N-Methylpyrrolidone (NMP) (≥99%), anhydrous N,N-Dimethylformamide (DMF) (99.8%), anhydrous N-Methylpyrrolidone (NMP) (99.5%), anhydrous pyridine (99.8%), methanol (≥99.9%), copper(I) iodide (CuI, 98%), 1,8-Diazabicyclo[5.4.0]undec-7-ene (DBU) (98%), potassium iodide (KI, >99.5%), dicyclohexylcarbodiimide (DCC) (60 wt% in xylenes), 4-(dimethylamino)pyridine (DMAP) (≥99%), phosphate buffer solution (PBS) tablets, potassium bromide (KI, ≥99%), acetaminophen (>99%), and 17β-estradiol   were purchased from Sigma-Aldrich. Celite Powder (Celite^{TM} 545 Filter Aid) was purchased from Fisher Chemical. Acetone (>99.5%) was purchased from EMD Millipore. All chemicals were of analytical grade and used without further purification. All the aqueous solutions were prepared with deionized (DI) water (resistivity ≥18 MΩ·cm). The 0.01 M phosphate buffer solutions (PBS) with pH 7.4 were prepared by dissolving one PBS tablet into 200 ml DI water. Tylenol® regular strength and Tylenol® Extra Strength tablets were purchased from a drugstore

3.2.2. Four modification techniques for MWCNT-βCD

Click chemistry (CC)

Preparation of 6^A-O-p-Toluenesulfonyl-β-Cyclodextrin (TsCl- βCD)): The preparation started with dissolving 12.5 g of NaOH in 750 ml of deionized water (DIW) with a big magnetic stirring bar. Next, we dissolved 25 g of βCD in the same solution. The reaction flask was then put into an ice-bath with continuous stirring for the solution temperature to be between 0 and 5 °C. After that, we added 10 g of *p*-toluenesulfonyl chloride (TsCl) and magnetically stirred vigorously for 2 hours followed by the addition of another 15 g of TsCl and stirring for 3 hours to get 6^A-O-*p*-toluenesulfonyl-β-cyclodextrin (TsCl-βCD), as shown in Figure 3-1(C). The TsCl-βCD solution was then filtered with Celite® powder on paper filter. We then added 175 ml of 10% HCl onto the filtrate and kept it in the refrigerator overnight to precipitate white aggregates of TsCl-βCD. The next day, we performed

vacuum filtration of the TsCl-βCD aggregates with a glass fiber filter paper to collect the white aggregates. We weighed the filter paper before and after filtration to measure the weight of the TsCl-βCD yield. After filtration, we took the TsCl-βCD aggregates in a glassware, grinded it to make it into more powder form, put aluminum foil cover with holes, and kept in a vacuum oven at 65 °C for two hours to remove the moisture. The TsCl-βCD dry powder was then kept in a refrigerator.
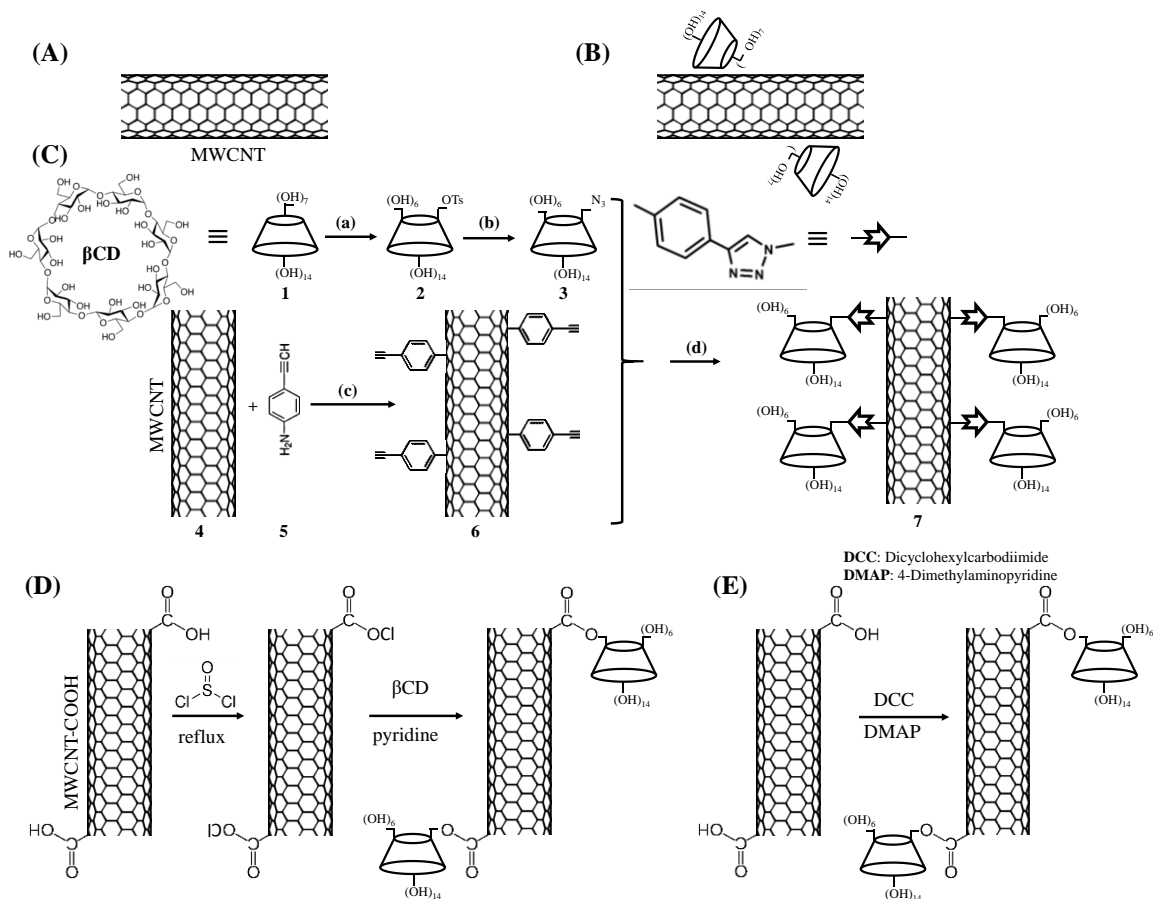
Figure 3-1. (A) Pure MWCNT, (B) Physically modified MWCNT with βCD, (C) Synthesis of βCD covalently modified MWNT through click chemistry. Reagents: (a) *p*-toluenesulfonyl chloride, NaOH, H_2O; (b) NaN_3, H_2O; (c) isopentyl nitrite, NMP, acetonitril, (d) CuI, DBU, DMF, (D) Synthesis of βCD covalently modified MWNT-COOH through thionyl chloride mediated esterification. (E) Synthesis of βCD covalently modified MWNT-COOH through Steglich esterification.

Preparation of Mono-2-azido-2deoxy-β-Cyclodextrin (Azido-βCD): A mixture of 5 g of TsCl-βCD and 3.9 g of sodium azide was dissolved in 25 ml of water and stirred at 80 °C for 1 day. After that, 25 ml of acetone was added to precipitate a white solid of azido-βCD and put into a refrigerator overnight (Figure 3-1(C)). In the next morning, the azido-βCD

precipitate was vacuum filtrated using a glass fiber filter paper, and then put into a vacuum oven at room temperature for 2 hours to remove the moisture, resulting in 3.25 g of azido-βCD with a product yield of 72% (mp: 220 °C).

Preparation of Alkyne Modified MWCNT (Alkyne-MWCNT): We weighed 100 mg of MWCNT, put it in a 100 ml flask and flowed Argon (Ar) with 99.99% purity for 5 min to remove any residual air. Then we added 25 ml of DMF followed by sonication for 15 to 30 minutes to get a uniform suspension. After that, we added 1.93 g of 4-Ethynylaniline to this suspension. We also added 1.93 g of isopentyl nitrite at room temperature, and the suspension was then stirred overnight at 60 °C under an Ar atmosphere. The resulting alkyne modified MWCNT (alkyne-MWCNT) suspension was diluted with 20 ml of DMF and filtered through a nylon membrane (Figure 3-1(C)). The collected solid was then washed thoroughly with DMF and methanol until the filtrate became colorless with a resulting yield of approximately 100 mg black powder.

Preparation of Click-Chemistry Mediated MWCNT-βCD (*MWCNT-βCD*(*CC*)): First, we dispersed 100 mg of alkyne-MWCNT in 25 ml of DMF by sonication for 15 min followed by bubbling with Ar for 10 minutes to remove any residual air and moisture. Then we added 1.93 g of azido-βCD, 316.67 mg of CuI and 2.5 g of DBU. The reaction mixture was then stirred under Ar bubbling flow at 70 °C for 48 hours to get MWCNT-βCD(CC) (Figure 3-1(C)). After that, the mixture was cooled to room temperature, and then diluted with additional 10 ml of DMF. The MWCNT-βCD(CC) suspension was then sonicated for 5 min, and filtered through a nylon membrane. The product was sonicated and re-dispersed in DMF and 1 mM aqueous KI solution, respectively. The product was again washed thoroughly with water and acetone, resulting in 13 mg βCD covalently modified MWCNT (i.e., pure MWCNT-βCD(CC)) obtained as a black powder after drying overnight in vacuum. A uniform, black suspension of MWCNT-βCD(CC) was prepared by dispersing 40 mg of the black powder into 20 ml of DIW using an ultrasonic preprocessor.

Thionyl chloride mediated esterification (TE)

We weighed 300 mg of MWCNT-COOH and put it into a reactor with continuous Ar flow so that no air and moisture can be trapped inside the reactor sidewall. Then, the reactor was pumped down with a vacuum pump to $<10^{-2}$ Pa. Also, hot air was blown around the reactor using a heat gun so that moisture from the inner wall and MWCNT-COOH are removed. After that, 5 ml of $SOCl_2$ was added into the MWCNT-COOH containing reactor, as shown in Figure 3-1(D). The MWCNT-COOH/$SOCl_2$ suspension was stirred at 65 °C for 24 hours. In a separate reactor, 450 mg of βCD was taken and dried up using a vacuum pump similar to the previous step, but with no heat gun blowing. The βCD reactor with vacuum pump was left running overnight. We then connected water cooling lines in the MWCNT-COOH reactor for condensation. The hot plate temperature under MWCNT-COOH reactor was raised to 110 °C to start boiling the $SOCl_2$ and to keep the MWCNT-COCl product in the reactor.

We removed the excess $SOCl_2$ under a reduced pressure of ~2×10^{-2} Pa using a small vacuum pump and collected the distilled $SOCl_2$ into the condenser collector. 10 ml of toluene was then added into the MWCNT-COCl product reactor and heated at 110 °C to perform azeotropic distillation, so that excess $SOCl_2$ was driven out by toluene. The MWCNT-COCl reactor was then cooled in a cold-water bath. 10 ml of anhydrous NMP was also transferred into the MWCNT-COCl. In parallel, we added 5 ml of anhydrous NMP into the βCD reactor. Also, a few drops of anhydrous pyridine were added into βCD-NMP solution. Finally, the βCD-NMP solution was inserted into the MWCNT-COCl reactor mixture. After 15 minutes of stirring at the cold-water bath, the stirring continued at 65 °C for 5 hours at 200 rpm of magnetic stirring. After the heating was turned off, stirring continued over 2 days with all the reactor inlet sealed to get chemically functionalized MWCNT-βCD(TE). A uniform, black suspension of MWCNT-βCD(TE) was made by dispersing 40 mg of the black powder into 20 ml of DIW using an ultrasonic preprocessor.

Steglich esterification (SE)

We weighed 300 mg of MWCNT-COOH and put it into a reactor with continuous Ar flow. We then added 25 ml of anhydrous DMF into the reactor and sonicated for 15 minutes to get a uniform suspension. We then added 100 mg of DMAP and 4 g of βCD. After that, we added 200 mg of DCC into the reaction mixture at 0° C and stirred it for 5 minutes at 0 °C and 5 hours at 20 °C. The precipitated MWCNT-βCD(SE) is then filtered through a nylon membrane and washed thoroughly with DMF and acetone to remove the DCC, DMAP and unreacted βCD, as shown in Figure 3-1(E). A uniform, black suspension of MWCNT-βCD(SE) was prepared by dispersing 40 mg of the black powder into 20 ml of DIW using an ultrasonic preprocessor.

Physical modification (Phys)

The weight percent of the carboxylic acid group in MWCNT-COOH is ~2.58 wt%, according to the manufacturer data sheet. If all the carboxylic groups are converted into ester groups through βCD modification in TE and SE modifications, then the approximate weight percent of βCD in MWCNT-βCD will be 36.5 wt%. Therefore, to study and compare the effect of βCD modification in electrochemical sensing, the physically modified MWCNT-βCD solution was prepared by dissolving 14.6 mg of βCD in 20 ml DI water followed by dispersion of 40 mg of MWCNTs using a probe ultrasonic preprocessor (Fisher Scientific™ Model 505 Sonic Dismembrator) for 10 minutes to give a MWCNT concentration of 2 mg·ml^{-1} (Figure 3-1(B)).

3.2.3. Characterization of the modified MWCNT-βCD

A field-emission scanning electron microscope (SEM, JSM-7001F, JEOL) was used to observe the surface morphologies of the drop-casted MWCNT-βCD on GCE. The SEM was operated at an acceleration voltage of 10 kV and emission current of ~80 μA. The βCD content in the modified/functionalized MWCNT-βCD were measured using a Q5000 IR (TA Instruments) thermogravimetric analyzer (TGA). About 15-20 mg black powder was obtained by evaporating water from 40 ml of each of the physically/chemically modified

MWCNT-βCD suspensions on a hotplate. The thermogravimetric (TG) analysis was carried out with a nitrogen gas (N$_2$, 99.99%) purge (20 mL·min^{-1}) and at a temperature ramp rate of 20 °C·min^{-1}. Fourier transform infrared (FTIR) spectra of the pure and modified βCD and MWCNT were recorded using a spectrometer (Vertex 70, Bruker) by making KBr-IR pellets. The chemical composition MWCNT-COOH, MWCNT-βCD(TE/SE/CC) were characterized by using X-ray Photoelectron Spectroscopy (XPS) (XPS, JPS-9200, JEOL, Mg-α source, 10 keV, 15 mA).
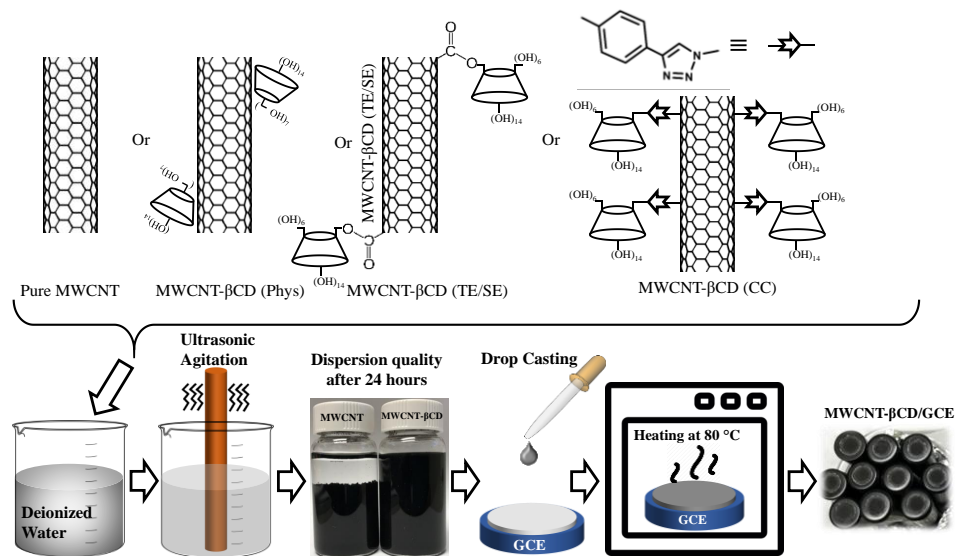
Figure 3-2. Fabrication process flow for the modification of glassy carbon electrode (GCE) with Pure MWCNT/ MWCNT-βCD(Phys/TE/SE/CC).

3.2.4. Fabrication of the MWCNT-βCD-modified electrodes

For a comparative analysis of the electrochemical sensing performance for the detection of acetaminophen (APAP) and 17β-estradiol (E2), five types of modified glassy carbon electrodes (GCE) were fabricated, as listed in the Table 3-1. A schematic overview of the electrode modification steps is shown in Figure 3-2. It was found that the dispersion quality of pristine MWCNT was not maintained beyond 24 hours after sonication. In fact, MWCNT cannot be highly dispersed in an aqueous solution without using a surfactant. However, the βCD functionalized MWCNT (i.e., MWCNT-βCD) were highly dispersed even after several weeks of storage, which was important to achieve reproducible drop-casted layers of the sensing materials. The amount of drop-casting volume of each

MWCNT/MWCNT-βCD was optimized based on their respective electrochemical sensing performance of 5 µM APAP to ensure a uniform basis of the comparison of MWCNT/MWCNT-βCD modified GCEs. The drop-cast volume of each sensing material was varied between 4 and 14 µl to find the optimum volumes that resulted in a maximum APAP oxidation peak current, as shown in Figure A- 1. The optimized drop-cast volumes for all electrodes are also listed in Table 3-1, which were then used throughout the rest of the experiments.

Table 3-1: List of MWCNT-βCD modification approaches and their corresponding acronyms, corresponding materials loading for the materials and the modified sensing electrodes.

Modification Approaches	Acronyms of the Modified MWCNT based GCE	Description of the Modification Approaches	Reagents Used	Number of Chemical Reaction Steps	Maximum Temperature Used	MWCNT/MWCNT-βCD Loading on Suspension	Volume drop-casted on GCE for Optimum Electrochemical Performance	Effective Surface Area (cm^2)	Charge Transfer Coefficient (α)	Heterogeneous Electron Transfer Rate Constant (k_s, s^{-1})
Unmodified	MWCNT/GCE	Pure MWCNT	N/A	N/A	RT	2 mg·ml^{-1} of MWCNT in DIW	6 µl	0.117±0.0040		
Physical Modification	MWCNT-βCD (Phys)/GCE	βCD modified MWCNT through **Phys**ical Mixing in water	N/A	N/A	RT	2 mg·ml^{-1} of MWCNT and 0.73 wt% of βCD in DIW	6 µl	0.122±0.0035	0.36	1.659
Chemical Modifications	MWCNT-βCD (CC)/GCE	βCD modified MWCNT through **C**lick **C**hemistry	*p*-toluene sulfonyl chloride, sodium azide, 4-ethynylaniline, isopentyl nitrite, DMF	4	80 °C	2 mg·ml^{-1} of MWCNT-βCD (CC) in DIW	12 µl	0.039±0.0012		
	MWCNT-βCD (TE)/GCE	βCD modified MWCNT through **T**hionyl **C**hloride based **E**sterification	Thionyl chloride, pyridine, DMF	2	110 °C	2 mg·ml^{-1} of MWCNT-βCD (TE) in DIW	10 µl	0.142±0.0028		
	MWCNT-βCD (SE)/GCE	βCD modified MWCNT through **S**teglich **E**sterification	dicyclohexylcarbodiimide, 4-(dimethylamino)pyridine, DMF	1	20 °C	2 mg·ml^{-1} of MWCNT-βCD (SE) in DIW	10 µl	0.149±0.0030	0.50	2.9

Acronyms:
RT: Room Temperature
DMF: Dimethylformamide

The fabrication of the MWCNT-βCD Modified Electrodes started with polishing the surface of each GCE electrode on fine emery paper and chamois leather containing alumina powder (Al_2O_3) with particle sizes of 1.0, 0.3, and 0.05 μm purchased from CHI Instruments. The polishing was done first using the large-particle-size alumina powder followed by the smaller ones. The GCE electrode surfaces were rinsed thoroughly with DI water between each polishing step, and then sonicated in DI water and dried with compressed air. An aliquot of 6 to 14 μl of physically/chemically modified MWCNT-βCD solution was drop-casted on the GCE electrodes. The electrodes were then dried in air for 20 min at 80 °C in an oven. The electrodes were cooled to room temperature before measurements. The electrodes were stored in a dry, well-ventilated are in the laboratory.

3.2.5. Measurement system

All electrochemical measurements were performed with a three-electrode conventional electrochemical workstation at room temperature. A PalmSens EmStat 3 potentiostat (PalmSens BV, Netherlands) was connected to a three-electrode cell. The potentiostat was operated by PSTrace 5.2 software. The three-electrode cell assembly consisted of a platinum wire as an auxiliary electrode and an Ag/AgCl electrode as the reference electrode. Unmodified/modified GCEs with pure/modified MWCNT-βCD were used as the working electrode with an exposed circular area of 3 mm diameter. All the electrodes were purchased from CHI instruments. Additionally, all the GCEs modified with pure MWCNT and modified MWCNT-βCD was measured in 10 mM $K_3[Fe(CN)_6]$ with 0.1 M KCl solution to obtain the cyclic voltammetry (CV) curves and analyze their electrochemically active surface areas. All measurements were performed at 23±2 °C.

3.2.6. Preparation of drinking water and urine samples

The APAP tablet solutions were prepared by grinding and dissolving one tablet of Tylenol® Regular Strength or Tylenol® Extra Strength, labeled 325 mg and 500 mg per tablet, respectively, into DIW water by magnetic stirring for 1 hour. The APAP tablet solution was then filtered by a 0.45 μm pore-diameter syringe filter membrane. The filtrate was

diluted with a pH 7.4 PBS solution to make 1 mM stock solution of APAP from the tablet. The E2 solution was made from the E2 purchased from Sigma-Aldrich. Urine samples were diluted four times with PBS (pH 7.4) without any further treatment. The diluted urine sample was spiked with different amounts of APAP and E2. The recovery tests were carried out using linear sweep voltammetry (LSV) for the determination of APAP and E2 in APAP tablet and E2 containing water and human urine.

3.3. Results and discussions

3.3.1. Electrochemical and surface properties of MWCNT with βCD

Physical and Chemical Modifications of MWCNT with βCD: The MWCNT was modified with βCD through physical mixing as well as chemical functionalization to compare their sensing performances for acetaminophen and 17β-estradiol (E2). The physical modification of MWCNT with βCD was done by mixing MWCNT and βCD directly in deionized water and then dispersing them using an ultrasonic preprocessor. The chemical functionalization of MWCNT with βCD was done with three different approaches: CC, TE and SE. The TE and SE approaches required the use of carboxylic acid functionalized MWCNT (MWCNT-COOH), where the carboxylic acid mediates the incorporation of βCD onto the MWCNT through ester bonds. In Figure 3-1(A) and (B), schematic representations of pure and physically modified MWCNT-βCD (i.e. MWCNT-βCD(Phys) are shown, respectively. In Figure 3-1(C), (D) and (E), schematics of the synthetic steps for the CC, TE and SE are shown, respectively. A summary of the MWCNT modification approaches and their corresponding acronyms that will be used throughout the paper is given in Table 3-1.

The CC modification has the ability to functionalize MWCNT from the side-walls through alkyne-mediated azide bonds. On the other hand, the TE and SE modifications can functionalize MWCNT mostly at the end of the one nanotube through the carboxyl group (–COOH) mediated esterification. Therefore, from the nature of the chemical modifications, it can be inferred the degree of βCD functionalization on to MWCNT is higher in CC modification than that of TE and SE, since the amount of the –COOH groups are limited in

the MWCNT-COOH (max. 2.58 wt%). Compared to CC [251] and TE [252], SE offers the advantage of accomplishing an one-step synthesis of βCD functionalized MWCNT with shorter reaction time and no requirement of air- and moisture-sensitive reagents. Therefore, DCC-DMAP mediated SE can be a promising approach for the development of functionalized CNTs.
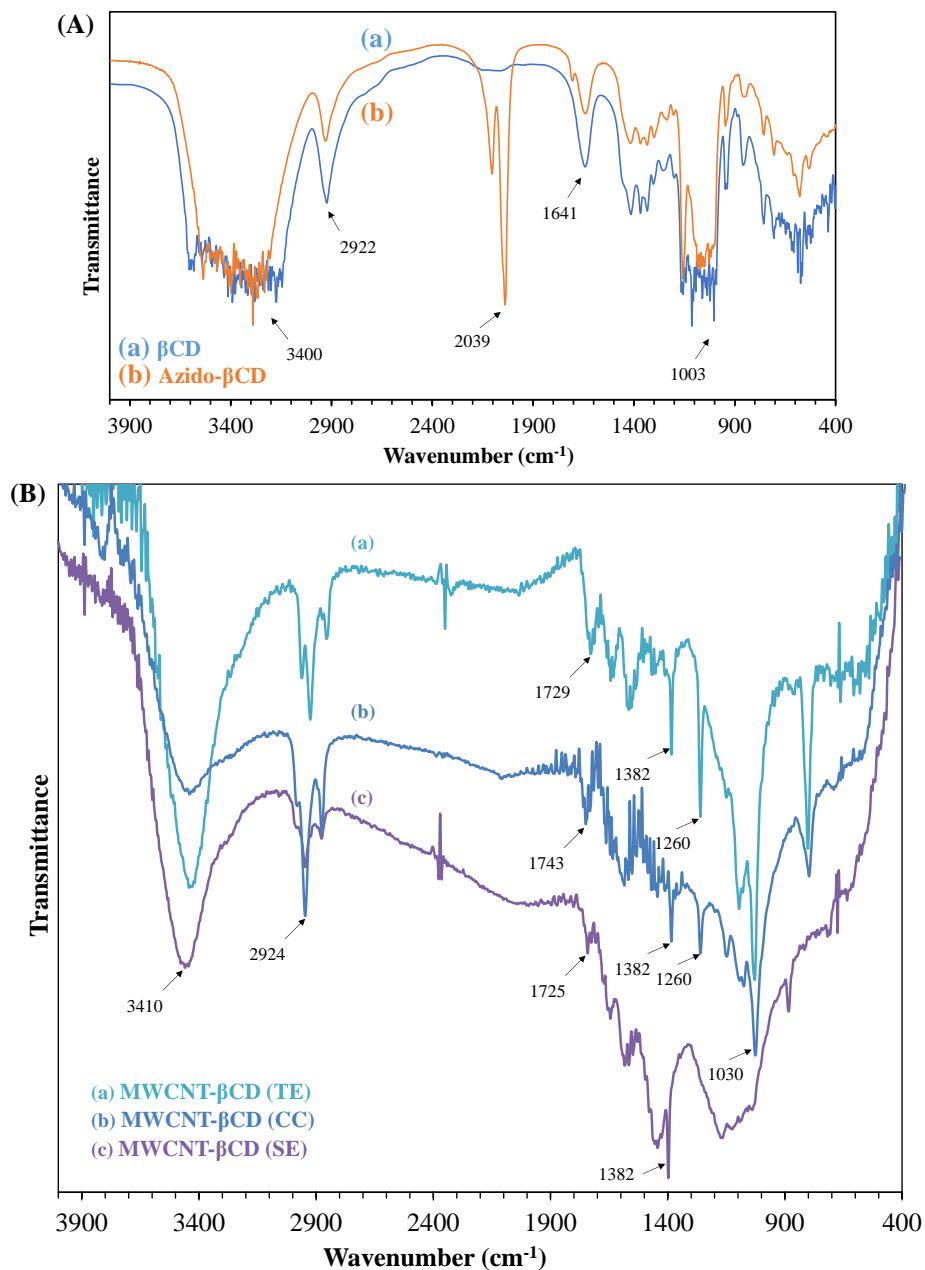
Figure 3-3. FTIR spectra of (A) βCD and Azido-βCD; and (B) MWCNT-βCD(TE/CC/SE) using KBr pellet.

The Attachment of βCD on MWCNT: The chemical attachments of βCD on MWCNT was confirmed from Fourier Transform Infrared (FTIR) spectroscopy, as shown in Figure 3-3. The characteristic infrared (IR) absorption peaks of βCD and azido-βCD are shown in Figure 3-3(A). In curve (a) of Figure 3-3(A), the broad peak near 3400 cm^{-1} was due to the –OH stretching vibration, the peak at 2922 cm^{-1} was due to the C-H stretching vibration, the fingerprint peaks located between 500 and 700 cm^{-1} could be due to –C-H bending vibrations, the peak at 1641 cm^{-1} was due to the C–C stretching of polysaccharides, and the fingerprint peaks near 1003 cm^{-1} were due to the C–O bonds in the ether and hydroxyl groups of β-CD, which are the characteristic absorption peaks of βCD [253,254], These characteristic peaks all appeared in curve (b) of Figure 3-3(A), and one additional peak at 2039 cm^{-1} due to the N=N=N symmetric stretching vibration [255]. The lower intensity peak at 2104 cm^{-1} was due asymmetric azide vibrations. The peaks at 2039 and 2104 cm^{-1} confirm the successful conversion of βCD into azido-βCD which is used for the subsequent click reactions of MWCNT-βCD (CC), as shown Figure 3-1(C).

The characteristic IR absorption peaks of MWCNT-βCD(TE/CC/SE) are shown in Figure 3(B). In curves (a) and (c) of Figure 3-3(B), the broad peak near 3410 cm^{-1} was due to the –OH stretching vibration, the peak at 2924 cm^{-1} was due to the C-H stretching vibration, the peak at 1729 and 1725 cm^{-1} were due to the C=O stretching vibration, and peak at 1382 cm^{-1} was due to the –COO$^-$ symmetric vibration [253,254]. The comparison of FTIR spectra of βCD (in Figure 3-3(A)) and MWCNT-βCD(TE/SE) (in Figure 3-3(B) curves (a) and (c)) shows that additional peaks appear at 1729, 1725 and 1382 cm^{-1}. The stretching vibration peak of C=O (at 1729 and 1725 cm^{-1}) and the symmetric vibration peak of –COO$^-$ (at 1382 cm^{-1}) are the characteristic peaks of ester groups present in the MWCNT-βCD(TE/SE). The curve (b) of Figure 3-3(B) shows that most of the characteristic peaks of MWCNT-βCD(TE/SE) are also present in the MWCNT-βCD(CC). Since phenyl-based ethynylaniline was introduced as a linker in the click reaction, the absorptions of phenyl framework vibration are observed at 1700–1382 cm^{-1}. Besides, the absorption at 2039 cm^{-1} of Figure 3-3(A) curve (b) disappeared, indicating successful reaction of alkyne-MWCNT with azido-βCD through 'click' coupling. Moreover, in Figure 3-3(B), the characteristic

absorption of C–O stretching vibration of βCD between 1260 and 1030 cm^{-1} can be seen. These results confirm the existence of βCD and validate the covalent modification of MWCNT through CC, TE and SE chemistries.
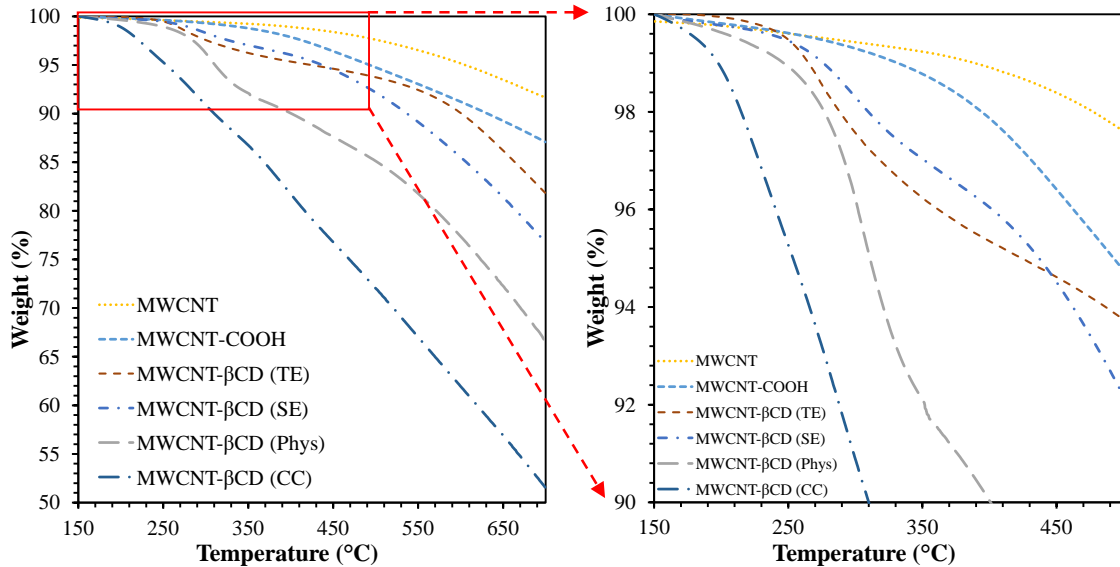
Figure 3-4. TGA test results of MWCNT, MWCNT-COOH and MWCNT-βCD (TE/SE/Phys/CC) acquired under nitrogen. The temperature profile involved a ramp of 20 °C·min^{-1} from room temperature to 500 °C.

In order to evaluate the amount of βCD attached on MWCNT, thermogravimetric analysis (TGA) measurements for as-received MWCNTs and modified MWCNTs were performed under nitrogen gas flow. Figure 3-4 shows the TGA weight loss profile from 150 to 700 °C for pure MWCNT and MWCNT-COOH, as well as physically and chemically modified MWCNT-βCD. As shown in the Figure 3-4, MWCNT has the smallest weight-loss over the full temperature range. The MWCNT-COOH has slightly more weight loss than that of MWCNT, indicating the decomposition of the –COOH groups from the MWCNT. On the other hand, the MWCNT-βCD(TE) and MWCNT-βCD(SE) showed even higher weight loss profiles than that of MWCNT and MWCNT-COOH. At around 480 °C, MWCNT-βCD(TE and SE) lost approximately 17% of their initial weight, signifying thermal decomposition of the attached βCD on MWCNT. At temperatures greater than 550 °C, the MWCNT-βCD(TE/SE) showed faster weight loss due to thermal decomposition of the chemically attached βCD. The MWCNT-βCD(Phys) had even higher weight loss from the lower temperature region than that of the MWCNT-βCD(TE/SE). This may be due to the

thermal decomposition of the non-covalently attached βCD with the MWCNT. However, the MWCNT-βCD(CC) showed the highest weight-loss profile compared to all other MWCNT-βCD. This significant weight-loss indicates substantially greater degree of functionalization of MWCNT with βCD from the side-walls compared to that of MWCNT-βCD(TE/SE), as depicted in the Figure 3-1(E).

Scanning electron microscope (SEM) and high-resolution transmission electron microscope (HRTEM) images were analyzed for visual confirmation of the high degree of βCD functionalization of MWCNT (Figure 3-5). Figure 3-5(A) and (B) show the SEM images of the surface morphology of the pristine MWCNT and MWCNT-βCD(CC), respectively. These images showed that the click chemistry mediated βCD functionalized MWCNT has a wider diameter than that of the pure MWCNT, which was due to the side-wall functionalization of MWCNT. The HRTEM images in Figure 3-5(C) and (D) also confirmed the wider diameter of MWCNT-βCD(CC) from the surface morphology of MWCNT before and after click chemistry modification. The sidewall of the pure and unmodified MWCNT is smooth, as shown in Figure 3-5(C). In contrast, the image of MWCNT-βCD in Figure 3-5(D) showed a ~3.2 nm thick amorphous layer of soft materials on the surfaces of MWCNT, signifying the presence of βCD [251]. The existence of this thick amorphous βCD layer on the surfaces of MWCNT significantly deteriorated the electrochemical sensing performances of the MWCNT-βCD(CC)/GCE, and this will be discussed in subsection 3.3.3.

The attachment of βCD with MWCNT was also experimentally investigated by using X-ray Photoelectron Spectroscopy (XPS) of (a) MWCNT-COOH, (b) MWCNT-βCD(TE), (c) MWCNT-βCD(SE), and (d) MWCNT-βCD(CC), as shown in Figure 3-6. βCD contains C-O-C/C-OH bonds, whereas MWCNT-COOH contains C=O and C-OH bonds. The C-C is present in both βCD and MWCNT-COOH [256]. Therefore, deconvolution of C-O-C/C-OH peak can provide an estimated quantification of βCD attached to the MWCNT. Figure 3-6(A) shows that the amount of C-O-C/C-OH is lowest for the all four materials, signifying small amount of –COOH group on MWCNT-COOH. The amount of C-O-C/C-

OH increased to 30% and 31% for MWCNT-βCD(TE) and MWCNT-βCD(SE), respectively (Figure 3-6(C) and (D)), indicating a moderate amount of βCD with MWCNT. However, the amount of C-O-C/C-OH is the highest (49%) for MWCNT-βCD(CC) among these materials (Figure 3-6(D)) confirming vigorous amount βCD attached to MWCNT. Therefore, the XPS analyses support the TGA and HRTEM results which indicate moderate and high amount of MWCNT-βCD attachment through TE/SE and CC methods, respectively.
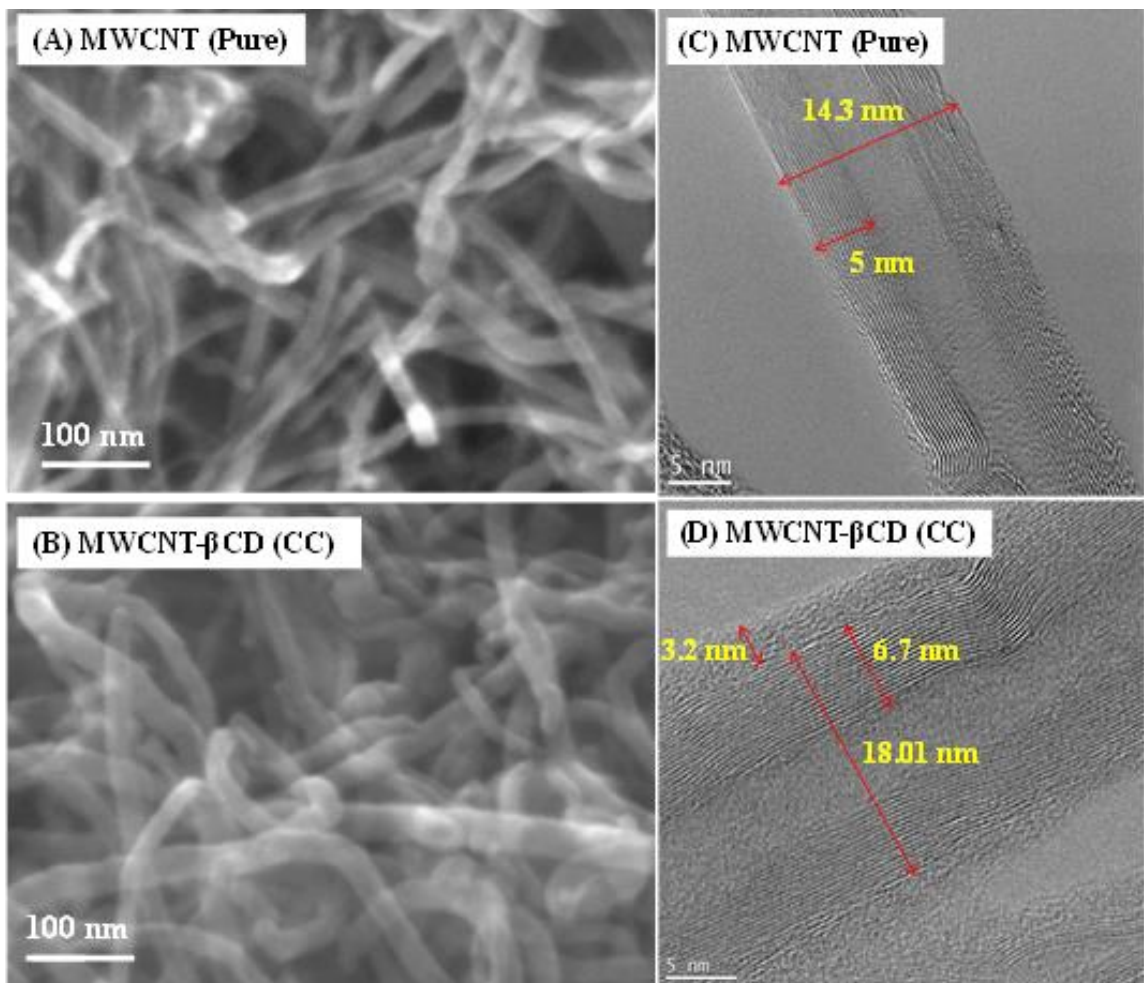
Figure 3-5. SEM images of (A) pure MWCNT and (B) MWCNT-βCD(CC). HRTEM images of (C) pure MWCNT and (D) MWCNT-βCD(CC).
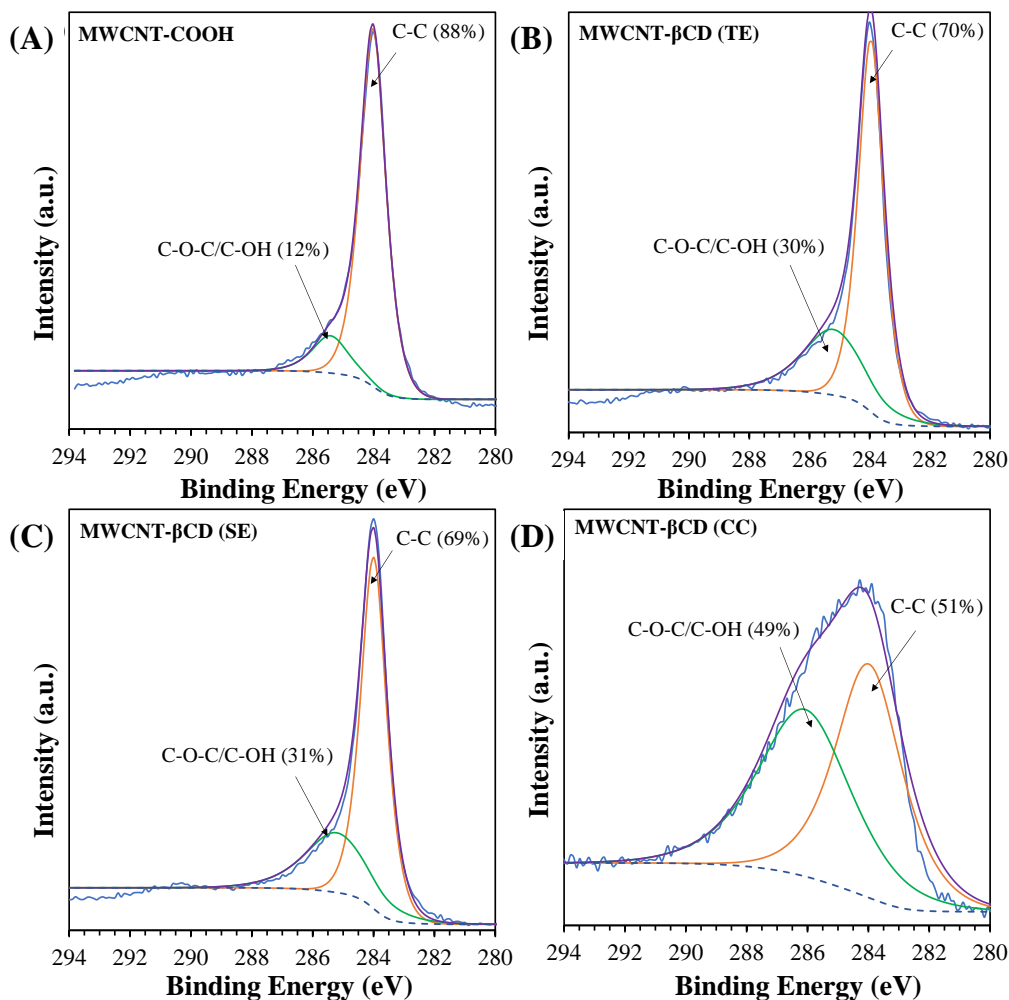
Figure 3-6. XPS narrow scan decomposed spectra of C_{1s} for (a) MWCNT-COOH, (b) MWCNT-βCD(TE), (c) MWCNT-βCD(SE), and (d) MWCNT-βCD(CC). Each figure shows the corresponding ratio of C-C and C-O-C/C-OH bonds signifying pure carbon and βCD, respectively.

3.3.2. Electrochemical sensing performance of MWCNT-βCD

Behavior of modified electrodes

The role of the electrode surface area on the modified electrodes' electrochemical behavior were investigated using a standard $K_3[Fe(CN)_6]$ redox probe. A schematic overview of the electrodes' fabrication steps is shown in Figure 3-2. The drop-cast volume of each sensing material was varied between 4 and 14 µl to find the optimum volumes that resulted in a maximum APAP oxidation peak current, as shown in Figure A- 1. The optimized drop-cast volumes for all the electrodes are listed in Table 3-1, which were then used throughout the

rest of the experiments. Moreover, the effect of surface topography of MWCNT with or without βCD was investigated in our previous manuscript [257]. It was observed that βCD improves the stability and homogeneity of the dispersion of MWCNT in water which resulted in smoother surface topography and uniform surface coverage of the sensing electrodes leading to higher stability.

Figure 3-7(A) shows the cyclic voltammetry (CV) curves of a bare GCE, MWCNT/GCE and MWCNT-βCD(CC/Phys/TE/SE)/GCE electrodes in an aqueous solution of 5.0 mM $K_3[Fe(CN_6)]$ containing 0.1 M KCl at a scan rate of 50 mV·s^{-1}. The bare GCE electrode showed two widely-separated redox peaks with a peak-to-peak separation (ΔE_p) of 500 mV. In the case of MWCNT/GCE and MWCNT-βCD(CC/Phys/TE/SE)/GCE, an increase in their redox peak currents (I_{pa}, I_{pc}) and a decrease in ΔE_p (115 mV) were observed. The increased peak currents and the decreased separation in peak-potentials indicate faster electron transfer at the modified electrodes compared to that of the bare GCE. This improved performance can be attributed to the excellent electrical conductivity and the large effective surface area of the MWCNT/GCE and MWCNT-βCD(CC/Phys/TE/SE)/GCE. The effective surface area of the modified electrodes was calculated using the Randles–Sevcik equation. In a reversible electrochemical reaction process, such as $K_3[Fe(CN_6)]$ based cyclic voltammetry, the peak current can be expressed as [211,258],

$$I_p = 2.69 \times 10^5 AD^{1/2}n^{3/2}v^{1/2}C, \tag{3-1}$$

where A is the effective surface area, C is the bulk concentration of $K_3[Fe(CN_6)]$, n is the number of electrons transferred ($n = 1$), D is the diffusion coefficient of $K_3[Fe(CN_6)]$ (6.67 $\times 10^{-6}$ cm^2·s^{-1}), and v is the scan rate.

From (3-1), a linear relationship exists in the peak current (I_p) vs square root of scan-rate ($v^{1/2}$), as shown in Figure 3-7(B) for MWCNT-βCD(SE)/GCE. The effective surface area of the electrode was calculated from the slope of the I_p-$v^{1/2}$ curve and equation (3-1). The area of the bare glassy carbon electrode was 0.070 cm^2, which was significantly improved to 0.149 cm^2 by the MWCNT-βCD(SE) film. Detailed scan-rate dependent redox behavior

of the MWCNT/GCE and MWCNT-βCD(Phys/TE/SE/CC)/GCE are shown in the Figure A- 2 to Figure A- 6, respectively. The effective surface areas of these electrodes were 0.117, 0.122, 0.142 and 0.035 cm^2 for pure MWCNT, MWCNT-βCD(Phys), MWCNT-βCD(TE), and MWCNT-βCD(CC) modifications, respectively. These results indicate that chemical modifications such as TE and SE can significantly improve the effective surface area compared to that of physical modifications.
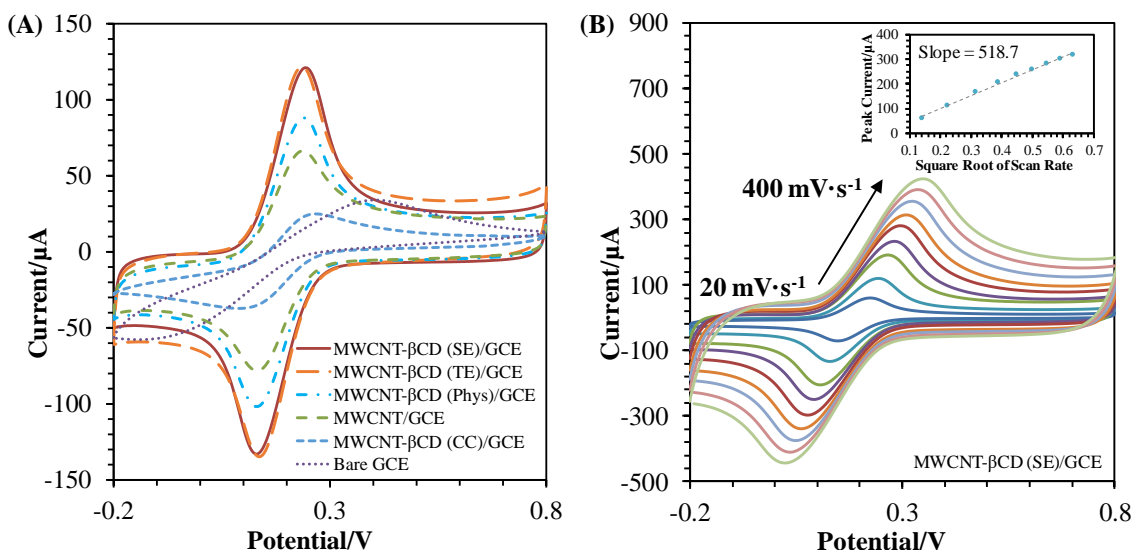
Figure 3-7. (A) Cyclic voltammetry curves of bare GCE, MWCNT/GCE and MWCNT-βCD(CC/Phys/TE/SE) in an aqueous solution of 5.0 mM K$_3$[Fe(CN)$_6$] containing 0.1 M KCl at a scan rate of 50 mV·s^{-1}. (B) Cyclic voltammetry curves of MWCNT-βCD(SE)/GCE in 5.0 mM K$_3$[Fe(CN)$_6$] containing 0.1 M KCl at different scan rates (20, 50, 100, 150, 200, 250, 300, 350, 400 mV·s^{-1}).

The increase in effective surface area can be attributed to the inclusion of a modest amount of βCD, which has a porous structure. In general, the modest amount of βCD attached to the edges of the MWCNT-COOH not only improved the porosity of the sensing surface but also retained the MWCNT backbone exposed, permitting ease of the redox reactions of the target molecule. However, CC-modified MWCNTs did not show an increased effective surface area. A high amount of βCD inclusion in the CC modification affected the conductivity of the MWCNT-βCD modified electrode surface due to the attachment of βCD molecule to MWCNT from the side wall (also shown in Figure 3-5(B) and (D)). This unexposed MWCNT surface hindered the redox reactions of the target molecule. Therefore,

MWCNT-βCD(SE) showed one of the best electrochemical performance among all the modified electrodes.

(A) APAP(5 μM)   **(B) E2 (5 μM)**
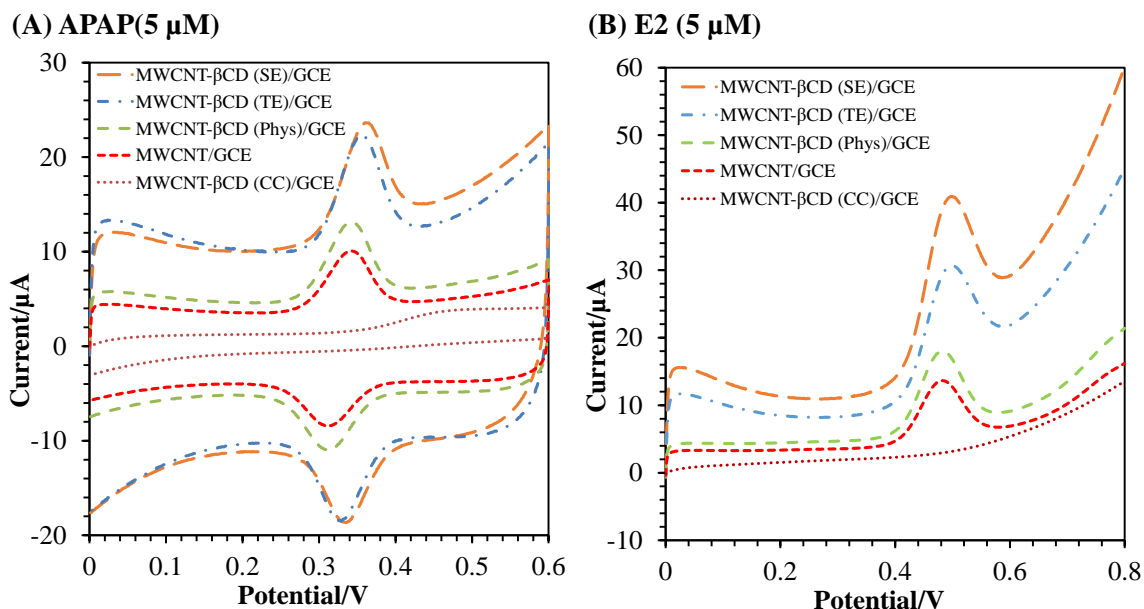
Figure 3-8. (A) Cyclic voltammetry curves of MWCNT/GCE, and MWCNT-βCD(CC/Phys/TE/SE)/GCE recorded in 0.01 M PBS (pH 7.4) in the presence of 5 μM APAP at a scan rate of 50 mV·s⁻¹. (B) Cyclic voltammetry curves of MWCNT/GCE, and MWCNT-βCD(CC/Phys/TE/SE)/GCE recorded in 0.01 M PBS (pH 7.4) in the presence of 5 μM E2 at a scan rate of 50 mV·s⁻¹. All the experiments were done with an open circuit potential of 300 seconds under magnetic stirring before measurements.

Sensing performance of MWCNT-βCD electrodes

Two major contributors to improved redox-based electrochemical sensing are the effective surface area and the analyte capturing ability of the sensing material. The prepared MWCNT-βCD composite has a high surface area from MWCNT and a high host-guest interaction from βCD [202,207,259]. Figure 3-8(A) shows the CV results of MWCNT/GCE and MWCNT-βC (Phys/TE/SE)/GCE in the presence of 5 µM APAP. Similar CV results were obtained when 1 and 10 µM APAP were used. Therefore, only the CV results for 5 µM APAP to compare the sensing performances of the modified electrodes are reported.

For MWCNT-βCD(CC)/GCE, a weak oxidation peak around 450 mV and no reduction peak were observed. For MWCNT/GCE, MWCNT-βCD(Phys/TE/SE)/GCE, strong and well-defined redox peaks were observed at the anodic peak potential (E_{pa}) of 340 mV and

the cathodic peak potential (E_{pc}) of 320 mV. Compared to that of MWCNT/GCE, the APAP oxidation peak current of MWCNT-βCD(Phys)/GCE and MWCNT-βCD(TE/SE)/GCE were improved by 30% and 80%, respectively. Hence, the TE and SE modifications effectively enhanced the APAP oxidation capability of MWCNT-βCD/GCE. Figure 3-8(B) shows the linear sweep voltammetry (LSV) results of MWCNT/GCE and MWCNT-βC (Phys/TE/SE)/GCE in the presence of 5 μM E2. Similarly, E2 oxidation peak current of MWCNT-βCD(Phys)/GCE and MWCNT-βCD(TE/SE)/GCE were also improved by 32% and ~85%, respectively, compared to that of MWCNT/GCE. The intensities and positions of the APAP redox peaks and E2 oxidation peaks signify that the fabricated MWCNT-βCD/GCE favors quasi-reversible and irreversible electrochemical reactions, respectively, as illustrated in Scheme 1 below:
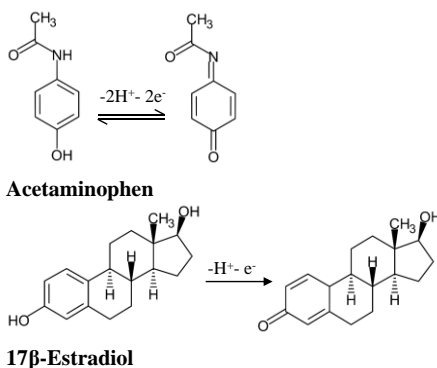
Scheme 1. Oxidation reduction reactions of acetaminophen and 17β-estradiol.

The oxidation and reduction processes involved two electrons and two protons for APAP, and the oxidation of E2 involved one electron and one proton, which will be discussed and characterized through their scan rate and pH dependent behavior in the following sub-sections. The improvement of the oxidation peak currents for both APAP and E2 with MWCNT-βCD(TE/SE)/GCE are correlated to their high effective surface area compared to that of MWCNT/GCE and MWCNT-βCD(Phys)/GCE, as discussed previously. Therefore, the scan rate and pH dependent behavior with APAP and E2 were only investigated with MWCNT-βCD(SE)/GCE due to its superior electrochemical sensing performance compared to that of other electrodes.

Charge-transfer properties of the modified electrodes

The charge transfer ability of the sensing electrodes for the redox of APAP is another important performance indicator. This can be estimated by analyzing scan rate (v) dependent redox peak currents (I_{pa}/I_{pc}) and peak potentials (E_{pa}/E_{pc}). Figure S7(A) shows the CVs of the MWCNT-βCD(SE)/GCE in the presence of 5 µM APAP for different scan rates from 20 to 400 mV·s^{-1}. The redox peak currents increased linearly with the increase of the scan rate, as indicated by the Randles-Sevcik equation (Eq. (3-1)), (Figure S7(B)). As shown in Figure S7(B), for the scan-rate dependent behavior of MWCNT-βCD(SE)/GCE in the presence of 5 µM APAP, the fitted regression equations were:

$$I_{pa}(\mu A) = 2.00 + 0.1651\ v\left(v:\ \mathrm{mV\cdot s^{-1}},\ R^2 = 0.9978\right), \tag{3-2}$$

$$I_{pc}(\mu A) = 1.99 - 0.1662\ v\left(v:\ \mathrm{mV\cdot s^{-1}},\ R^2 = 0.9988\right), \tag{3-3}$$

The linear relationship of the peak currents (I_{pa} or I_{pc}) with the increase of scan rate (v) confirmed that the electrochemical reaction of APAP at MWCNT-βCD(SE)/GCE is a surface controlled process [260]. The effect of scan rate on the peak potential was also analyzed by the relationship between the peak potentials and the logarithmic values of the scan rates (log v), as shown in Appendix A. The positive shifting of the oxidation peaks potentials and negative shifting of the reduction peak potentials can be attributed to the quasi-reversible nature of the redox of APAP where the rate of electron transfer becomes comparable to the mass transport rate [215]. The E_{pa} and E_{pc} were proportional with the log v at higher scan rates from 200 to 400 mV·s^{-1}, with the linear regression equations:

$$E_{pa}(V) = 0.26 + 0.0495\ \log v\left(v:\ \mathrm{mV\cdot s^{-1}},\ R^2 = 0.9895\right), \tag{3-4}$$

$$E_{pc}(V) = 0.42 - 0.0495\ \log v\left(v:\ \mathrm{mV\cdot s^{-1}},\ R^2 = 0.9895\right), \tag{3-5}$$

According to Laviron's theory [216], the slopes of the two regression lines are equal to $2.3RT/(1 − α)nF$ and $−2.3RT/αnF$ for the anodic and cathodic peaks, respectively. Here, R is the ideal gas constant (Joules per Kelvin per mole), T is the temperature in Kelvin and F is the Faraday's constant. Based on the slopes of the two straight lines, the charge transfer coefficient, $α$, was calculated to be 0.5 using the following equation:

$$\log \frac{k_a}{k_c} = \log \frac{\alpha}{1-\alpha} \quad \text{or} \quad \frac{k_a}{k_c} = \frac{\alpha}{1-\alpha}, \tag{3-6}$$

where k_a and k_c are the slopes of the straight lines for E_{pa} vs. log v and E_{pc} vs. log v, respectively. Also, the apparent heterogeneous electron transfer rate constant, k_s, was calculated based on the following equation [216]:

$$\log k_S = \alpha \log(1-\alpha) + (1-\alpha)\log \alpha - \log \frac{RT}{nFv} - \frac{\alpha(1-\alpha)nF\Delta E_p}{2.3RT}, \tag{3-7}$$

where n is the number of electrons involved in the reaction, ΔE_p is the peak-to-peak potential separation, α is the charge transfer coefficient, v is the scan rate, and other symbols have their usual meanings. The number of electrons involved in the reaction of APAP is 2. Therefore, the heterogeneous electron transfer rate constant (k_s) was calculated to be 2.9 s^{-1}, which is higher than that of the physically modified MWCNT-βCD/GCE (1.659 s^{-1}) reported in Ref [261]. The high value of k_s indicates that the MWCNT-βCD(SE)/GCE electrode provides rapid electron transfer properties during the redox based sensing of APAP [217].

The electron transfer number of the sensing electrodes for the oxidation of E2 is another important performance indicator. This was investigated from the scan rate dependent behavior of the MWCNT-βCD(SE)/GCE in the presence of E2. The relationships between peak potential (E_p) and scan rate (v) were studied using linear potential sweep voltammetry (LSV), as shown in Figure A- 7(D) and Figure A- 7(E). In the range of 0.02 to 0.3 $V \cdot s^{-1}$, the linear relationship between I_{pa} and $v^{1/2}$ is:

$$I_{pa} = 5.5471 \ v^{1/2} - 18.06 \quad (R^2 = 0.9951), \tag{3-8}$$

This result indicated that the electrode process was diffusion controlled. Also, for a totally irreversible electrochemical process like this, the E_{pa} is defined by the following equations [262]:

$$E_{pa} = E_0' + m\left[0.78 + \ln\left(\frac{D^{1/2}}{k_s}\right) - 0.5\ln m\right] + 0.5 \times 2.303 \times \left(\frac{RT}{\alpha n_\alpha F}\right)\log v \,, \tag{3-9}$$

$$E_{pa} - E_{p/2} = \frac{1.857RT}{(\alpha n_\alpha F)} = \left(\frac{47.7}{\alpha n_\alpha}\right)mV \text{ (at 25 °C)}, \tag{3-10}$$

where E_0' is the standard electrode potential, k_s is the standard heterogeneous rate constant, D is the diffusion coefficient of E2, α is the transfer coefficient of the oxidation of E2, $E_{p/2}$ is the potential where $i = I_{p/2}$ in the LSV, and other symbols have their usual meanings. In this experiment, as shown in Figure A- 7(F), E_{pa} can be expressed with the following equation:

$$E_{pa} = 0.0642 \log v + 0.4134 \quad (R^2 = 0.9903) \tag{3-11}$$

From Equations (3-9) and (3-11), we obtain:

$$0.5 \times 2.303 \times \left(\frac{RT}{\alpha n_\alpha F}\right) = 0.0642 \,, \tag{3-12}$$

From equation (3-12), the value of αn_α was calculated to be 0.46. On the other hand, the average value of $(E_p - E_{p/2})$ is 93.5 mV for v from 20 to 400 mV·s⁻¹. The value of αn_α from equation (3-10) was 0.51. The two values are almost equal with the average value of 0.485. In general, in a totally irreversible electrode process, the value of α is assumed as 0.5. Therefore, the electron transfer number (n_α) calculated as 0.97, is close to 1. This indicates that one electron was involved in the oxidation process of E2. Although a larger I_{pa} can be achieved at a higher scan rate, the background current will also increase at the higher scan rate and the shape of peak might become distorted. Therefore, an optimum scan rate of 0.05 V·s⁻¹ was chosen for the electrochemical sensing of APAP and E2.

The pH of a solution is an important parameter since it influences the variation in acid-base dissociation of APAP and E2. This, in turn, alters their electrochemical detection by shifting the redox peak potential towards more positive or negative directions and changing the redox peak currents [215] The effect of pH on the redox reaction of APAP was studied in our previous work [261] with the MWCNT-βCD(Phys)/GCE electrode. The highest

redox peak current was observed at pH 7.4. On the other hand, Figure A- 8 shows the effect of pH variation on the E2 oxidation peaks. A small increase in the oxidation peak current was observed at pH 5. However, the peak current was almost stable from pH 7 to 8. Therefore, pH 7.4 was chosen as the standard pH for the detection of both APAP and E2. The oxidation (E_{pa}) peak potential of E2 shifted negatively with the increase of pH. The linear regression equation for the pH dependent shift of E_{pa} can be expressed as:

$$E_{pa} = -0.0713 \, \text{pH} + 1.0281 \left(R^2 = 0.9962 \right), \tag{3-13}$$

The slope of the equation (3-13) can be used to determine the ratio of proton and electron involved in the oxidation reaction from the following equation [220]:

$$\frac{dE_{pa}}{d\text{pH}} = 2.303 \frac{mRT}{nF}, \tag{3-14}$$

where m is the number of protons, and n is the number of electrons. The m/n ratios were calculated to be 1.2 for the oxidation process, which is close to unity. Therefore, the number of protons and electrons involved in the oxidation of E2 were equal, suggesting a one-electron and a one-proton process [260].

3.3.3. Determination of acetaminophen and 17β-estradiol

Comparison of MWCNT-βCD-modified electrodes

The comparison of the electrochemical performance of the modified MWCNT with βCD in the previous subsection showed that the sensing performance of MWCNT-βCD(SE)/GCE was comparable to that of MWCNT-βCD(TE)/GCE and better than that of MWCNT/GCE and MWCNT-βCD(Phys)/GCE. The electrochemical sensing performance of MWCNT-βCD(SE)/GCE was also compared in determining APAP and E2 over wide concentration ranges to identify the sensors linear response range. Figure 3-9(A) and Figure 3-10(A) show the linear sweep voltammetry (LSV) curves for the concentration ranges of 0.005 to 20 μM APAP and 0.01 to 15 μM E2, respectively, using MWCNT-βCD(SE)/GCE. Similarly, Figure 3-9(B) and Figure 3-10(B) show the calibration curves for the concentration ranges of 0.005 to 20 μM APAP and 0.01 to 15 μM E2, respectively, for

MWCNT-βCD(SE)/GCE along with that of MWCNT-βCD(Phys)/GCE and MWCNT/GCE. The linear regression equations for APAP are:

$$I_p(\mu A) = 9.2C + 0.57(\mu M), (R^2 = 0.99)$$
$$C: 0.005 - 0.1\mu M, \left[\text{MWCNT-}\beta\text{CD(SE)/GCE}\right] \quad , \tag{3-15}$$

$$I_p(\mu A) = 1.80C + 1.27(\mu M), (R^2 = 0.99)$$
$$C: 0.1\text{-}20\ \mu M, \left[\text{MWCNT-}\beta\text{CD(SE)/GCE}\right] \quad , \tag{3-16}$$

$$I_p(\mu A) = 1.27C + 0.87(\mu M)\ (R^2 = 0.99),\ [\text{MWCNT-}\beta\text{CD(Phys)/GCE}], \tag{3-17}$$

$$I_p(\mu A) = 0.93C + 0.58(\mu M)\ (R^2 = 0.99),\ [\text{MWCNT/GCE}], \tag{3-18}$$

Also, the linear regression equations for E2 are:

$$I_p(\mu A) = 11.9C + 0.74(\mu M), (R^2 = 0.99),$$
$$C: 0.01 - 0.1\mu M, \left[\text{MWCNT-}\beta\text{CD(SE)/GCE}\right] \quad , \tag{3-19}$$

$$I_p(\mu A) = 2.40C + 1.84(\mu M)\ (R^2 = 0.99),$$
$$C: 0.1 - 15\mu M, \left[\text{MWCNT-}\beta\text{CD(SE)/GCE}\right] \quad , \tag{3-20}$$

$$I_p(\mu A) = 1.84C + 0.39(\mu M)\ (R^2 = 0.99),\ [\text{MWCNT-}\beta\text{CD(Phys)/GCE}], \tag{3-21}$$

$$I_p(\mu A) = 1.26C + 0.46(\mu M)\ (R^2 = 0.99),\ [\text{MWCNT/GCE}]. \tag{3-22}$$
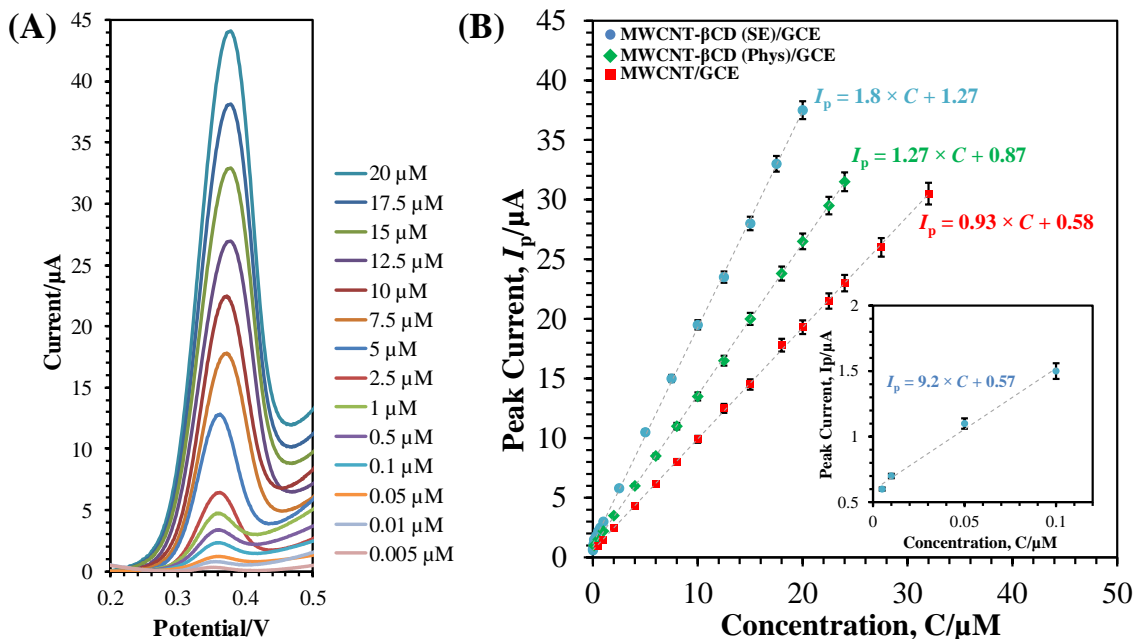
Figure 3-9. (A) LSVs of MWCNT-βCD(SE)/GCE in 0.01 M PBS (pH 7.4) in the presence of 0.005–20 μM APAP. (B) Calibration curve (i.e., peak current vs APAP concentration) for MWCNT/GCE and MWCNT-βCD(Phys/SE)/GCE. All the experiments were done with an open circuit potential of 300 seconds under magnetic stirring before measurements.
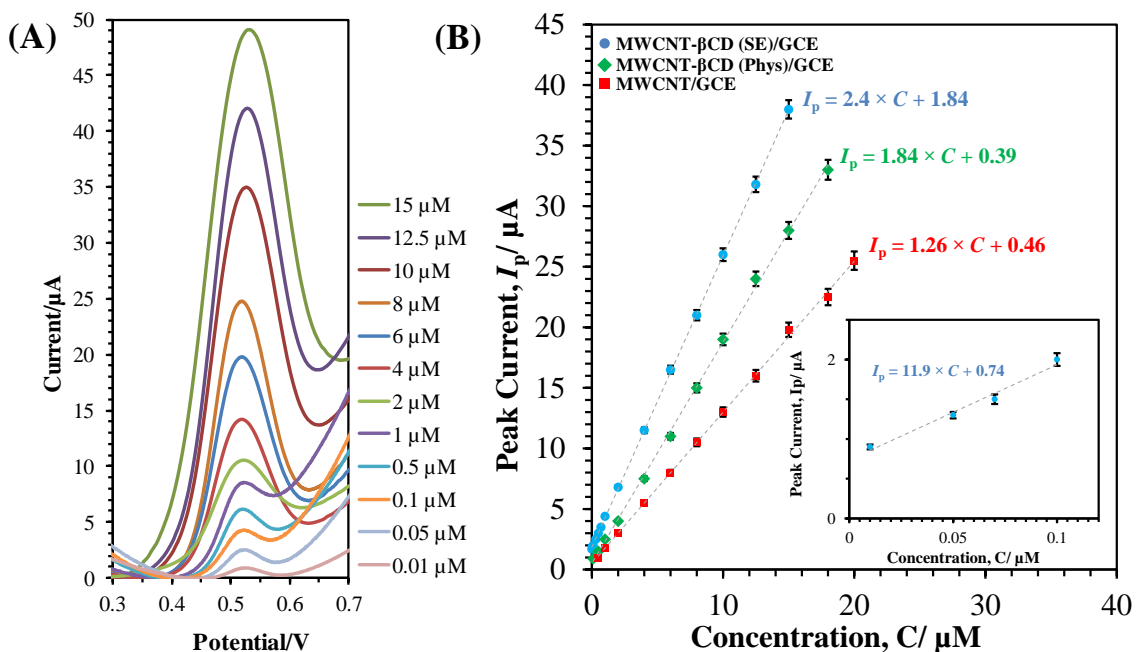
Figure 3-10. (A) LSVs of MWCNT-βCD(SE)/GCE in 0.01 M PBS (pH 7.4) in the presence of 0.01–15 μM E2. (B) Calibration curve (i.e., peak current vs E2 concentration) for MWCNT/GCE and MWCNT-βCD(Phys/SE)/GCE. All the experiments were done with an open circuit potential of 300 seconds under magnetic stirring before measurements.

The I_p-C curve started to deviate from its linear behavior and became saturated after 20 µM concentration of APAP and 15 µM concentration of E2 for MWCNT-βCD(SE)/GCE (Figure A- 9). The deviation from the linear response might be due to the saturation of the kinetic behavior of the sensing electrode [235]. The MWCNT-βCD(SE)/GCE showed two linear regions for both APAP and E2 detection, as shown in equations 3-15, 3-16 and 3-19, 3-20, respectively. The sensitivity slope of APAP and E2 linear ranges was improved for MWCNT-βCD(SE)/GCE compared to that of MWCNT/GCE and MWCNT-βCD(Phys)/GCE. Also, the inset images of the Figure 3-9(B) and Figure 3-10 (B) show that the lower limit of the concentration linear ranges had been reduced significantly with MWCNT-βCD(SE)/GCE compared to that of MWCNT/GCE and MWCNT-βCD(Phys)/GCE due to higher sensitivity slope in lower concentration range. Using MWCNT-βCD(SE)/GCE, the limit-of-detection, defined as LoD = $3s/m$ (where s is the standard deviation of the blank solution (10 nA), and m is the slope of the calibration curve at the lower concentration range), was estimated to be 3.3 nM and 2.5 nm for APAP and E2, respectively [156]. As shown in Table 3-2 and Table 3-3, the linear ranges and LoDs of APAP and E2 using MWCNT-βCD(SE)/GCE had improved performance compared to other reported results that utilized modified electrodes based on CNT.

The MWCNT-βCD(SE)/GCE electrode achieved the lowest LoD of 3.3 nM and a modest linear range for APAP compared to results reported in the literature and listed in Table 3-3. For example, MWCNT/BPPGE [231] based electrode showed the lowest reported LoD, with similar linear range compared to that of MWCNT-βCD(SE)/GCE. On the other hand, MWCNT-βCD(SE)/GCE also showed LoD of 2.5 nM for E2, which is very close to the lowest LoD, as shown in Table 3-3. Although the LoD of CTAB-Nafion/GCE [263] and MWCNT-IL-BMIMPF6/GCE [264] has the lowest LoD, they showed very narrow linear range of 0.025 to 1.5 µM and 0.01 to 1 µM, respectively, compared to that of MWCNT-βCD(SE)/GCE. Therefore, the MWCNT-βCD(SE)/GCE sensors are very promising for sensitive determination of pharmaceutical contaminants such as APAP and E2.

Table 3-2: Comparison of nanomaterials based electrochemical sensors for the detection of acetaminophen (APAP).

Configuration of the Sensor	Method of Detection	Limit-of-Detection, LoD (μM)	Linear Range (μM)	Reference
SWCNT/CCE	DPV	0.05	0.08−200	[225]
MWCNT-PDDA-PSS/GE	CA	0.5	25−400	[226]
N-DHPB/MWCNT/CPE	DPV	10	15−270	[227]
EF-NiO/MWCNT/CPE	SWV	0.5	0.8−600	[229]
SWCNT-GNS/GCE	SWV	0.038	0.05−64.5	[205]
MWCNT-GNS/GCE	DPV	0.1	0.8−110	[230]
MWCNT/BPPGE	AdsSV	0.01	0.01−2/2−20	[231]
fMWCNT/GCE	DPV	0.6	3−300	[183]
ED-CMWCNT/GCE	DPV	0.092	1−200	[184]
Chitosan/MWCNT/GCE	DPV	0.17	1−145/4−200	[232]
AuNP-PGA-SWCNT/PET	DPV	1.18	8.3−145.6	[234]
MWCNT-βCD(SE)/GCE	LSV	0.0033	0.005−0.1/0.1−20	This Work

Table 3-3: Comparison of nanomaterials based electrochemical sensors for the detection of 17β-estradiol (E2).

Configuration of the Sensor	Method of Detection	Limit-of-Detection, LoD (μM)	Linear Range (μM)	References
CTAB–Nafion/GCE	LSV	0.001	0.025−1.5	[263]
nanoAl$_2$O$_3$/GCE	LSV	0.08	0.4−40	[265]
MWNT-nafion/GCE	SWV	0.01	0.25−10	[266]
CNT-Ni(Cyclam)/GCE	SWV	0.06	0.5−40	[267]
Poly(L-serine)/GCE	LSV	0.02	0.1−30	[268]
MWCNT-IL-BMIMPF$_6$/GCE	LSV	0.002	0.01−1	[264]
RGO-DHP/GCE	LSAdSV	0.077	0.4−20	[269]
Exfoliated graphene	DPV	0.0049	0.01−1.5	[270]
MWCNT-βCD(SE)/GCE	LSV	0.0025	0.01−0.1/0.1−15	This Work

(A) MWCNT/GCE

(B) MWCNT-βCD (Phys)/GCE

(C) MWCNT-βCD (TE/SE)/GCE

(D) MWCNT-βCD (CC)/GCE
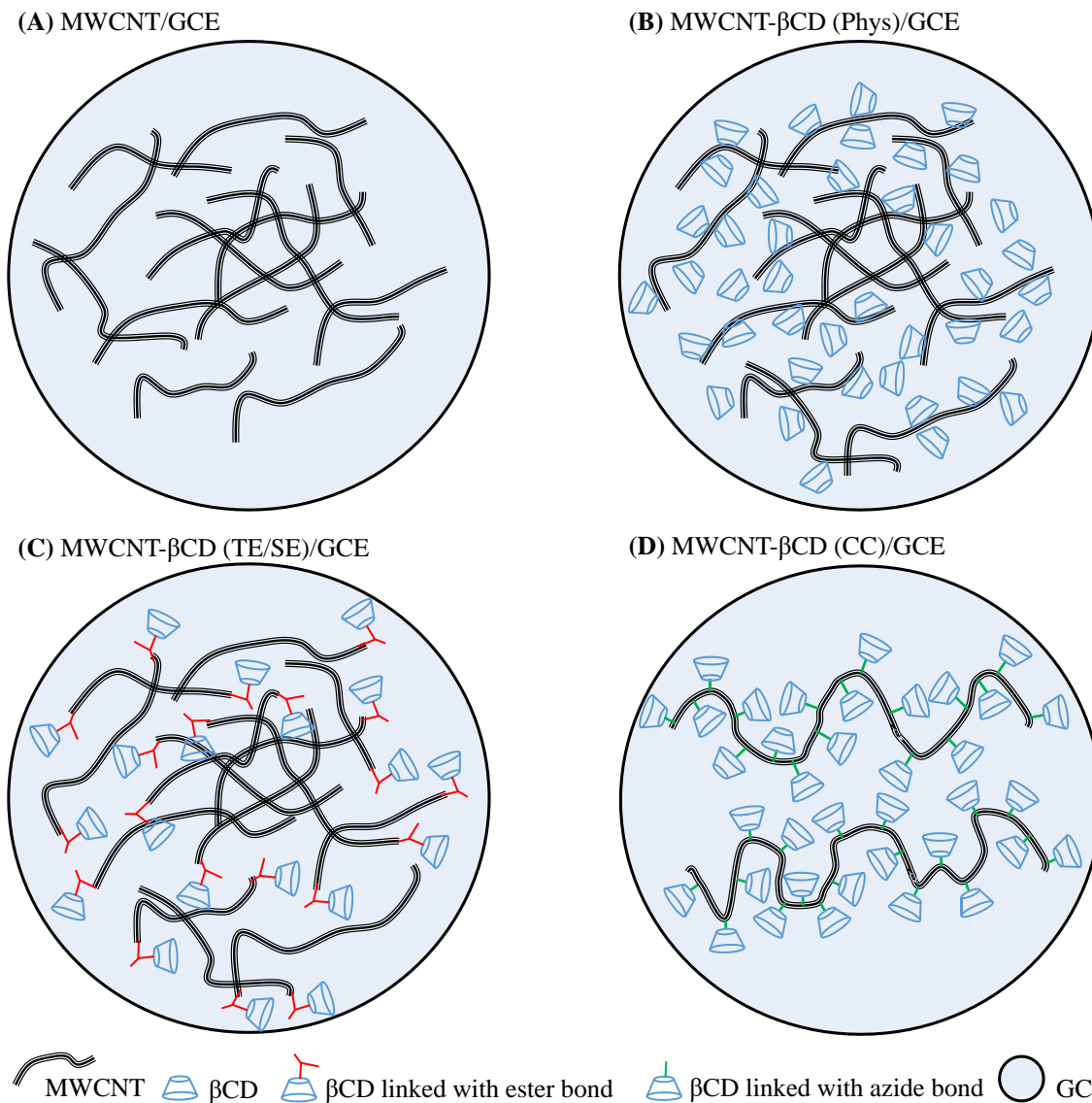
Figure 3-11. Schematic illustration of the modified GCE electrodes with (A) MWCNT, (B) MWCNT-βCD(Phys), (C) MWCNT-βCD(TE/SE), and (D) MWCNT-βCD(CC) to explain their electrochemical sensing mechanisms. The dimensions of the components of the images are not to the scale and are drawn for qualitative explanation of the sensing performances of the electrodes only.

Sensing mechanisms

The electrochemical sensing mechanisms of MWCNT/GCE and MWCNT-βCD(Phys/TE/SE/CC)/GCE can be explained with the schematic illustrations in Figure 3-11. The illustration represents the relative amount of MWCNT and βCD on the surface of the GCE electrodes along with their molecular orientations. The MWCNT-

βCD(Phys)/GCE and MWCNT-βCD(TE/SE)/GCE have almost similar amounts of MWCNT compared to that of MWCNT/GCE. In contrast, MWCNT-βCD(CC)/GCE has lower amounts of MWCNT due to the significant functionalization by βCD. The illustration also shows the relative amounts of βCD and its linkage orientations. The MWCNT-βCD(TE/SE)/GCE has lower amount of βCD compared to that of MWCNT-βCD(Phys)/GCE and MWCNT-βCD(CC)/GCE. The significant improvement in the APAP and E2 sensitivity of the MWCNT-βCD(SE/TE)/GCE can, therefore, be attributed to the following factors.

The inherent materials properties, such as high conductivity and electron transfer ability of MWCNT, provides enhanced electrocatalytic activity for the oxidation of APAP and E2 (Figure 3-11(A), (B) and (C)). The high surface-to-volume ratio of the MWCNT provides enhanced pathways towards oxidation of APAP and E2 (Figure 3-11(A), (B) and (C)). The covalently bonded βCD with MWCNT in MWCNT-βCD(TE/SE)/GCE produces a synergistic effect by introducing even higher surface area of the sensor by dispersing the MWCNT and providing a direct electron transfer path from the redox reactions of APAP and E2 (Figure 3-11(B)). In the case of pure MWCNT, APAP/E2 form a single-layer adsorption on the MWCNT surface. However, in the case of MWCNT-βCD(TE/SE), the covalently bonded βCD provides a hydrophilic outer surface with its hydrophobic inner core on top/edges of the MWCNT, forming a multilayer surface structure with higher electrochemically active surface area (Figure 3-11(B)). This multilayer surface structure attracts more APAP and E2 on the electrode surface compared to that of the single layer adsorption in MWCNT. The presence of βCD onto the top/edges of MWCNT improved detection sensitivity of APAP through the formation of supramolecular host-guest complexes between βCD and APAP/E2 [207]. Therefore, the combined effect of the βCD and MWCNT in covalently bonded MWCNT-βCD(TE/SE) provided enhanced redox sensitivity.

The poor electrochemical sensing performance of MWCNT-βCD(CC)/GCE with APAP and E2 can be attributed to the poor electron transfer ability due to excessive surface coverage of the MWCNT with insulating βCD, as shown in Figure 3-11(D). This result is

consistent with our previous finding of poor redox activity of the MWCNT-βCD(CC)/GCE with standard $K_3[Fe(CN)_6]$. The electrochemical sensing performance of MWCNT-βCD(CC)/GCE was also analyzed by mixing pure MWCNT with MWCNT-βCD(CC), as shown in Figure A- 10. It was observed that the intensity of the oxidation peak currents was increased by the increase of pure MWCNT ratio with MWCNT-βCD(CC) (i.e., $1\times$ and $3\times$ MWCNT than that of MWCNT-βCD(CC)). This result confirms that the role of βCD on electrochemical sensing can be optimized with their controlled modification ratio with MWCNT.

3.3.4. Interference, stability, and sample analysis

Interference

The interference study was to observe the effects of the presence of interfering ions and biological molecules on the selective measurement of APAP and E2 concentrations. The interference experiments were performed in PBS solutions (pH 7.4) with 5 µM APAP, and E2, respectively. The response peak currents before and after adding different interfering species were compared. Common interfering species in drinking water are ionic in nature, whereas urines contain biochemical species. Therefore, tests with common interfering species in 10 mM of Na^+, K^+, Mg^{2+}, Ca^{2+}, Cl^-, SO_4^{2-} and glucose, and 100 µM dopamine, ascorbic acid, uric acid, L-serine, and L-proline on APAP and E2 sensing were conducted. These interferers had no significant effect on the sensed signal, causing less than 3% changes in the APAP and E2 peak currents. However, the interferences of bisphenol A and tyrosine resulted in significant decrease in the peak current for the determination of E2. This interference is caused by their similar molecular structure with E2. To reduce such interferences, a molecularly imprinted polymer (MIP) layer on top of the electrode surface may be used for selective determination of the target analyte. The MIP layer can also be used to eliminate the interferences from other species present in real samples [271]. Therefore, it can be considered that this MWCNT-βCD(SE)/GCE electrode showed satisfactory selectivity for the detection of APAP and E2 in the presence of common interfering species.

Reproducibility and stability

The reproducibility and stability of the MWCNT-βCD(SE)/GCE sensors were investigated by performing sensing measurements over time and with multiple electrodes. The MWCNT-βCD(SE)/GCE sensors prepared in the same batch were tested for the determination of 5 µM APAP and E2 in 0.01 M PBS (pH 7.4). A relative standard deviation (RSD) of 1.8% was observed with twelve different electrodes of the same batch, confirming excellent reproducibility of the MWCNT-βCD (SE)/GCE electrode. Two MWCNT-βCD(SE)/GCE electrodes were stored in room temperature (25 °C) in a dry environment and the APAP/E2 sensing tests were performed every week over a 4-week period to analyze their long-term stability. A relative standard deviation (RSD) of 1.5% was observed, confirming the stable performance of the MWCNT-βCD(SE)/GCE electrodes for detecting APAP and E2. Therefore, the MWCNT-βCD(SE)/GCE electrode showed excellent reproducibility and stability for determining APAP and E2.

Table 3-4: Determination results of APAP in Tylenol® tablets by using MWCNT-βCD(SE)/GCE.

Sample[a]	Prepared Concentration (µM)	Found (µM)[†]	Recovery
1	0.10	0.098±0.0019	98.0%±1.96%
2	1.0	1.02±0.02	102.0%±2.0%
3	5.0	5.06±0.10	101.2%±%2.02%

[a] Tylenol® Regular Strength tablets (Acetaminophen: 325 mg).

[†] Average values were calculated from three determinations.

Table 3-5: Determination results of E2 in urine by using MWCNT-βCD(SE)/GCE.

Sample	Added (µM)	Found (µM)[†]	Recovery
1	0.10	0.099±0.00198	99.0%±1.98%
2	1.0	0.98±0.0196	98.0%±1.96%
3	5.0	4.05±0.081	101.0%±2.02%

[†] Average values were calculated from three determinations.

Drinking water and urine samples analysis

The MWCNT-βCD(SE)/GCE electrode was also used to determining the concentrations of APAP and E2 in real samples made from APAP tablets and human urine. The recovery

tests of APAP were carried out using LSV under optimized parameters through the standard addition method. In this method, the 0.1 mM stock solution made from the APAP tablets were added to 0.01 M PBS solution (pH 7.4) to make certain concentrations of APAP (e.g., 0.1, 1 and 5 μM). Table 3-4 shows that the sensor exhibited an excellent recovery from 98% to 102%. Similarly, the standard addition method was also applied to the determination of E2 in urine samples. In this method, certain concentrations of E2 (e.g., 0.1, 1 and 5 μM) were added to the urine sample diluted by 0.01 M PBS solution. Table 3-5 shows that a recovery of the experimental results was obtained from 98% to 101%. These results indicate that the developed sensor can detect APAP and E2 in water and urine samples.

3.4. Conclusions

We developed a one-step covalent modification of MWCNT with βCD through Steglich esterification to fabricate highly sensitive electrochemical sensors for the determination of acetaminophen (APAP) and 17β-estradiol (E2). The sensor demonstrated excellent sensing performance for detecting APAP and E2 with limits-of-detection of 3.3 and 2.5 nM, respectively. We compared the sensing performances of the Steglich modified MWCNT-βCD with that of physically modified MWCNT-βCD and two other chemical modification approaches to demonstrate the advantages of the proposed approach that resulted in higher effective surface area and electron transfer capability. The Steglich modified MWCNT-βCD based sensing electrodes exhibited high stability, good reproducibility and considerable selectivity for the detection of acetaminophen and 17β-estradiol in the presence of common interfering species, with recovery of more than 98% in real samples. Therefore, the developed sensor may be used in low-cost sensing systems for pharmaceutical and organic micro-pollutants monitoring in water.

Chapter 4

Electrochemical Sensing of Lead in Drinking Water Using β-Cyclodextrin-Modified MWCNT[*]

Heavy metal pollution is a severe environmental problem affecting many water resources. The non-biodegradable nature of the heavy metals such as lead (Pb) causes severe human health issues, so their cost-effective, sensitive and rapid detection is needed. In this work, we describe a simple, facile and low-cost modification of multiwalled carbon nanotubes (MWCNT) with β-cyclodextrin (βCD) through a physical (Phys) or a covalent approach via Steglich esterification (SE). The Phys modification approach results in Pb detection with a limit-of-detection (LoD) of 0.9 ppb, while the SE approach shows an LoD of 2.3 ppb, both of which are well below the WHO Pb concentration guideline of 10 ppb. The modified electrodes showed negligible interference with other common heavy metal ions such as Cd^{2+} and Zn^{2+}, and improved reusability. The proposed MWCNT-βCD based electrodes offer a promising technology in developing a highly affordable and sensitive electrochemical sensing system for monitoring the Pb level in drinking water.

---

[*] Part of this work will be submitted for consideration for publication as: A. U. Alam, M. M. R. Howlader, N.-X. Hu, and M. J. Deen, Electrochemical Sensing of Lead in Drinking Water Using MWCNTs and β-Cyclodextrin, April 2019. (in preparation).

4.1. Background

Accessibility to potable water is increasingly challenging in developing and in some developed countries due to contamination of their source waters by heavy metal ion and other pollutants [60]. Heavy metals such as lead (Pb) are non-biodegradable and widely distributed, and its presence in drinking water causes greater risks to human health [272]. The effects of Pb include behavioral disorder and neurodevelopmental problems in children; increased blood pressure and renal dysfunction in adults; and even cancer in kidneys, lung, or brain due to its long-term presence in source and drinking water [56–59,273]. According to World Health Organization (WHO) guidelines, the maximum acceptable concentration of Pb in drinking water should be 10 µg/L or 10 ppb.[57] However, drinking water authorities such as in Canada are proposing an even stricter limit (e.g., 5 ppb) for Pb in drinking water [57]. Major challenges in implementing the stricter limit include the lack of on-site monitoring techniques, and detecting contaminant levels across distributed water sources. Therefore, a simple, low-cost and easy to use sensor for the detection of a heavy metal such as Pb is highly desirable to maintain water safety in resource-limited areas.

Conventional analytical techniques, such as inductively coupled plasma mass spectrometry and atomic absorption spectroscopy, require qualified testing laboratories and trained personnel [274,275]. Recently, electrochemical methods have made considerable progress towards simple, on-site and low-cost detection capabilities to allow adequate time for taking safety measures in case of a contamination [123]. The electrochemical sensors, commonly referred as "electrodes", are ideal candidates as they can be fabricated with low-cost to detect Pb with higher precision and accuracy. The material system of a sensing electrode is the key ingredient in maximizing overall performance of an electrochemical analysis. Specifically, electrode materials based on carbon nanomaterials [276], metal nanoparticles [277–279], and a number of selectivity-enhancing polymeric or organic materials [280–282] have attracted tremendous research interest for their collective attributes such as high effective surface area, enhanced electron transfer, ability to be

miniaturized, and improved selectivity. More notably, nanomaterials based electrodes made up of easily available electrode materials by a facile and scalable synthesis method can be exploited to fabricate low cost electrodes for the analysis of multiple environmental targets, including heavy metals such as lead, and pharmaceutical contaminants such as acetaminophen and estrogen in drinking water [257,283]. The ability to detect multiple environmental targets at low cost and in an easy-to-use manner requires careful selection of sensing materials to provide high sensitivity and selectivity, development of simple modification approaches and user-friendly analysis steps.

In electrochemical sensing of heavy metals, the sensing materials should possess two important characteristics. First, the sensing electrode should have a good electron transfer capability. Second, the electrode materials should consist of some sort of moieties for easy capture of the heavy metal analyte. These two characteristics can be realized with the use of multiwalled carbon nanotubes (MWCNTs). MWCNTs are excellent electrode material to fabricate simple, low cost and easy-to-use electrochemical sensors because of their wide electrical potential window, fast electron transfer rate and large surface area [284]. MWCNTs can be used in different forms, such as unmodified and modified MWCNTs. For example, unmodified MWCNTs, directly grown in the form of tower, array, and thread structures, were used as an electrode material. The unmodified MWCNTs provided considerable simplicity in electrode fabrication [285]. However, unmodified MWCNTs suffer from limited sensing performances since they do not disperse well in water and most common organic solvents due to the high Van der Waals force between them that lead to aggregation and bundling [123].

Modified MWNCTs can be tailored to accomplish better sensitivity and selectivity by enhancing their dispersion quality and attaching analyte capturing sites. The dispersion quality can be enhanced through non-covalent and covalent modifications of MWCNTs. For example, non-covalent modification of MWCNTs with organic modifiers such dodecylbenzene sulfonate and Nafion showed improved sensing performances due to their improved dispersion [276]. However, non-covalent modifications cannot significantly improve the sensing performance of the electrode since individual nanotube becomes less

interconnected, thus facilitating fewer electron transfer [276]. A better electron transfer can be achieved through covalent modification of MWCNTs by chemical functionalization. Covalent modification of MWCNTs was accomplished with chemical functionalization with amino (–NH$_2$) [286] and thiol groups (–SH) [287], and electrochemical functionalization with amino acids [288]. However, the covalent modification approaches often require tedious chemical reaction procedures and thus may increase fabrication complexity.

The use of β-cyclodextrin (βCD), a porous sugar ring molecule, has shown improved electrochemical sensing performances [257]. The improved sensing performances stemmed from the facts that βCD improves the dispersion quality of MWCNTs leading to enhanced sensitivity, and the porous structure of the molecule offers better analyte capturing. In our recent studies we demonstrated that non-covalent and covalent modifications of MWCNTs with β-cyclodextrin (βCD) molecule offers enhanced sensing performance due to improved dispersion of MWCNTs in the presence of βCD, and the inclusion complex formation property of βCD towards the detection of emerging pharmaceutical contaminants such as acetaminophen and estrogen in drinking water [257,283]. The sensing performance of the electrodes was not only influenced by the presence of βCD, but also the way βCD was incorporated (i.e., non-covalent/covalent modifications) with the MWCNTs. In another study, βCD have also shown selective formation of inclusion complexes with Pb ions (Pb^{2+}) which can be exploited for the detection Pb^{2+} [282]. Also, βCD functionalized gold nanoparticles have shown selective detection of Pb^{2+} [281].

Therefore, in this work, we show that the enhanced electrochemical properties of MWCNTs can be combined with the inclusion capability of βCD through their non-covalent and covalent modifications towards the sensitive detection of Pb^{2+}. We demonstrate that the non-covalent modification of MWCNTs with βCD offers better sensing performances towards the detection of Pb^{2+} with an impact on achieving better sensitivity. On the other hand, the simple and one-step covalent modification of MWCNTs with βCD offers moderate sensitivity to Pb^{2+} sensing with an impact on improving the

sensor reusability and reliability. Thus, the type of modifications between MWCNTs and βCD, that is, non-covalently and covalently modified MWCNT-βCD, significantly controls the sensing performance of the electrodes.
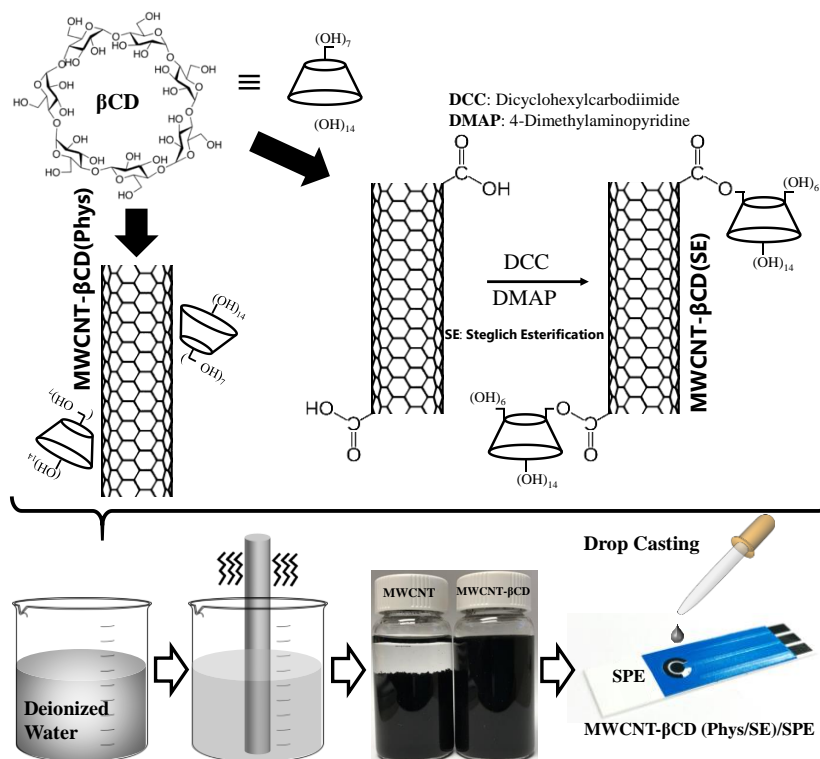
Figure 4-1. Schematic diagram of the MWCNT-βCD (Phys/SE)/SPE electrode fabrication processes.

4.2. Sample preparation

4.2.1. Non-covalent modification of MWCNT and βCD

The non-covalent modification of MWCNTs and βCD was done by physically mixing them in **D**e-**I**onized **W**ater (DIW). Twenty milligram of MWCNTs (purchased from U.S. Research Nanomaterials Inc., outer diameter (OD): 5−15 nm, length: ~50 µm, and purity: ≥ 95 wt%) was dispersed by using an ultrasonic preprocessor in 10 ml of βCD solution (2 wt%) in DIW to give a 2 mg mL^{-1} stable black suspension (Figure 4-1). The resulting suspension will be termed as MWCNT-βCD (Phys) since the modification process is based on physical mixing of MWCNTs and βCD. An aliquot of 10 μL of 2 mg mL^{-1} MWCNT-

106

βCD (Phys) solution was drop-casted on a commercial **S**creen **P**rinted **E**lectrode (SPE) (Zensor, purchased from CH Instruments, with Carbon working and counter electrode, and Ag/AgCl reference electrode). The drop-casted MWCNT-βCD (Phys) solution was dried in air for 20 min at 80 °C in an oven resulting in MWCNT-βCD (Phys)/SPE electrode (Figure 4-1).

4.2.2. Covalent modification of MWCNT and βCD

The covalent modification of MWCNTs and βCD was accomplished by a simple, one-step chemical reaction based on **S**teglich **e**sterification (SE) principle [283]. Briefly, MWCNT-COOH (purchased from U.S. Research Nanomaterials Inc., OD: 5−15 nm, length: ~50 µm, and purity: ≥ 95 wt%) was first dispersed in anhydrous *N,N*-dimethylformamide (DMF) under Ar environment. The mixture in the reactor was then sonicated to get a uniform suspension. After that 4-(dimethylamino)pyridine (DMAP) and βCD and dicyclohexylcarbodiimide (DCC) were added into the reaction mixture at 0 °C, and the resulting suspension was stirred for five hours at 20 °C. The precipitated material, MWCNT-βCD (SE)), was then filtered through a nylon membrane and washed repeatedly with DMF and acetone to remove the DCC, DMAP, and unreacted βCD. The SE process couples MWCNT-COOH and βCD through ester bonds resulting in the chemically or covalently modified MWCNTs with βCD. A uniform, black suspension of the covalently modified MWCNT-βCD (SE) was prepared by dispersing 40 mg of the black MWCNT-βCD (SE) powder into 20 mL of DIW using an ultrasonic preprocessor. Finally, an aliquot of 10µL 2 mg ml^{-1} MWCNT-βCD (SE) solution was drop-casted on SPE and then dried in air for 20 min at 80 °C in an oven resulting in MWCNT-βCD (SE)/SPE electrode (Figure 4-1). For comparison, an SPE electrode was also modified by drop casting only MWCNT (i.e., 2mg/mL MWCNT dispersed in DIW using ultrasonic preprocessor) and dried to get MWCNT/SPE.

4.2.3. Apparatus

The Pb^{2+} ion sensing was done by **D**ifferential **P**ulse **A**nodic **S**tripping **V**oltammetry (DPASV) method. The test solutions with different Pb^{2+} ion concentrations were made by dissolving appropriate amount of $Pb(NO_3)_2$ salt in 0.1 M acetate buffer (pH 5). A miniature USB powered potentiostat (EmStat3 from PalmSens) with PSTrace 5.5 data analyzer software was used in the electrochemical measurements. At the beginning of the electrochemical measurement, a deposition potential of −0.8 V was applied at the working electrode for 600 s under magnetic stirring (250 rpm) in 50 mL solution to reduce Pb^{2+} ions to Pb^0. The electrodeposited Pb atoms were then stripped from the working electrodes by anodically sweeping the electrode potential from −0.8 to −0.2 V. The optimized DPASV parameters were 4 mV, 50 mV, 50 ms and 40 mV/s for step potential, pulse amplitude, pulse time and scan rate, respectively. The peak currents were measured with respect to linear base line of the current vs. potential curve.
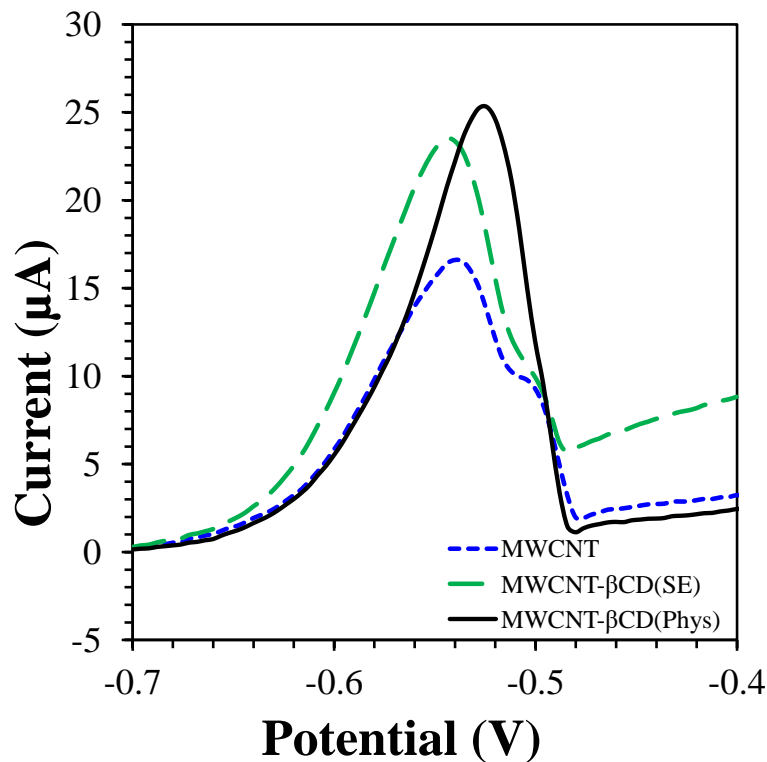
Figure 4-2. DPASV of MWCNT/SPE (blue smaller dashed curve), MWCNT-βCD (SE)/SPE (green larger dashed curve), and MWCNT-βCD (Phys)/SPE (black solid curve) recorded in 0.1 M acetate buffer (pH 5) in the presence of 1 μM (207 ppb) Pb^{2+} ion.

4.3. Results and Discussions

4.3.1. Surface area effects

There are two major approaches to improve the performance of an electrochemical sensor. First, the effective surface area of the working electrode plays a key role in achieving high sensitivity. The effective surface area of the MWCNT-βCD (Phys)/SPE and MWCNT-βCD (SE)/SPE is higher compared to that of MWCNT/SPE [283]. Second, the target-capturing ability of the sensing material system can improve its selectivity and dynamic range. A comparison of the sensing performance of the prepared MWCNT-βCD (Phys)/SPE and MWCNT-βCD (SE)/SPE with that of MWCNT/SPE in the presence of 1 μM (207 ppb) Pb^{2+} is shown in Figure 4-2. The peak current for MWCNT/SPE was 15.1 µA. The MWCNT-βCD (SE)/SPE showed increased current peak of 19.3 µA, whereas the MWCNT-βCD (Phys)/SPE showed the highest peak current of 24.4 µA. The peak potential of MWCNT-βCD (Phys)/SPE was slightly shifted towards more positive direction and this could be due to modification in the oxidation potential in the presence of βCD.

The enhanced electrochemical sensing of Pb^{2+} ion with MWCNT-βCD (Phys)/SPE can be attributed to higher amount of Pb^0 deposition during application of the deposition potential or −0.8 V. To confirm this phenomenon, we performed **S**canning **E**lectron **M**icroscopy (SEM) observations of the three different electrodes (MWCNT/SPE, MWCNT-βCD (SE)/SPE and MWCNT-βCD (Phys)/SPE) taken out of the electrochemical cell just after the deposition step. These electrodes were used since performing the stripping step will cause anodization induced-stripping of the Pb^0. Figure 4-3 shows the corresponding SEM images of the modified electrodes with low (on top, x200) and high (on bottom, x1000) magnifications. The SEM images were taken using a JEOL 7100F SEM microscope with an acceleration voltage of 15 kV and working distance of 6 mm. Figure 4-3(a) shows that the MWCNT/SPE has dendritic structures of the electrodeposited Pb^0. On the other hand, as shown in Figure 4-3(b), the MWCNT-βCD (SE)/SPE surface has island structures of the electrodeposited Pb^0, which covers more surface area to that of MWCNT/SPE. However, as shown in Figure 4-3(c), the MWCNT-βCD (Phys)/SPE surface is covered with leaf-like

structure of the accumulated Pb^0. All the low and high magnification SEM images are scaled equally. Therefore, Figure 4-3 shows that the MWCNT-βCD (Phys)/SPE has the highest amount of surface coverage by the electrodeposited Pb^0. The highest surface coverage of Pb^0 resulted in the largest peak current due to anodic oxidation stripping from the MWCNT-βCD (Phys)/SPE electrode (Figure 4-2).
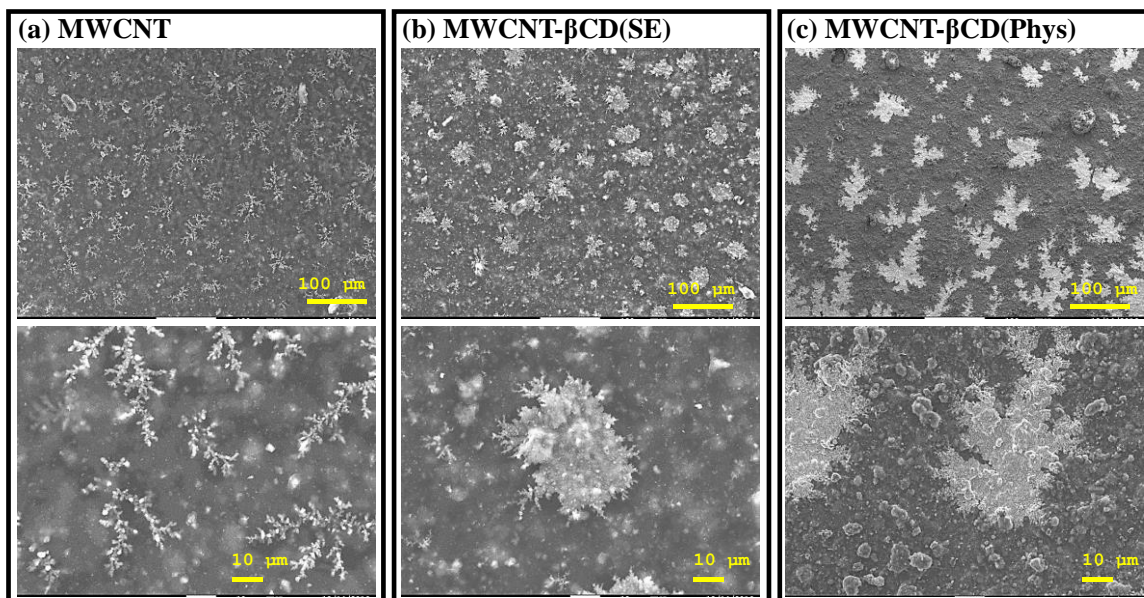
Figure 4-3. DPASV of MWCNT/SPE (blue smaller dashed curve), MWCNT-βCD (SE)/SPE (green larger dashed curve), and MWCNT-βCD (Phys)/SPE (black solid curve) recorded in 0.1 M acetate buffer (pH 5) in the presence of 1 μM (207 ppb) Pb^{2+} ion.

4.3.2. β-cyclodextrin effects

The difference in the surface coverage by Pb in the three types of electrodes could be related to the amount of βCD present with the MWCNTs. We demonstrated before that the amount of βCD is highest in MWCNT-βC (Phys) compared to that of MWCNT-βCD (SE) [283]. In fact, there are 1:2 weight ratio of βCD:MWCNTs present in the MWCNT-βCD (Phys) suspension through physical/non-covalent mixing. On the contrary, MWCNT-βC (SE) has much smaller amount of βCD since the chemical attachment of βCD with MWCNT (i.e., the Steglich esterification) depends on the amount of –COOH groups present in the precursor MWCNT-COOH material. It was found that MWCNT-βC (SE) has only ~1:10

weight ratio of βCD:MWCNTs [283]. Thus, it is confirmed that MWCNT-βC (Phys)/SPE electrode has the highest amount of βCD which are physically/non-covalently attached with MWCNTs. Hence, the increased amount of βCD in MWCNT-βCD (Phys)/SPE facilitated improved electrochemical sensing of Pb^{2+}.

The improved electrochemical sensing performance of MWCNT-βCD (Phys)/SPE compared to that of MWCNT/SPE and MWCNT-βCD (SE)/SPE could also be attributed to the formation of the inclusion complexes between βCD and Pb^{2+}. The βCD molecule has a porous structure with an average diameter of 18–20 nm which is capable to form host-guest interaction based inclusion complexes with other molecules. A number of researches had investigated its host-guest interaction properties with phenolic organic molecules and steroid hormones [257,283]. These organic molecules and hormones are attracted to the hydrophobic inner core of the βCD molecule and facilitates redox-based electrochemical sensing of the guest molecules.

The βCD also showed affinity towards metal ions. For example, βCD functionalized gold-iron nanoparticles was used for selective and sensitive colorimetric sensing of Cr^{6+} ion. In another study [289], carboxymethyl-β-cyclodextrin polymer modified Fe_3O_4 nanoparticles (CDpoly-MNPs) were utilized for selective removal of Pb^{2+}, Cd^{2+}, and Ni^{2+} ions from water. The CDpoly-MNPs showed preferential adsorption towards Pb^{2+} ions with an affinity order of $Pb^{2+} \gg Cd^{2+} \gg Ni^{2+}$. Moreover, βCD functionalized gold nanoparticles were used for the selective detection of Pb^{2+} ions from aqueous solution. The electrochemical evidence of the interaction between the Pb^{2+} ions and the βCD was also described where the formation constants of surface inclusion complexes between Pb^{2+} and βCD were electrochemically measured (727.5 ± 20.2 M^{-1}) using a carbon paste electrode [282],[290]. Therefore, in this study, the inclusion complex formation of βCD has been combined with the superior electrochemical properties of MWCNTs towards sensing of Pb^{2+} ion.
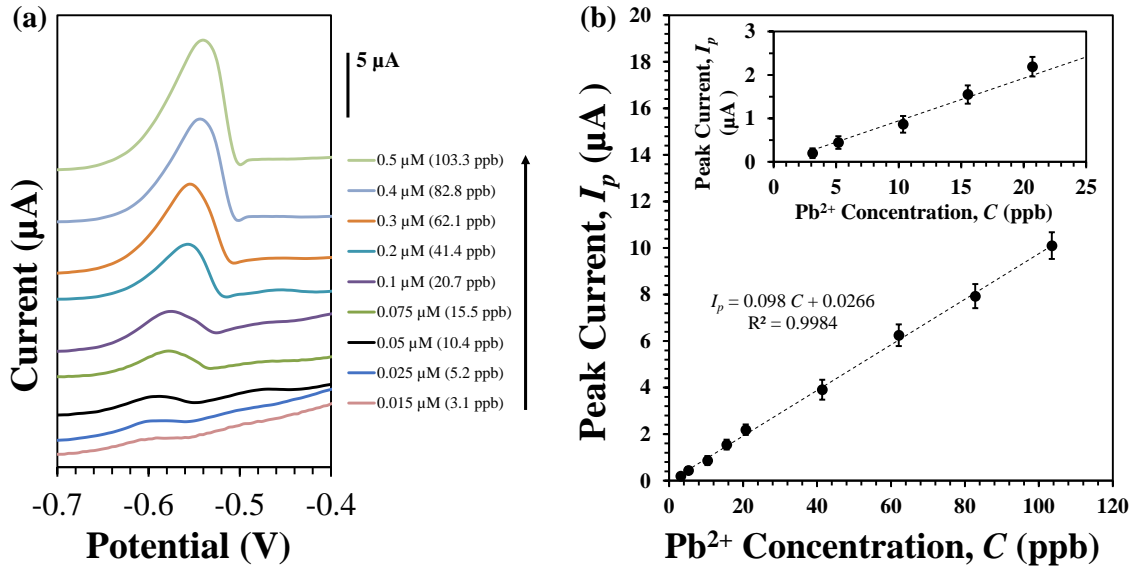
Figure 4-4. DPASV of MWCNT/SPE (blue smaller dashed curve), MWCNT-βCD (SE)/SPE (green larger dashed curve), and MWCNT-βCD (Phys)/SPE (black solid curve) recorded in 0.1 M acetate buffer (pH 5) in the presence of 1 μM (207 ppb) Pb^{2+} ion.

4.3.3. Sensing mechanisms

The linear detection range of MWCNT-βCD (Phys)/SPE electrode for the detection of Pb2+ ion was measured to determine its feasibility for use in drinking water monitoring. Figure 4-4 shows the DPASV curves and the corresponding linear calibration curve in the presence of 0.015−20 μM (3.1–103.3 ppb) Pb^{2+} ion. The optimized DPASV conditions used in these measurements are similar to that of Figure 4-2. Figure 4-4(a) shows that the current peak for lowest Pb^{2+} ion concentration is located at −0.6 V. The peak current slightly shift towards more anodic value with the increased concentration of Pb^{2+} ion. This peak shifting could be due to diffusional control reaction influenced by concentration difference [291]. Figure 4-4(b) shows the calibration curves for the concentration ranges of 0.015–20 μM (3.1-103.3 ppb). The error bars for each data point was calculated by taking six measurements using newly prepared sensors each time and by multiplying Student's *t*-distribution *k* value of 2.57 to get 95% confidence interval. The linear regression equations can be expressed as $I_p = 0.098\,C + 0.0266$, where I_p is the peak current (in μA) and C is the Pb^{2+} concentration (in ppb).
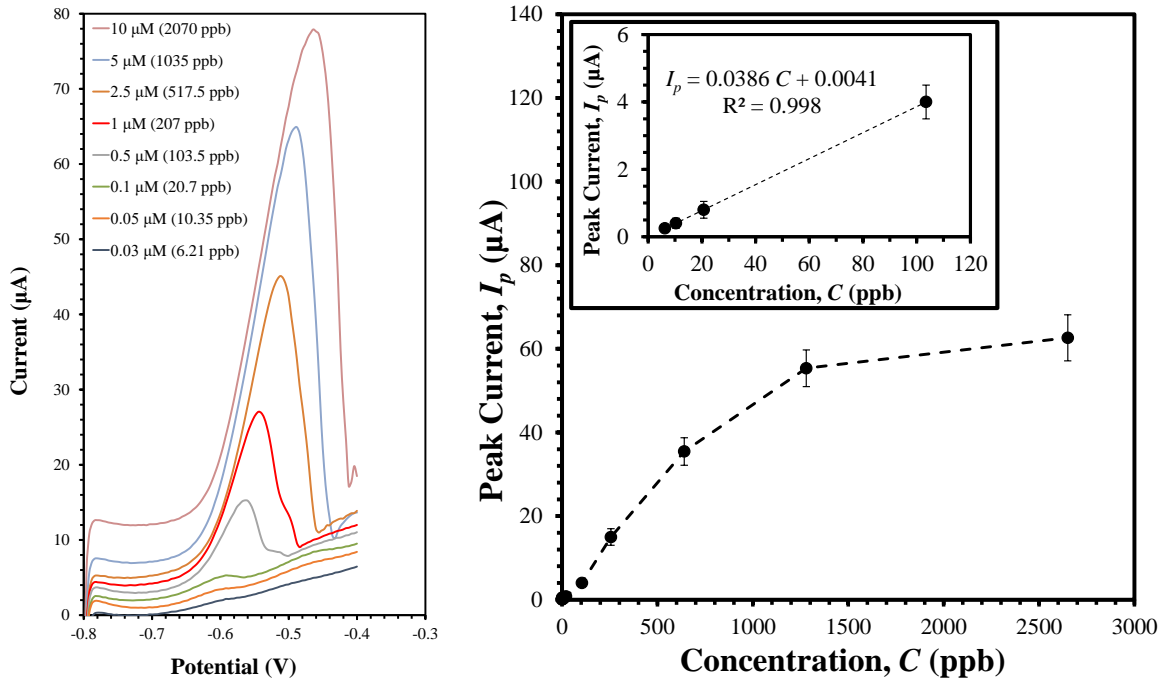
Figure 4-5. (a) DPASV of MWCNT-βCD (SE)/SPE in 0.1 M acetate buffer (pH 5) in the presence of 0.025−20 μM (6.2–103.3 ppb) Pb^{2+}. (b) Calibration curve (i.e., peak current vs Pb^{2+} concentration) for MWCNT-βCD (Phys)/SPE. All of the experiments were done with a deposition potential of −0.8 V for 600 s under magnetic stirring before measurements.

The sensitivity of the MWCNT-βCD (Phys)/SPE electrode is 98 nA/ppb. The limit of detection (LoD), defined as LoD = 3s/m (where, s is the standard deviation of the blank solution (0.03 μA), and m is the slope of the calibration curve), was estimated to be 0.9 ppb. Therefore, the linear range and the LoD value of the MWCNT-βCD (Phys)/SPE sensor to detect lead concentration in drinking water are much better than those specified by the WHO guideline. The LoD value is compared with other recent reports for the detection of Pb^{2+} using electrodes based on MWCNTs, as shown in Table 4-1. It is observed that the MWCNT-βCD (Phys)/SPE sensor has comparable linear range and one of the lowest limit of detection (LoD) for the detection of Pb^{2+}. For comparison, the linear range and calibration curves of MWCNT-βCD (SE)/SPE electrode was also measured and are shown in Figure 4-5. The MWCNT-βCD (SE)/SPE electrode showed a linear detection range of 6.2 – 103.5 ppb with an LoD of 2.3 ppb. Thus, the sensitivity of the MWCNT-βCD (SE)/SPE electrode is 38.6 nA/ppb, which is ~2.5 times lower than that of MWCNT-βCD

(Phys)/SPE. However, the MWCNT-βCD (SE)/SPE electrode showed better performance in terms of stability.
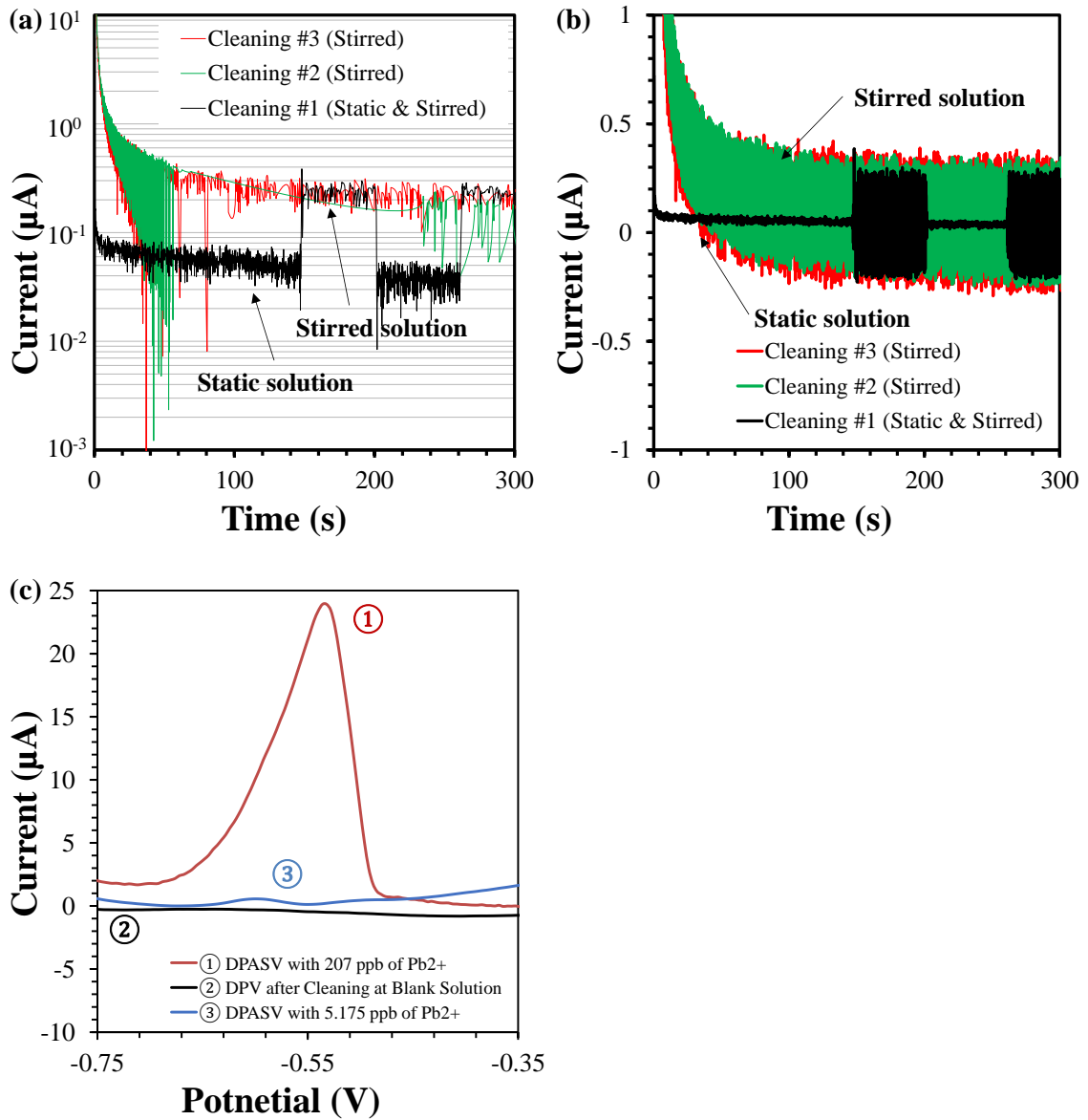
Figure 4-6. Electrochemical process of electrode surface cleaning/regeneration by applying a +0.31 V under magnetic stirring for 300 s. The resulting current response of the electrodes are shown with logarithmic (a) and (b) general numbers with respect to elapsed time. (c) The DPASV curves for new sensor (①), cleaned sensor (②) and reused sensor ③ for the detection of 207 ppb, blank and 5.2 ppb of Pb^{2+}.

Table 4-1: Comparison of the MWCNTs-based electrochemical sensors for Pb^{2+}

Electrode	Modifications	Linear Range	Detection Limit	Comments	[Ref.]
MWCNT-GC	Poly(PCV)/Bi	1-200 ppb	0.4 ppb	MWCNT modified with poly(PCV) and Bi film	[292]
MWCNT-GC	BiOCl/Nafion	5-50 ppb	0.57 ppb	Bismuth-oxychloride particle-MWCNT composite	[293]
MWCNTs/Bi-GC	-SH, -NH2, -COO-, -OH	2-50 ppb	0.3 ppb	N-doping and thiol-modification of MWCNT	[287]
AuNPs-CNFs-GCE	Isopropanol/Nafion	20.7-207.2 ppb	20.7 ppb	AuNPs/CNFs fabricated via electrospinning and in situ thermal reduction	[294]
CNT Thread	None	207-1035 ppb	0.12 ppb	Electrochemical cell fabricated by CNT thread	[295]
MWCNT-IIP/Pt	Ion Imprinted polymer	1-5 ppm	0.02 ppb	Binding sites for lead ions sculpted with lead ion as template and NNMBA-crosslinked polyacrylamide as the solid matrix on MWCNTs	[296]
MWCNT-βCD	Physical, Steglich esterification	3.1-103.3 ppb	0.9 ppb	Physically and Steglich esterification modified MWCNT and βCD	This work

4.3.4. Sensing performances

Stability and reusability

The stability of the MWCNT-βCD (Phys)/SPE and MWCNT-βCD (SE)/SPE electrodes were investigated to examine their repeatability and reusability. The two types of electrode were repeatedly reused in similar and different concentrations of Pb^{2+} solutions. Before reusing the electrodes, they were electrochemically cleaned/regenerated by applying 0.31 V under magnetic stirring in a blank solution for 300 s to desorb the Pb molecules from the electrode surface, as shown in Figure 4-6. The cleaning procedure was found to be more effective and faster when magnetic stirring was used, as shown in Figure 4-6(a) and Figure 4-6(b). Figure 4-6(c) shows the DPASV response of a newly prepared MWCNT-βCD (Phys)/SPE electrode with 207 ppb of Pb^{2+} (curve ①), which was then electrochemically cleaned to give a DPASV curve in blank solution with no peak current (curve ②), signifying successful regeneration of the electrode. After that, the same electrode was used to DPASV measurement of 5.2 ppb of Pb^{2+} with peak current of 0.4 µA (curve ③), which is within the error bar range of the calibration line of MWCNT-βCD (Phys)/SPE. However,

the MWCNT-βCD (Phys)/SPE electrode showed stable sensing performance when reused/regenerated for four consecutive measurements of 207 ppb of Pb^{2+} solutions.

On the other hand, the MWCNT-βCD (Phys)/SPE electrode performed at least six consecutive reuse/regeneration cycles with negligible degradation in sensing performance when low concentrations of Pb^{2+} solution (in the range of 5−20 ppb) were used. Therefore, the MWCNT-βCD (Phys)/SPE electrode tends to degrade faster when measuring higher concentration of Pb^{2+}. This could be due to dissolution of βCD molecule from the electrode surface when increased amounts of Pb^{0} molecules adsorb which ultimately leads to delamination and disintegration of the MWCNTs network during the electrode regeneration step. In contrast, the MWCNT-βCD (SE)/SPE electrode showed reusability for at least 10 reuse/regeneration cycles at both low and high concentrations of Pb^{2+}. The better reusability of the MWCNT-βCD (SE)/SPE electrode can be attributed to the chemical/covalent attachment of βCD with MWCNTs which is stronger than that of the MWCNT-βCD (Phys) that provides better electrode surface adhesion during cleaning/regeneration steps. Consequently, the MWCNT-βCD (SE)/SPE can provide better reusability when measuring higher levels of Pb^{2+}, and the MWCNT-βCD (Phys)/SPE can offer better sensitivity as well as reusability when lower levels of Pb^{2+} is measured.

Cost-effectiveness of the fabrication

The MWCNT-βCD (Phys)/SPE and MWCNT-βCD (SE)/SPE electrodes are low cost and can be used utilized in resource limited areas. The low cost of fabrication of these electrodes is due to the simple MWCNTs modification processes (covalent/non-covalent), use of simple equipment and low-cost commercial carbon SPE electrodes. Furthermore, apart from the electrochemical cleaning/regeneration procedure described above, the SPE electrode can also be reused by simply wiping off the MWCNT-βCD from its surface using Kim Wipes and cleaning with solvents like isopropyl alcohol followed by drop-casting another aliquot of 10 µL of MWCNT-βCD solution. The SPE electrode showed negligible degradation in sensing performance over at least 50 cycles of cleaning and remaking of the electrodes.

Table 4-2: Breakdown of materials cost to fabricate a single MWCNT-βCD (Phys/SE)/SPE electrode

Name of Materials	Unit Price	Price (each)	Price (for one sensor)	Price for one experiment
MWCNTs	$125/25gm	$.005 (each mg)	0.02 mg × $0.005 = $0.0001 [10 µL solution with 2 mg/mL concentration of MWCNT]	
βCD	$220/100gm	$0.0022 (each mg)	0.02mg × $0.0022 = $0.00044 [10 µL solution with 2 mg/mL concentration of βCD]	
SPE	$50/40 pieces	$1.25 (each)	$1.25 (each)	
MWCNT-βCD			2.64×10^{-3} Cost of one drop of **MWCNT-βCD** with respect to one **SPE** = 2.64×10^{-3} / $1.25 = 0.21%	2.64×10^{-4} [for reusing 10 times]
MWCNT-βCD /SPE			$1.25+$0.0001+$0.00044 = $1.25054	$0.0250108 [for 50 measurements]

The reusability of the SPE electrode provides further economic benefits to reduce the overall cost to run a single experiment. Table 4-2 shows the breakdown of materials cost (in US$) to fabricate a new MWCNT-βCD (Phys)/SPE or MWCNT-βCD (SE)/SPE electrode and to run a single experiment to highlight the cost-effectiveness of the proposed Pb^{2+} sensor. Table 4-2 shows that the materials cost a 10 µL drop of MWCNT-βCD (Phys/SE) required to fabricate a single sensor is only $0.0026 which is only 0.21% compared to the price of a single SPE ($1.25). Additionally, the prices included on Table 4-2 can be reduced more since it lists the retail prices. Also, if a MWCNT-βCD (Phys/SE)/SPE sensor is cleaned/regenerated for 10 times, then the cost of each measurement will be much smaller. Therefore, the MWCNT-βCD (Phys/SE)/SPE electrode can be fabricated with extremely low cost. The fabrication costs can be further reduced by fabricating the SPE electrode also instead of using the commercial one.

Interference studies

An important performance parameter of an electrochemical heavy metal sensor is its selectivity in the presence of other interfering ions in the solution. The selectivity of the

MWCNT-βCD(Phys)/SPE electrode with 103.5 ppb of Pb^{2+} was measured in the presence of 207 ppb of Cadmium (Cd^{2+}) and Zinc (Zn^{2+}) ions (Figure 4-7). The Cd^{2+} peak was clearly separated from the Pb^{2+} peak. Also, the Pb^{2+} peak showed negligible change in the peak current. However, the Zn^{2+} peak was not observed since the oxidation potential of Zn^{2+} is lower than −1.2 V and the deposition potential (−0.8 V) did not cause any deposition of Zn^{0} molecule on the electrode surface. The peak current for 207 ppb of Cd^{2+} was very small compared to that of Pb^{2+}. Therefore, the MWCNT-βCD(Phys)/SPE electrode showed more selectivity towards Pb^{2+} ion.
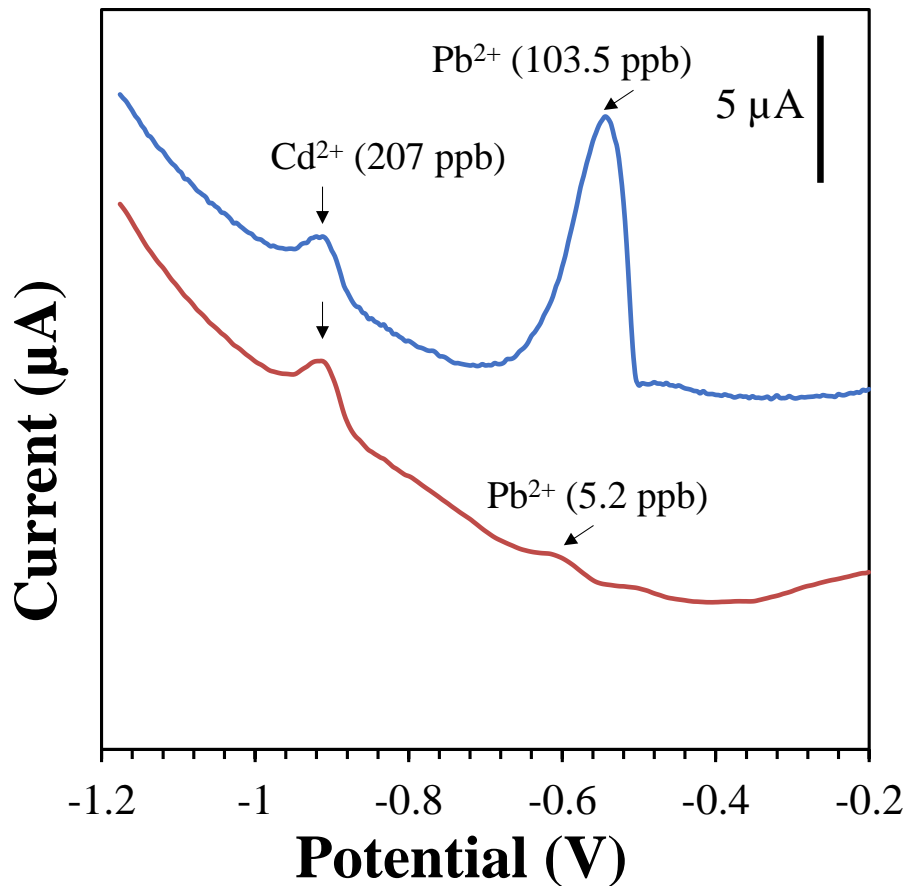
Figure 4-7. DPASV of MWCNT-βCD(Phys)/SPE with 5.2 ppb and 103.5 ppb of Pb^{2+} in the presence of 207 ppb of Zn^{2+} and Cd^{2+} in 0.1 M acetate buffer (pH = 5).

4.3.5. Perspectives of the sensor

A careful comparison between the sensitivity/LoD and reliability/reusability of MWCNT-βCD (Phys)/SPE and MWCNT-βCD(SE)/SPE electrodes shows that the presence of βCD has a role in determining their sensing performances. First, the sensitivity/LoD of the electrode is controlled by the amount of βCD present with the MWCNTs. For example, the MWCNT-βCD(Phys)/SPE had higher number of βCD than that of MWCNT-βCD(SE)/SPE, which allowed higher sensitivity and lower limit of detection. It is worth noting that MWCNT-βCD(SE)/SPE can only have a maximum amount of βCD which is limited by the number of –COOH (~2.5 wt%) present in the precursor MWCNT-COOH. Second, reliability/reusability of the electrode is controlled by the robustness of the βCD attached to the MWCNTs. For example, MWCNT-βCD(SE)/SPE had covalently attached βCD with MWCNTs which offered improved robustness of the electrode that resulted in better reliability/reusability to that of MWCNT-βCD (Phys)/SPE. An optimum sensing performance in terms of both the sensitivity/LoD and reliability/reusability can be achieved through accommodating higher number of covalently attached βCD with the MWCNTs.

4.4. Conclusions

In summary, in this research work, we developed low-cost and easy-to-use electrochemical sensors for the determination of Pb^{2+} using non-covalent/physical and a one-step covalent modifications (Steglich esterification) of MWCNT with βCD. The modified MWCNT-βCD electrodes demonstrated excellent sensing performance for the detection of Pb^{2+} with limits-of-detection of 0.9 and 2.3 ppb for the non-covalent/physical and covalent modifications, respectively. The physically modified MWCNT-βCD based electrode exhibited the higher sensitivity, whereas the covalently modified MWCNT-βCD showed better reliability and reusability, which were governed by the amount of βCD and type of βCD modifications, respectively. The electrodes fabrications and materials were of extremely low cost which was calculated to be only $2.64 per 1000 MWCNT-βCD modifications. The final cost of each measurement could be further reduced because of the

reusability of the MWCNT-βCD based electrodes for at least four times. The sensors also showed good selectivity in the presence of other interfering heavy metal ions such as Zn^{2+} and Cd^{2+} with very high concentrations. The developed sensor may be used in low-cost and point-of-care sensing systems for drinking water quality monitoring.

Chapter 5

Noise in MWCNTs and nanomaterials based water monitoring sensors[*]

The sensitivity of electrochemical sensors depends on several design parameters, such as electrode area and materials properties. However, the fidelity of the signals provided by an electrochemical sensor might be limited by random fluctuations, often referred to as noise, which usually is described by signal-to-noise ratio (SNR) of the sensor.

The noise behavior of the electrochemical electrodes is not well-studied and rarely addressed in the literature [297–299]. Therefore, an experimental study of noise in electrochemical sensors is carried out. The noise levels were examined for several designs and conditions of the electrochemical sensors, as follows. Two electrolytes were used, in particular, Phosphate Buffer Saline (PBS) and Potassium Ferricyanide ($K_3[Fe(CN)_6]$). The electrode materials and fabrication were Screen Printed Electrode (SPE), and SPE functionalized with Multi-Walled Carbon Nanotubes (MWCNT) and β-cyclodextrin (βCD).

The noise of the three-electrode sensors was measured at various biasing conditions in a set-up similar to potentiostat for current-voltage measurement, adding low-noise amplifiers and dual-input spectrum analyzer (SR785 Dynamic Signal Analyzer). The Power Spectral Density (PSD) of the noise in currents and voltages, the cross-correlation and coherence are obtained from the spectrum analyzer, which acquires the signals in the time domain and uses Fast Fourier Transform (FFT) to convert and analyze the signals in the frequency domain. The noise experiments indicate that the bias voltages and current have negligible

---

[*] Part of this work will be submitted for consideration for publication as: A. U. Alam, O. Marinov, S. Majumder, C. H. Chen, and M. J. Deen, Study of noise in electrochemical sensors, April 2019. (in preparation)

influence on the levels of the $1/f$ noise. This is a favorable property of the electrochemical sensor applications, having similar noise level while varying the potentials of the reference and working electrodes in a wide range in excess of 0.5 V. Functionalization of the SPE electrode increases the noise levels, but the increase of the sensitivity is much higher. Thus, the functionalization improves the SNR.

5.1. Background

The study of noise mechanisms in electrochemical sensors is critical for accurate in-vivo detection of analytes [300]. The detection efficiency of an electrochemical sensor depends on its ability to recognise small changes in the transduction signals that also brings uncertainty [297]. Therefore, an improved understanding of the sources of noises in an electrochemical sensor is crucial to accomplish high sensitivity and low limit of detection. Understanding of noise sources can help in developing new models and designs for the electrochemical sensors towards an improved system level integration. For example, the noise behavior of an electrochemical sensor can provide insights into the optimization of sensor performance. The sensor performance is generally modified with different nanomaterials and functionalization. While noise phenomena are well-understood in solid-state electrical and electronic devices, noise in electrochemical sensing systems with solid-liquid interfaces are rarely investigated.

Noise fluctuations have been well-understood in common electronic components. These fluctuations are generally classified in three different types based on their spectral densities, such as thermal noise, shot noise and flicker noise [301]. The noise power spectral density (PSD) of the Johnson-Nyquist thermal current noise of a resistor is expressed as:

$$S_R = 4k_BTR \tag{5-1}$$

where k_B is the Boltzmann's constant, T is the temperature and R is the resistance of the resistor. Shot noise is an electronic noise that comes from the discrete nature of electric charge (when overcoming a barrier). Equation (5−1) shows that thermal noise is

proportional to temperature and does not depend on frequency. However, shot noise does not depend on both temperature and frequency. The frequency independent behavior of the thermal and shot noise gave rise to their name White noise, in analogy with the spectrum of the white light. In contrast, the flicker noise PSD depends reciprocally on the frequency, therefore, is often called $1/f$ noise. For devices showing these three types of noises, the $1/f$ noise is the dominant one at lower frequencies.

Many experimental and theoretical studies on $1/f$ noise suggested that the $1/f$ noise is inversely proportional to active area in electronic devices [302], and the electrode area of electrochemical device [303]. Another study made some conclusions about the type of graphitic electrode material that can minimize flow-associated noise [304]. The major contribution to the understanding of noise in electrochemical systems originates from faradaic interfacial processes, which were divided into two fundamental areas such as: (1) the method of creating perturbation of an equilibrium followed by measuring the induced current and the associated transfer function of the interface phenomena [305,306], and (2) the noise that naturally occurs in the interfaces as homogeneous processes [307–314]. In both cases, a few fundamental insights into noise processes have emerged. Specifically, fundamental noise sources such as Johnson-Nyquist thermal noise and shot noise have been discussed, are ignored here due to their very low magnitudes compared to $1/f$ noise.

In recent years, nanomaterials have attracted great attention in electrochemical sensing and biosensing applications due to their unique electronic, physical and chemical properties leading to highly sensitive and robust sensing/biosensing platforms [135]. In particular, carbon based nanomaterials such as carbon nanotubes, were widely investigated as an efficient electrode modifier that enhanced the efficiency of the electrochemical sensors/biosensors [136]. For example, modification of sensing electrodes with multiwalled carbon nanotubes (MWCNT) with/without β-cyclodextrin (βCD) resulted in improved charge transfer efficiency and better sensing performances [257,283]. However, the behavior of noise in electrochemical sensors that operate in the voltammetric modes with or without nanomaterials modifications is still not well-understood.

In this work, we realize an experimental set up that mimics the voltammetric operation conditions, and then study the noise of the unmodified/modified SPE electrodes under different conditions at low frequencies. The effect of the bias voltage and the two types of electrolyte solutions (Phosphate Buffer Saline (PBS) and Potassium Ferricyanide ($K_3[Fe(CN)_6]$)) on the noise level is investigated. The effect of using sensing electrodes functionalized with MWCNT and βCD on the electrochemical potential and noise level is investigated. We also study the noise of palladium/ palladium oxide (Pd/PdO) based pH sensor (in potentiometric configuration), amine-modifed carbon electrode based free chlorine sensor (in voltammetric configuration), and PEDOT:PSS/silicon based thermistors. The experimental set up is described in section 5.2, followed by noise characterization results and discussions in section 5.3.

5.2. Experimental setup

5.2.1. Materials and reagents

Carbon based Screen Printed Electrodes (SPE) (Zensor), a glass based Ag/AgCl reference electrode and platinum counter electrode were purchased from CH Instruments. Potassium Ferricyanide ($K_3[Fe(CN)_6]$) in the form of powder and Phosphate Buffer Saline (PBS) tablets were purchased from Sigma. The $K_3[Fe(CN)_6]$ powder was dissolved into deionized (DI) water to get 5 mM concentration. Each PBS tablet was dissolved into 200 ml of DI water to get 0.01 M PBS buffer with pH 7.4.

5.2.2. Preparation of electrodes

Modifications of the SPE was done with Multi-Walled Carbon Nanotubes (MWCNT) and β-cyclodextrin to get three types of modified SPEs such as: MWCNT/SPE, MWCNT-βCD(Phys)/SPE and MWCNT-βCD(SE)/SPE. The MWCNT/SPE electrode was modified with only pure MWCNT. The MWCNT-βCD(Phys)/SPE electrode was modified by MWCNT which was non-covalently (i.e., physically) functionalized with βCD. The MWCNT-βCD(SE)/SPE electrode was modified by MWCNT which was covalently (i.e.,

Steglich esterification) functionalized with βCD. The detailed MWCNT modification processes were described previously in Chapter 3.

The preparations of the pH, free chlorine and temperature sensors are described in Chapter 6. In summary, the Pd/PdO based pH sensing electrode was prepared according to a modified spin-coating technique, in which Pd/PdO thin film was fabricated on a Kapton polyimide tape using thermolysis of Pd-organometallic precursor ink, and then transferred to another glass substrate. The free chlorine sensor was fabricated by a carbon electrode electrochemically modified by ammonium carbamate. The temperature sensor consists of two pairs of PEDOT:PSS and silicon thermistors connected in a Wheatstone-bridge configuration. The PEDOT:PSS thermistor was fabricated by simply drop-casting on a glass substrate. The silicon thermistor was fabricated by sputter-deposited contact and subsequent dicing and gluing on a glass substrate.

5.2.3. Apparatus

The noise measurements of the electrochemical sensors were done in a three electrode configuration similar to a potentiostat configuration that performs cyclic voltammetry or differential pulse voltammetry, as shown in Figure 5-1. A dynamic signal analyzer (SR785, Stanford Research Systems) was used to acquire and analyze the noise signal coming from the working electrode (Channel B of SR785) (i.e., bare SPE, MWCNT/SPE, MWCNT-βCD(Phys)/SPE and MWCNT-βCD(SE)/SPE electrodes). The reference and the counter electrodes were connected to a low-noise voltage amplifier (SR560, Stanford Research Systems) to the negative and positive input terminals, respectively. Another low noise current amplifier (SR570, Stanford Research Systems) was used to amplify the output current of the working electrode. A custom-made battery cell with potentiostat was used as the bias voltage source. Three multimeters were used to monitor the voltage values at the biasing battery source, the reference electrode and the output of the current amplifier which corresponds to current from the working electrode by the factor of the amplifier gain ranging from 0.5 to 10 μA/V.

Cross-correlation and coherence between voltages and currents were examined. The coherence was low, always below 30%, which indicates that the noise at different terminals of the electrodes are independent.
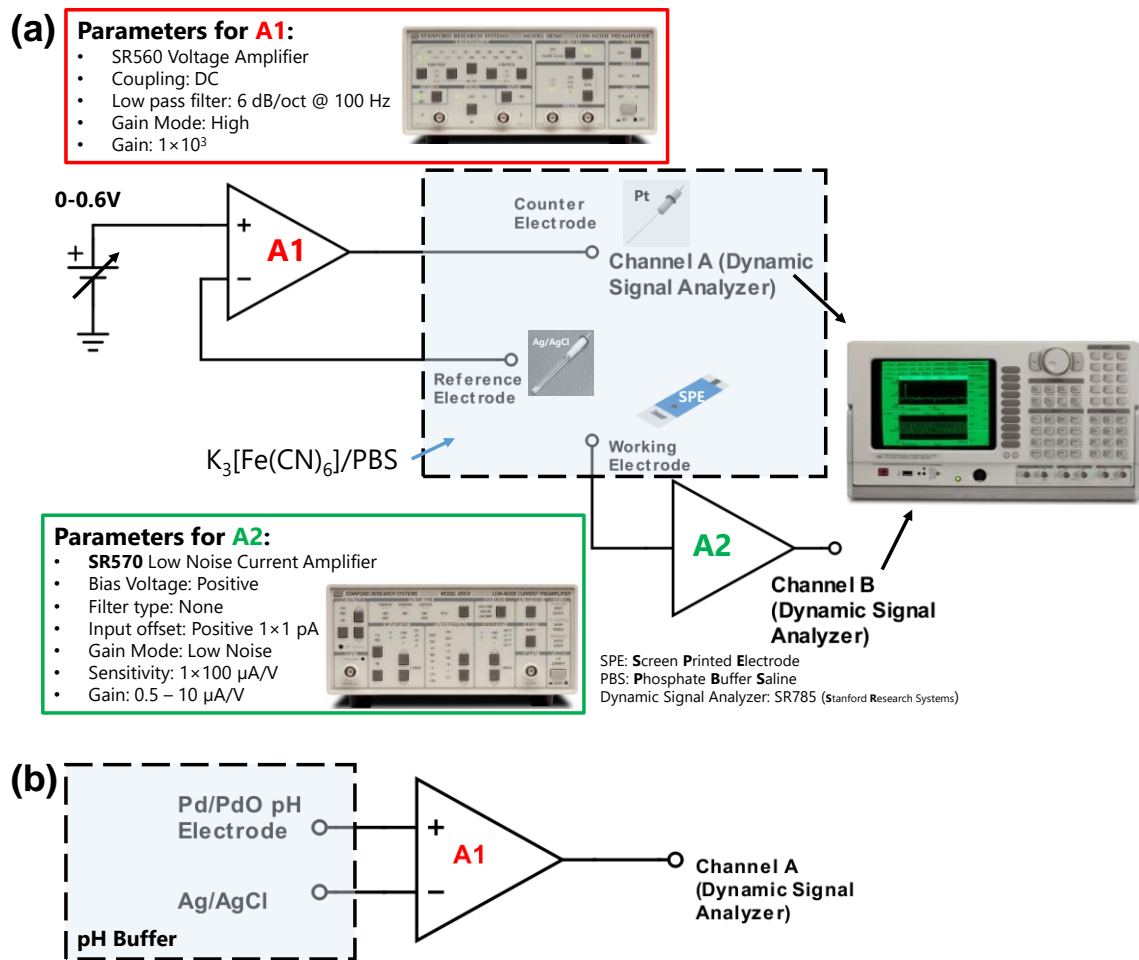
Figure 5-1. The experimental setup for the noise measurement of (a) SPE electrodes modified with multi-walled carbon nanotubes and β-cyclodextrin, and amine modified carbon electrodes; (b) Pd/PdO based pH sensing electrode.

Table 5-1: The noise measurement setup with different electrolytes, sensing electrodes and biasing voltages.

Type of Electrolyte	Type of Electrode		Bias Voltages
$K_3[Fe(CN)_6]$ (5mM)	SPE		0.0 V 0.1 V 0.2 V 0.3 V 0.4 V 0.5 V 0.6 V
	MWCNT-SPE		
	MWCNT-βCD(Phys)/SPE		
	MWCNT-βCD(SE)/SPE		
PBS (pH 7.4, 0.01 M)	SPE		
	MWCNT/SPE		
	MWCNT-βCD(Phys)/SPE		
	MWCNT-βCD(SE)/SPE		
pH Buffer	Pd/PdO based pH sensing electrode		-
PBS (pH 7.4, 0.01 M)	Amine modified carbon electrode		0.0 V 0.1 V
Tap Water	Silicon and PEDOT:PSS thermistors		-

5.2.4. Noise data processing and analysis procedure

The noise data processing and analysis procedure is schematically shown in Figure 5-2. In step 1, the raw data of noise signal from the Dynamic Signal Analyzer (SR785) equipment is extracted to a personal computer in *.csv file format using VEE Pro 9.33 software developed by Keysight Technologies. The extracted noise spectra contained 60 Hz harmonics signal which was due to interference from electrical power networks. In step 2, the 60 Hz harmonics were removed from the spectra using a MATLAB code which allowed for faster data processing. In step 3, the clean data from the MATLAB processing was then scaled with the gain of the current amplifier (SR570). In step 4, the current voltage (I-V)

characteristics were obtained along with other noise related parameters (not shown in the Figure 5-2).
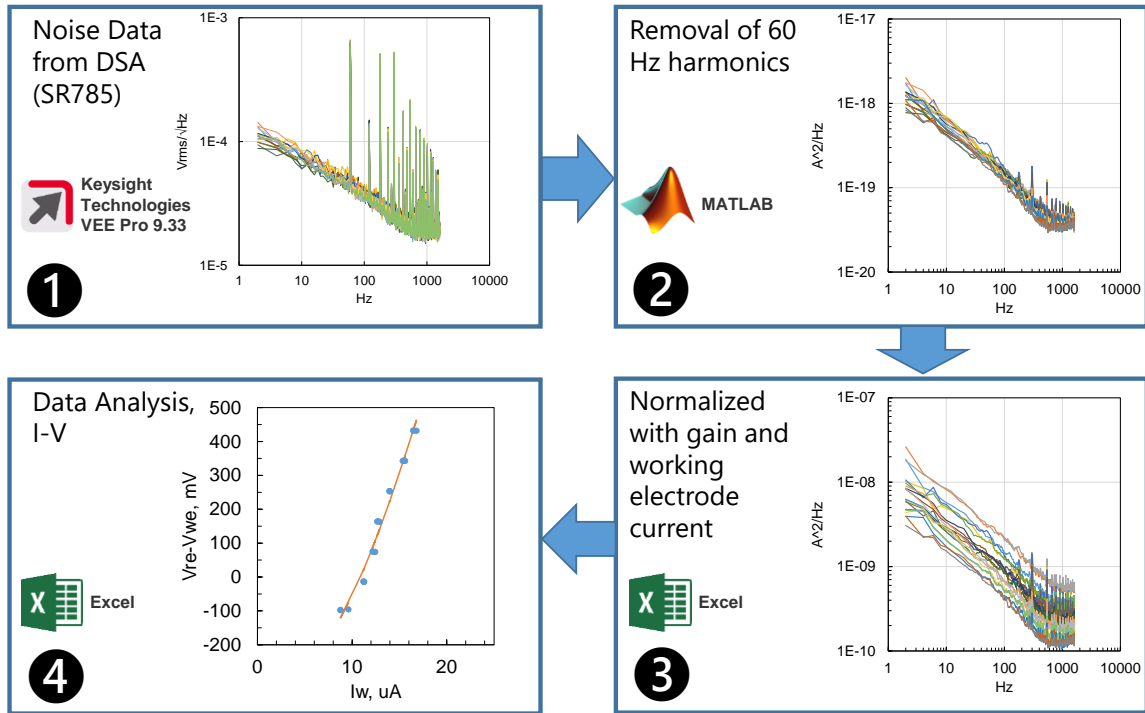
Figure 5-2. Noise data extraction and analysis procedure: ❶ extraction of data from SR785 using VEE Pro 9.33 software, ❷ removal of 60 Hz harmonics using MATLAB, ❸ normalization of the signal with gain of the current amplifier and output current of the working electrode, and ❹ additional analysis of noise data (for example, the current-voltage characteristics) using Microsoft Excel.

5.3. Results and discussions

The noise measurement setup for the electrochemical sensing electrodes was based on the potentiostat three-electrode configuration, since the actual electrochemical measurements also use the same configuration. In this potentiostat configuration (Figure 5-1), we analyzed the current noise fluctuations at the working electrode. In electrochemical sensing measurements, the applied bias voltages are scanned between two voltages, which is usually in the range of few hundred millivolts. Therefore, we also used multiple bias voltages from 0 V to 0.6 V to analyze the effect of the bias voltages on the senor noise. Figure 5-3 shows the power spectral density (PSD) spectra of the noise current when the

electrodes were immersed into $K_3[Fe(CN)_6]$ (a-d) and PBS (e-h) solutions. In each type of electrode, the bias voltage applied between the reference and counter electrodes was set at 0, 0.1, 0.2, 0.3, 0.4, 0.5 and 0.6 V. The frequency range of the PSD spectra is from 2 Hz to 1.6 kHz. Each spectrum is an average of 64 acquisitions.

5.3.1. Noise in the pharmaceutical/heavy metal sensor

Noise coherence/correlation in three-electrode system

To investigate noise correlation between the working electrode and the reference/counter electrode, we performed correlation/coherence measurement with the Dynamic Signal Analyzer (SR785) equipment. First, we performed correlation between the between the voltage and currents of all electrode terminals. However, there was no significant correlation between the terminals. This signifies that the noise originating from the electrode terminals were based on independent processes that only happens within the vicinity of the corresponding electrode and does not affect the other two electrodes. After that, we performed coherence measurement which showed coherence value of less than 30%, again signifying negligible coherence between the noise sources of all electrode terminals.

Effect of biases/materials/solutions on noise characteristics

The current noise PSD spectra on each figure of Figure 5-3(a-d) and Figure 5-4(a-d) shows seven noise PSD spectra which were recorded with seven different applied bias voltages ranging from 0 V to 0.6 V. There is no specific pattern or variation of the seven different noise PSD spectra showing very weak dependence on the applied bias. However, there is small increase in the noise PSD level from $\sim 10^{-18}$ A²/Hz to $\sim 10^{-17}$ A²/Hz in lower frequency range (2-10 Hz) when the bare SPE electrode is modified with MWCNT and MWCNT-βCD(Phys/SE), as shown in Figure 5-3(a-d) and Figure 5-4(a-d). The increase in the noise level with the addition of MWCNT on the SPE electrode may indicate that the noise behavior are due to the inherent materials properties of the electrodes. Again, the noise may also be related to the concentrations of ions of the solutions going into the working electrode. However, when the electrodes are changed from $K_3[Fe(CN)_6]$ solution to PBS

buffer solution, the noise level remains almost the same, which means that the noise does not depend on the type or concentration of ions that are present in the electrolyte solution. Thus, the noise behavior that are observed in Figure 5-3(a-d) and Figure 5-4(a-d) are simply due to characteristics of each electrode itself.

(a) $K_3[Fe(CN)_6]$-SPE

(b) $K_3[Fe(CN)_6]$-MWCNT

(c) $K_3[Fe(CN)_6]$-MWCNT-βCD(Phys)

(d) $K_3[Fe(CN)_6]$-MWCNT-βCD(SE)
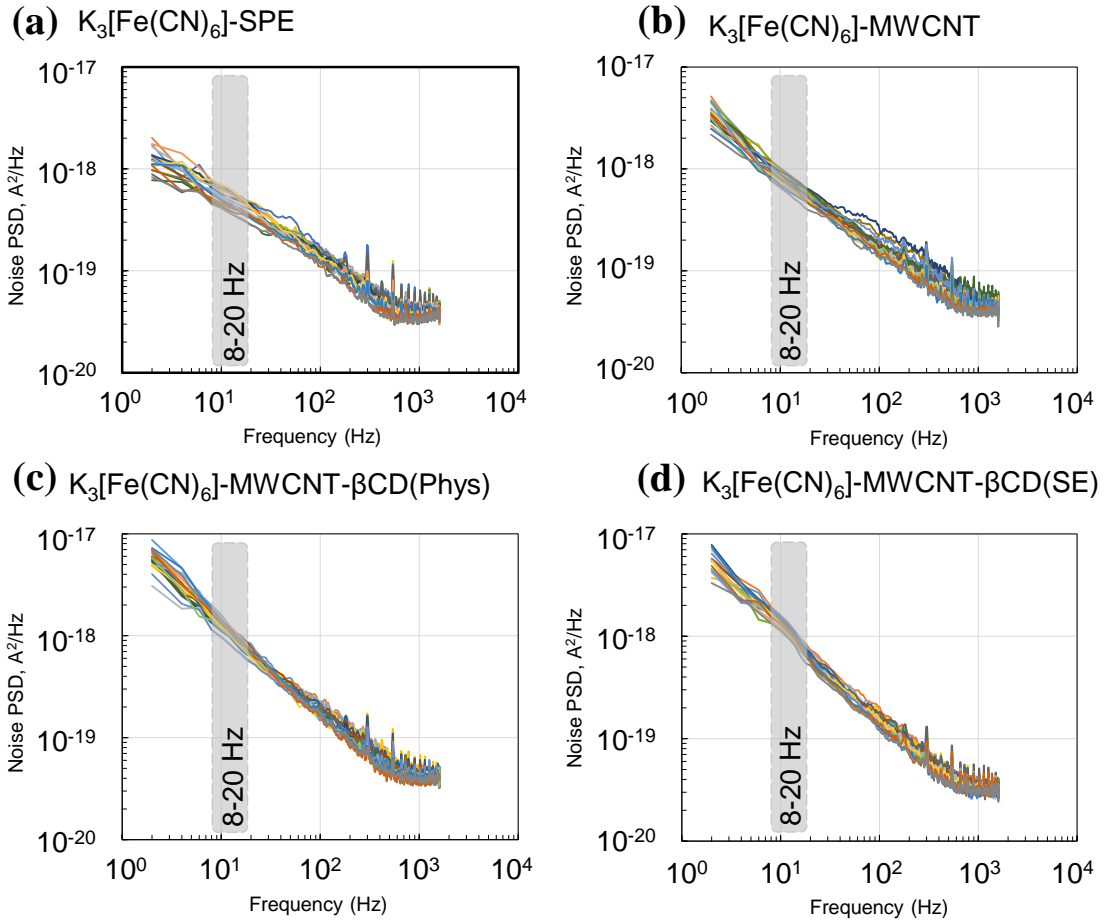
Figure 5-3. The power spectral density (PSD) spectra of the noise current (at the working electrode) with $K_3[Fe(CN)_6]$ solution for (a) SPE, (b) MWCNT/SPE, (c) MWCNT-βCD(Phys)/SPE, and (d) MWCNT-βCD(SE)/SPE electrodes.

The noise PSD spectra shown in Figure 5-3(a-d) for $K_3[Fe(CN)_6]$ solution shows $1/f$ noise characteristics since the level of the noise spectra decreases by one decade per decade of frequency. The $1/f$ noise refers to the phenomenon of the spectral density, S(f), of a stochastic process having the form [315]:

130
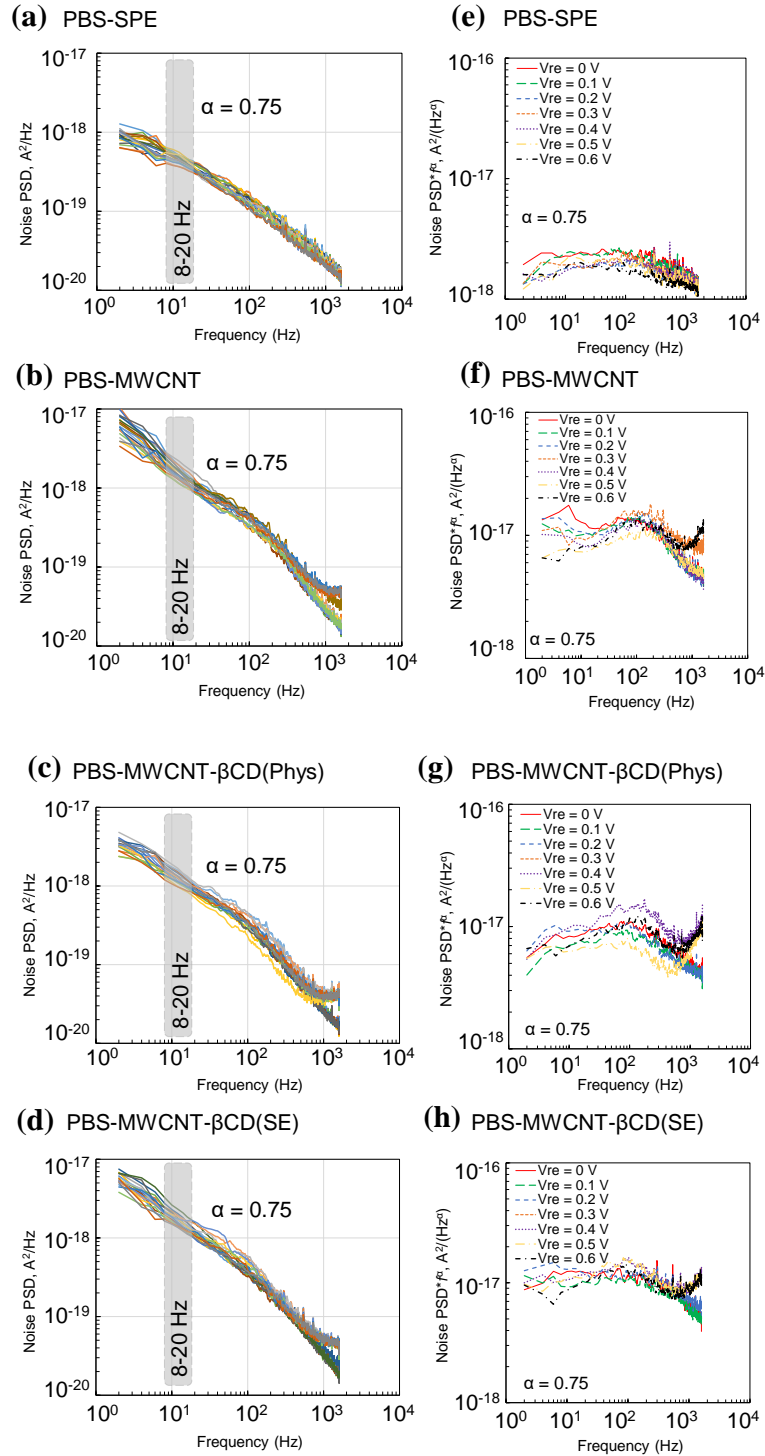
Figure 5-4. The power spectral density (PSD) spectra of the noise current (at the working electrode) with PBS solution for (a) SPE, (b) MWCNT/SPE, (c) MWCNT-βCD(Phys)/SPE, and (d) MWCNT-βCD(SE)/SPE electrodes. The noise PSD spectra multiplied with frequency for (e) SPE, (f) MWCNT/SPE, (g) MWCNT-βCD(Phys)/SPE, and (h) MWCNT-βCD(SE)/SPE electrodes.

$$S(f) = \frac{K_F (I_{avg} \text{ or } V_{avg})^2}{f^{\alpha}}, \tag{5-2}$$

where f is frequency, I_{avg} or V_{avg} are the average current/voltage of the sensor, K_F is the flicker noise coefficient, and the exponent α is in the range of $0.8 < \alpha < 1.2$, which is usually close to 1 and known as pink or flicker noise. $1/f$ fluctuations are widely found in nature. The noise PSD spectra shown in Figure 5-4(a-d) for PBS solution are, however, not purely pink noise. In this case, the value of α is somewhere between 0.5 and 1. Moreover, the noise PSD spectra in Figure 5-4(a-d) also show very weak Lorentzian humps at around frequency of 100 Hz, which could be due to defect-assisted generation-recombination (GR) processes [316] or other bistable random fluctuation [317]. Figure 5-4(e-h) shows the noise PSD spectra multiplied with frequency to identify the level of $1/f$ noise and the frequency at which the Lorenztian humps are observed. The initial flat region of the curves in Figure 5-4(e-h) in the lower frequency range provides the level of $1/f$ noise. It is observed from Figure 5-4(e-h) that the $1/f$ noise increases by only few times when the electrodes are modified with MWCNT and βCD. Also, the Lorenztian humps are observed at around 100 Hz for all the electrodes.

Effect of bias on electrochemical potential and noise level

Figure 5-5 (a) shows the "V_{re}-V_{we}" vs I_w, where V_{re} is the voltage in the reference electrode, V_{we} is the voltage at the working electrode, and I_w is the current in the working electrode. This current-voltage relationship of the working electrode with respect to the reference electrode (i.e., V_{re}-V_{we}) shows two different types of characteristic curves of the set of electrodes due to the two electrolyte solutions (i.e., $K_3[Fe(CN)_6]$ and PBS solutions, separated by a dashed gray line). In case of PBS, the I_w ranges from ~0.1 µA to ~8 µA, whereas in case of $K_3[Fe(CN)_6]$, the current varies in a narrow range between ~9 µA to ~11 µA. If we extrapolate the I-V, their intercept of on the vertical axis will provide corresponding electrochemical potential of the electrodes. The electrochemical potential of the SPE and modified SPE electrodes in PBS solution can be estimated to be close to 0 mV. However, the electrochemical potential can be extrapolated to at least below −200 mV

when $K_3[Fe(CN)_6]$ solution was used. It is also observed in Figure 5-5(a) that the electrochemical potential reduces with the functionalization of the SPE electrode with MWCNT and MWCNT-βCD(Phys/SE).
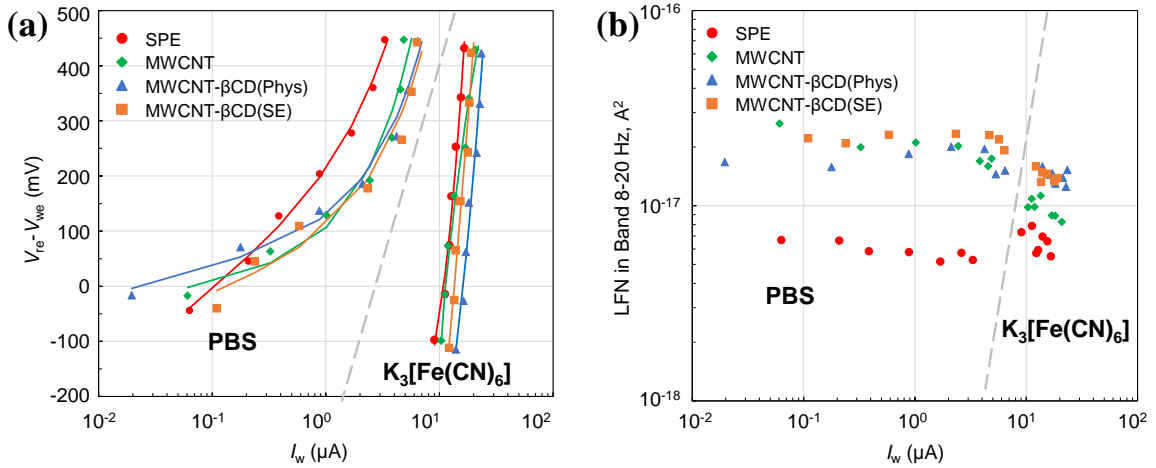
Figure 5-5. (a) Current voltage characteristics of SPE and modified SPE working electrodes with PBS and $K_3[Fe(CN)_6]$ solutions measured in potentiostatic configuration, (b) Low frequency noise of SPE and modified SPE working electrodes with PBS and $K_3[Fe(CN)_6]$ solutions in frequency band of 8-20 Hz with respect to the current at the working electrodes.

Figure 5-5(b) shows the "Low Frequency Noise (LFN) between 8 and 20 Hz" vs I_w in the working electrode. These curves were derived from the normalized noise PSD spectra (i.e., Step 4 in Figure 5-2). Similar to the case as shown in Figure 5-5(a), the I_w has a wider range when PBS solution is used as the electrolyte compared to that of $K_3[Fe(CN)_6]$ solution. However, the LFN in band 8-20 Hz remains almost constant at different current of the working electrode (I_w, which is proportional to the bias voltages), signifying negligible bias dependence of the LFN noise level. However, the level of LFN noise increases around three times when the SPE electrode is modified with MWCNT and MWCNT-βCD(Phys/SE).

Reduction of SNR with MWCNT functionalization of surface

In summary, the noise level of the SPE and modified SPE electrodes have negligible bias dependence and a very small dependence on the electrode materials. In fact, the noise level only increases by ~3 times when MWCNT or MWCNT-βCD(Phys/SE) is attached to the SPE electrode. The increase of the noise level is not significant compared to the increase

of the electrochemical sensing signals when MWCNT based modification are done. Moreover, since the noise level has a negligible bias dependence, the signal-to-noise ratio of the electrodes during actual sensing experiments will not depend much upon the range of the scanning potential. Therefore, these results signifies that the modification of SPE with MWCNT and functionalized MWCNT will not introduce significant noise to the electrochemical sensing signals.
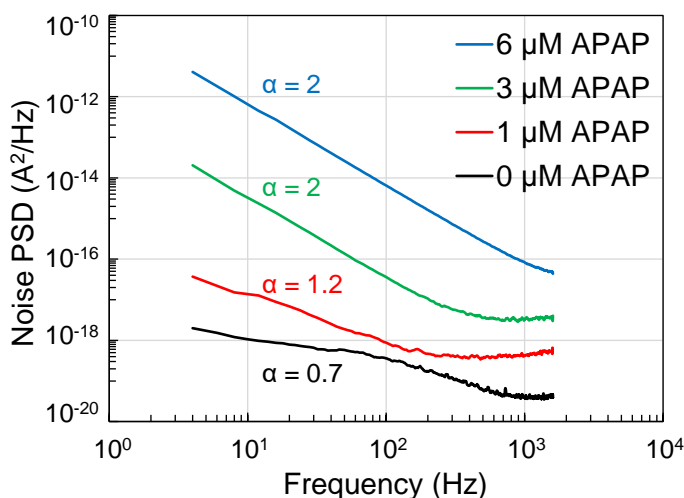
Figure 5-6. Noise with different APAP concentration using MWCNT-βCD(Phys)SPE electrode.

Effect of analyte concentration

The influence of the analyte concentration on the noise of the pharmaceutical sensor was investigated by using three different concentrations of acetaminophen (APAP) with the MWCNT-βCD(Phys)/SPE electrode. The three concentrations of APAP were 1, 3 and 6 µM, which were prepared in PBS (7.4) buffer solution. The bias voltage used in the noise measurement was 0.3 V that is close to the APAP oxidation potential. Applying this bias voltage mimics the actual conditions during the sensing experiment so that the noise behavior can be estimated related to the experimental conditions. The APAP concentration dependent noise behavior is shown in Figure 5-6. It is observed that the low frequency noise power increases by around one to two orders of magnitude when the concentration of APAP is increased. However, the peak current at the oxidation potential is at least few orders of magnitude higher than the base-line current. Therefore, the increase in the noise due to

higher APAP concentration does not significantly deteriorate the overall noise, as shown in Table 5-2. Also, the increase of noise at very low concentration of APAP (<1µM) is also insignificant compared to the noise at high APAP concentration (e.g., 6 µM). Another noise characteristic is the value of α corresponding to $1/f^{\alpha}$ noise parameter. In the case of blank PBS solution, the value of α is 0.7 which increases to 2 with high concentrations of APAP (i.e., 6 µM). Higher value of α corresponds to sharper decrease of slope of the noise power.

Table 5-2: Noise K_F and LFN in different sensors compared to the noises during actual measurements.

Sensor	Analyte	α	Signal (in actual measurement)	Noise K_F	Noise (in actual measurement)	LFN in band 8-20 Hz
MWCNT-βCD(Phys)	0 µM APAP	0.7	0.6 µA	1.56×10^{-5}	< 10 nA	3.64 nA
	1 µM APAP	1.2	~3 µA	1.16×10^{-5}	< 0.1 µA	9.14 nA
	3 µM APAP	2.0	~5 µA	2.26×10^{-3}	< 0.5 µA	0.11 µA
	6 µM APAP	2.0	~8 µA	1.77×10^{-1}	< 2 µA	1.55 µA
Pd/PdO	pH 4	2.0	~60 mV	2.08×10^{-14}	< 0.1 mV	2.12 nV
	pH 7	2.0	~200 mV	1.92×10^{-16}	< 0.1 mV	0.74 nV
	pH 10	2.0	~400 mV	4.7×10^{-16}	< 0.1 mV	2.14 nV
Free chlorine	PBS 7.4	2.0	~100 to 1500 nA	$< 1.84\times10^{-1}$	< 20 nA	11 nA
Temperature	Si	1.3	~100 to 800 mV	$< 3.97\times10^{-14}$	< 0.1 mV	10 nV
	PEDOT:PSS	0.45	~100 to 800 mV	$< 1.86\times10^{-14}$	< 0.1 mV	55 nV

5.3.2. Noise in the pH sensor

The noise in Pd/PdO based pH sensors was studied by using three different pH buffers (i.e., 4, 7 and 10). As the pH sensors are operated in potentiometric configurations, where the pH of the solution is transduced into corresponding output potential, the noise PSD of the pH sensor was measured by connecting the pH sensor and a reference electrode to the positive and negative terminal of a low-noise amplifier, respectively. As shown in Figure 5-7, the value of α in the noise PSD is 2 for all the pH buffers in the frequency range of 4-100 Hz. Also, the noise power increases by one order of magnitude in pH buffer 4 and 10 compared to that of pH 7 in lower frequency range. The increase in the noise power at pH 4 and 10 may be attributed to the higher concentrations of H_3O^+ and OH^- ions, respectively, compared to that of neutral pH 7. However, the noise power levels (i.e., nanovolts square) for different pH are significantly smaller than the signal of the pH sensors, which are in the

range of few hundred millivolts. Thus, the noise power of the pH sensor does not introduce any additional experimental uncertainty during the pH measurement.
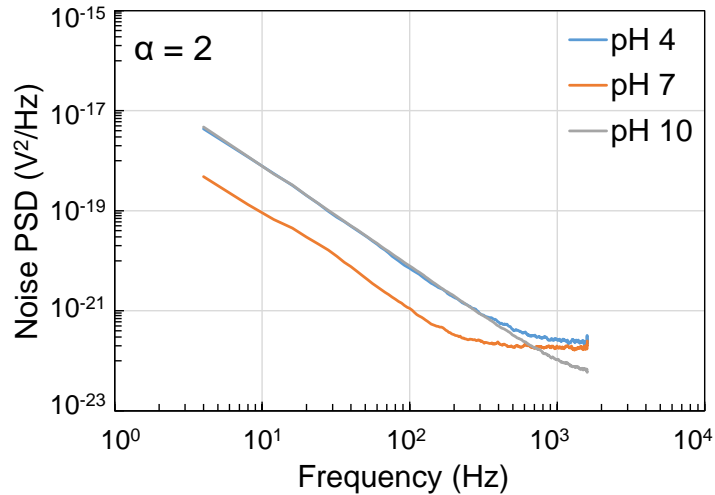
Figure 5-7. Noise with different pH buffer using Pd/PdO based pH sensing electrode.
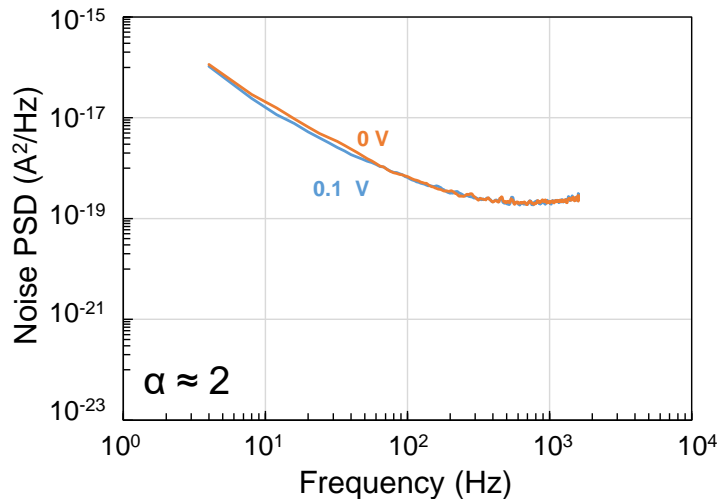
Figure 5-8. Noise with different bias voltages using ammonium carbamate modified and carbon based free chlorine sensing electrode.

5.3.3. Noise in the free chlorine sensor

The noise in the amine-modified carbon electrode-based free chlorine sensor was studied by using the electrode in a three-electrode voltammetric configuration along with an Ag/AgCl reference electrode and a platinum counter electrode, as shown in Figure 5-8. The

bias voltages used in the noise were 0 V and 0.1 V, since the free chlorine sensor operated only in these two biasing conditions in chronoamperometry measurement. It is observed that the noise behavior does not change with the biasing voltages. Also, the value α in $1/f^{\alpha}$ parameter is 2 in both biasing conditions. Moreover, the noise power is in the range of less than few nanovolts square per Hz, whereas, the minimum current detected in the free chlorine sensing is in the range of few tens of nanovolts. Therefore, the noise behavior of the free chlorine sensor does not introduce additional degradation in the sensitivity and Lod of the sensing signal.
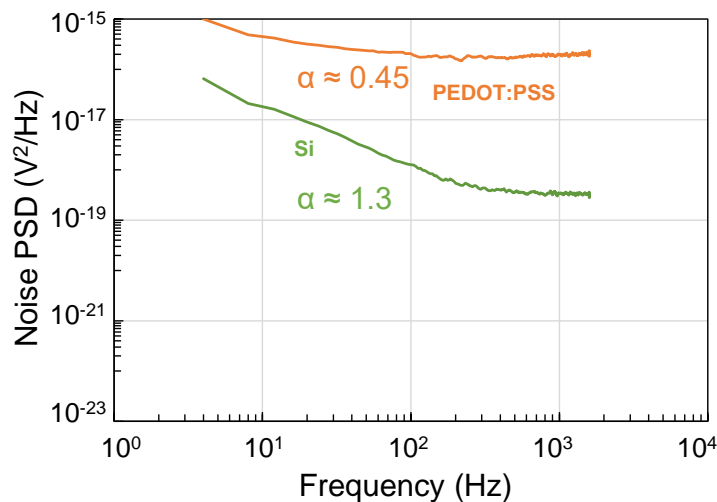
Figure 5-9. Noise in the PEDT:PSS and silicon thermistors used for temperature sensing.

5.3.4. Noise in the temperature sensor

The temperature sensor used in the integrated water quality monitoring system was based on a Wheatstone-bridge based temperature sensor made of PEDOT:PSS and silicon (Si), as describe in Chapter 6. Therefore, the output signal of the temperature sensor is a potential difference. The overall noise behavior of the temperature sensor depends on the individual PEDOT:PSS and Si thermistors. Thus, we studied the voltage noise of the individual thermistors, as shown in Figure 5-9. The noise power of the PEDOT:PSS thermistor was ~1-3 orders of magnitude higher than that of the Si thermistor. This could be due to polymeric nature of the PEDOT:PSS thermistor which possesses higher molecular irregularity/defects compared to that of silicon, where the atoms are arranged in an almost

perfectly crystalline structure. Also, the $1/f^{\alpha}$ parameters shown that the value of α were 0.45 and 1.3 for PEDOT:PSS and Si, respectively. This difference in the α value could be related to the transport mechanism of the two types of semiconductors. The noise power levels for both of the thermistors were in the range of few nanovolts square, which is much below the temperature induced voltage difference in the range of few hundreds of millivolts.

5.4. Conclusions

In this study on noise in electrochemical sensors, several experiments were reported in an effort to understand the dependence of noise level on the type of electrolyte solutions, bias voltages and electrode materials, this would allow us to identify possible effect of noise on electrochemical sensing performances. Analyte types and electrode modifications, as well as bias voltages dependent $1/f$ noise are studied in screen printed electrode (SPE) and MWCNT/MWCNT-βCD(Phys/SE) modified SPE. Measurements show that the noise level remains almost constant, independent on the type of the electrolyte solutions or the bias voltages. However, a slight increase of the noise level (about three times) is observed when SPE electrode was modified with MWCNT and MWCNT-βCD(Phys/SE). The PBS solution showed wider current range of the working electrode to that of $K_3[Fe(CN)_6]$ solution. Also, the electrochemical potential of the electrodes in PBS solution was close to 0 mV, whereas it was below -200 mV for $K_3[Fe(CN)_6]$ solution. The increase of the noise level due to MWCNT and MWCNT-βCD(Phys/SE) modifications has negligible impact on the signal-to-noise ratio in the electrochemical sensing measurements. In fact, SNR improves when surfaces are functionalized with MWCNT. The noise in pH, free chlorine and temperature sensors are also analyzed. From the noise measurements, it is shown that there was negligible influence on the sensing signal, and the nosie is lower than the LoD reported in previous chapters.

Chapter 6

Fully integrated, simple and low-cost electrochemical sensors array for drinking water quality monitoring[*]

Rapid, accurate and inexpensive monitoring of water quality parameters is indispensable for continued water safety in resource-limited areas. Conventional sensing systems either can only monitor one parameter at a time or lack on-site monitoring capability, thus, demanding full system integration. Here, we report fully-integrated electrochemical sensor arrays for *in situ* water quality monitoring, which offers simultaneous monitoring of pH (57.5 mV/pH), free Cl (186 nA/ppm), and temperature (16.9 mV/°C); and on-demand monitoring of acetaminophen and 17β-estradiol (<10 nM), and heavy-metal (<10 ppb of lead) – bridging the technological gap between signal transduction, processing, wireless-transmission and smartphone interfacing by merging nanomaterials, and carbon nanotubes based sensors fabricated on two microscope glass slide controlled by a custom-designed readout circuit, potentiostat and Android app. We demonstrate the integrated system for monitoring tap, swimming pool and lake water. This integrated sensor platform can facilitate a wide range of water monitoring and sensing applications.

6.1. Background

Water quality monitoring is critical to preserve and protect the safety of water resources that are used for drinking, recreation and consumer usage [48,54,318–321]. Water quality is dependent on its chemical, physical, and microbial features which are mutually dependent. Typical water quality parameters include pH, free chlorine, dissolved oxygen, organic pollutants, heavy metals, turbidity, conductivity, temperature, and microbes [3]. Many conventional water quality monitoring systems are incomplete in terms of integration, require separate sample collection and analysis, and are expensive – failing to provide a real-time profile of water quality parameters [48,322]. Moreover, these systems are mostly capable of measuring only one parameter such as pH [323] or free chlorine [324] in a single measurement [99]. Therefore, a fully integrated sensing platform with high sensitivity, lower cost, high accuracy, reliability, user-friendliness is desirable for continuous or on-demand monitoring of critical water quality parameters to guarantee an improved water safety and associated public health.

Recently, integrated sensing systems have shown promises in wearable sweat biomarkers monitoring and diabetes monitoring/treatment [325–327]. These systems possess high spatial and temporal sensing resolution, and the integrated electronics can perform simultaneous on-site signal processing. Integrated sensors have also been developed for water quality monitoring for measuring dissolved oxygen, conductivity, temperature, pH, bacteria, and cell nutrients/metabolites [107,328–331]. However, an integrated system capable of monitoring pH, free chlorine (Cl), temperature, emerging pharmaceutical contaminants and heavy metals together with stand-alone and on-site monitoring ability are yet to be developed. Also, the interdependent mechanisms that are involved in water quality monitoring call for a practical strategy to develop a fully integrated, low-cost, highly sensitive, accurate, and multiplexed sensing system to extract the water quality parameters in a reliable and easy-to-use manner.

Here, we present a fully integrated water quality monitoring system (FIWQMS) for simultaneous measurement of the pH, free Cl concentration, and temperature, and on-

demand monitoring of pharmaceuticals and heavy metal in water. Our design bridges the existing technological gap between signal transduction, conditioning, processing and low-power wireless transmission of the electrochemical sensors signals by merging commercially available integrated-circuits, microcontrollers and open-source software and hardware technologies consolidated on a custom-designed, compact and stacked (i.e., multi-layered) printed circuit board, with low-cost electrochemical sensor technologies fabricated on a single glass substrate. This method eliminates the rigorous fabrication and associated high-costs at the sensor level and electronics design requirements at the signal analysis level, while employing the strengths of the underlying technologies at the same time.

In summary, the potentiometric pH sensor was fabricated by spin-coating of palladium/palladium oxide (Pd/PdO) ink as the sensing electrode and hand-drawn silver/silver chloride (Ag/AgCl) as the reference electrode – which showed a high sensitivity and did not require signal conditioning for data analysis. A potentiostat-free, calibration-free and amperometric free chlorine sensor was fabricated on the same glass substrate by electrochemically modifying a hand-drawn carbon electrode and an Ag/AgCl reference electrode. The pharmaceuticals (APAP and E2) and heavy metal (Pb) sensing was accomplished with a single carbon electrode glued on the same glass substrate and modified by functionalized multi-walled carbon nanotubes and β-cyclodextrin (MWCNT-βCD). A Wheatstone-bridge-based temperature sensor was fabricated on a separate glass substrate using bulk silicon wafer and poly(3,4-ethylenedioxythiophene) polystyrene sulfonate (PEDOT:PSS). All the sensors fabricated on the two glass substrate were connected to an Arduino-controlled printed circuit board, wirelessly (Bluetooth Low Energy) interfaced with an Android application (app) for on-site monitoring of real water samples. This integrated sensing platform is a promising tool for rapid, low-cost, easy-to-use, accurate and real-time water quality monitoring.

6.2. Materials, methods and system design

6.2.1. Chemicals and reagents

Isopropanol (IPA, 8600-1), acetic acid (HOAc, 1000-1), and toluene (9200-1) were purchased from Caledon Laboratory Chemicals. Sodium hypochlorite (NaOCl) solution (239305), silver chloride (AgCl, 227927), phosphoric acid (H_3PO_4, 695017), boric acid (H_3BO_3, 339067), phosphate buffered saline (PBS) tablet (P4417), sodium chloride (NaCl, 793566), sodium acetate (CH_3COONa, S2889), sodium phosphate dibasic (Na_2HPO_4, S0876), ammonium carbamate (292834), sodium hydroxide (NaOH) pellets (S5881), lead nitrate ($Pb(NO_3)_2$, 228621), acetaminophen (A7085), and 17β-estradiol (E8875) were from Sigma-Aldrich. Pd precursor solution (Pd-25c) was obtained from Xerox Research Centre of Canada. Carbon ink paste (C2130925D1), Ag/AglCl paste (C2130809D5), and polymer dielectric paste (D2020823P2) were purchased from Gwent Group. Five-minute epoxy and super glue were purchased from a local store.

6.2.2. Fabrication and integration of the sensors

The fabrication processes of the electrochemical sensors array for water quality monitoring are detailed in Figure 6-1. The potentiometric pH sensor (with voltage output) was based on spin-coating of Palladium (Pd) ink. The amperometric free Cl sensor (with current output) was based on carbon paste electrode electrochemically modified by ammonium carbamate. A common Ag/AgCl electrode works as the reference electrode for pH and free Cl sensors. The pH and free Cl sensor fabrication processes are schematically described in Figure 6-1(a-i). In summary, a three inch silicon wafer was first taken (Figure 6-1(a)) as a smooth substrate which was then covered by a Kapton polyimide tape (Figure 6-1(b)). After that, few millilitre of Pd ink was slowly drop-casted with a dropper so that no air bubble is trapped inside the viscous ink (Figure 6-1(c)). The drop-casted ink was then spin-coated onto the Si/Kapton substrate at 3000 RPM to get a very thin and uniform Pd ink layer (Figure 6-1(d)) followed by annealing in ambient with a hotplate at 200 °C for 48 hours to get Pd/PdO thin film (Figure 6-1(e)). A small piece of the resulting Pd/PdO on Kapton (5

mm × 100 mm) was then cut (Figure 6-1(f)) and transferred into a glass slide followed by hand-drawing of carbon ink and one Ag/AgCl ink (Figure 6-1(g)). The carbon and Ag/AgCl lines drawn on the substrates were then annealed in ambient at 60 °C for 30 minutes using a hotplate (Figure 6-1(h)). The carbon ink was electrochemically modified with ammonium carbamate according to the process described in Ref [332] (Figure 6-1(i)).
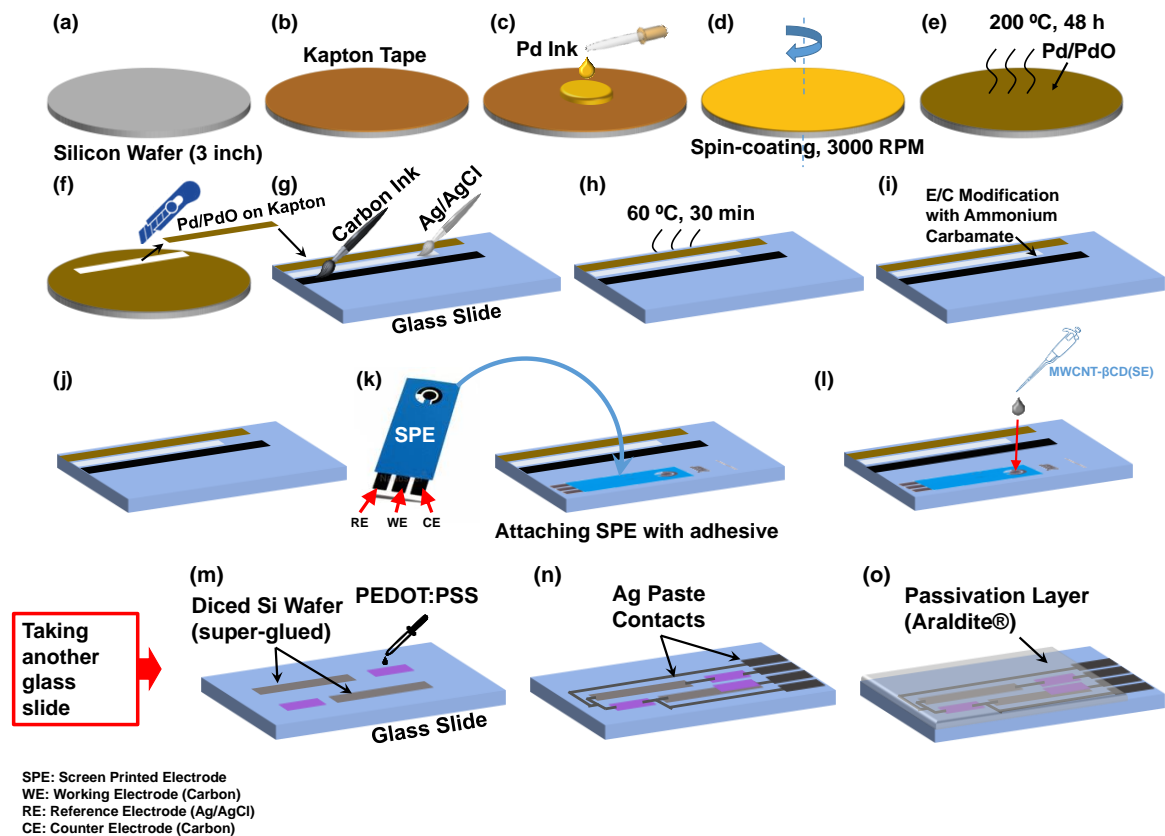
Figure 6-1. Fabrication processes of the fully integrated water quality monitoring sensors. (a-i) Fabrication steps for pH and free chlorine sensors. (j-l) Fabrication steps for APAP/E2/Pb^{2+} sensor. (m-o) Fabrication steps for temperature sensor.

The pharmaceutical contaminants (i.e., APAP and E2) and heavy-metal (Pb) sensors were fabricated by first gluing a commercial paper-based screen printed electrode (SPE) onto the substrate containing the pH and free Cl sensors (Figure 6-1(j-k)). The attached SPE was then modified by β-cyclodextrin functionalized multi walled carbon nanotubes (MWCNT-βCD(SE)) as described in Chapter 3 (Figure 6-1(l)). The resistance-based temperature sensor was realized by fabricating a Wheatstone bridge resistor network using p-type Si

(super-glued) and poly(3,4-ethylenedioxythiophene) polystyrene sulfonate (PEDOT:PSS) on a separate glass substrate (Figure 6-1(m-n)). A 5-minute epoxy resin was used as an insulating layer to ensure sensor isolation from water samples (Figure 6-1(o)).
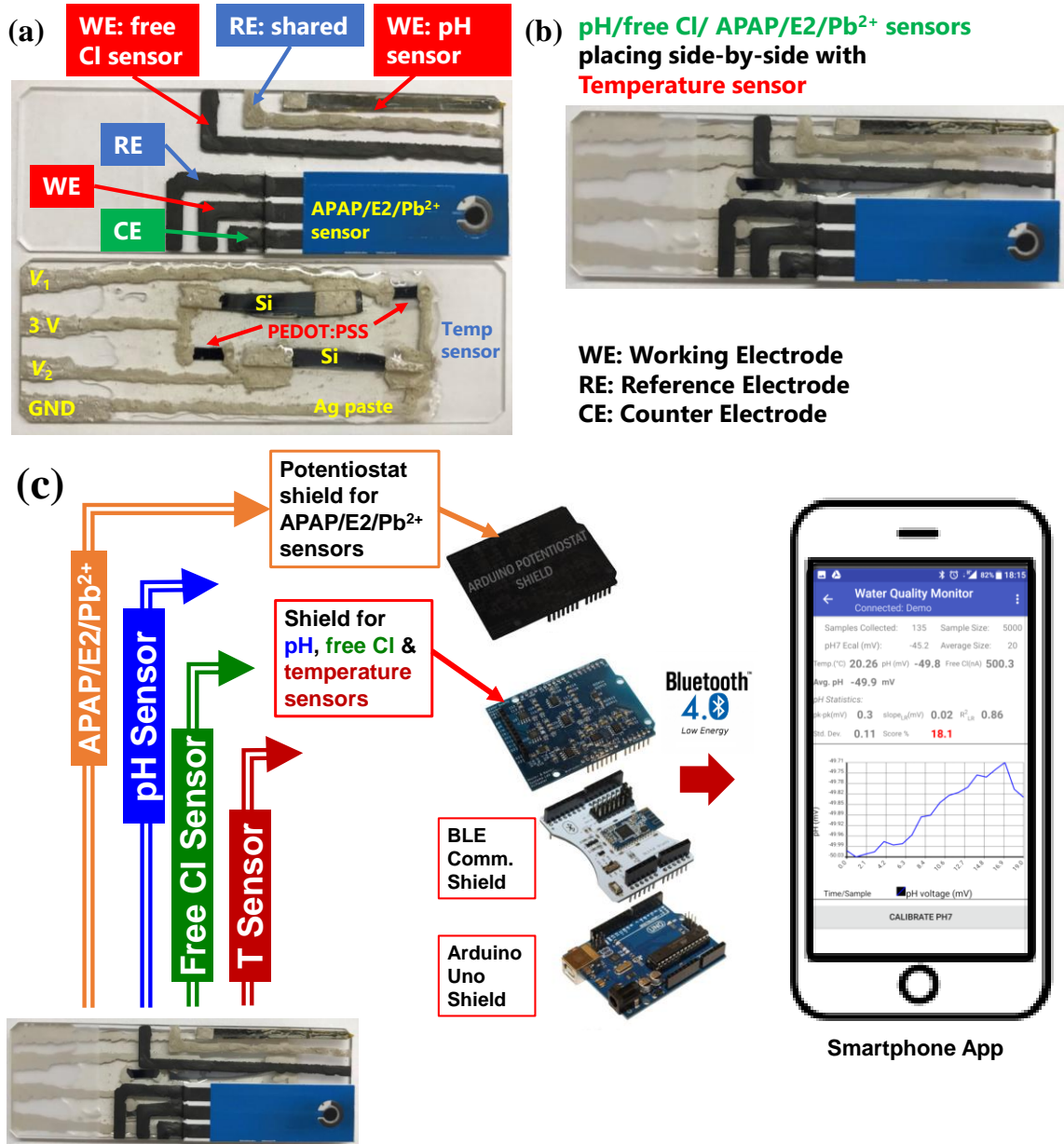
Figure 6-2. (a) Photograph of FIWQMS sensors on two glass slides. Top one contains the pH, free Cl and APAP/E2/Pb^{2+} sensors, and the bottom one contains the temperature sensor. (b) Photograph of the two glass slides placed side-by-side containing all the water quality monitoring sensors. (c) Schematic of the connection of the integrated water quality monitoring sensors with Arduino Uno microcontroller based shields along with Bluetooth shied for wireless connectivity with a custom-designed Android smartphone app.

6.2.3. System design

The FIWQMS allows simultaneous and on-site measurement of pH, free Chlorine (Cl) and temperature as well as on-demand monitoring of pharmaceuticals and heavy metal in water. The sensors were fabricated on two pieces of microscope glass slide substrates, resulting in a low-cost and compact sensor integration (Figure 6-2(a-b)), while vertically stacked printed circuit board technology was exploited to incorporate the critical signal conditioning, processing, and wireless transmission functionalities using readily available integrated-circuit components and open-source software and hardware architecture Figure 6-2(c) [333][210]. The panel of water quality parameters and temperature was selected to evaluate the quality of a water sample. For example, the free Cl concentration should be accurately monitored for the safety of drinking, recreational, and food processing water – as recommended by the World Health Organization; and water temperature is needed to compensate for and eliminate the influence of temperature variation in the measurements of the pH and other electrochemical sensors.

The pH and free Cl sensors autonomously generate voltage and current signals proportional to the presence of the H^+/OH^- ions and free Cl, respectively, between the working electrode and the Ag/AgCl electrode. The on-demand measurement of pharmaceutical contaminants (i.e., APAP and E2) and heavy-metal (Pb) was facilitated through the use of the SPE modified by β-cyclodextrin functionalized multi walled carbon nanotubes (MWCNT-βCD). By utilizing differential pulse voltammetry, linear sweep voltammetry and anodic stripping voltammetry, the MWCNT-βCD(SE)/SPE electrode detected APAP, E2 and Pb with three well-separated peak potentials for on-demand measurements with negligible interferences.

Figure 6-3 illustrates the system-level block diagram of the signal transduction, conditioning, processing, and wireless transmission routes that facilitate simultaneous and on-demand water quality monitoring. Figure 6-4 shows the photographs of the FIWQMS system. The readout circuit of the FIWQMS has two shields or PCB boards, such as Water Quality Monitoring (WQM) Shield, and the Potentiostat Shield. The WQM Shield is

connected to pH, free chlorine and temperature sensors, whereas the Potentiostat Shield is connected to the pharmaceuticals/heavy metal sensor. The circuits are designed to capture the analog signals from each sensor with fine resolution while staying within the input voltage range of the analogue-to-digital converter. An Arduino Uno microcontroller is used to calibrate, compensate, and dispatch the conditioned signals to an on-board wireless transceiver. The transceiver enables wireless data transmission to a Bluetooth-enabled mobile handset with a custom-developed application, and a user-friendly interface for uploading the data to cloud servers. The circuit schematics, programming codes and screenshot of the FIWQMS are given in Appendix B.
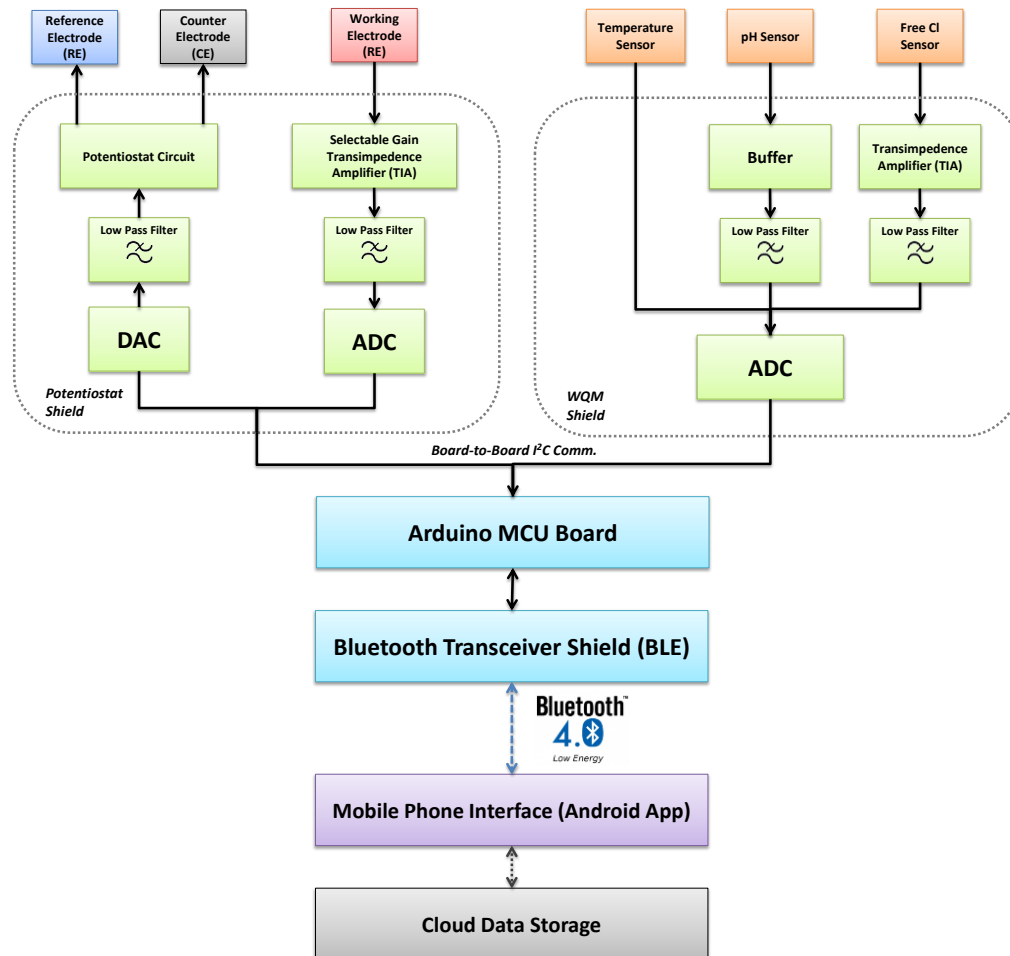
Figure 6-3. System-level block diagram of the FIWQMS system showing the signal transduction (orange) (with potential *V*, current *I* and resistance *R* outputs), signal conditioning (green), signal processing (blue) and wireless transmission (blue) paths from the integrated sensors to the custom-designed Android smartphone application (purple).
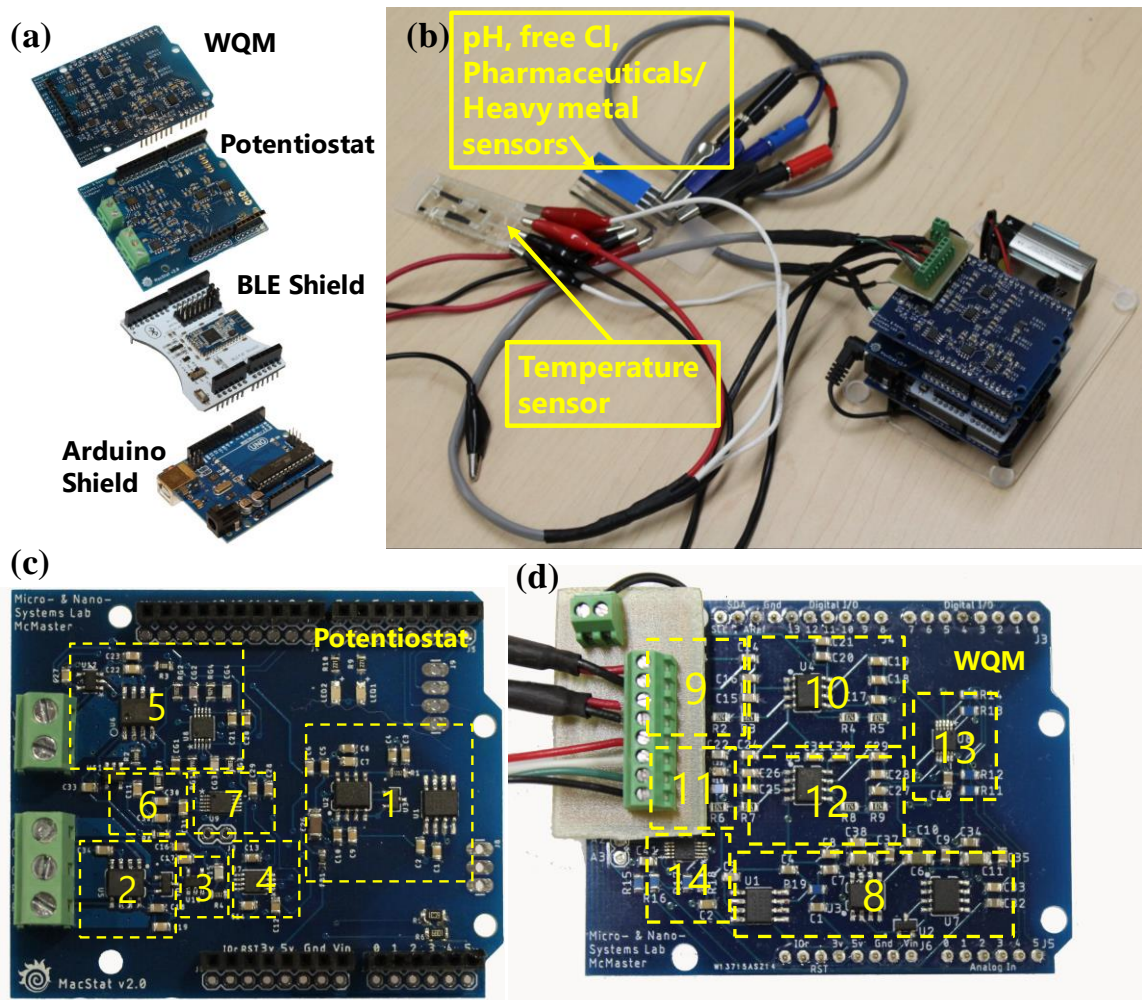
Figure 6-4. (a) Stacked view of the FIWQMS readout circuit system. (b) Photograph of the FIWQMS system with the sensors. Top view of (c) the Potentiostat shield, and (d) the WQM shield. The numbered yellow boxes indicate the locations of the integrated circuit components. (1 & 8) Power Supply, (2) Potentiostat Circuit, (3) LPF (DAC output filter), (4) DAC, (5 & 11) TIA, (6) LPF (ADC input filter), (7) ADC, (9) Buffer, (10) LPF (pH), (12) LPF (Cl), (13) ADC (Cl + pH), (14) ADC (Temp.)

6.2.4. Sensor characterization

Pharmaceuticals and heavy metal sensor

The pharmaceuticals and heavy metal sensing were performed with a PalmSens EmStat 3 potentiostat (PalmSens BV, Netherlands) connected to the three-electrodes of MWCNT-βCD(SE)/SPE. The potentiostat was run by PSTrace 5.2 software. The three-electrode cell

assembly consisted of screen-printed carbon as an auxiliary electrode and Ag/AgCl electrode as the reference electrode. Modifications of the working electrode of the SPE was done with MWCNT-βCD(SE) which had an exposed circular area of 3 mm diameter. All of the measurements were performed at 25±2 °C. Preparation of the samples and experimental conditions for pharmaceuticals and heavy metal sensing are described in Chapter 3 and Chapter 4, respectively.

pH sensor

The Britton-Robinson pH test buffer solutions with pH value of 4, 5, 6, 7, 8, 9, and 10 were prepared by mixing 0.04 M H_3PO_4, 0.04 M HOAc, 0.04 M H_3BO_3 solutions with 0.2 M NaOH solution. A commercial pH meter (PHB-600R, OMEGA) with a glass electrode (PHE1311, OMEGA) was used to monitor the pH of the buffer solutions. Characterization of the spin-coated pH sensors was done in a potentiometric configuration using a semiconductor parameter analyzer (B1500A, Agilent). The pH dependent open-circuit potential between the Pd/PdO and Ag/AgCl electrodes was recorded every 2 s for 90 s during immersion of the electrodes in pH buffer solutions without magnetic stirring. The transfer of the electrodes between different pH buffers was done without cleaning or drying. The pH sensing measurements were performed at 25±2 °C.

Free chlorine sensor

Different concentrations of free chlorine (Cl) solutions were prepared by diluting the as-received NaOCl solution with necessary volume of PBS solution (0.01 M, pH = 7.4). A DPD-based colorimetric test kit (CN-70, Hach) was used to calibrate the prepared free chlorine concentrations. The free chlorine sensor was characterized by a simplified amperometric measurement configuration. In this configuration, the modified carbon electrode was used as the working electrodes; and the hand-drawn Ag/AgCl film worked as the reference/counter electrode. The free Cl dependent current flow that were going through the working and the reference/counter electrodes was recorded using a commercial PalmSens EmStat 3 potentiostat (PalmSens BV, Netherlands) every 1 s for 50 s when the

electrodes were immersed in free chlorine solutions. Similar to the pH sensor, the electrodes were transferred into other free chlorine test solutions without additional cleaning or drying. The free chlorine sensing measurements were also performed at 25 ± 2 °C.

Temperature sensor

The characterization of the Wheatstone-bridge-based temperature sensor performed in a reliability test chamber (ESL-2CA, ESPEC) in water with the temperature varying between 0°C and 50°C. A commercial thermometer (HI98509 Checktemp 1, HANNA) was used to monitor the water temperature. A bias voltage of 3 V was used for the temperature sensor when the output voltage was recorded using a semiconductor parameter analyzer (B1500A, Agilent).

6.3. Results and discussions

6.3.1. Pharmaceutical and heavy metal sensor

The acetaminophen (APAP) and 17β-estradiol (E2) sensing performances of the pharmaceutical sensor have been discussed in Chapter 3 (Section 3.3) by using glassy carbon electrode (GCE) as the base electrode. GCE is an expensive electrode. Moreover, it's pen-like shape is not suitable for the integration with the other water sensors in the FIWQMS system. Therefore, we used a low-cost and paper-based screen printed electrode (SPE) purchased from Zensor which was glued beside with the pH and free Cl sensors on the same glass substrate, followed by modifications with MWCNT-βCD(SE), as described in Chapter 3. Since, the MWCNT-βCD(SE)/SPE electrode can only be used once for any pharmaceutical sensing due to contamination of the electrode surface with residues of APAP and E2, we reused the SPE electrode by cleaning the MWCNT-βCD(SE) with IPA solutions and newly re-drop-casting MWCNT-βCD(SE) solution onto the SPE working electrode followed by drying in ambient air.

The Figure 6-5 and Figure 6-6 show the APAP and E2 determination performances, respectively, using the MWCNT-βCD(SE)/SPE electrode of the FIWQMS characterized

by a commercial PalmSens EmStat 3 potentiostat (PalmSens BV, Netherlands). The APAP sensing was done by Differential Pulse Voltammetry (DPV) between 0.01 to 15 µM, as shown in Figure 6-5(a). Figure 6-5(b) shows the linear calibration curve for APAP determination which shows two linear regions of 0.01-0.1 µM and 0.1-15 µM with slopes of 5.18 µA/µM and 1.75 µA/µM, respectively. The E2 sensing was done by Linear Sweep Voltammetry (LSV) between 0.01 to 15 µM, as shown in Figure 6-6(a). Figure 6-6(b) shows the linear calibration curve for E2 determination which shows two linear regions of 0.01-0.1 µM and 0.1-15 µM with slopes of 8.37 µA/µM and 2.07 µA/µM, respectively. The limit of detection, defined as LoD $= 3s/m$ (where s is the standard deviation of the blank solution (30 nA) and m is the slope of the calibration curve), was estimated to be 17 nM and 11 nm for APAP and E2, respectively. In these cases, the slope of the lower concentration ranges was used to calculate the LoD of APAP and E2.

The lead ion (lead, Pb^{2+}) sensing performances of the heavy metal sensor have been discussed in Chapter 3 (Section 3.3) by using screen printed electrode (SPE) as the base electrode and both the MWCNT-βCD(Phys) and MWCNT-βCD(SE) modifications. The MWCNT-βCD(Phys)/SPE showed better sensitivity than that of the MWCNT-βCD(SE)/SPE, as shown in Figure 4-3 and 4-4 of Chapter 4. Since the MWCNT-βCD(SE)/SPE electrode is reusable for at least 10 times by electrochemically cleaning and regenerating in blank solution under magnetic stirring, the same electrode can be used for all the three analytes such as Pb^{2+} detection followed by cleaning/regeneration for APAP or E2 detection without making a new SPE electrode modification. The ability to detect all the three types of analyte using a single MWCNT-βCD(SE)/SPE electrode provides substantial simplicity and overall lower cost of the FIWQMS system.
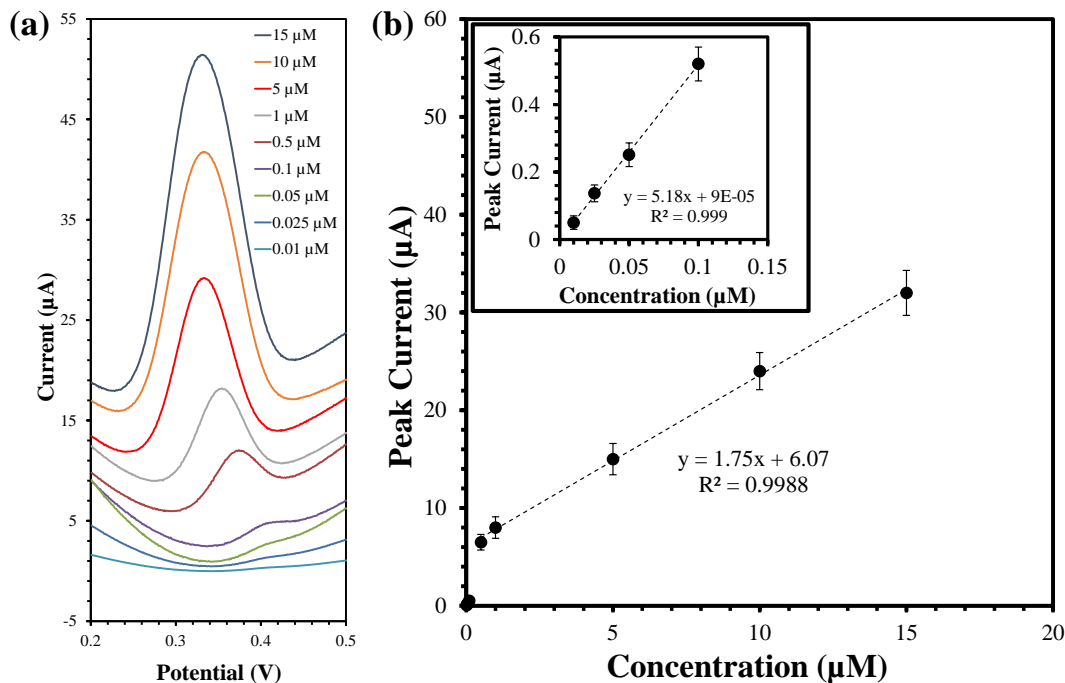
Figure 6-5. (a) DPVs of MWCNT-βCD(SE)/SPE in 0.01 M PBS (pH 7.4) in the presence of 0.01–15 μM APAP. (b) Calibration curve (i.e., peak current vs APAP concentration) for MWCNT-βCD(SE)/SPE. All the experiments were done with an open circuit potential of 300 seconds under magnetic stirring before measurements.
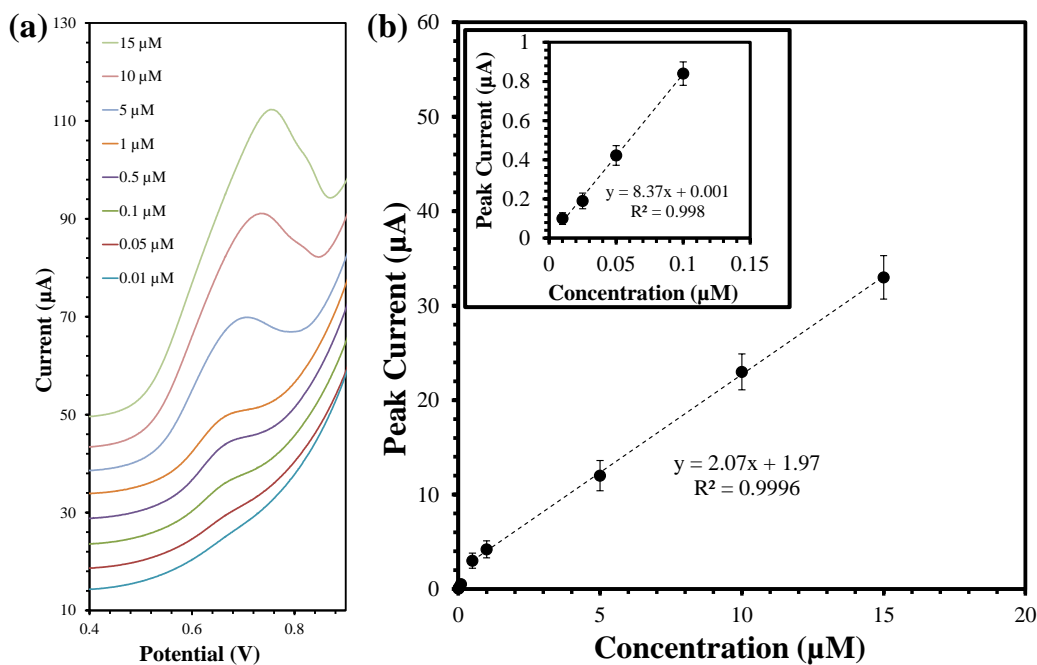
Figure 6-6. (a) LSVs of MWCNT-βCD(SE)/SPE in 0.01 M PBS (pH 7.4) in the presence of 0.01–15 μM E2. (b) Calibration curve (i.e., peak current vs E2 concentration) for MWCNT-βCD(SE)/SPE. All the experiments were done with an open circuit potential of 300 seconds under magnetic stirring before measurements.

6.3.2. pH sensor

The Pd/PdO based potentiometric pH sensor was chosen as the pH sensing material due to its higher sensitivity and stability than that of other metal/metal-oxides and carbon-based materials [334]. Moreover, the Pd/PdO-based pH sensing electrode is very inexpensive ($<$ 10 cent) due to its very small consumption of the Pd ink precursor solution ($< 10\,\mu L$) in the spin-coating fabrication process. The use of a Kapton$^®$ tape as a substrate resulted in limiting the spread of the Pd ink only on the tape, as compared to the full area of the glass slide, thus reducing the waste of the precursor Pd ink during spin-coating process. The pH sensing mechanism of the Pd/PdO electrode is based on the following redox reaction [335]:

$$PdO + 2H_3O^+ + 2e^- \leftrightarrow Pd + 3H_2O. \tag{6-1}$$

The redox potential can be calculated by the following Nernst equation:

$$E = E^0 - \frac{2.303RT}{F}pH, \tag{6-2}$$

where E^0 is the standard electrode potential, R is the gas constant (8.31 J/mol/K), T is the absolute temperature, and F is Faraday's constant (96485.33 C/mol). The sensor showed a large, stable, and low-noise output voltage in the range of 0–400 mV (which is within the input range of the ADC) corresponding to the pH variation of the water sample between 4 and 10. The output the pH sensor was compatible with the ADC voltage in the FIWQMS system. Therefore, the readout circuit of the pH sensor did not require the use of any external power supply, amplifier, or low-pass filter for driving the sensor or signal conditioning. The sensor showed a fast response time (~20 s) enabling real-time monitoring of the water pH level. The sensitivity of three pH sensors were ~57.5 mV/pH, which was close to the theoretical Nernstian response (59.53 mV/pH at 27◦C), as shown in Figure 6-7. The variation of the sensitivity between three sensors was ±0.16 mV/pH which is ~0.28% of the sensitivity. Also, different sensors exhibited a difference of ~38 mV for standard electrode potential (E^0) which accounts for a variation of ~0.7 pH unit. Therefore, an improved sensing accuracy can be achieved with single-point calibration (normally at pH = 7) for each sensor to find its standard electrode potential (E^0). However, the

FIWQMSM system has the options for three-point calibration (at pH 4, 7, and 10) in case of utilizing sensors with different sensitivity and linearity. According to, equation (6-2), the pH sensitivity also varies with temperature, which was experimentally found to be ~0.22 mV/pH/∘C, requiring temperature compensation for the pH sensitivity. The following equation is used for calculating the pH value which considers the pH sensor calibration as well as temperature compensation:

$$pH = 7 + \frac{E_{cal} - E_{meas}}{57.5 + (T_{meas} - 27) \times 0.22}, \tag{6-3}$$

The equation (6-3) was thus programmed into the Arduino microprocessor of the FIWQMS system, where E_{cal} (in mV) corresponds to the recorded voltage when the sensor is dipped into the calibration solution (pH = 7), E_{meas} (in mV) is the measured voltage during pH sensing, and T_{meas} (in °C) is the measured temperature of the water sample.
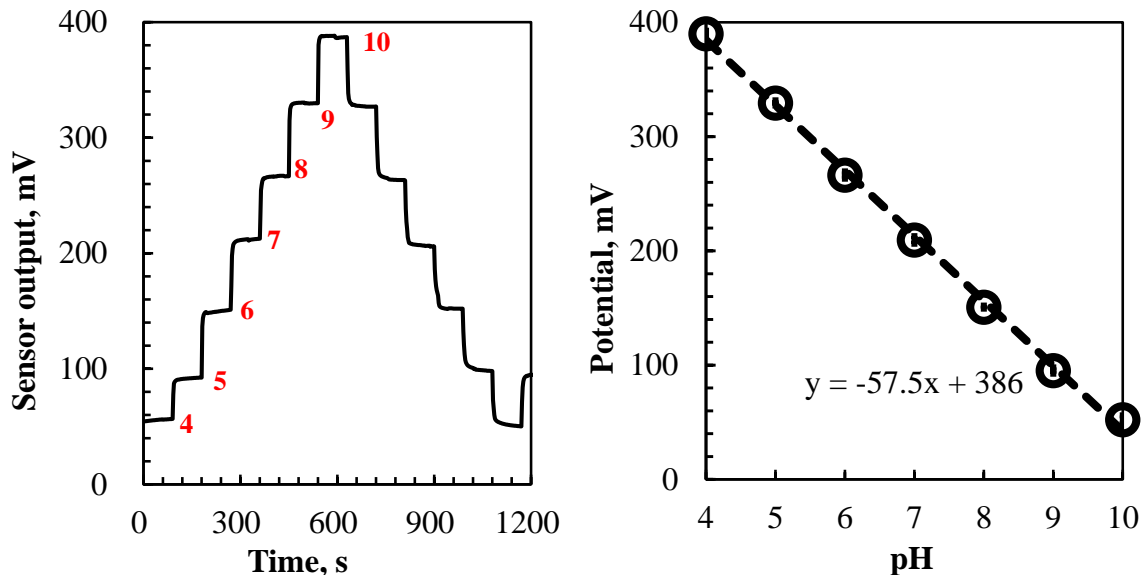
Figure 6-7. (a) Temporal response of the spin-coated pH sensor for pH between 4 and 10. (b) Calibration curves for three printed pH sensors.

The resolution of the pH sensor depends on its hysteresis. The average hysteresis of the pH sensor was 9.8 mV when the water pH was cycled between 4 and 10, corresponding to a resolution of 0.17 pH for the sensor. The selectivity of the sensor was calculated by measuring solutions containing different concentrations of interfering ions (e.g. K^+, Na^+,

Ca^{2+}, Mg^{2+}, Cl^-, SO_4^{2-}, NO_3^-), which showed negligible response to common anions and cations because of the specific redox reaction as shown in equation (6-1). The developed pH sensor has the following advantages compared to conventional glass electrodes and other microelectronics-based pH sensors or sensing systems [54,336]:

(1) The sensor shows a higher sensitivity of ∼57.5 mV/pH than many ion-selective field-effect transistors (∼55 mV/pH).

(2) The sensor is portable and easy-to-use due to integration of the reference electrode in the same glass substrate [337][338]. The sensor can be used with a single point calibration because of its reproducible sensitivity and linear response.

(3) The sensor fabricated by spin-coating technique followed by transfer of the Kapton adhesive is of low-cost.

(4) The pH sensing method does not require any external power supply, amplifier, or filter circuits, which simplifies the integration and signal processing to enable continuous pH monitoring.

6.3.3. Free chlorine sensor

The free chlorine sensor was fabricated by an amine-modified carbon electrode (hand-drawn) as the working electrode [332]. During the amperometric sensing process, the HOCl (free Cl) undergoes electrochemical reduction at the working electrode according to the following chemical reaction, resulting in an output current proportional to the HOCl concentration:

$$HOCl + 2e^- \rightarrow Cl^- + OH^-, \tag{6-4}$$

Conventional amperometric sensor requires three electrodes and a potentiostat circuit for external biasing as well as readout of the response current. However, our free Cl sensor has significantly reduced its complexity by combining the reference and counter electrodes into a single, hand-drawn Ag/AgCl film, which is actually shared with the pH sensor as a common reference electrode, thus further simplifying the fabrication complexity of

integrated sensors. A reduction voltage of 0 V was used to eliminate the use of an external power supply (i.e., potentiostat) in this simplified two-electrode sensing system [327]. The concentration of HOCl in the water sample is measured by this sensor, which is then used to calculate the free chlorine concentration (both HOCl and OCl⁻) [332]. The output current of the sensor varied between 0 and −5000 nA (Figure 6-8) as the free chlorine concentration of the water sample was varied between 1 and 8 ppm. The output current of the sensor was converted to a voltage signal between 0 and 1 V A using a transimpedance amplifier with a gain of 196 kΩ (Appendix B). A resistor-capacitor low-pass filter with a cut-off frequency of 0.06 Hz was used to suppress the noise introduced by the transimpedance amplifier.
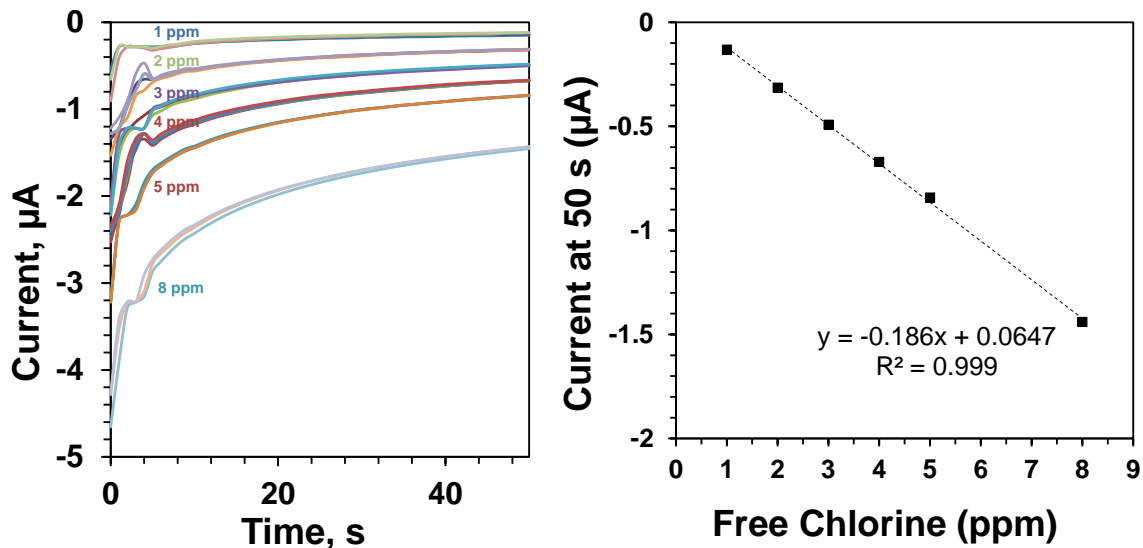
Figure 6-8. (a) Temporal response of three free chlorine sensor for free chlorine concentrations between 1 and 8 ppm. (b) Calibration curves for the three free chlorine sensors.

The output current of the sensor requires some time (at least 10 s, depends on the concentration of free Cl) to reach to a steady-state value. Also, if the water sample is not stirred, the current starts to fluctuate after long period of time (few minutes) due to the depletion of free Cl at the vicinity of the sensor surface. Moreover, stirring of the sample introduces additional noises to the current signal, thereby reducing the sensitivity of the sensor. Hence, we chose the current value at 50 s that corresponds to the concentration of free Cl. In this design, the response time of the free Cl sensor was ∼50 s, which is suitable for on-site monitoring. After one measurement, we turned off the sensor for 10 s so that the

sensor surface is in contact with an equilibrium free Cl concentration near the sensor surface. This turning on/off procedure of the sensor was facilitated by a digital switch connected at the end of the readout circuit (Appendix B). The elimination of sample stirring and the addition of a digital on/off switch significantly improved the sensing performance of the free Cl sensor.

The average sensitivity of 5 free Cl sensors fabricated in the same batch was ~186 nA/ppm, and the sensitivity variation was only ±9 nA/ppm (~5% of the sensitivity) (Figure 6-8(b)). The high reproducibility of the sensor is an attractive feature for its use in a continuous and online monitoring system since calibration is not required before each measurement once the calibration equation is stored in the microcontroller of FIWQMS readout circuit. Though the absolute sensitivity value was not as high as that of other reported free chlorine sensors, this sensor has the advantage of long-term stability of more than six months. The sensitivity of the free chlorine sensor can be improved by utilizing nano-structured carbon materials with a larger surface area (e.g. carbon nanotubes, graphene, and nanoporous carbon) as the working electrode [339]. The larger surface area can enable higher amount of immobilization of amine-sites to react with HOCl for a more sensitive output signal.

The sensitivity of the free chlorine sensor was calculated at 3 °C, 15 °C, 27 °C and 40 °C to study its dependence on temperature, which was calculated to be ~6.2 nA/ppm/°C. As a result, the calibration equation of the free chlorine sensor was used as follows to compensate for temperature-induced variation of the sensitivity towards an improved accuracy of the free chlorine measurement:

$$I_{out} = \left[186 + \left(T_{meas} - 27\right) \times 6.2\right] C_{NaOCl} + 64.7,$$

(6-5)

where I_{out} (in nA) is the amplitude of the output current of the free chlorine sensor (input current of the signal conditioning circuit), T_{meas} (in °C) is the measured temperature of the water sample, and C_{NaOCl} (in ppm) is the concentration of NaOCl in the water sample for sensor characterization. The transfer function of the signal conditioning circuit (i.e., transimpedance amplifier and low-pass filter) is given as follows:

$$V = 0.196 I_{out} + 35.4, \tag{6-6}$$

where V (in mV) is the output voltage of the signal conditioning circuit. Consequently, the free chlorine concentration was calculated by considering the following equation which takes into account the pH and temperature of the water sample, and was thus programmed into the microprocessor [340]:

$$C_{free\ chlorine} = 0.57 \times \frac{\frac{V-35.4}{0.196}-64.7}{186+\left(T_{meas}-27\right)\times 6.2} \times \left\{1+10^{pH-\left[\frac{3000}{T_{meas}+273}-10.0686+0.0253\left(T_{meas}+273\right)\right]}\right\} \tag{6-7}$$

The resolution of the free chlorine sensor was determined from its hysteresis by cycling the free chlorine concentration from 1 to 8, and back to 1 ppm, which resulted in an average hysteresis of 11 nA corresponding to a resolution of 0.06 ppm. The selectivity of the sensor was studied by measuring the sensor response by adding 0.2 mL of 5% interfering solutions (with an equivalent concentration of ∼400 ppm) into 25 mL of 2 ppm NaOCl solution (Fig. 4(d)). The free Cl sensor showed negligible response to the interfering solution of KNO_3, K_2SO_4, Na_2CO_3, $NaHCO_3$, NaCl, $(NH_4)_2SO_4$, $NaHPO_4$ and NaOAc and was able to perform free Cl sensing measurements successfully right after the selectivity test. The developed free chlorine sensor showed the following advantages compared to conventional three-electrodes based amperometric sensors and other free chlorine sensors fabricated by microfabrication technologies [54],[336]:

(1) The sensitivity of the free chlorine sensor is high enough for drinking water monitoring purposes. The sensing accuracy is further improved due to its integration with pH and temperature sensors for signal compensation.

(2) The highly reproducibility of the sensor resulted in nearly calibration-free sensing, since the calibration is only required for one sensor before the first use.

(3) The sensor readout circuit does not need any potentiostat to activate the sensor, resulting in simplicity of the integration.

(4) The sensing procedure does not require any sample preconditioning steps (e.g. oxidation, dilution, pH adjustment) using chemicals are not needed, thereby reduces the operation complexity.

(5) The use of carbon paste and Ag/AgCl paste, and hand-drawing those directly on the glass substrate have greatly enhanced cost-effectiveness of the sensor.
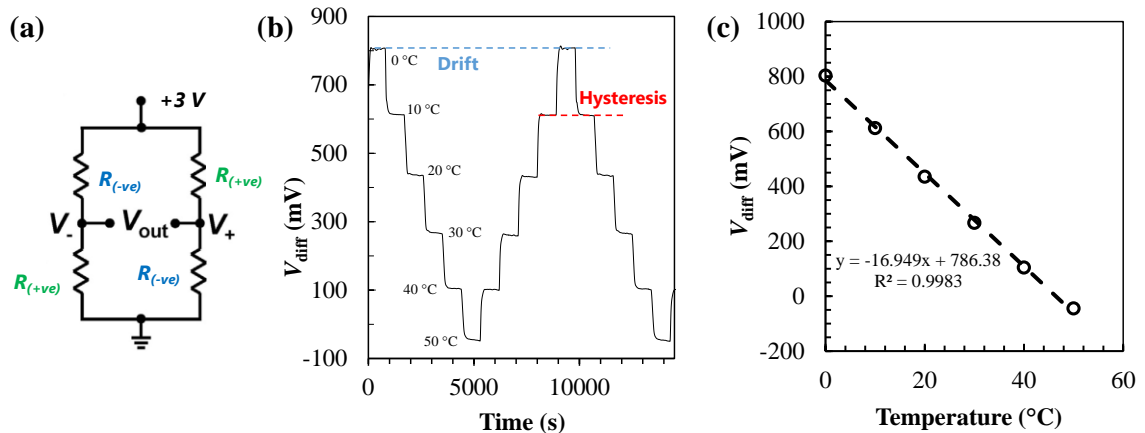
Figure 6-9. (a) Circuit diagram of the Wheatstone-bridge-based temperature sensor with 4 thermistors. (b) Temporal response of the temperature sensor for temperatures between 0 and 50 °C. (c) Calibration curve of the temperature sensor.

6.3.4. Temperature sensor

We used a Wheatstone bridge circuit for the temperature sensor (Fig. 5(a)), where $R_{Si1,2}$ were two pieces of p-type silicon wafer (1 cm × 10 cm) that have a positive TCR value of 1%/∘C (Figure B- 1), and $R_{PEDOT:PSS1,2}$ were drop-casted PEDOT:PSS films that have a negative TCR value of −0.32%/∘C (Figure B- 2) [341,342]. The Si and PEDOT:PSS were used as-received which simplified the integration process. Also, their high TCR values resulted in higher temperature sensitivity with negligible drift. The resistance values of the four thermistors in the Wheat-stone bridge circuit were chosen to be $R_{Si1} = 800$ Ω, $R_{Si2} = 1300$ Ω, $R_{PEDOT:PSS1} = 1500$ Ω, and $R_{PEDOT:PSS2} = 800$ Ω (Figure 6-9(a)) so that (1) the output voltage stays within the range of −1 to +1 V to be able to be read by the ADC for a temperature range of $0 − 50$ °C (for most water quality monitoring applications), (2) the sensitivity is maximized for higher accuracy, (3) the equivalent resistance of the bridge is

159

large enough to prevent self-heating-induced drift of the sensor output, and (4) the overall area of the sensor remains small enough for an adequate spatial resolution.

The temporal response (between $0 - 50\,°C$) was measured for the temperature sensor which showed increased and decreased resistances R_{Si} and $R_{PEDOT:PSS}$, respectively, with the increase of temperature. This resulted in an increased voltage of V^- and decreased voltage of V^+ decreases with overall decrease for $V_{out} = V^+ - V^-$ also decreases) as the temperature increases. This differential voltage phenomenon defines the temperature sensitivity, dVout/dT, of the Wheatstone bridge. Moreover, the temperature induced output voltage showed a fast and linear response with the change of temperature change, to facilitate real-time compensation of the pH and free chlorine sensors. The sensitivity of the temperature sensor was calculated to be ~ 16.95 mV/$\circ$C (Figure 6-9(b)), which was lower than the theoretical value (~ 18.5 mV/°C). The reduced sensitivity might be due to the mismatch in the thermal expansion coefficient and temperature induced stress of the epoxy coating on the four thermistors to that of Si and PEDOT:PSS. The following calibration equation was programmed into the microprocessor for the calculation of temperature:

$$T_{meas} = \frac{786.38 - V_{out}}{16.95}, \tag{6-8}$$

where T_{meas} (in °C) is the measured temperature of the water sample and V_{out} (in mV) is the output voltage of the temperature sensor. In summary, the developed temperature sensor has the following advantages:

(1) The Wheatstone-bridge-based configuration of the temperature sensor provided higher sensitivity than a single-resistor based thermistor.

(2) The sensor is fabricated by directly drop-casting PEDOT:PSS liquid and cutting/gluing silicon on to a glass substrate, therefore, the sensor is inexpensive and easy-to-integrate.

Table 6-1: Measurement of pH, free chlorine concentration and temperature of real water samples (average values from 5 measurements)

	Tap water (Hamilton)		Lake water (Lake Ontario)		Swimming pool water (McMaster University)	
	FIWQMS system	Reference	FIWQMS system	Reference	FIWQMS system	Reference
pH	8.25 ± 0.30	8.15 ± 0.06	7.29 ± 0.23	7.53 ± 0.05	6.85 ± 0.20	7.21 ± 0.08
Free Cl, ppm	1.01 ± 0.05	0.97 ± 0.04	0.00 ± 0.00	0.00 ± 0.00	2.55 ± 0.26	2.18 ± 0.22
Temperature, °C	16.05 ± 0.25	16.20 ± 0.10	4.35 ± 0.18	4.44 ± 0.14	25.86 ± 0.45	27.23 ± 0.10

Table 6-2: Determination results of APAP and E2 in Hamilton tap water using MWCNT-βCD(SE)/SPE (Average values were calculated from five determinations).

	Prepared Concentration (μM)	Found (μM)	Recovery
APAP	0.50	0.48 ± 0.015	$96.0\%\pm3.0\%$
E2	0.50	0.53 ± 0.012	$106.0\%\pm2.4\%$
Pb^{2+}	0.50	0.51 ± 0.013	$102.0\%\pm2.6\%$

6.3.5. Measurement of water samples

The integrated sensors were connected to the programmed Arduino based FIWQMS board for the monitoring of tap water, lake water, and swimming pool water. Table 6-1 shows the comparison of the pH, free chlorine, and temperature measurements taken from the FIWQMS system with measurements taken from reference methods. A commercial pH meter with a glass electrode was used as the reference for pH sensing. A DPD-based colorimetric test kit was used as the reference for free chlorine sensing. A thermometer was used as the reference for temperature sensing. Table 6-2 shows the comparison of the pharmaceuticals (i.e., APAP and E2) and heavy metal (Pb^{2+}) sensing measurements taken from the FIWQMS system with their known spiked concentrations. The pharmaceuticals and heavy metal sensing was done by spiking tap water with APAP, E2 and Pb^{2+}. The measurements taken using the FIWQMS system were close to those measured from reference methods, with a difference less than 5%, 15%, and 5% for pH, free chlorine, temperature. The APAP, E2 and Pb^{2+} determination in spiked tap water showed recovery results between 96%−106%.

6.3.6. Costs of the sensor system

The total costs of the FIWQMS system include the costs of the sensors and the readout circuitry. The cost of the sensors is very low compared to that of the one-time cost of the readout circuitry. Table 6-3 shows the item-wise costs breakdown of the FIWQMS system. The cost of the data acquisition system is approximately $333 CAD, which is a one-time cost and can be reduced significantly if made in large scale and with custom-designed chips. On the other hand, the cost of the electrochemical sensors is below $2.46 CAD, which is can also be further reduced if fabricated in large commercially. Therefore, the FIWQMS system is suitable for their ubiquitous use, especially in developing and under-developed countries. In addition, the fabrication procedure of the sensors, the circuit schematics and source codes are publicly available for use in non-commercial and research purposes by students and researchers for further development.

Table 6-3: Costs breakdown of the FIWQMS system. The green texts correspond to the electrochemical sensors and their associated costs, and the red texts corresponds to the data acquisition system and its costs.

Name of main parts	Subparts	Price (CAD)
Pharmaceutical/heavy metal sensor	Screen printed electrode (SPE)	$1.25
	MWCNT-βCD	< $0.01
pH sensor	Pd/PdO ink (6 µl)	< $1
	Ag/AgCl paste reference	
Free chlorine sensor	Carbon electrode modified by ammonium carbamate	< $0.1
	Ag/AgCl paste reference	
Temperature sensor	Diced silicon wafer	< $0.1
	PEDOT:PSS (~6 µl)	
	Silver paste	
Data acquisition system	Arduino Uno Rev3	$28
	Bluetooth (BLE) Shield	$25
	Water Quality Monitor (WQM) shield: for pH, free chlorine and temperature sensors	$80
	Potentiostat shield	$200
	Android App (Custom-made)	-
Total Cost of the FIWQMS	Data acquisition system + Sensors	$333 + (< $2.46)

6.4. Conclusions

We have developed a fully integrated water quality monitoring system (FIWQMS) for the simultaneous detection of water parameters including pH, free chlorine concentration, and temperature. The FIWQMS system included integrated sensors array with spin-coated pH sensor, hand-drawn and electrochemically modified free chlorine sensor, hand-made/hand-drawn temperature sensors, and a multi-walled carbon nanotubes and β-cyclodextrin modified screen printed electrode for pharmaceuticals and heavy metal sensor all in just two pieces of glass substrates. These sensors were compact in size with a total size of two 25 mm × 75 mm, glass slides sandwiched together that offered high sensitivity, fast response time, and user-friendly operation at low cost (~$336 CAD only). The measurement accuracy of pH, free chlorine and temperature sensors was >85%, and the pharmaceuticals and heavy metal sensor showed sensing recovery of 96%−106%. The FIWQMS system shows that it can be a promising tool for practical application of the integrated sensing system for on-site water quality monitoring due to the miniaturization and simplification of the conventional laboratory-based analytical methods in a portable format. The similar sensing platform can also be utilized with simple modifications to monitor other water quality parameters such as conductivity, dissolved oxygen, and bacteria. A modified version of this system can be used for promising applications such as wearable molecular monitoring of human sweat.

Chapter 7

Conclusions and recommendations

7.1. Conclusions

Conventional laboratory-based analytical techniques provide highly accurate and reliable results regarding water quality parameters. However, these analytical techniques require trained personnel, long sample pre-processing, expensive equipment, which limits their application to realize continued water safety in resource limited and highly populated areas. Recent research activities demonstrated individual electrochemical sensors for low-cost and highly sensitive water quality monitoring, yet these electrochemical sensors are still difficult to be integrated into a functional monitoring system. Therefore, the purpose of this research was to develop an integrated, low-cost, easy-to-use, and highly sensitive pharmaceuticals, heavy metal, pH, temperature, and free chlorine sensing system for real-time, multi-parameter water quality monitoring.

This thesis focuses on the design, fabrication, and characterization of electrochemical sensors for pharmaceuticals, heavy metal, pH, temperature, and free chlorine sensors. An integrated system is demonstrated using these five sensors in this thesis. For pharmaceuticals sensing, multi-walled carbon nanotubes (MWCNT) and β-cyclodextrin (βCD) were used in three-electrode potentiostatic configuration due to the materials high sensitivity, and simple fabrication. For heavy metal sensing, the same MWCNT-βCD based electrochemical sensor was used, which simplified the integrated sensor configuration at low cost. For pH sensing, Pd/PdO thin films were used in two-electrode potentiometric sensing configuration due to the material's high pH sensitivity, short response time, and high stability. For temperature sensing, a Wheatstone bridge consisting of two silicon thermistors with positive TCR, and two PEDOT:PSS thermistors with negative TCR were

employed to increase the sensitivity. For free chlorine sensing, an amperometric sensor was developed for continuous monitoring in a simplified two-electrode configuration with amine-modified carbon electrode. The abovementioned sensing materials and sensor configurations provided highly sensitive and efficient measurement.

The cost efficiency of the system was improved by fabricating the sensors on two glass substrates using solution-based processes: ultrasonic preprocessing, one-step chemical synthesis, and electrochemical modification. These fabrication techniques consumed a small amount of materials without the use of any cleanroom environment, high-temperature/pressure conditions, and/or high-vacuum equipment.

The integrated sensor was connected to two signal conditioning circuit board (potentiostat board: pharmaceuticals/heavy metal; WQM board: pH/free chlorine, temperature) and a programmed Arduino Uno microcontroller board with a Bluetooth shield for signal processing and display. The portable and integrated water quality monitoring system was able to accurately measure the spiked pharmaceuticals and heavy metal, pH value, temperature, and free chlorine concentration in tap water and lake water.

In Chapter 1, the background of water quality (pharmaceuticals, heavy metal, pH and free chlorine) monitoring was presented, followed by a comprehensive overview of the electrochemical sensors for pharmaceuticals, heavy metal, pH and free chlorine. By comparing different types of sensor configurations and sensing materials, we choose to use MWCNT and βCD- based voltammetric sensor pharmaceuticals and heavy metal sensing, metal/metal oxide-based potentiometric sensor for pH monitoring, and functionalized carbon materials for free chlorine sensing.

In Chapter 2, we studied the acetaminophen sensing mechanism and property of MWCNT-βCD modified electrochemical sensor. We fabricated a simple, rapid, and low-cost electrochemical sensor for precise sensing of acetaminophen based on MWCNT-βCD

modification of glassy carbon electrode. XPS, SEM, and AFM studies were used to determine the surface morphology of the drop-casted MWCNT-βCD films and the chemical composition when exposed to solutions containing acetaminophen [343]. The sensor demonstrated excellent redox activity towards acetaminophen sensing with limit of detection of 11 nM. Also, a wide two-step linear detection ranges from 0.05–1 μM and 1–300 μM was observed. The sensor exhibited high stability, good reproducibility and selectivity towards acetaminophen sensing in the presence of common interfering species. We investigated the sensing performance of the sensor using commercially available acetaminophen tablets and human urine. A recovery of more than 95% was observed. The superior acetaminophen sensing behavior may be related to the novel process that combines the adsorption properties of βCD with high surface area of carbon nanotubes.

In Chapter 3, we tailored MWCNT-βCD functionalization processes and compared their electrochemical sensing performance for sensitive detection of acetaminophen and estrogen. A systematic investigation of four types of modified MWCNT-βCD: (1) physical mixing, (2) "click reaction", (3) thionyl chloride esterification, and (4) Steglich esterification was reported. Steglich esterification, a one-step approach with shorter reaction time, lower reaction temperature, was developed which eliminated the handling of air/moisture-sensitive reagents. The Steglich esterification based MWCNT-βCD facilitated moderate βCD loading (5–10 wt %), with large effective surface area, and fast electron transfer. Sensitive detection of acetaminophen (APAP) and 17β-estradiol (E2, a primary female sex hormone) was observed due to the host–guest interaction of βCD and redox properties of MWCNT. The sensing ranges of APAP and E2 were 0.005–20 and 0.01–15 μM, with low detection limits of 3.3 and 2.5 nM, respectively. The proposed sensor also demonstrated accurate detection results of pharmaceutical compositions in water and urine samples.

In Chapter 4, we demonstrated low-cost and easy-to-use electrochemical sensors for the determination of Pb^{2+} using physical and a one-step chemical modification (Steglich

esterification) of MWCNT with βCD developed in Chapter 3. The modified MWCNT-βCD electrodes demonstrated excellent electrochemical sensing performance for the detection of Pb^{2+} with limits-of-detection of 0.9 and 2.3 ppb for physical and covalent modifications, respectively. Higher sensitivity was observed with the physically modified MWCNT-βCD based electrode. On the other hand, better reliability and reusability were observed with the covalently modified MWCNT-βCD based electrode. The high sensitivity and better reliability/reusability aspects of the physical and covalent modification approaches could be attributed to the amount of βCD and type of βCD modifications, respectively. The cost for electrodes fabrications and the materials was calculated to be only \$2.64 per 1000 MWCNT-βCD modifications. The reusability of the MWCNT-βCD based electrodes for at least four times further reduced the final cost of each measurement. The sensors also showed good selectivity in the presence of other interfering heavy metal ions such as Zn^{2+} and Cd^{2+} with very high concentrations. The developed sensor is suitable to be integrated in a low-cost and portable sensing system for drinking water quality monitoring.

In Chapter 5, we studied noises in electrochemical sensors to understand the dependence of noise level on the type of electrolyte solutions, bias voltages and electrode materials. This study identified possible effect of noise on electrochemical sensing performances. The type of the electrolytes, electrode modifications, as well as bias voltage dependent $1/f$ noise were studied in screen printed electrode (SPE) and MWCNT-βCD modified SPE electrode. The noise level remained almost constant irrespective of the type of the electrolyte solutions or the bias voltages. However, a slight increase of the noise level (only about three times) was observed after modification of the electrodes with MWCNT and βCD. A wider current range of the working electrode was observed with the PBS solution compared to that of $K_3[Fe(CN)_6]$ solution. Also, the electrochemical potential of the electrodes in PBS solution was more closer to 0 mV compared to $K_3[Fe(CN)_6]$ solution, which was < -200 mV. The increase of the noise level due to MWCNT and βCD modifications showed negligible impact on the signal-to-noise ratio in the electrochemical sensing measurements.

In Chapter 6, we developed an integrated water quality monitoring system for the simultaneous detection of water quality parameters including pharmaceuticals, heavy metal, pH, free chlorine concentration, and temperature. The system consisted of an integrated sensing probe with MWCNT-βCD modified screen printed carbon electrode for pharmaceuticals and heavy metal sensing, spin-coated Pd/PdO for pH sensing, electrochemically modified carbon electrode for free chlorine sensing, and a silicon/PEDOT:PSS-based Wheatstone-bridge for temperature sensing. These sensors were highly sensitive, small in sizes and user-friendly with fast response time which were achieved at low cost. Water samples were monitored with high accuracy using the integrated sensors with a programmed Arduino Uno microcontroller board which controlled two other data acquisition boards. This study demonstrates the feasibility and practical application of the integrated sensing system as a simple and low cost alternative of the conventional laboratory-based analytical methods for on-site water quality monitoring.

7.2. Recommendations

This research work focused on developing an integrated and easy-to-use sensing system using low-cost, highly sensitive electrochemical sensors for water quality monitoring. However, few features of the sensors and the integrated sensing system need to be improved in the future.

Pharmaceuticals and heavy metal sensors

Sensor repeatability and reliability

- The main difficulty in using the electrochemical sensor for pharmaceuticals and heavy metal sensing is the requirement of the use of freshly modified electrode for each measurement. Although, the sensor can be reused for a few times for heavy metal sensing, the sensor needs to be electrochemically cleaned before doing repeated measurements. Therefore, the reusability of the MWCNT-βCD modified electrodes needs to be improved.

- The major impediment towards reusing MWCNT-βCD modified electrodes for pharmaceuticals and heavy metal sensing is that the analytes (i.e., APAP and E2) becomes adsorbed on the surface of the electrode, which requires to be desorbed from the electrode surface, also known as electrode regeneration. The most common technique for the desorption of the analytes is cyclic voltammetry by sweeping between two voltages (typically ±1 V) in a strong acid solution. However, the use of strong acids during voltammetric sweeping may cause the MWCNT-βCD to be delaminated from the electrode surface. Therefore, an efficient and sustainable electrode regeneration process needs to be developed.

- Also, the time required to regenerate the one MWCNT-βCD modified electrode is almost comparable to making a freshly prepared electrode by cleaning the electrode surface and drop-casting a new drop of MWCNT-βCD. However, the drop-casting process is done by hand which is prone to human error, and thereby, can cause measurement inaccuracy. Therefore, an improved and more accurate drop-casting process should be developed.

Sensor fabrication scale-up

- Accurate drop-casting can be accomplished by other deposition methods such as screen-printing and ink-jet printing. For each of the printing process, the viscosity and surface tension of the MWCNT-βCD solution needs to be adjusted by adding some other chemicals and solvents. Addition of other reagents may incur additional complexity in the fabrication processes as well as the sensing performance.

Sensor robustness

- The electrode delamination can be avoided by ensuring proper adhesion of MWCNT-βCD on the surface of the electrode. One approach could be direct growth of MWCNT on an electrode substrate surface and subsequent modification of MWCNT with βCD. Another approach could be the use of an adhesion-

improvement layer such as self-assembled monolayer of (3-aminopropyl)triethoxysilane (APTES). However, use of such monolayer needs careful consideration of their impact on the sensing performances.

Sensitivity and linearity

- The linear range and limit of detection of the MWCNT-βCD modified electrodes can be further improved by optimizing the βCD attachment to MWCNT. In Chapter 3, we observed that chemically modified MWCNT-βCD through Steglich esterification provides the best sensing performances. On the other hand, chemically modified MWCNT-βCD through Click reaction does not provide any sensitivity to the pharmaceuticals. The main reason for this discrepancy in sensing behaviour was attributed to the molecular orientation of βCD with MWCNT. In case of Steglich esterification, βCD is attached to the end of the nanotubes, rather than on the nanotubes sidewall as observed in Click reaction. Therefore, we concluded that attachment of βCD to the end of nanotubes improves the sensing performance. It suggests that if we can attach more βCD on the end of nanotubes, we may achieve even better sensing performances. However, the number of βCD that can be attached on the end of the nanotubes is limited by the number of –COOH groups, which is controlled by the MWCNT functionalization process. Therefore, MWCNT with varying amount of –COOH can be utilized in future to analyse the relative sensing performance of the MWCNT-βCD modified electrode.

- Also, the sensing performance of MWCNT-βCD modified electrodes are not as good as biosensors. Improving sensing performance of the MWCNT-βCD modified electrodes requires further research on developing multi-layer and multifunctional sensing materials and structures. For example, MWCNT-βCD modified electrodes may be incorporated with other metallic nanoparticles which possess high electrocatalytic behaviour in electrooxidation or electroreduction of pharmaceuticals and heavy metals.

Selectivity

- The selectivity of the MWCNT-βCD modified electrodes are not as good as biosensors. There may be mixture of hundreds of other pharmaceuticals that may be present in drinking water having very closely located redox peak potentials. Therefore, the selectivity of the sensor should be improved by introducing an additional layer that only permits the intended pharmaceuticals or heavy metals into electrode surface. One approach could be the use molecularly imprinted polymer (MIP) layer on top of the modified electrode surface. However, the use MIP has its own challenges associated with it that require careful consideration.

Calibration

- The major difficulty in using the pH sensor is the requirement of the calibration step. Calibration is needed due to the variation in the sensor sensitivity, and/or the drift of the sensor output voltage. Thus, the stability of the Pd/PdO sensing electrode needs to be improved for a calibration-free sensor.
    - We observed that the sensitivity of the pH sensing electrode was affected by the electrode surface area. A smaller surface area (< 10 mm^2) resulted in a sub-Nernstian sensitivity. Also, mechanical delamination of the Pd/PdO film was observed, which further reduced the electrode area, hence a lower sensitivity. Therefore, the mechanical adhesion between the Pd/PdO film and the substrate can be improved, for example, by applying an adhesion-improvement layer between them.
    - The drift and hysteresis of the pH sensor was attributed to the buried sites in the Pd/PdO film. High temperature (> 600 °C), high pressure, and/or vacuum-based post processing steps may be used to eliminate the buried sites. These post-processing steps improves the film quality by using external energies to remove chemical contaminants, reconstructing the crystal structures, and reducing the amount of defects in the film.

pH, free chlorine and temperature sensor

Stability

- The stability of the pH sensor also depends on the drift behaviour of the Ag/AgCl reference electrode. Thus, the stability of the reference electrode needs to be improved. The potential drift of the reference electrode is generally caused by the leaching of KCl in the solid electrolyte layer when the electrode is immersed in water. In theory, a stable reference electrode potential can be generated by a constant and very slow leaching of KCl. However, in practical situations, faster KCl leaching may pose greater challenges. Therefore, alternative structures/materials of the reference electrode should be considered.

Sensitivity

- The sensitivity of the pH sensor can also be improved by using three-dimensional nano structures at the electrode surface. In this case, a smaller electrode area can be used as long as the effective sensing area is >10 mm^2 to obtain a near-Nernstian response. The three-dimensional nano structures provide surface areas in the vertical direction so that the horizontal area of the electrode can be reduced. This will also to fabricate miniaturized pH sensor that can be applied for measurements requiring high spatial resolution, and for implantable applications [333].

System miniaturization

- The size of the temperature sensor needs to be reduced. In Chapter 6, the temperature sensor had a size of ~20 mm × 60 mm, which was limited by the size of the individual thermistors with large resistance values. The sensor size can be reduced by using thermistors with lower resistance which can be utilized by using a lower bias voltage.

- In the integrated water quality monitoring system, the electronics part, including the two data acquisition shields, Bluetooth shield and the Arduino Uno shield can be

combined into a single and smaller PCB by combining and redesigning the integrated circuits. Also, a result display unit may be developed in the future.

Linearity

- The sensing range of the amine-modified free chlorine sensor needs to be increased. The free chlorine sensor was able to accurately monitor free chlorine concentrations of 0-8 ppm in drinking water and swimming pool water, the sensing range is too narrow for the monitoring of food processing waters which is in the range of 50-200 ppm. A wide sensing range can be obtained by attaching more amine groups to the carbon electrode by the use of three-dimensional nanostructures.

The work presented in this thesis was a pilot research and development project. The target of this research was to develop an integrated, easy-to-use, accurate, and low-cost sensing system for water quality monitoring. It is demonstrated that solution-based, low cost electrochemical sensors could be proper candidates to fabricate and integrate multiple types of sensors with high sensing performance. This research provides the feasibility, challenges, and potential solutions to develop water quality monitoring systems for practical applications.

References

[1]   WHO | Progress on drinking water, sanitation and hygiene, WHO. (2017). https://www.who.int/water_sanitation_health/publications/jmp-2017/en/ (accessed January 22, 2019).

[2]   WHO, Pharmaceuticals in drinking-water - World Health Organization, in: 2012. http://www.who.int/water_sanitation_health/publications/2011/pharmaceuticals/en/ .

[3]   USEPA, Water Sentinel online water quality monitoring as an indicator of drinking water contamination, 2005.

[4]   C. Hignite, D.L. Azarnoff, Drugs and drug metabolites as environmental contaminants: chlorophenoxyisobutyrate and salicyclic acid in sewage water effluent., Life Sci. 20 (1977) 337–41. http://www.ncbi.nlm.nih.gov/pubmed/839964.

[5]   C.D. Watts, B. Crathorne, M. Fielding, C.P. Steel, Analysis of organic micropollutants in water, Reidel, Dordr. (1983) 120–131.

[6]   T. Heberer, Occurrence, fate, and removal of pharmaceutical residues in the aquatic environment: a review of recent research data, 2002. doi:10.1016/S0378-4274(02)00041-3.

[7]   T.A. Ternes, Occurrence of drugs in German sewage treatment plants and rivers1Dedicated to Professor Dr. Klaus Haberer on the occasion of his 70th birthday.1, Water Res. 32 (1998) 3245–3260. doi:10.1016/S0043-1354(98)00099-2.

[8]   O.A.H. Jones, N. Voulvoulis, J.N. Lester, Human Pharmaceuticals in the Aquatic Environment a Review, Environ. Technol. 22 (2001) 1383–1394. doi:10.1080/09593330.2001.11090873.

[9]   D. Ashton, M. Hilton, K.V. Thomas, Investigating the environmental transport of human pharmaceuticals to streams in the United Kingdom, Sci. Total Environ. 333 (2004) 167–184. doi:10.1016/j.scitotenv.2004.04.062.

[10]   C.G. Daughton, T.A. Ternes, Pharmaceuticals and personal care products in the environment: agents of subtle change?, Environ. Health Perspect. 107 (1999) 907–938. doi:10.1289/ehp.99107s6907.

[11]   O.A. Jones, N. Voulvoulis, J.N. Lester, Potential impact of pharmaceuticals on environmental health., Bull. World Health Organ. 81 (2003) 768–9. http://www.ncbi.nlm.nih.gov/pubmed/14758440.

[12]   O.A.H. Jones, N. Voulvoulis, J.N. Lester, Potential Ecological and Human Health Risks Associated With the Presence of Pharmaceutically Active Compounds in the Aquatic Environment, Crit. Rev. Toxicol. 34 (2004) 335–350. doi:10.1080/10408440490464697.

[13]   K. Kummerer, Resistance in the environment, J. Antimicrob. Chemother. 54 (2004)

311–320. doi:10.1093/jac/dkh325.

[14] R. Hirsch, T. Ternes, K. Haberer, K.-L. Kratz, Occurrence of antibiotics in the aquatic environment, Sci. Total Environ. 225 (1999) 109–118. doi:10.1016/S0048-9697(98)00337-4.

[15] O.A.H. Jones, N. Voulvoulis, J.N. Lester, Human Pharmaceuticals in the Aquatic Environment a Review, Environ. Technol. 22 (2001) 1383–1394. doi:10.1080/09593332208618186.

[16] H. Li, Z. Dong, Q. Weng, C.-C. Chang, B. Liu, Emerging Pollutants – Part I: Occurrence, Fate and Transport, Water Environ. Res. 87 (2015) 1849–1872. doi:10.2175/106143015X14338845156425.

[17] B. Petrie, R. Barden, B. Kasprzyk-Hordern, A review on emerging contaminants in wastewaters and the environment: Current knowledge, understudied areas and recommendations for future monitoring, Water Res. 72 (2015) 3–27. doi:10.1016/j.watres.2014.08.053.

[18] J.P. Bound, N. Voulvoulis, Household Disposal of Pharmaceuticals as a Pathway for Aquatic Contamination in the United Kingdom, Environ. Health Perspect. 113 (2005) 1705–1711. doi:10.1289/ehp.8315.

[19] I. Rodríguez, J.. Quintana, J. Carpinteiro, A.. Carro, R.. Lorenzo, R. Cela, Determination of acidic drugs in sewage water by gas chromatography–mass spectrometry as tert.-butyldimethylsilyl derivatives, J. Chromatogr. A. 985 (2003) 265–274. doi:10.1016/S0021-9673(02)01528-5.

[20] T. Heberer, Tracking persistent pharmaceutical residues from municipal sewage to drinking water, J. Hydrol. 266 (2002) 175–189. doi:10.1016/S0022-1694(02)00165-8.

[21] B. Ferrari, N. Paxéus, R. Lo Giudice, A. Pollio, J. Garric, Ecotoxicological impact of pharmaceuticals found in treated wastewaters: study of carbamazepine, clofibric acid, and diclofenac, Ecotoxicol. Environ. Saf. 55 (2003) 359–370. doi:10.1016/S0147-6513(02)00082-9.

[22] E.C.E. Commission, Priority Substances Daughter Directive-Directive 2008/105/EC of the European Parliament and of the Council of 16 December 2008 on environmental quality standards in the field of water policy Accessed 23/05/2012 at http://eur-lex. europa. eu/LexUriServ, LexUriServ. Do. (2008).

[23] B. Petrie, R. Barden, B. Kasprzyk-Hordern, A review on emerging contaminants in wastewaters and the environment: Current knowledge, understudied areas and recommendations for future monitoring, Water Res. 72 (2015) 3–27. doi:10.1016/j.watres.2014.08.053.

[24] R.D. Bruce, D.J. Versteeg, A statistical procedure for modeling continuous toxicity data, Environ. Toxicol. Chem. 11 (1992) 1485–1494. doi:10.1002/etc.5620111014.

[25] H.H. Lützhøft, B. Halling-Sørensen, S.E. Jørgensen, Algal toxicity of antibacterial agents applied in Danish fish farming., Arch. Environ. Contam. Toxicol. 36 (1999) 1–6. http://www.ncbi.nlm.nih.gov/pubmed/9828255.

[26] R.A. Brain, D.J. Johnson, S.M. Richards, M.L. Hanson, H. Sanderson, M.W. Lam,

C. Young, S.A. Mabury, P.K. Sibley, K.R. Solomon, Microcosm evaluation of the effects of an eight pharmaceutical mixture to the aquatic macrophytes Lemna gibba and Myriophyllum sibiricum, Aquat. Toxicol. 70 (2004) 23–40. doi:10.1016/j.aquatox.2004.06.011.

[27] B. Halling-Sørensen, Algal toxicity of antibacterial agents used in intensive farming., Chemosphere. 40 (2000) 731–9. http://www.ncbi.nlm.nih.gov/pubmed/10705551.

[28] B.D. Giudice, T.M. Young, The antimicrobial triclocarban stimulates embryo production in the freshwater mudsnail *Potamopyrgus antipodarum*, Environ. Toxicol. Chem. 29 (2010) 966–970. doi:10.1002/etc.105.

[29] M. Terasaki, M. Makino, N. Tatarazako, Acute toxicity of parabens and their chlorinated by-products with *Daphnia magna* and *Vibrio fischeri* bioassays, J. Appl. Toxicol. 29 (2009) 242–247. doi:10.1002/jat.1402.

[30] M. DellaGreca, M.R. Iesce, M. Isidori, A. Nardelli, L. Previtera, M. Rubino, Phototransformation products of tamoxifen by sunlight in water. Toxicity of the drug and its derivatives on aquatic organisms, Chemosphere. 67 (2007) 1933–1939. doi:10.1016/j.chemosphere.2006.12.001.

[31] M. Isidori, A. Nardelli, L. Pascarella, M. Rubino, A. Parrella, Toxic and genotoxic impact of fibrates and their photoproducts on non-target organisms., Environ. Int. 33 (2007) 635–41. doi:10.1016/j.envint.2007.01.006.

[32] M. Isidori, M. Lavorgna, A. Nardelli, L. Pascarella, A. Parrella, Toxic and genotoxic evaluation of six antibiotics on non-target organisms, Sci. Total Environ. 346 (2005) 87–98. doi:10.1016/j.scitotenv.2004.11.017.

[33] B.W. Brooks, P.K. Turner, J.K. Stanley, J.J. Weston, E.A. Glidewell, C.M. Foran, M. Slattery, T.W. La Point, D.B. Huggett, Waterborne and sediment toxicity of fluoxetine to select organisms, Chemosphere. 52 (2003) 135–142. doi:10.1016/S0045-6535(03)00103-6.

[34] R. Andreozzi, V. Caprio, C. Ciniglia, M. de Champdoré, R. Lo Giudice, R. Marotta, E. Zuccato, Antibiotics in the Environment: Occurrence in Italian STPs, Fate, and Preliminary Assessment on Algal Toxicity of Amoxicillin, Environ. Sci. Technol. 38 (2004) 6832–6838. doi:10.1021/es049509a.

[35] E.U. TGD, Technical guidance document on risk assessment in support of commission directive 93/67/EEC on risk assessment for new notified substances, Commission Regulation (EC) No 1488/94 on Risk Assessment for existing substances, and Directive 98/8/EC of the Euro, Part II. Eur. Comm. Jt. Res. Centre. EUR. 20418 (2003).

[36] M. Cleuvers, Aquatic ecotoxicity of pharmaceuticals including the assessment of combination effects, Toxicol. Lett. 142 (2003) 185–194. doi:10.1016/S0378-4274(03)00068-7.

[37] F. Stuer-Lauridsen, M. Birkved, L.P. Hansen, H.-C. Holten Lützhøft, B. Halling-Sørensen, Environmental risk assessment of human pharmaceuticals in Denmark after normal therapeutic use, Chemosphere. 40 (2000) 783–793. doi:10.1016/S0045-

6535(99)00453-1.

[38]   D.J. Caldwell, F. Mastrocco, P.D. Anderson, R. Länge, J.P. Sumpter, Predicted-no-effect concentrations for the steroid estrogens estrone, 17β-estradiol, estriol, and 17α-ethinylestradiol., Environ. Toxicol. Chem. 31 (2012) 1396–406. doi:10.1002/etc.1825.

[39]   W.F. Boron, E.L. Boulpaep, Medical physiology, n.d.

[40]   WHO | Guidelines for drinking-water quality, 2nd edition: Volume 2 - Health criteria and other supporting information, WHO. (2018).

[41]   Guidelines for Canadian Drinking Water Quality: Guideline Technical Document – Chlorine - Canada.ca, 2009. https://www.canada.ca/en/health-canada/services/publications/healthy-living/guidelines-canadian-drinking-water-quality-chlorine-guideline-technical-document.html (accessed January 24, 2019).

[42]   USEPA, "Nitrification," Office of Water, Washington, D.C., USA, 2002.

[43]   J.M. Willey, L. Sherwood, C.J. Woolverton, L.M. Prescott, Prescott, Harley, and Klein's microbiology, McGraw-Hill Higher Education, 2008. https://archive.org/details/Microbiology_7_edition_by_Joanne_Willey_Linda_Sherwood_Chris_Woolverton/page/n1 (accessed January 24, 2019).

[44]   W.W. Group, Health impact of acidic deposition, Sci. Total Environ. 52 (1986) 157–187. doi:10.1016/0048-9697(86)90118-X.

[45]   E.I. Gill, A. Arshak, K. Arshak, O. Korostynska, Investigation of Thick-Film Polyaniline-Based Conductimetric pH Sensors for Medical Applications, IEEE Sens. J. 9 (2009) 555–562. doi:10.1109/JSEN.2009.2016608.

[46]   R. Sadiq, S. Imran, V. Kleiner, IWA Publishing., Water Environment Research Foundation., Examining the impact of water quality on the integrity of distribution infrastructure, Water Environment Research Foundation, 2007.

[47]   Organisation for Economic Co-operation and Development., World Health Organization., Assessing microbial safety of drinking water : improving approaches and methods, OECD, 2003.

[48]   M.H. Banna, S. Imran, A. Francisque, H. Najjaran, R. Sadiq, M. Rodriguez, M. Hoorfar, Online drinking water quality monitoring: Review on available and emerging technologies, Crit. Rev. Environ. Sci. Technol. 44 (2014) 1370–1421. doi:10.1080/10643389.2013.781936.

[49]   G.F. Connell, The chlorination/chloramination handbook, American Water Works Association, 1996.

[50]   WHO | Guidelines for drinking-water quality, 3rd edition: Volume 1 - Recommendations, WHO. (2018). https://www.who.int/water_sanitation_health/publications/gdwq3rev/en/ (accessed January 24, 2019).

[51]   US EPA, National Primary Drinking Water Regulations, (n.d.). https://www.epa.gov/ground-water-and-drinking-water/national-primary-drinking-water-regulations (accessed January 24, 2019).

[52]   K. Senthilkumar, J.-M. Zen, Free chlorine detection based on EC' mechanism at an

electroactive polymelamine-modified electrode, Electrochem. Commun. 46 (2014) 87–90. doi:10.1016/j.elecom.2014.06.018.

[53]   Y. Qin, S. Pan, M.M.R. Howlader, R. Ghosh, N.-X. Hu, M.J. Deen, Paper-Based, Hand-Drawn   Free   Chlorine   Sensor   with   Poly(3,4-ethylenedioxythiophene):Poly(styrenesulfonate)., Anal. Chem. 88 (2016) 10384–10389. doi:10.1021/acs.analchem.6b03211.

[54]   Y. Qin, H.-J. Kwon, M.M.R. Howlader, M.J. Deen, Microfabricated electrochemical pH and free chlorine sensors for water quality monitoring: recent advances and research challenges, RSC Adv. 5 (2015) 69086–69109. doi:10.1039/C5RA11291E.

[55]   Lead   poisoning   and   health,   (n.d.).   https://www.who.int/news-room/fact-sheets/detail/lead-poisoning-and-health (accessed January 24, 2019).

[56]   Childhood   Lead   Poisoning,   (n.d.). http://www.who.int/ceh/publications/leadguidance.pdf (accessed November 5, 2018).

[57]   Lead   in   Drinking   Water,   (n.d.).   https://www.canada.ca/en/health-canada/programs/consultation-lead-drinking-water/document.html   (accessed November 5, 2018).

[58]   B.P. Lanphear, K. Dietrich, P. Auinger, C. Cox, Cognitive deficits associated with blood lead concentrations <10 microg/dL in US children and adolescents., Public Health Rep. 115 (n.d.) 521–9. http://www.ncbi.nlm.nih.gov/pubmed/11354334.

[59]   R.A. Goyer, Lead toxicity: current concerns., Environ. Health Perspect. 100 (1993) 177–187. doi:10.1289/ehp.93100177.

[60]   Gobal   Water   Crisis: The   Facts,   (n.d.).   http://inweh.unu.edu/wp-content/uploads/2017/11/Global-Water-Crisis-The-Facts.pdf (accessed November 5, 2018).

[61]   C.W. Pifer, E.G. Wollish, M. Schmall, Titration of Pharmaceuticals in Nonaqueous Solvents *, J. Am. Pharm. Assoc. (Scientific Ed.). 42 (1953) 509–521. doi:10.1002/jps.3030420902.

[62]   N. Alizadeh, F. Keyhanian, SIMPLE, SENSITIVE AND SELECTIVE SPECTROPHOTOMETRIC   ASSAY   OF   NAPROXEN   IN   PURE, PHARMACEUTICAL PREPARATION AND HUMAN SERUM SAMPLES., Acta   Pol.   Pharm.   72   (n.d.)   867–75. http://www.ncbi.nlm.nih.gov/pubmed/26665392.

[63]   K. Pavić, O. Čudina, D. Agbaba, S. Vladimirov, Quantitative analysis of cyproterone acetate and ethinylestradiol in tablets by use of planar chromatography, J. Planar Chromatogr. – Mod. TLC. 16 (2003) 45–47. doi:10.1556/JPC.16.2003.1.9.

[64]   M. Calcara, V. Enea, A. Pricoco, F. Miano, Capillary electrophoresis assay of netilmicin   sulphate,   J.   Pharm.   Biomed.   Anal.   38   (2005)   344–348. doi:10.1016/j.jpba.2004.12.019.

[65]   M.R. Siddiqui, Z.A. AlOthman, N. Rahman, Analytical techniques in pharmaceutical analysis: A review, Arab. J. Chem. 10 (2017) S1409–S1421. doi:10.1016/j.arabjc.2013.04.016.

[66] H. Marona, Development and validation of a nonaqueous titration with perchloric acid to determine sparfloxacin in tablets, Eur. J. Pharm. Biopharm. 52 (2001) 227–229. doi:10.1016/S0939-6411(01)00177-1.

[67] N. Matei, N. Matei, S. Birghila, V. Popescu, S. Dobrinas, A. Soceanu, C. Oprea, V. Magearu, KINETIC STUDY OF VITAMIN C DEGRADATION FROM PHARMACEUTICAL PRODUCTS, (2006). http://citeseerx.ist.psu.edu/viewdoc/summary?doi=10.1.1.553.5704 (accessed January 25, 2019).

[68] S. Görög, Ultraviolet-Visible Spectrophotometry in Pharmaceutical Analysis, CRC Press, 2018. doi:10.1201/9781351077422.

[69] S. Küçükkolbaşı, B. Gündüz, E. Kılıç, Development of a Spectrofluorimetric Method for Determination of Albendazole in Tablets, Anal. Lett. 41 (2008) 104–118. doi:10.1080/00032710701746857.

[70] K. Venugopal, R.N. Saha, New, simple and validated UV-spectrophotometric methods for the estimation of gatifloxacin in bulk and formulations, Farm. 60 (2005) 906–912. doi:10.1016/j.farmac.2005.08.010.

[71] C.V.S. Ieggli, S.G. Cardoso, L.P. Belle, Validation of UV spectrophotometric and nonaqueous titration methods for the determination of carvedilol in pharmaceutical formulations., J. AOAC Int. 88 (n.d.) 1299–303. http://www.ncbi.nlm.nih.gov/pubmed/16385978.

[72] S.B. Shuker, P.J. Hajduk, R.P. Meadows, S.W. Fesik, Discovering High-Affinity Ligands for Proteins: SAR by NMR, Science (80-.). 274 (1996) 1531–1534. doi:10.1126/science.274.5292.1531.

[73] U. Holzgrabe, R. Deubner, C. Schollmayer, B. Waibel, Quantitative NMR spectroscopy—Applications in drug analysis, J. Pharm. Biomed. Anal. 38 (2005) 806–812. doi:10.1016/j.jpba.2005.01.050.

[74] C. Cimpoiu, A. Hosu, S. Hodisan, Analysis of some steroids by thin-layer chromatography using optimum mobile phases, J. Pharm. Biomed. Anal. 41 (2006) 633–637. doi:10.1016/j.jpba.2005.12.004.

[75] J. Tang, J. Peng, L. Zhang, Y. Xiao, High performance liquid chromatography (HPLC) method coupled with resonance Rayleigh scattering detection for the determination of isepamicin, Anal. Methods. 4 (2012) 1833. doi:10.1039/c2ay25127b.

[76] Y. Zuo, L. Zhang, J. Wu, J.W. Fritz, S. Medeiros, C. Rego, Ultrasonic extraction and capillary gas chromatography determination of nicotine in pharmaceutical formulations, Anal. Chim. Acta. 526 (2004) 35–39. doi:10.1016/j.aca.2004.09.035.

[77] W.M.. Niessen, State-of-the-art in liquid chromatography–mass spectrometry, J. Chromatogr. A. 856 (1999) 179–197. doi:10.1016/S0021-9673(99)00480-X.

[78] A. D'Avolio, M. Simiele, M. Siccardi, L. Baietto, M. Sciandra, S. Bonora, G. Di Perri, HPLC–MS method for the quantification of nine anti-HIV drugs from dry plasma spot on glass filter and their long term stability in different conditions, J. Pharm. Biomed. Anal. 52 (2010) 774–780. doi:10.1016/j.jpba.2010.02.026.

[79] J.-D. Berset, R. Brenneisen, C. Mathieu, Analysis of llicit and illicit drugs in waste, surface and lake water samples using large volume direct injection high performance liquid chromatography – Electrospray tandem mass spectrometry (HPLC–MS/MS), Chemosphere. 81 (2010) 859–866. doi:10.1016/j.chemosphere.2010.08.011.

[80] J. Zhou, X. Dai, X. Fang, H. Li, Y. Zhao, A. Gong, DETERMINATION OF CORTISOL IN HUMAN SERUM USING ULTRASONIC EXTRACTION COUPLED WITH ISOTOPE DILUTION LIQUID CHROMATOGRAPHY–MASS SPECTROMETRY, Instrum. Sci. Technol. 39 (2011) 522–533. doi:10.1080/10739149.2011.623209.

[81] D.S. Tarbell, A.T. Tarbell, The development of the pH meter, J. Chem. Educ. 57 (1980) 133. doi:10.1021/ed057p133.

[82] F. Haber, Z. Hlemensiewicz, Über elektrische Phasengrenzkräfte, Zeitschrift Für Phys. Chemie. 67U (1909). doi:10.1515/zpch-1909-6720.

[83] P. Kurzweil, Metal Oxides and Ion-Exchanging Surfaces as pH Sensors in Liquids: State-of-the-Art and Outlook., Sensors (Basel). 9 (2009) 4955–85. doi:10.3390/s90604955.

[84] G. Gordon, D.L. Sweetin, K. Smith, G.E. Pacey, Improvements in the N,N-diethyl-p-phenylenediamine method for the determination of free and combined residual chlorine through the use of FIA., Talanta. 38 (1991) 145–9. http://www.ncbi.nlm.nih.gov/pubmed/18965120.

[85] J.D. Johnson, R. Overby, Stabilized neutral o-tolidine, SNORT, colorimetric method for chlorine, Anal. Chem. 41 (1969) 1744–1750. doi:10.1021/ac60282a027.

[86] M. Zenki, H. Komatsubara, K. Tôei, Determination of residual chlorine in tap water by flow-injection spectrophotometry, Anal. Chim. Acta. 208 (1988) 317–320. doi:10.1016/S0003-2670(00)80763-1.

[87] K.K. Verma, A. Jain, A. Townshend, Determination of free and combined residual chlorine by flow-injection spectrophotometry, Anal. Chim. Acta. 261 (1992) 233–240. doi:10.1016/0003-2670(92)80196-E.

[88] S.G. Dmitrienko, O.A. Sviridova, L.N. Pyatkova, V.A. Zhukova, Y.A. Zolotov, Rapid determination of free active chlorine in water by diffuse reflectance spectroscopy after reaction with polyurethane foams, Anal. Chim. Acta. 405 (2000) 231–237. doi:10.1016/S0003-2670(99)00751-5.

[89] G.C. White, The handbook of chlorination, Van Nostrand Reinhold Co, 1986.

[90] J. Ellis, P.L. Brown, Determination of residual chlorine by derivatisation with 2,6-dimethylphenol and gas chromatographic separation, Anal. Chim. Acta. 124 (1981) 431–436. doi:10.1016/S0003-2670(01)93593-7.

[91] T. Nakagama, M. Yamada, T. Hobo, Chemiluminescence sensor with uranine immobilized on an anion-exchange resin for monitoring free chlorine in tap water, Anal. Chim. Acta. 231 (1990) 7–12. doi:10.1016/S0003-2670(00)86390-4.

[92] F. Kodera, M. Umeda, A. Yamada, Determination of free chlorine based on anodic voltammetry using platinum, gold, and glassy carbon electrodes, Anal. Chim. Acta. 537 (2005) 293–298. doi:10.1016/j.aca.2005.01.053.

[93]   F.J. Del Campo, O. Ordeig, F.J. Muñoz, Improved free chlorine amperometric sensor chip for drinking water applications, Anal. Chim. Acta. 554 (2005) 98–104. doi:10.1016/j.aca.2005.08.035.

[94]   J.C. Morris, The Acid Ionization Constant of HOCl from 5 to 35°, J. Phys. Chem. 70 (1966) 3798–3805. doi:10.1021/j100884a007.

[95]   Y. Moser, M.A.M. Gijs, Miniaturized Flexible Temperature Sensor, J. Microelectromechanical Syst. 16 (2007) 1349–1354. doi:10.1109/JMEMS.2007.908437.

[96]   J.P. Bentley, Temperature sensor characteristics and measurement system design, J. Phys. E. 17 (1984) 430–439. doi:10.1088/0022-3735/17/6/002.

[97]   A.W. Van Herwaarden, P.M. Sarro, Thermal sensors based on the seebeck effect, Sensors and Actuators. 10 (1986) 321–346. doi:10.1016/0250-6874(86)80053-1.

[98]   M. Kimura, K. Toshima, Thermistor-like pn junction temperature-sensor with variable sensitivity and its combination with a micro-air-bridge heater, Sensors Actuators A Phys. 108 (2003) 239–243. doi:10.1016/S0924-4247(03)00290-5.

[99]   M. Badihi-Mossberg, V. Buchner, J. Rishpon, Electrochemical Biosensors for Pollutants in the Environment, Electroanalysis. 19 (2007) 2015–2028. doi:10.1002/elan.200703946.

[100] G. Hanrahan, D.G. Patil, J. Wang, Electrochemical sensors for environmental monitoring: design, development and applications., J. Environ. Monit. 6 (2004) 657–64. doi:10.1039/b403975k.

[101] N. Jaffrezic-Renault, S. Dzyadevych, Conductometric Microbiosensors for Environmental Monitoring, Sensors. 8 (2008) 2569–2588. doi:10.3390/s8042569.

[102] M. Yuqing, C. Jianrong, F. Keming, New technology for the detection of pH, J. Biochem. Biophys. Methods. 63 (2005) 1–9. doi:10.1016/j.jbbm.2005.02.001.

[103] D.V.B. Malkov, B. Zachman, Tom, K.T. Scribner, Comparison of On-line Chlorine Analysis Methods and Instrumentation Built on Amperometric and Colorimetric Technologies, (2010). https://www.semanticscholar.org/paper/Comparison-of-On-line-Chlorine-Analysis-Methods-and-Malkov-Zachman/58de227b9fe12e70afd0f661771ff0a1c0be4918 (accessed January 25, 2019).

[104] Y. Qin, M. Howlader, M. Deen, Low-Temperature Bonding for Silicon-Based Micro-Optical Systems, Photonics. 2 (2015) 1164–1201. doi:10.3390/photonics2041164.

[105] M.M.R. Howlader, M.J. Deen, T. Suga, Nanobonding: A key technology for emerging applications in health and environmental sciences, Jpn. J. Appl. Phys. 54 (2015) 030201. doi:10.7567/JJAP.54.030201.

[106] M.M.R. Howlader, P.R. Selvaganapathy, M.J. Deen, T. Suga, Nanobonding Technology Toward Electronic, Fluidic, and Photonic Systems Integration, IEEE J. Sel. Top. Quantum Electron. 17 (2011) 689–703. doi:10.1109/JSTQE.2010.2080261.

[107] M.H. Banna, H. Najjaran, R. Sadiq, S.A. Imran, M.J. Rodriguez, M. Hoorfar,

Miniaturized water quality monitoring pH and conductivity sensors, Sensors Actuators B Chem. 193 (2014) 434–441. doi:10.1016/j.snb.2013.12.002.

[108] G. Gerlach, M. Guenther, J. Sorber, G. Suchaneck, K.-F. Arndt, A. Richter, Chemical and pH sensors based on the swelling behavior of hydrogels, Sensors Actuators B Chem. 111–112 (2005) 555–561. doi:10.1016/j.snb.2005.03.040.

[109] Q. Thong Trinh, G. Gerlach, J. Sorber, K.-F. Arndt, Hydrogel-based piezoresistive pH sensors: Design, simulation and output characteristics, Sensors Actuators B Chem. 117 (2006) 17–26. doi:10.1016/j.snb.2005.10.041.

[110] Y. Zhang, H. Ji, D. Snow, R. Sterling, G.M. Brown, A pH Sensor Based on a Microcantilever Coated with Intelligent Hydrogel, Instrum. Sci. Technol. 32 (2004) 361–369. doi:10.1081/CI-120037668.

[111] Z. Cheng, M.J. Deen, H. Peng, A Low-Power Gateable Vernier Ring Oscillator Time-to-Digital Converter for Biomedical Imaging Applications, IEEE Trans. Biomed. Circuits Syst. 10 (2016) 445–454. doi:10.1109/TBCAS.2015.2434957.

[112] M.J. Deen, F. Pascal, Electrical characterization of semiconductor materials and devices—review, J. Mater. Sci. Mater. Electron. 17 (2006) 549–575. doi:10.1007/s10854-006-0001-8.

[113] M. Jamal Deen, B. Iñiguez, O. Marinov, F. Lime, Electrical studies of semiconductor–dielectric interfaces, J. Mater. Sci. Mater. Electron. 17 (2006) 663–683. doi:10.1007/s10854-006-0018-z.

[114] M.J. Deen, P.K. (Prasanta K. Basu, Silicon photonics : fundamentals and devices, Wiley, 2012. https://www.wiley.com/en-us/Silicon+Photonics%3A+Fundamentals+and+Devices-p-9780470517505 (accessed January 25, 2019).

[115] D. Wencel, T. Abel, C. McDonagh, Optical Chemical pH Sensors, Anal. Chem. 86 (2014) 15–29. doi:10.1021/ac4035168.

[116] J.N. Tiwari, V. Vij, K.C. Kemp, K.S. Kim, Engineered Carbon-Nanomaterial-Based Electrochemical Sensors for Biomolecules, ACS Nano. 10 (2016) 46–80. doi:10.1021/acsnano.5b05690.

[117] J. Kirsch, C. Siltanen, Q. Zhou, A. Revzin, A. Simonian, Biosensor technology: recent advances in threat agent detection and medicine., Chem. Soc. Rev. 42 (2013) 8733–68. doi:10.1039/c3cs60141b.

[118] M. Govindhan, T. Lafleur, B.-R. Adhikari, A. Chen, Electrochemical Sensor Based on Carbon Nanotubes for the Simultaneous Detection of Phenolic Pollutants, Electroanalysis. 27 (2015) 902–909. doi:10.1002/elan.201400608.

[119] S. Kurbanoglu, S.A. Ozkan, Electrochemical carbon based nanosensors: A promising tool in pharmaceutical and biomedical analysis, J. Pharm. Biomed. Anal. 147 (2018) 439–457. doi:10.1016/j.jpba.2017.06.062.

[120] C. Zhu, G. Yang, H. Li, D. Du, Y. Lin, Electrochemical Sensors and Biosensors Based on Nanomaterials and Nanostructures, Anal. Chem. 87 (2015) 230–249. doi:10.1021/ac5039863.

[121] A. Cernat, M. Terti??, R. S??ndulescu, F. Bedioui, A. Cristea, C. Cristea,

Electrochemical sensors based on carbon nanomaterials for acetaminophen detection: A review, Anal. Chim. Acta. 886 (2015) 16–28. doi:10.1016/j.aca.2015.05.044.

[122] S.R. Gunatilake, V.K. Munasinghe, R. Ranaweera, T.E. Mlsna, K. Xia, Recent advancements in analytical methods for the determination of steroidal estrogen residues in environmental and food matrices, Anal. Methods. 8 (2016) 5556–5568. doi:10.1039/C6AY01422D.

[123] G. Aragay, J. Pons, A. Merkoçi, Recent trends in macro-, micro-, and nanomaterial-based tools and strategies for heavy-metal detection, Chem. Rev. 111 (2011) 3433–3458. doi:10.1021/cr100383r.

[124] A. Rahi, K. Karimian, H. Heli, Nanostructured materials in electroanalysis of pharmaceuticals, Anal. Biochem. 497 (2016) 39–47. doi:10.1016/j.ab.2015.12.018.

[125] PalmSens, PSTrace Help Menu, (2018).

[126] M. Tertis, A. Florea, R. Sandulescu, C. Cristea, Carbon Based Electrodes Modified with Horseradish Peroxidase Immobilized in Conducting Polymers for Acetaminophen Analysis, Sensors. 13 (2013) 4841–4854. doi:10.3390/s130404841.

[127] L. Asturias-Arribas, M. Asunción Alonso-Lomillo, O. Domínguez-Renedo, M. Julia Arcos-Martínez, Cytochrome P450 2D6 based electrochemical sensor for the determination of codeine, Talanta. 129 (2014) 315–319. doi:10.1016/j.talanta.2014.05.053.

[128] V. Sima, C. Cristea, E. Bodoki, G. Duţu, R. Sāndulescu, Screen-printed electrodes modified with HRP-zirconium alcoxide film for the development of a biosensor for acetaminophen detection, Open Chem. 8 (2010). doi:10.2478/s11532-010-0070-7.

[129] J.R. Camargo, M. Baccarin, P.A. Raymundo-Pereira, A.M. Campos, G.G. Oliveira, O. Fatibello-Filho, O.N. Oliveira, B.C. Janegitz, Electrochemical biosensor made with tyrosinase immobilized in a matrix of nanodiamonds and potato starch for detecting phenolic compounds, Anal. Chim. Acta. 1034 (2018) 137–143. doi:10.1016/j.aca.2018.06.001.

[130] L. Asturias-Arribas, M. Asunción Alonso-Lomillo, O. Domínguez-Renedo, M. Julia Arcos-Martínez, Screen-printed biosensor based on the inhibition of the acetylcholinesterase activity for the determination of codeine, Talanta. 111 (2013) 8–12. doi:10.1016/j.talanta.2013.03.042.

[131] E. Khaled, M.S. Kamel, H.N.A. Hassan, H. Abdel-Gawad, H.Y. Aboul-Enein, Performance of a portable biosensor for the analysis of ethion residues, Talanta. 119 (2014) 467–472. doi:10.1016/j.talanta.2013.11.001.

[132] R.M. Pemberton, T.T. Mottram, J.P. Hart, Development of a screen-printed carbon electrochemical immunosensor for picomolar concentrations of estradiol in human serum extracts, J. Biochem. Biophys. Methods. 63 (2005) 201–212. doi:10.1016/j.jbbm.2005.05.002.

[133] A.B. Iliuk, L. Hu, W.A. Tao, Aptamer in Bioanalytical Applications, Anal. Chem. 83 (2011) 4440–4452. doi:10.1021/ac201057w.

[134] G. Contreras Jiménez, S. Eissa, A. Ng, H. Alhadrami, M. Zourob, M. Siaj, Aptamer-

Based Label-Free Impedimetric Biosensor for Detection of Progesterone, Anal. Chem. 87 (2015) 1075–1082. doi:10.1021/ac503639s.

[135] Q. Liu, Q. Zhou, G. Jiang, Nanomaterials for analysis and monitoring of emerging chemical pollutants, TrAC - Trends Anal. Chem. 58 (2014) 10–22. doi:10.1016/j.trac.2014.02.014.

[136] J. Wang, Carbon-Nanotube Based Electrochemical Biosensors: A Review, Electroanalysis. 17 (2005) 7–14. doi:10.1002/elan.200403113.

[137] P.J. Britto, K.S. V. Santhanam, A. Rubio, J.A. Alonso, P.M. Ajayan, Improved Charge Transfer at Carbon Nanotube Electrodes, Adv. Mater. 11 (1999) 154–157. doi:10.1002/(SICI)1521-4095(199902)11:2<154::AID-ADMA154>3.0.CO;2-B.

[138] M. Musameh, N.S. Lawrence, J. Wang, Electrochemical activation of carbon nanotubes, Electrochem. Commun. 7 (2005) 14–18. doi:10.1016/j.elecom.2004.10.007.

[139] J.J. Gooding, Nanostructuring electrodes with carbon nanotubes: A review on electrochemistry and applications for sensing, Electrochim. Acta. 50 (2005) 3049–3060. doi:10.1016/j.electacta.2004.08.052.

[140] Y. Shao, J. Wang, H. Wu, J. Liu, I.A. Aksay, Y. Lin, Graphene Based Electrochemical Sensors and Biosensors: A Review, Electroanalysis. 22 (2010) 1027–1036. doi:10.1002/elan.200900571.

[141] J. Losada, I. del Peso, L. Beyer, Redox and electrocatalytic properties of electrodes modified by films of polypyrrole nickel(II) Schiff-base complexes, J. Electroanal. Chem. 447 (1998) 147–154. doi:10.1016/S0022-0728(97)00608-6.

[142] H. Heli, F. Faramarzi, N. Sattarahmady, Voltammetric investigation and amperometric detection of the bisphosphonate drug sodium alendronate using a copper nanoparticles-modified electrode, J. Solid State Electrochem. 14 (2010) 2275–2283. doi:10.1007/s10008-010-1069-x.

[143] L. Chen, S. Xu, J. Li, Recent advances in molecular imprinting technology: current status, challenges and highlighted applications, Chem. Soc. Rev. 40 (2011) 2922. doi:10.1039/c0cs00084a.

[144] D. Tong, C. Heényi, Z. Bikádi, J.-P. Gao, S. Hjertén, Some studies of the chromatographic properties of gels ('Artificial antibodies/receptors') for selective adsorption of proteins, Chromatographia. 54 (2001) 7–14. doi:10.1007/BF02491825.

[145] T. Zhou, K. Zhang, T. Kamra, L. Bülow, L. Ye, Preparation of protein imprinted polymer beads by Pickering emulsion polymerization, J. Mater. Chem. B. 3 (2015) 1254–1260. doi:10.1039/C4TB01605J.

[146] A.M. Bossi, P.S. Sharma, L. Montana, G. Zoccatelli, O. Laub, R. Levi, Fingerprint-Imprinted Polymer: Rational Selection of Peptide Epitope Templates for the Determination of Proteins by Molecularly Imprinted Polymers, Anal. Chem. 84 (2012) 4036–4041. doi:10.1021/ac203422r.

[147] D. Dechtrirat, N. Gajovic-Eichelmann, F.F. Bier, F.W. Scheller, Hybrid Material for Protein Sensing Based on Electrosynthesized MIP on a Mannose Terminated Self-

Assembled Monolayer, Adv. Funct. Mater. 24 (2014) 2233–2239. doi:10.1002/adfm.201303148.

[148] P. Gou, N.D. Kraut, I.M. Feigel, H. Bai, G.J. Morgan, Y. Chen, Y. Tang, K. Bocan, J. Stachel, L. Berger, M. Mickle, E. Sejdić, A. Star, Carbon Nanotube Chemiresistor for Wireless pH Sensing, Sci. Rep. 4 (2014). doi:10.1038/srep04468.

[149] P. Bergveld, Thirty years of ISFETOLOGY, Sensors Actuators B Chem. 88 (2003) 1–20. doi:10.1016/S0925-4005(02)00301-5.

[150] A. Fog, R.P. Buck, Electronic semiconducting oxides as pH sensors, Sensors and Actuators. 5 (1984) 137–146. doi:10.1016/0250-6874(84)80004-9.

[151] S. Safari, P.R. Selvaganapathy, A. Derardja, M.J. Deen, Electrochemical growth of high-aspect ratio nanostructured silver chloride on silver and its application to miniaturized reference electrodes, Nanotechnology. 22 (2011) 315601. doi:10.1088/0957-4484/22/31/315601.

[152] S. Safari, P.R. Selvaganapathy, M.J. Deen, Microfluidic Reference Electrode with Free-Diffusion Liquid Junction, J. Electrochem. Soc. 160 (2013) B177–B183. doi:10.1149/2.007310jes.

[153] J. JIN, Y. SUZUKI, N. ISHIKAWA, T. TAKEUCHI, A Miniaturized FIA System for the Determination of Residual Chlorine in Environmental Water Samples, Anal. Sci. 20 (2004) 205–207. doi:10.2116/analsci.20.205.

[154] F. Lichtenberg, The impact of new drug launches on longevity: evidence from longitudinal disease-level data from 52 countries, 1982-2001, Cambridge, MA, 2003. doi:10.3386/w9754.

[155] Y. Lu, P. Hernandez, D. Abegunde, T. Edejer, The World Medicines Situation 2011, (n.d.) p 32. http://apps.who.int/medicinedocs/documents/s18767en/s18767en.pdf.

[156] B.R. Adhikari, M. Govindhan, A. Chen, Sensitive detection of acetaminophen with graphene-based electrochemical sensor, Electrochim. Acta. 162 (2015) 198–204. doi:10.1016/j.electacta.2014.10.028.

[157] B.D. Blair, J.P. Crago, C.J. Hedman, R.D. Klaper, Pharmaceuticals and personal care products found in the Great Lakes above concentrations of environmental concern, Chemosphere. 93 (2013) 2116–2123. doi:10.1016/j.chemosphere.2013.07.057.

[158] J.P. Bound, N. Voulvoulis, Predicted and measured concentrations for selected pharmaceuticals in UK rivers: Implications for risk assessment, Water Res. 40 (2006) 2885–2892. doi:10.1016/j.watres.2006.05.036.

[159] M. Gros, M. Petrović, A. Ginebreda, D. Barceló, Removal of pharmaceuticals during wastewater treatment and environmental risk assessment using hazard indexes, Environ. Int. 36 (2010) 15–26. doi:10.1016/j.envint.2009.09.002.

[160] J. Radjenovic, M. Petrovic, D. Barceló, Analysis of pharmaceuticals in wastewater and removal using a membrane bioreactor, Anal. Bioanal. Chem. 387 (2007) 1365–1377. doi:10.1007/s00216-006-0883-6.

[161] J. Pascual-Aguilar, V. Andreu, Y. Picó, An environmental forensic procedure to analyse anthropogenic pressures of urban origin on surface water of protected coastal

agro-environmental wetlands (L'Albufera de Valencia Natural Park, Spain), J. Hazard. Mater. 263 (2013) 214–223. doi:10.1016/j.jhazmat.2013.07.052.

[162] P. Guerra, M. Kim, A. Shah, M. Alaee, S.A. Smyth, Occurrence and fate of antibiotic, analgesic/anti-inflammatory, and antifungal compounds in five wastewater treatment processes, Sci. Total Environ. 473–474 (2014) 235–243. doi:10.1016/j.scitotenv.2013.12.008.

[163] B.D. Sites, M.L. Beach, M.A. Davis, Increases in the Use of Prescription Opioid Analgesics and the Lack of Improvement in Disability Metrics Among Users, Reg. Anesth. Pain Med. 39 (2014) 6–12. doi:10.1097/AAP.0000000000000022.

[164] Health Canada taking new action to improve acetaminophen safety, reminds Canadians about safe use, (2015). http://healthycanadians.gc.ca/recall-alert-rappel-avis/hc-sc/2015/54178a-eng.php (accessed November 28, 2016).

[165] M. Doherty, C. Hawkey, M. Goulder, I. Gibb, N. Hill, S. Aspley, S. Reader, A randomised controlled trial of ibuprofen, paracetamol or a combination tablet of ibuprofen/paracetamol in community-derived people with knee pain, Ann. Rheum. Dis. 70 (2011) 1534–1541. doi:10.1136/ard.2011.154047.

[166] E. Roberts, V. Delgado Nunes, S. Buckner, S. Latchem, M. Constanti, P. Miller, M. Doherty, W. Zhang, F. Birrell, M. Porcheret, K. Dziedzic, I. Bernstein, E. Wise, P.G. Conaghan, Paracetamol: not as safe as we thought? A systematic literature review of observational studies, Ann. Rheum. Dis. 75 (2015) 1–8. doi:10.1136/annrheumdis-2014-206914.

[167] L.L. Mazaleuskaya, K. Sangkuhl, C.F. Thorn, G.A. FitzGerald, R.B. Altman, T.E. Klein, PharmGKB summary: pathways of acetaminophen metabolism at the therapeutic versus toxic doses., Pharmacogenet. Genomics. 25 (2015) 416–26. doi:10.1097/FPC.0000000000000150.

[168] G. Burgot, F. Auffret, J.-L. Burgot, Determination of acetaminophen by thermometric titrimetry, Anal. Chim. Acta. 343 (1997) 125–128. doi:10.1016/S0003-2670(96)00613-7.

[169] R. Săndulescu, S. Mirel, R. Oprean, The development of spectrophotometric and electroanalytical methods for ascorbic acid and acetaminophen and their applications in the analysis of effervescent dosage forms., J. Pharm. Biomed. Anal. 23 (2000) 77–87. doi:10898157.

[170] S. Ravisankar, Reversed-phase HPLC method for the estimation of acetaminophen, ibuprofen and chlorzoxazone in formulations, Talanta. 46 (1998) 1577–1581. doi:10.1016/S0039-9140(98)00043-5.

[171] A. Trettin, A.A. Zoerner, A. Böhmer, F.-M. Gutzki, D.O. Stichtenoth, J. Jordan, D. Tsikas, Quantification of acetaminophen (paracetamol) in human plasma and urine by stable isotope-dilution GC–MS and GC–MS/MS as pentafluorobenzyl ether derivative, J. Chromatogr. B. 879 (2011) 2274–2280. doi:10.1016/j.jchromb.2011.06.012.

[172] W. Ruengsitagoon, S. Liawruangrath, A. Townshend, Flow injection chemiluminescence determination of paracetamol, Talanta. 69 (2006) 976–983.

doi:10.1016/j.talanta.2005.11.050.

[173] C.B. Jacobs, M.J. Peairs, B.J. Venton, Review: Carbon nanotube based electrochemical sensors for biomolecules, Anal. Chim. Acta. 662 (2010) 105–127. doi:10.1016/j.aca.2010.01.009.

[174] E.B. Bahadır, M.K. Sezgintürk, Electrochemical biosensors for hormone analyses., Biosens. Bioelectron. 68 (2015) 62–71. doi:10.1016/j.bios.2014.12.054.

[175] S. Shi, S. Reisberg, G. Anquetin, V. Noël, M.C. Pham, B. Piro, General approach for electrochemical detection of persistent pharmaceutical micropollutants: Application to acetaminophen, Biosens. Bioelectron. 72 (2015) 205–210. doi:10.1016/j.bios.2015.05.010.

[176] M. Yang, Y. Yang, Y. Liu, G. Shen, R. Yu, Platinum nanoparticles-doped sol–gel/carbon nanotubes composite electrochemical sensors and biosensors, Biosens. Bioelectron. 21 (2006) 1125–1131. doi:10.1016/j.bios.2005.04.009.

[177] F.S. Omar, N. Duraisamy, K. Ramesh, S. Ramesh, Conducting polymer and its composite materials based electrochemical sensor for Nicotinamide Adenine Dinucleotide (NADH), Biosens. Bioelectron. 79 (2016) 763–775. doi:10.1016/j.bios.2016.01.013.

[178] Y. Zhang, X. Bo, A. Nsabimana, A. Munyentwali, C. Han, M. Li, L. Guo, Green and facile synthesis of an Au nanoparticles@polyoxometalate/ordered mesoporous carbon tri-component nanocomposite and its electrochemical applications, Biosens. Bioelectron. 66 (2015) 191–197. doi:10.1016/j.bios.2014.11.022.

[179] Z. Wang, Z. Dai, Carbon nanomaterial-based electrochemical biosensors: an overview, Nanoscale. 7 (2015) 6420–6431. doi:10.1039/C5NR00585J.

[180] H. Beitollahi, H. Karimi-Maleh, H. Khabazzadeh, Nanomolar and Selective Determination of Epinephrine in the Presence of Norepinephrine Using Carbon Paste Electrode Modified with Carbon Nanotubes and Novel 2-(4-Oxo-3-phenyl-3,4-dihydro-quinazolinyl)- N ′-phenyl-hydrazinecarbothioamide, Anal. Chem. 80 (2008) 9848–9851. doi:10.1021/ac801854j.

[181] M. Mazloum-Ardakani, B. Ganjipour, H. Beitollahi, M.K. Amini, F. Mirkhalaf, H. Naeimi, M. Nejati-Barzoki, Simultaneous determination of levodopa, carbidopa and tryptophan using nanostructured electrochemical sensor based on novel hydroquinone and carbon nanotubes: Application to the analysis of some real samples, Electrochim. Acta. 56 (2011) 9113–9120. doi:10.1016/j.electacta.2011.07.021.

[182] H. Beitollahi, J.-B. Raoof, H. Karimi-Maleh, R. Hosseinzadeh, Electrochemical behavior of isoproterenol in the presence of uric acid and folic acid at a carbon paste electrode modified with 2,7-bis(ferrocenyl ethyl)fluoren-9-one and carbon nanotubes, J. Solid State Electrochem. 16 (2012) 1701–1707. doi:10.1007/s10008-011-1578-2.

[183] Z.A. Alothman, N. Bukhari, S.M. Wabaidur, S. Haider, Simultaneous electrochemical determination of dopamine and acetaminophen using multiwall carbon nanotubes modified glassy carbon electrode, Sensors Actuators B Chem. 146

(2010) 314–320. doi:10.1016/j.snb.2010.02.024.

[184] Y. Li, S. Feng, S. Li, Y. Zhang, Y. Zhong, A high effect polymer-free covalent layer by layer self-assemble carboxylated MWCNTs films modified GCE for the detection of paracetamol, Sensors Actuators B Chem. 190 (2014) 999–1005. doi:10.1016/j.snb.2013.09.052.

[185] M. Li, L. Jing, Electrochemical behavior of acetaminophen and its detection on the PANI–MWCNTs composite modified electrode, Electrochim. Acta. 52 (2007) 3250–3257. doi:10.1016/j.electacta.2006.10.001.

[186] A. Kutluay, M. Aslanoglu, Modification of electrodes using conductive porous layers to confer selectivity for the voltammetric detection of paracetamol in the presence of ascorbic acid, dopamine and uric acid, Sensors Actuators B Chem. 185 (2013) 398–404. doi:10.1016/j.snb.2013.05.025.

[187] M.R. Akhgar, H. Beitollahi, M. Salari, H. Karimi-Maleh, H. Zamani, Fabrication of a sensor for simultaneous determination of norepinephrine, acetaminophen and tryptophan using a modified carbon nanotube paste electrode, Anal. Methods. 4 (2012) 259–264. doi:10.1039/C1AY05503H.

[188] L. Vaisman, H.D. Wagner, G. Marom, The role of surfactants in dispersion of carbon nanotubes, Adv. Colloid Interface Sci. 128–130 (2006) 37–46. doi:10.1016/j.cis.2006.11.007.

[189] G. Crini, M. Morcellet, Synthesis and applications of adsorbents containing cyclodextrins, J. Sep. Sci. 25 (2002) 789–813. doi:10.1002/1615-9314(20020901)25:13<789::AID-JSSC789>3.0.CO;2-J.

[190] N. Morin-Crini, G. Crini, Environmental applications of water-insoluble β-cyclodextrin–epichlorohydrin polymers, Prog. Polym. Sci. 38 (2013) 344–368. doi:10.1016/j.progpolymsci.2012.06.005.

[191] İ. Abay, A. Denizli, E. Bişkin, B. Salih, Removal and pre-concentration of phenolic species onto β-cyclodextrin modified poly(hydroxyethylmethacrylate–ethyleneglycoldimethacrylate) microbeads, Chemosphere. 61 (2005) 1263–1272. doi:10.1016/j.chemosphere.2005.03.079.

[192] A. Alsbaiee, B.J. Smith, L. Xiao, Y. Ling, D.E. Helbling, W.R. Dichtel, Rapid removal of organic micropollutants from water by a porous β-cyclodextrin polymer, Nature. 529 (2015) 190–194. doi:10.1038/nature16185.

[193] S. Menuel, J.-P. Joly, B. Courcot, J. Elysée, N.-E. Ghermani, A. Marsura, Synthesis and inclusion ability of a bis-β-cyclodextrin pseudo-cryptand towards Busulfan anticancer agent, Tetrahedron. 63 (2007) 1706–1714. doi:10.1016/j.tet.2006.10.070.

[194] T.R. Thatiparti, A.J. Shoffstall, H.A. von Recum, Cyclodextrin-based device coatings for affinity-based release of antibiotics, Biomaterials. 31 (2010) 2335–2347. doi:10.1016/j.biomaterials.2009.11.087.

[195] S. Kohata, K. Jyodoi, A. Ohyoshi, Thermal decomposition of cyclodextrins (α-, β-, γ-, and modified β-CyD) and of metal—(β-CyD) complexes in the solid phase, Thermochim. Acta. 217 (1993) 187–198. doi:10.1016/0040-6031(93)85107-K.

[196] J. Hu, D. Shao, C. Chen, G. Sheng, J. Li, X. Wang, M. Nagatsu, Plasma-Induced

Grafting of Cyclodextrin onto Multiwall Carbon Nanotube/Iron Oxides for Adsorbent Application, J. Phys. Chem. B. 114 (2010) 6779–6785. doi:10.1021/jp911424k.

[197] H. Wang, L. Li, L. Zhang, F. Ran, The unique morphology role of thorn surface in determining electrochemical performance of polyaniline nano-fibers via one-step method, J. Appl. Polym. Sci. 132 (2015) n/a-n/a. doi:10.1002/app.42266.

[198] H.J. Lee, Y.D. Lee, S. Il Moon, W.S. Cho, Y.-H. Lee, J.K. Kim, S.W. Hwang, B.K. Ju, Enhanced surface morphologies of screen-printed carbon nanotube films by heat treatment and their field-emission properties, Carbon N. Y. 44 (2006) 2625–2630. doi:10.1016/j.carbon.2006.04.038.

[199] Y. Bai, F. Wu, D. Lin, B. Xing, Aqueous stabilization of carbon nanotubes: effects of surface oxidization and solution chemistry, Environ. Sci. Pollut. Res. 21 (2014) 4358–4365. doi:10.1007/s11356-013-2304-7.

[200] Y. Qin, H.-J. Kwon, A. Subrahmanyam, M.M.R. Howlader, P.R. Selvaganapathy, A. Adronov, M.J. Deen, Inkjet-printed bifunctional carbon nanotubes for pH sensing, Mater. Lett. 176 (2016) 68–70. doi:10.1016/j.matlet.2016.04.048.

[201] Q. Cheng, L. Ji, K. Wu, W. Zhang, Morphology-dependent Electrochemical Enhancements of Porous Carbon as Sensitive Determination Platform for Ascorbic Acid, Dopamine and Uric Acid, Sci. Rep. 6 (2016) 22309. doi:10.1038/srep22309.

[202] R. Jain, S. Sharma, Glassy carbon electrode modified with multi-walled carbon nanotubes sensor for the quantification of antihistamine drug pheniramine in solubilized systems, J. Pharm. Anal. 2 (2012) 56–61. doi:10.1016/j.jpha.2011.09.013.

[203] A. Abbaspour, A. Noori, A cyclodextrin host–guest recognition approach to an electrochemical sensor for simultaneous quantification of serotonin and dopamine, Biosens. Bioelectron. 26 (2011) 4674–4680. doi:10.1016/j.bios.2011.04.061.

[204] B. Habibi, M. Jahanbakhshi, M.H. Pournaghi-Azar, Differential pulse voltammetric simultaneous determination of acetaminophen and ascorbic acid using single-walled carbon nanotube-modified carbon–ceramic electrode, Anal. Biochem. 411 (2011) 167–175. doi:10.1016/j.ab.2011.01.005.

[205] X. Chen, J. Zhu, Q. Xi, W. Yang, A high performance electrochemical sensor for acetaminophen based on single-walled carbon nanotube-graphene nanosheet hybrid films, Sensors Actuators, B Chem. 161 (2012) 648–654. doi:10.1016/j.snb.2011.10.085.

[206] L. Jiang, S. Gu, Y. Ding, F. Jiang, Z. Zhang, Facile and novel electrochemical preparation of a graphene-transition metal oxide nanocomposite for ultrasensitive electrochemical sensing of acetaminophen and phenacetin., Nanoscale. 6 (2014) 207–14. doi:10.1039/c3nr03620k.

[207] M. El-Kemary, S. Sobhy, S. El-Daly, A. Abdel-Shafi, Inclusion of Paracetamol into β-cyclodextrin nanocavities in solution and in the solid state, Spectrochim. Acta Part A Mol. Biomol. Spectrosc. 79 (2011) 1904–1908. doi:10.1016/j.saa.2011.05.084.

[208] Z. Yang, M. Xu, Y. Liu, F. He, F. Gao, Y. Su, H. Wei, Y. Zhang, Nitrogen-doped,

carbon-rich, highly photoluminescent carbon dots from ammonium citrate, Nanoscale. 6 (2014) 1890–1895. doi:10.1039/C3NR05380F.

[209] A.U. Alam, M.M.R. Howlader, M.J. Deen, Oxygen Plasma and Humidity Dependent Surface Analysis of Silicon, Silicon Dioxide and Glass for Direct Wafer Bonding, ECS J. Solid State Sci. Technol. 2 (2013) P515–P523. doi:10.1149/2.007312jss.

[210] A.U. Alam, M.M.R. Howlader, M.J. Deen, The effects of oxygen plasma and humidity on surface roughness, water contact angle and hardness of silicon, silicon dioxide and glass, J. Micromechanics Microengineering. 24 (2014) 035010. doi:10.1088/0960-1317/24/3/035010.

[211] A.J. Bard, L.R.. Faulkner, Electrochemical Methods, 2nd ed., Wiley, New York, 2011.

[212] Y. Yaman, S. Abaci, Sensitive Adsorptive Voltammetric Method for Determination of Bisphenol A by Gold Nanoparticle/Polyvinylpyrrolidone-Modified Pencil Graphite Electrode, Sensors. 16 (2016) 756. doi:10.3390/s16060756.

[213] A. Martin Santos, A. Wong, A. Ara?jo Almeida, O. Fatibello-Filho, Simultaneous determination of paracetamol and ciprofloxacin in biological fluid samples using a glassy carbon electrode modified with oxide of graphene and nickel oxide nanoparticles, Talanta. (2017). doi:10.1016/j.talanta.2017.06.040.

[214] D. Aşangil, İ. Hüdai Taşdemir, E. Kılıç, Adsorptive stripping voltammetric methods for determination of aripiprazole, J. Pharm. Anal. 2 (2012) 193–199. doi:10.1016/j.jpha.2012.01.009.

[215] D.A.C. Brownson, C.E. Banks, Interpreting Electrochemistry, in: Handb. Graphene Electrochem., Springer London, London, 2014: pp. 23–77. doi:10.1007/978-1-4471-6428-9_2.

[216] E. Laviron, General expression of the linear potential sweep voltammogram in the case of diffusionless electrochemical systems, J. Electroanal. Chem. Interfacial Electrochem. 101 (1979) 19–28. doi:10.1016/S0022-0728(79)80075-3.

[217] I. Dumitrescu, P. V. Dudin, J.P. Edgeworth, J. V. Macpherson, P.R. Unwin, Electron Transfer Kinetics at Single-Walled Carbon Nanotube Electrodes using Scanning Electrochemical Microscopy, J. Phys. Chem. C. 114 (2010) 2633–2639. doi:10.1021/jp908830d.

[218] Y. Fang, D. Long, J. Ye, Study of acetaminophen by parallel incident spectroelectrochemistry, Anal. Chim. Acta. 342 (1997) 13–21. doi:10.1016/S0003-2670(96)00619-8.

[219] D.J. Miner, J.R. Rice, R.M. Riggin, P.T. Kissinger, Voltammetry of acetaminophen and its metabolites, Anal. Chem. 53 (1981) 2258–2263. doi:10.1021/ac00237a029.

[220] E. Laviron, Adsorption, autoinhibition and autocatalysis in polarography and in linear potential sweep voltammetry, J. Electroanal. Chem. Interfacial Electrochem. 52 (1974) 355–393. doi:10.1016/S0022-0728(74)80448-1.

[221] F. Ghorbani-Bidkorbeh, S. Shahrokhian, A. Mohammadi, R. Dinarvand, Simultaneous voltammetric determination of tramadol and acetaminophen using

carbon nanoparticles modified glassy carbon electrode, Electrochim. Acta. 55 (2010) 2752–2759. doi:10.1016/j.electacta.2009.12.052.

[222] S.A. Kumar, C.-F. Tang, S.-M. Chen, Electroanalytical determination of acetaminophen using nano-TiO2/polymer coated electrode in the presence of dopamine, Talanta. 76 (2008) 997–1005. doi:10.1016/j.talanta.2008.04.057.

[223] J. Osteryoung, Pulse voltammetry, J. Chem. Educ. 60 (1983) 296. doi:10.1021/ed060p296.

[224] A.P. Brown, F.C. Anson, Cyclic and differential pulse voltammetric behavior of reactants confined to the electrode surface, Anal. Chem. 49 (1977) 1589–1595. doi:10.1021/ac50019a033.

[225] B. Habibi, M. Jahanbakhshi, M. Abazari, A modified single-walled carbon nanotubes/carbon-ceramic electrode for simultaneous voltammetric determination of paracetamol and caffeine, J. Iran. Chem. Soc. 11 (2014) 511–521. doi:10.1007/s13738-013-0324-3.

[226] R. Manjunatha, D.H. Nagaraju, G.S. Suresh, J.S. Melo, S.F. D'Souza, T.V. Venkatesha, Electrochemical detection of acetaminophen on the functionalized MWCNTs modified electrode using layer-by-layer technique, Electrochim. Acta. 56 (2011) 6619–6627. doi:10.1016/j.electacta.2011.05.018.

[227] A.A. Ensafi, H. Karimi-Maleh, S. Mallakpour, M. Hatami, Simultaneous determination of N-acetylcysteine and acetaminophen by voltammetric method using N-(3,4-dihydroxyphenethyl)-3,5-dinitrobenzamide modified multiwall carbon nanotubes paste electrode, Sensors Actuators B Chem. 155 (2011) 464–472. doi:10.1016/j.snb.2010.12.048.

[228] J.B. Raoof, M. Baghayeri, R. Ojani, A high sensitive voltammetric sensor for qualitative and quantitative determination of phenobarbital as an antiepileptic drug in presence of acetaminophen, Colloids Surfaces B Biointerfaces. 95 (2012) 121–128. doi:10.1016/j.colsurfb.2012.02.038.

[229] M.R. Shahmiri, A. Bahari, H. Karimi-Maleh, R. Hosseinzadeh, N. Mirnia, Ethynylferrocene-NiO/MWCNT nanocomposite modified carbon paste electrode as a novel voltammetric sensor for simultaneous determination of glutathione and acetaminophen, Sensors Actuators, B Chem. 177 (2013) 70–77. doi:10.1016/j.snb.2012.10.098.

[230] M. Arvand, T.M. Gholizadeh, Simultaneous voltammetric determination of tyrosine and paracetamol using a carbon nanotube-graphene nanosheet nanocomposite modified electrode in human blood serum and pharmaceuticals, Colloids Surfaces B Biointerfaces. 103 (2013) 84–93. doi:10.1016/j.colsurfb.2012.10.024.

[231] R.T. Kachoosangi, G.G. Wildgoose, R.G. Compton, Sensitive adsorptive stripping voltammetric determination of paracetamol at multiwalled carbon nanotube modified basal plane pyrolytic graphite electrode, Anal. Chim. Acta. 618 (2008) 54–60. doi:10.1016/j.aca.2008.04.053.

[232] A. Babaei, M. Afrasiabi, M. Babazadeh, A Glassy Carbon Electrode Modified with Multiwalled Carbon Nanotube/Chitosan Composite as a New Sensor for

Simultaneous Determination of Acetaminophen and Mefenamic Acid in Pharmaceutical Preparations and Biological Samples, Electroanalysis. 22 (2010) 1743–1749. doi:10.1002/elan.200900578.

[233] M.M. Barsan, C.T. Toledo, C.M.A. Brett, New electrode architectures based on poly(methylene green) and functionalized carbon nanotubes: Characterization and application to detection of acetaminophen and pyridoxine, J. Electroanal. Chem. 736 (2015) 8–15. doi:10.1016/j.jelechem.2014.10.026.

[234] M.-P.N. Bui, C.A. Li, K.N. Han, X.-H. Pham, G.H. Seong, Determination of acetaminophen by electrochemical co-deposition of glutamic acid and gold nanoparticles, Sensors Actuators B Chem. 174 (2012) 318–324. doi:10.1016/j.snb.2012.08.012.

[235] E. Haghshenas, T. Madrakian, A. Afkhami, A novel electrochemical sensor based on magneto Au nanoparticles/carbon paste electrode for voltammetric determination of acetaminophen in real samples, Mater. Sci. Eng. C. 57 (2015) 205–214. doi:10.1016/j.msec.2015.07.054.

[236] H. Beitollahi, J.B. Raoof, R. Hosseinzadeh, Fabrication of a nanostructure-based electrochemical sensor for simultaneous determination of N-acetylcysteine and acetaminophen, Talanta. 85 (2011) 2128–2134. doi:10.1016/j.talanta.2011.07.054.

[237] A. Kumaravel, M. Chandrasekaran, Electrochemical determination of imidacloprid using nanosilver Nafion®/nanoTiO2 Nafion® composite modified glassy carbon electrode, Sensors Actuators B Chem. 158 (2011) 319–326. doi:10.1016/j.snb.2011.06.028.

[238] M.J. Benotti, R.A. Trenholm, B.J. Vanderford, J.C. Holady, B.D. Stanford, S.A. Snyder, Pharmaceuticals and Endocrine Disrupting Compounds in U.S. Drinking Water, Environ. Sci. Technol. 43 (2009) 597–603. doi:10.1021/es801845a.

[239] M. Adeel, X. Song, Y. Wang, D. Francis, Y. Yang, Environmental impact of estrogens on human, animal and plant life: A critical review, Environ. Int. 99 (2017) 107–119. doi:10.1016/j.envint.2016.12.010.

[240] Y. He, S. Xie, X. Yang, R. Yuan, Y. Chai, Electrochemical Peptide Biosensor Based on in Situ Silver Deposition for Detection of Prostate Specific Antigen, ACS Appl. Mater. Interfaces. 7 (2015) 13360–13366. doi:10.1021/acsami.5b01827.

[241] B.-B. Kou, L. Zhang, H. Xie, D. Wang, Y.-L. Yuan, Y.-Q. Chai, R. Yuan, DNA Enzyme-Decorated DNA Nanoladders as Enhancer for Peptide Cleavage-Based Electrochemical Biosensor, ACS Appl. Mater. Interfaces. 8 (2016) 22869–22874. doi:10.1021/acsami.6b07017.

[242] W. Wang, L. Ge, X. Sun, T. Hou, F. Li, Graphene-Assisted Label-Free Homogeneous Electrochemical Biosensing Strategy based on Aptamer-Switched Bidirectional DNA Polymerization, ACS Appl. Mater. Interfaces. 7 (2015) 28566–28575. doi:10.1021/acsami.5b09932.

[243] X. Zhou, A. Wang, C. Yu, S. Wu, J. Shen, Facile Synthesis of Molecularly Imprinted Graphene Quantum Dots for the Determination of Dopamine with Affinity-Adjustable, ACS Appl. Mater. Interfaces. 7 (2015) 11741–11747.

doi:10.1021/am5078478.

[244] S. Wang, J. Shang, Q. Wang, W. Zhang, X. Wu, J. Chen, W. Zhang, S. Qiu, Y. Wang, X. Wang, Enhanced Electrochemical Performance by Strongly Anchoring Highly Crystalline Polyaniline on Multiwalled Carbon Nanotubes, ACS Appl. Mater. Interfaces. 9 (2017) 43939–43949. doi:10.1021/acsami.7b11567.

[245] K. Rajavel, M. Lalitha, J.K. Radhakrishnan, L. Senthilkumar, R.T. Rajendra Kumar, Multiwalled Carbon Nanotube Oxygen Sensor: Enhanced Oxygen Sensitivity at Room Temperature and Mechanism of Sensing, ACS Appl. Mater. Interfaces. 7 (2015) 23857–23865. doi:10.1021/acsami.5b04869.

[246] X. Ran, L. Yang, J. Zhang, G. Deng, Y. Li, X. Xie, H. Zhao, C.-P. Li, Highly sensitive electrochemical sensor based on β-cyclodextrin–gold@3, 4, 9, 10-perylene tetracarboxylic acid functionalized single-walled carbon nanohorns for simultaneous determination of myricetin and rutin, Anal. Chim. Acta. 892 (2015) 85–94. doi:10.1016/j.aca.2015.08.046.

[247] X. Yu, Y. Chen, L. Chang, L. Zhou, F. Tang, X. Wu, β-cyclodextrin non-covalently modified ionic liquid-based carbon paste electrode as a novel voltammetric sensor for specific detection of bisphenol A, Sensors Actuators B Chem. 186 (2013) 648–656. doi:10.1016/j.snb.2013.06.089.

[248] A. Alsbaiee, B.J. Smith, L. Xiao, Y. Ling, D.E. Helbling, W.R. Dichtel, Rapid removal of organic micropollutants from water by a porous β-cyclodextrin polymer, Nature. 529 (2015) 190–194. doi:10.1038/nature16185.

[249] A.K. Chatjigakis, C. Donze, A.W. Coleman, P. Cardot, Solubility behavior of .beta.-cyclodextrin in water/cosolvent mixtures, Anal. Chem. 64 (1992) 1632–1634. doi:10.1021/ac00038a022.

[250] Y. Gao, Y. Cao, D. Yang, X. Luo, Y. Tang, H. Li, Sensitivity and selectivity determination of bisphenol A using SWCNT-CD conjugate modified glassy carbon electrode, J. Hazard. Mater. 199–200 (2012) 111–118. doi:10.1016/j.jhazmat.2011.10.066.

[251] Z. Guo, L. Liang, J.-J. Liang, Y.-F. Ma, X.-Y. Yang, D.-M. Ren, Y.-S. Chen, J.-Y. Zheng, Covalently β-cyclodextrin modified single-walled carbon nanotubes: a novel artificial receptor synthesized by 'click' chemistry, J. Nanoparticle Res. 10 (2008) 1077–1083. doi:10.1007/s11051-007-9338-z.

[252] X. Wang, X.-J. Song, H. Xuan, F. Yang, Preparation of β-cyclodextrin-modified multi-walled CNTs and its application in capturing β-naphthol from wastewater, Micro Nano Lett. 7 (2012) 892–895. doi:10.1049/mnl.2012.0426.

[253] S. Mosivand, I. Kazeminezhad, Functionalization and characterization of electrocrystallized iron oxide nanoparticles in the presence of β-cyclodextrin, CrystEngComm. 18 (2016) 417–426. doi:10.1039/C5CE01789K.

[254] N. V. Roik, L.A. Belyakova, Thermodynamic, IR spectral and X-ray diffraction studies of the "β-cyclodextrin-para-aminobenzoic acid" inclusion complex, J. Incl. Phenom. Macrocycl. Chem. 69 (2011) 315–319. doi:10.1007/s10847-010-9737-0.

[255] E. Lieber, C.N.R. Rao, T.S. Chao, C.W.W. Hoffman, Infrared Spectra of Organic

Azides, Anal. Chem. 29 (1957) 916–918. doi:10.1021/ac60126a016.

[256] Y. Niu, T. Huang, Z. Zhou, G. Xu, L. Zhang, T. Wei, Formation of cyclodextrin monolayer through a host–guest interaction with tailor-made phenyltriethoxysilane self-assembled monolayer, Colloids Surfaces A Physicochem. Eng. Asp. 470 (2015) 224–229. doi:10.1016/j.colsurfa.2015.01.088.

[257] A.U. Alam, Y. Qin, M.M.R. Howlader, N.-X. Hu, M.J. Deen, Electrochemical sensing of acetaminophen using multi-walled carbon nanotube and β-cyclodextrin, Sensors Actuators B Chem. 254 (2018) 896–909. doi:10.1016/j.snb.2017.07.127.

[258] T.-Y. Huang, C.-W. Kung, H.-Y. Wei, K.M. Boopathi, C.-W. Chu, K.-C. Ho, A high performance electrochemical sensor for acetaminophen based on a rGO–PEDOT nanotube composite modified electrode, J. Mater. Chem. A. 2 (2014) 7229–7237. doi:10.1039/c4ta00309h.

[259] E. Albers, B.W. Müller, Complexation of Steroid Hormones with Cyclodextrin Derivatives: Substituent Effects of the Guest Molecule on Solubility and Stability in Aqueous Solution, J. Pharm. Sci. 81 (1992) 756–761. doi:10.1002/jps.2600810808.

[260] W. Zhu, H. Huang, X. Gao, H. Ma, Electrochemical behavior and voltammetric determination of acetaminophen based on glassy carbon electrodes modified with poly(4-aminobenzoic acid)/electrochemically reduced graphene oxide composite films, Mater. Sci. Eng. C. 45 (2014) 21–28. doi:10.1016/j.msec.2014.08.067.

[261] A.U. Alam, Y. Qin, M.M.R. Howlader, N.-X. Hu, M.J. Deen, Electrochemical sensing of acetaminophen using multi-walled carbon nanotube and β-cyclodextrin, Sensors Actuators B Chem. 254 (2018) 896–909. doi:10.1016/j.snb.2017.07.127.

[262] R.S. Nicholson, I. Shain, Theory of Stationary Electrode Polarography. Single Scan and Cyclic Methods Applied to Reversible, Irreversible, and Kinetic Systems., Anal. Chem. 36 (1964) 706–723. doi:10.1021/ac60210a007.

[263] S. Hu, K. Wu, H. Yi, D. Cui, Voltammetric behavior and determination of estrogens at Nafion-modified glassy carbon electrode in the presence of cetyltrimethylammonium bromide, Anal. Chim. Acta. 464 (2002) 209–216. doi:10.1016/S0003-2670(02)00496-8.

[264] H. Tao, W. Wei, X. Zeng, X. Liu, X. Zhang, Y. Zhang, Electrocatalytic oxidation and determination of estradiol using an electrode modified with carbon nanotubes and an ionic liquid, Microchim. Acta. 166 (2009) 53–59. doi:10.1007/s00604-009-0163-1.

[265] Q. He, S. Yuan, C. Chen, S. Hu, Electrochemical properties of estradiol at glassy carbon electrode modified with nano-Al2O3 film, Mater. Sci. Eng. C. 23 (2003) 621–625. doi:10.1016/S0928-4931(03)00053-5.

[266] N. Terui, B. Fugetsu, S. Tanaka, Voltammetric Behavior and Determination of 17 β-Estradiol at Multi-Wall Carbon Nanotube-Nafion Modified Glassy Carbon Electrode, Anal. Sci. 22 (2006) 895–898. doi:10.2116/analsci.22.895.

[267] X. Liu, D.K.Y. Wong, Electrocatalytic detection of estradiol at a carbon nanotube|Ni(Cyclam) composite electrode fabricated based on a two-factorial design, Anal. Chim. Acta. 594 (2007) 184–191. doi:10.1016/j.aca.2007.05.043.

[268] J. Song, J. Yang, X. Hu, Electrochemical determination of estradiol using a poly(l-serine) film-modified electrode, J. Appl. Electrochem. 38 (2008) 833–836. doi:10.1007/s10800-008-9520-8.

[269] B.C. Janegitz, F.A. dos Santos, R.C. Faria, V. Zucolotto, Electrochemical determination of estradiol using a thin film containing reduced graphene oxide and dihexadecylphosphate, Mater. Sci. Eng. C. 37 (2014) 14–19. doi:10.1016/j.msec.2013.12.026.

[270] L. Hu, Q. Cheng, D. Chen, M. Ma, K. Wu, Liquid-phase exfoliated graphene as highly-sensitive sensor for simultaneous determination of endocrine disruptors: Diethylstilbestrol and estradiol, J. Hazard. Mater. 283 (2015) 157–163. doi:10.1016/j.jhazmat.2014.08.067.

[271] D. Futra, L.Y. Heng, M.Z. Jaapar, A. Ulianas, K. Saeedfar, T.L. Ling, A novel electrochemical sensor for 17β-estradiol from molecularly imprinted polymeric microspheres and multi-walled carbon nanotubes grafted with gold nanoparticles, Anal. Methods. 8 (2016) 1381–1389. doi:10.1039/C5AY02796A.

[272] Adverse Health Effects of Heavy Metals in Children, (n.d.). http://www.who.int/ceh/capacity/heavy_metals.pdf (accessed November 5, 2018).

[273] R.L. Canfield, C.R. Henderson, D.A. Cory-Slechta, C. Cox, T.A. Jusko, B.P. Lanphear, Intellectual Impairment in Children with Blood Lead Concentrations below 10 μg per Deciliter, N. Engl. J. Med. 348 (2003) 1517–1526. doi:10.1056/NEJMoa022848.

[274] G.A. Jenner, H.P. Longerich, S.E. Jackson, B.J. Fryer, ICP-MS — A powerful tool for high-precision trace-element analysis in Earth sciences: Evidence from analysis of selected U.S.G.S. reference samples, Chem. Geol. 83 (1990) 133–148. doi:10.1016/0009-2541(90)90145-W.

[275] J.C. Smith, G.P. Butrimovitz, W.C. Purdy, Direct measurement of zinc in plasma by atomic absorption spectroscopy., Clin. Chem. 25 (1979) 1487–91. http://www.ncbi.nlm.nih.gov/pubmed/455691.

[276] T. Wang, W. Yue, Carbon Nanotubes Heavy Metal Detection with Stripping Voltammetry: A Review Paper, Electroanalysis. 29 (2017) 2178–2189. doi:10.1002/elan.201700276.

[277] P. Podešva, I. Gablech, P. Neužil, Nanostructured Gold Microelectrode Array for Ultrasensitive Detection of Heavy Metal Contamination, Anal. Chem. 90 (2018) 1161–1167. doi:10.1021/acs.analchem.7b03725.

[278] T.Z. Redhwan, A.U. Alam, Y.M. Haddara, M.M.R. Howlader, Copper and liquid crystal polymer bonding towards lead sensing, Jpn. J. Appl. Phys. 57 (2018) 02BB03. doi:10.7567/JJAP.57.02BB03.

[279] T.Z. Redhwan, A.U. Alam, Y.M. Haddara, M.M.R. Howlader, Bonding mechanism and electrochemical impedance of directly bonded liquid crystal polymer and copper, in: Proc. 2017 5th Int. Work. Low Temp. Bond. 3D Integr. LTB-3D 2017, 2017. doi:10.23919/LTB-3D.2017.7947436.

[280] muxin Lu, Y. Deng, Y. Luo, J. Lv, T. Li, J. Xu, S.-W. Chen, J. Wang, Graphene

Aerogel−Metal-Organic Framework-Based Electrochemical Method for Simultaneous Detection of Multiple Heavy Metal Ions, Anal. Chem. (2018) acs.analchem.8b03764. doi:10.1021/acs.analchem.8b03764.

[281] B. Aswathy, G.S. Avadhani, S. Suji, G. Sony, Synthesis of β-cyclodextrin functionalized gold nanoparticles for the selective detection of Pb 2+ ions from aqueous solution, Front. Mater. Sci. 6 (2012) 168–175. doi:10.1007/s11706-012-0165-5.

[282] G. Roa-Morales, L. Galicia, A. Rojas-Hernández, M.T. Ramírez-Silva, Electrochemical study on the selective formation of [Pb(cyclodextrin)2+]surfaceinclusion complexes at the carbon paste electrode/ClO4-1 M interphase, Electrochim. Acta. 50 (2005) 1925–1930. doi:10.1016/j.electacta.2004.09.001.

[283] A.U. Alam, Y. Qin, M. Catalano, L. Wang, M.J. Kim, M.M.R. Howlader, N.-X. Hu, M.J. Deen, Tailoring MWCNTs and β-Cyclodextrin for Sensitive Detection of Acetaminophen and Estrogen, ACS Appl. Mater. Interfaces. 10 (2018) 21411–21427. doi:10.1021/acsami.8b04639.

[284] V. Schroeder, S. Savagatrup, M. He, S. Lin, T.M. Swager, Carbon Nanotube Chemical Sensors, Chem. Rev. (2018) acs.chemrev.8b00340. doi:10.1021/acs.chemrev.8b00340.

[285] D. Zhao, X. Guo, T. Wang, N. Alvarez, V.N. Shanov, W.R. Heineman, Simultaneous Detection of Heavy Metals by Anodic Stripping Voltammetry Using Carbon Nanotube Thread, Electroanalysis. 26 (2014) 488–496. doi:10.1002/elan.201300511.

[286] Y. Wei, R. Yang, X. Chen, L. Wang, J.-H. Liu, X.-J. Huang, A cation trap for anodic stripping voltammetry: NH3–plasma treated carbon nanotubes for adsorption and detection of metal ions, Anal. Chim. Acta. 755 (2012) 54–61. doi:10.1016/j.aca.2012.10.021.

[287] X. Li, H. Zhou, C. Fu, F. Wang, Y. Ding, Y. Kuang, A novel design of engineered multi-walled carbon nanotubes material and its improved performance in simultaneous detection of Cd(II) and Pb(II) by square wave anodic stripping voltammetry, Sensors Actuators B Chem. 236 (2016) 144–152. doi:10.1016/j.snb.2016.05.149.

[288] X.C. Fu, J. Wu, J. Li, C.G. Xie, Y.S. Liu, Y. Zhong, J.H. Liu, Electrochemical determination of trace copper(II) with enhanced sensitivity and selectivity by gold nanoparticle/single-wall carbon nanotube hybrids containing three-dimensional l-cysteine molecular adapters, Sensors Actuators, B Chem. 182 (2013) 382–389. doi:10.1016/j.snb.2013.02.074.

[289] A.Z.M. Badruddoza, Z.B.Z. Shawon, W.J.D. Tay, K. Hidajat, M.S. Uddin, Fe 3O 4/cyclodextrin polymer nanocomposites for selective heavy metals removal from industrial wastewater, Carbohydr. Polym. 91 (2013) 322–332. doi:10.1016/j.carbpol.2012.08.030.

[290] J. Szejtli, Introduction and General Overview of Cyclodextrin Chemistry, Chem. Rev. 98 (1998) 1743–1754. doi:10.1021/cr970022c.

[291] Y. Dai, C.C. Liu, A simple, cost-effective sensor for detecting lead ions inwater using under-potential deposited bismuth sub-layer with differential pulse voltammetry (DPV), Sensors (Switzerland). 17 (2017). doi:10.3390/s17050950.

[292] M.A. Chamjangali, H. Kouhestani, F. Masdarolomoor, H. Daneshinejad, A voltammetric sensor based on the glassy carbon electrode modified with multi-walled carbon nanotube/poly(pyrocatechol violet)/bismuth film for determination of cadmium and lead as environmental pollutants, Sensors Actuators B Chem. 216 (2015) 384–393. doi:10.1016/j.snb.2015.04.058.

[293] S. Cerovac, V. Guzsvány, Z. Kónya, A.M. Ashrafi, I. Švancara, S. Rončević, Á. Kukovecz, B. Dalmacija, K. Vytřas, Trace level voltammetric determination of lead and cadmium in sediment pore water by a bismuth-oxychloride particle-multiwalled carbon nanotube composite modified glassy carbon electrode, Talanta. 134 (2015) 640–649. doi:10.1016/j.talanta.2014.12.002.

[294] B. Zhang, J. Chen, H. Zhu, T. Yang, M. Zou, M. Zhang, M. Du, Facile and green fabrication of size-controlled AuNPs/CNFs hybrids for the highly sensitive simultaneous detection of heavy metal ions, Electrochim. Acta. 196 (2016) 422–430. doi:10.1016/j.electacta.2016.02.163.

[295] D. Zhao, D. Siebold, N.T. Alvarez, V.N. Shanov, W.R. Heineman, Carbon Nanotube Thread Electrochemical Cell: Detection of Heavy Metals, Anal. Chem. 89 (2017) 9654–9663. doi:10.1021/acs.analchem.6b04724.

[296] M. Sebastian, B. Mathew, Ion imprinting approach for the fabrication of an electrochemical sensor and sorbent for lead ions in real samples using modified multiwalled carbon nanotubes, J. Mater. Sci. 53 (2018) 3557–3572. doi:10.1007/s10853-017-1787-x.

[297] S.S. Ghoreishizadeh, G. Nanda, S. Carrara, G. De Micheli, Empirical study of noise dependence in electrochemical sensors, in: 5th IEEE Int. Work. Adv. Sensors Interfaces IWASI, IEEE, 2013: pp. 36–39. doi:10.1109/IWASI.2013.6576080.

[298] D. Kingrey, P.G. Collins, Noise in carbon nanotube electronics (Invited Paper), in: J.A. Bergou, J.M. Smulko, M.I. Dykman, L. Wang (Eds.), 2005: p. 92. doi:10.1117/12.609278.

[299] S. Xu, P. Wang, Y. Dong, Measuring Electrolyte Impedance and Noise Simultaneously by Triangular Waveform Voltage and Principal Component Analysis, Sensors. 16 (2016) 576. doi:10.3390/s16040576.

[300] D.M. Morgan, S.G. Weber, Noise and signal-to-noise ratio in electrochemical detectors, Anal. Chem. 56 (1984) 2560–2567. doi:10.1021/ac00277a065.

[301] R.F. Voss, 1/f (Flicker) Noise: A Brief Review, in: 33rd Annu. Symp. Freq. Control, IEEE, 1979: pp. 40–46. doi:10.1109/FREQ.1979.200297.

[302] S. Kim, T. Rim, K. Kim, U. Lee, E. Baek, H. Lee, C.-K. Baek, M. Meyyappan, M.J. Deen, J.-S. Lee, Silicon nanowire ion sensitive field effect transistor with integrated Ag/AgCl electrode: pH sensing and noise characteristics, Analyst. 136 (2011) 5012. doi:10.1039/c1an15568g.

[303] J. Lankelma, H. Poppe, Design and characterization of a coulometric detector with

a glassy carbon electrode for high-performance liquid chromatography, J. Chromatogr. A. 125 (1976) 375–388. doi:10.1016/S0021-9673(00)83369-5.

[304] D.E. Weisshaar, D.E. Tallman, J.L. Anderson, Kel-F-graphite composite electrode as an electrochemical detector for liquid chromatography and application to phenolic compounds, Anal. Chem. 53 (1981) 1809–1813. doi:10.1021/ac00235a022.

[305] S.K. Rangarajan, Random processes in electrochemistry, J. Electroanal. Chem. Interfacial Electrochem. 62 (1975) 43–50. doi:10.1016/0022-0728(75)80026-X.

[306] R.J. Schwall, A.M. Bond, D.E. Smith, On-line fast Fourier transform faradaic admittance measurements: real-time deconvolution of heterogeneous charge transfer kinetic effects for thermodynamic and analytical measurements, Anal. Chem. 49 (1977) 1805–1812. doi:10.1021/ac50020a042.

[307] V.A. Tyagai, Electrochemical noise of reversible electrode reactions, Electrochim. Acta. 18 (1973) 229–230. doi:10.1016/0013-4686(73)80017-9.

[308] M. Fleischmann, J.W. Oldfield, Generation-recombination noise in weak electrolytes, J. Electroanal. Chem. Interfacial Electrochem. 27 (1970) 207–218. doi:10.1016/S0022-0728(70)80183-8.

[309] G.C. Barker, Noise connected with electrode processes, J. Electroanal. Chem. Interfacial Electrochem. 21 (1969) 127–136. doi:10.1016/S0022-0728(69)80032-X.

[310] G.C. Barker, Flicker noise connected with the hydrogen evolution reaction on mercury, J. Electroanal. Chem. Interfacial Electrochem. 39 (1972) 484–488. doi:10.1016/S0022-0728(72)80172-4.

[311] G.C. Barker, Faradaic reaction noise, J. Electroanal. Chem. Interfacial Electrochem. 82 (1977) 145–155. doi:10.1016/S0022-0728(77)80254-4.

[312] G. Blanc, C. Gabrielli, M. Keddam, Measurement of the electrochemical noise by a cross correlation method, Electrochim. Acta. 20 (1975) 687–689. doi:10.1016/0013-4686(75)90069-9.

[313] G. Blanc, I. Epelboin, C. Gabrielli, M. Keddam, Electrochemical noise generated by anodic dissolution or diffusion processes, J. Electroanal. Chem. Interfacial Electrochem. 75 (1977) 97–124. doi:10.1016/S0022-0728(77)80074-0.

[314] I. Epelboin, C. Gabrielli, M. Keddam, L. Raillon, A study of potentiostat noise, J. Electroanal. Chem. Interfacial Electrochem. 93 (1978) 155–161. doi:10.1016/S0022-0728(78)80229-0.

[315] F.N. Hooge, 1/f noise, Phys. B+C. 83 (1976) 14–23. doi:10.1016/0378-4363(76)90089-9.

[316] E.A. Gutierrez-D., M.J. Deen, C.L. Claeys, Low temperature electronics : physics, devices, circuits, and applications, Academic Press, 2001.

[317] O. Marinov, M.J. Deen, J.A. Jimenez Tejada, Theory of microplasma fluctuations and noise in silicon diode in avalanche breakdown, J. Appl. Phys. 101 (2007) 064515. doi:10.1063/1.2654973.

[318] World Health Organization, Guidelines for drinking-water quality, 4th editio, 2017.

[319] D. Chapman, ed., Water Quality Assessments, Taylor & Francis, Abingdon, UK, 1992. doi:10.4324/9780203476710.

[320] M. V. Storey, B. van der Gaag, B.P. Burns, Advances in on-line drinking water quality monitoring and early warning systems, Water Res. 45 (2011) 741–747. doi:10.1016/j.watres.2010.08.049.

[321] A.U. Alam, Y. Qin, S. Nambiar, J.T.W. Yeow, M.M.R. Howlader, N.-X. Hu, M.J. Deen, Polymers and organic materials-based pH sensors for healthcare applications, Prog. Mater. Sci. 96 (2018) 174–216. doi:10.1016/j.pmatsci.2018.03.008.

[322] B. Ahmed, A.U. Alam, E.H. Chowdhury, T.E. Mursalin, Analysis of visual cortex-event-related fMRI data using ICA decomposition, Int. J. Biomed. Eng. Technol. 7 (2011). doi:10.1504/IJBET.2011.044415.

[323] S.J. and, R.B. Brown*, Chemical Sensors with Integrated Electronics, (2008). doi:10.1021/CR068113+.

[324] Y. Feng, D.W. Smith, J.R. Bolton, Photolysis of aqueous free chlorine species (HOCl and OCl −) with 254 nm ultraviolet light, J. Environ. Eng. Sci. 6 (2007) 277–284. doi:10.1139/s06-052.

[325] H. Lee, T.K. Choi, Y.B. Lee, H.R. Cho, R. Ghaffari, L. Wang, H.J. Choi, T.D. Chung, N. Lu, T. Hyeon, S.H. Choi, D.-H. Kim, A graphene-based electrochemical device with thermoresponsive microneedles for diabetes monitoring and therapy, Nat. Nanotechnol. 11 (2016) 566–572. doi:10.1038/nnano.2016.38.

[326] H.Y.Y. Nyein, W. Gao, Z. Shahpar, S. Emaminejad, S. Challa, K. Chen, H.M. Fahad, L.-C. Tai, H. Ota, R.W. Davis, A. Javey, A wearable electrochemical platform for noninvasive simultaneous monitoring of Ca2+ and pH, ACS Nano. 10 (2016) 7216–7224. doi:10.1021/acsnano.6b04005.

[327] W. Gao, S. Emaminejad, H.Y.Y. Nyein, S. Challa, K. Chen, A. Peck, H.M. Fahad, H. Ota, H. Shiraki, D. Kiriya, D.H. Lien, G.A. Brooks, R.W. Davis, A. Javey, Fully integrated wearable sensor arrays for multiplexed in situ perspiration analysis, Nature. 529 (2016) 509–514. doi:10.1038/nature16521.

[328] Z. Xu, Q. Dong, B. Otieno, Y. Liu, I. Williams, D. Cai, Y. Li, Y. Lei, B. Li, Real-time in situ sensing of multiple water quality related parameters using micro-electrode array (MEA) fabricated by inkjet-printing technology (IPT), Sensors Actuators B Chem. (2016). doi:10.1016/j.snb.2016.09.040.

[329] S. Mross, T. Zimmermann, N. Winkin, M. Kraft, H. Vogt, Integrated multi-sensor system for parallel in-situ monitoring of cell nutrients, metabolites, cell density and pH in biotechnological processes, Sensors Actuators B Chem. 236 (2016) 937–946. doi:10.1016/j.snb.2016.03.086.

[330] D. Kirsanov, A. Korepanov, D. Dorovenko, E. Legin, A. Legin, Indirect monitoring of protein A biosynthesis in E.coli using potentiometric multisensor system, Sensors Actuators B Chem. 238 (2017) 1159–1164. doi:10.1016/j.snb.2016.02.073.

[331] B. Zhou, C. Bian, J. Tong, S. Xia, Fabrication of a Miniature Multi-Parameter Sensor Chip for Water Quality Assessment, Sensors. 17 (2017) 157. doi:10.3390/s17010157.

[332] S. Pan, M.J. Deen, R. Ghosh, Low-cost graphite-based free chlorine sensor, Anal. Chem. 87 (2015) 10734–10737. doi:10.1021/acs.analchem.5b03164.

[333] H. Jin, Y. Qin, S. Pan, A.U. Alam, S. Dong, R. Ghosh, M.J. Deen, Open-Source Low-Cost Wireless Potentiometric Instrument for pH Determination Experiments, J. Chem. Educ. 95 (2018) 326–330. doi:10.1021/acs.jchemed.7b00479.

[334] Y. Qin, A.U. Alam, M.M.R. Howlader, N.-X. Hu, M.J. Deen, Inkjet Printing of a Highly Loaded Palladium Ink for Integrated, Low-Cost pH Sensors, Adv. Funct. Mater. 26 (2016) 4923–4933. doi:10.1002/adfm.201600657.

[335] Y. Qin, A.U. Alam, S. Pan, M.M.R. Howlader, R. Ghosh, P.R. Selvaganapathy, Y. Wu, M.J. Deen, Low-temperature solution processing of palladium/palladium oxide films and their pH sensing performance, Talanta. 146 (2016) 517–524. doi:10.1016/j.talanta.2015.08.062.

[336] J. Orozco, A. Baldi, R. Baena, A. Cadarso, A. Bratov, C. Jimenez, Portable system based on microsensors for environmental monitoring applications, Meas. Sci. Technol. 18 (2007) 935–940. doi:10.1088/0957-0233/18/3/048.

[337] A.U. Alam, Y. Qin, M.R. Howlader, M.J. Deen, Direct bonding of liquid crystal polymer to glass, RSC Adv. 6 (2016). doi:10.1039/C6RA17729H.

[338] T.Z. Redhwan, A.U. Alam, M. Catalano, L. Wang, M.J. Kim, Y.M. Haddara, M.M.R. Howlader, Direct bonding of copper and liquid crystal polymer, Mater. Lett. 212 (2018) 214–217. doi:10.1016/j.matlet.2017.10.099.

[339] A. Santos, M.J. Deen, L.F. Marsal, Low-cost fabrication technologies for nanostructures: state-of-the-art and potential, Nanotechnology. 26 (2015) 042001. doi:10.1088/0957-4484/26/4/042001.

[340] Y. Qin, A.U. Alam, S. Pan, M.M.R. Howlader, R. Ghosh, N.-X. Hu, H. Jin, S. Dong, C.-H. Chen, M.J. Deen, Integrated water quality monitoring system with pH, free chlorine, and temperature sensors, Sensors Actuators B Chem. 255 (2018) 781–790. doi:10.1016/j.snb.2017.07.188.

[341] S.S. Li, W.R. Thurber, The dopant density and temperature dependence of electron mobility and resistivity in n-type silicon, Solid. State. Electron. 20 (1977) 609–616. doi:10.1016/0038-1101(77)90100-9.

[342] I.W. Kwon, H.J. Son, W.Y. Kim, Y.S. Lee, H.C. Lee, Thermistor behavior of PEDOT:PSS thin film, Synth. Met. 159 (2009) 1174–1177. doi:10.1016/j.synthmet.2009.02.006.

[343] A.U. Alam, Surface Analysis of Materials for Direct Wafer Bonding, McMaster University, 2014. https://macsphere.mcmaster.ca/handle/11375/13627.

Appendix A

Supporting Information for Chapter 3

Optimization of drop-cast volume from oxidation peak currents
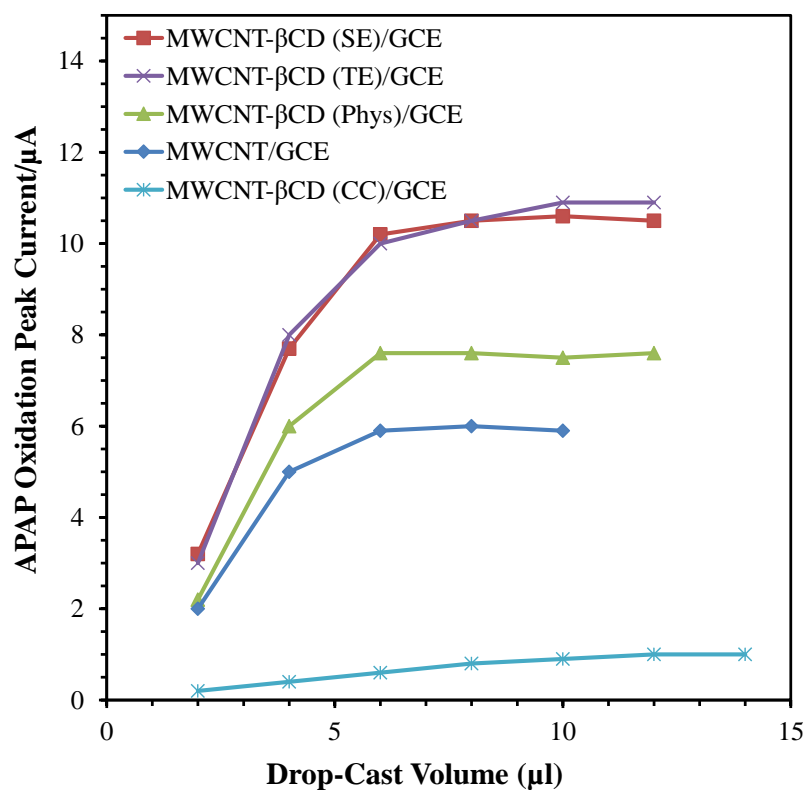
Figure A- 1: Oxidation peak currents vs drop-cast volume from cyclic voltammetry curves of MWCNT/GCE, and MWCNT-βCD (CC/Phys/TE/SE)/GCE recorded in 0.01 M PBS (pH 7.4) in the presence of 5 μM APAP at a scan rate of 50 mV·s^{-1}. All the experiments were done with an open circuit potential of 300 seconds under magnetic stirring before measurements.

Scan-rate dependent redox behaviour of the sensing electrodes
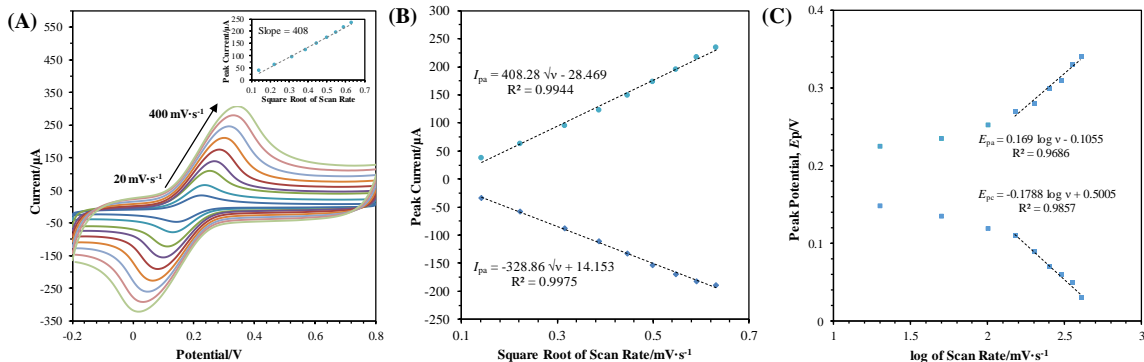
Figure A- 2: (A) Cyclic Voltammetry curves of MWCNT/GCE in 5.0 mM $K_3[Fe(CN)_6]$ containing 0.1 M KCl at different scan rates (20, 50, 100, 150, 200, 250, 300, 350, 400 mV·s^{-1}). (B) The relationship between redox peak currents and the scan rates. (C) The dependence of the redox peak potentials on log of scan rates.
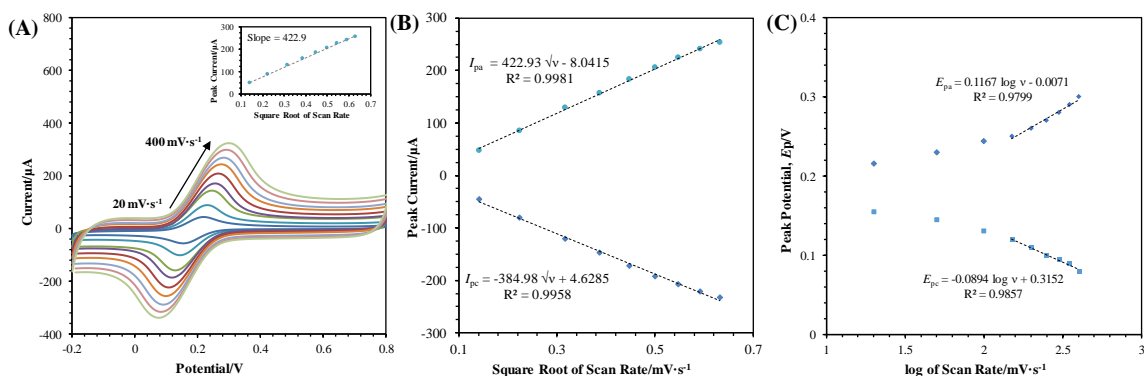
Figure A- 3: (A) Cyclic Voltammetry curves of MWCNT-βCD (Phys)/GCE in 5.0 mM $K_3[Fe(CN)_6]$ containing 0.1 M KCl at different scan rates (20, 50, 100, 150, 200, 250, 300, 350, 400 mV·s^{-1}). (B) The relationship between redox peak currents and the scan rates. (C) The dependence of the redox peak potentials on log of scan rates.
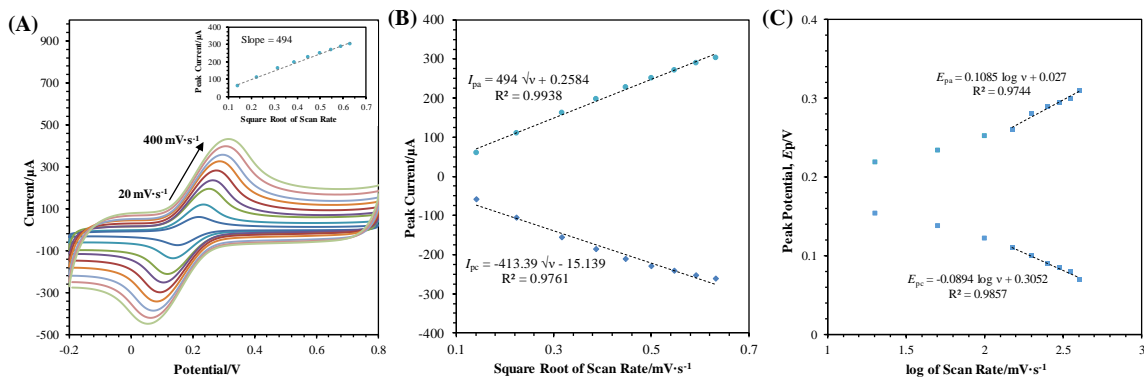
Figure A- 4: (A) Cyclic Voltammetry curves of MWCNT-βCD (TE)/GCE in 5.0 mM $K_3[Fe(CN)_6]$ containing 0.1 M KCl at different scan rates (20, 50, 100, 150, 200, 250, 300, 350, 400 mV·s^{-1}). (B) The relationship between redox peak currents and the scan rates. (C) The dependence of the redox peak potentials on log of scan rates.
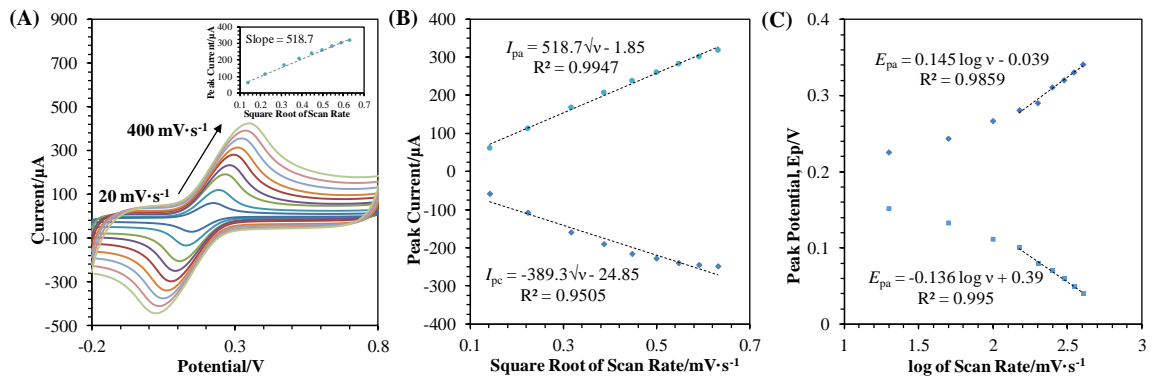
Figure A- 5: (A) Cyclic Voltammetry curves of MWCNT-βCD (SE)/GCE in 5.0 mM $K_3[Fe(CN)_6]$ containing 0.1 M KCl at different scan rates (20, 50, 100, 150, 200, 250, 300, 350, 400 mV·s^{-1}). (B) The relationship between redox peak currents and the scan rates. (C) The dependence of the redox peak potentials on log of scan rates.
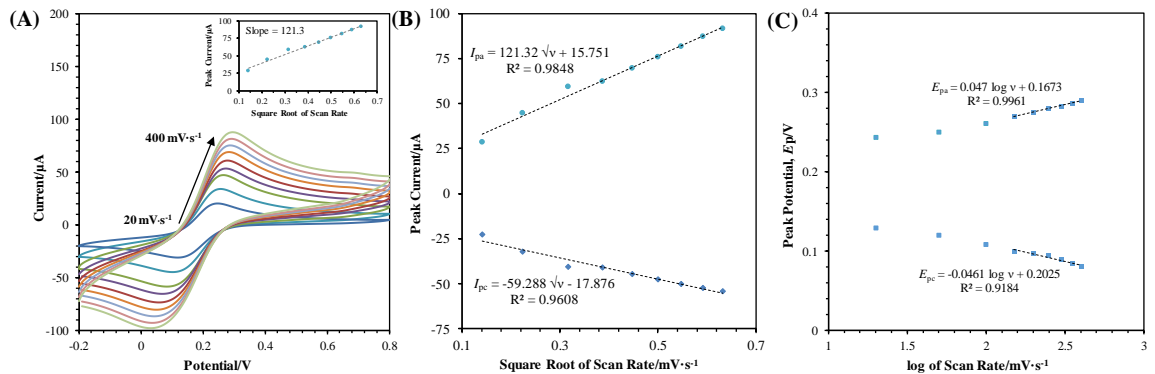
Figure A- 6: (A) Cyclic Voltammetry curves of MWCNT-βCD (CC)/GCE in 5.0 mM $K_3[Fe(CN)_6]$ containing 0.1 M KCl at different scan rates (20, 50, 100, 150, 200, 250, 300, 350, 400 mV·s^{-1}). (B) The relationship between redox peak currents and the scan rates. (C) The dependence of the redox peak potentials on log of scan rates.

Charge transfer properties of the modified electrodes
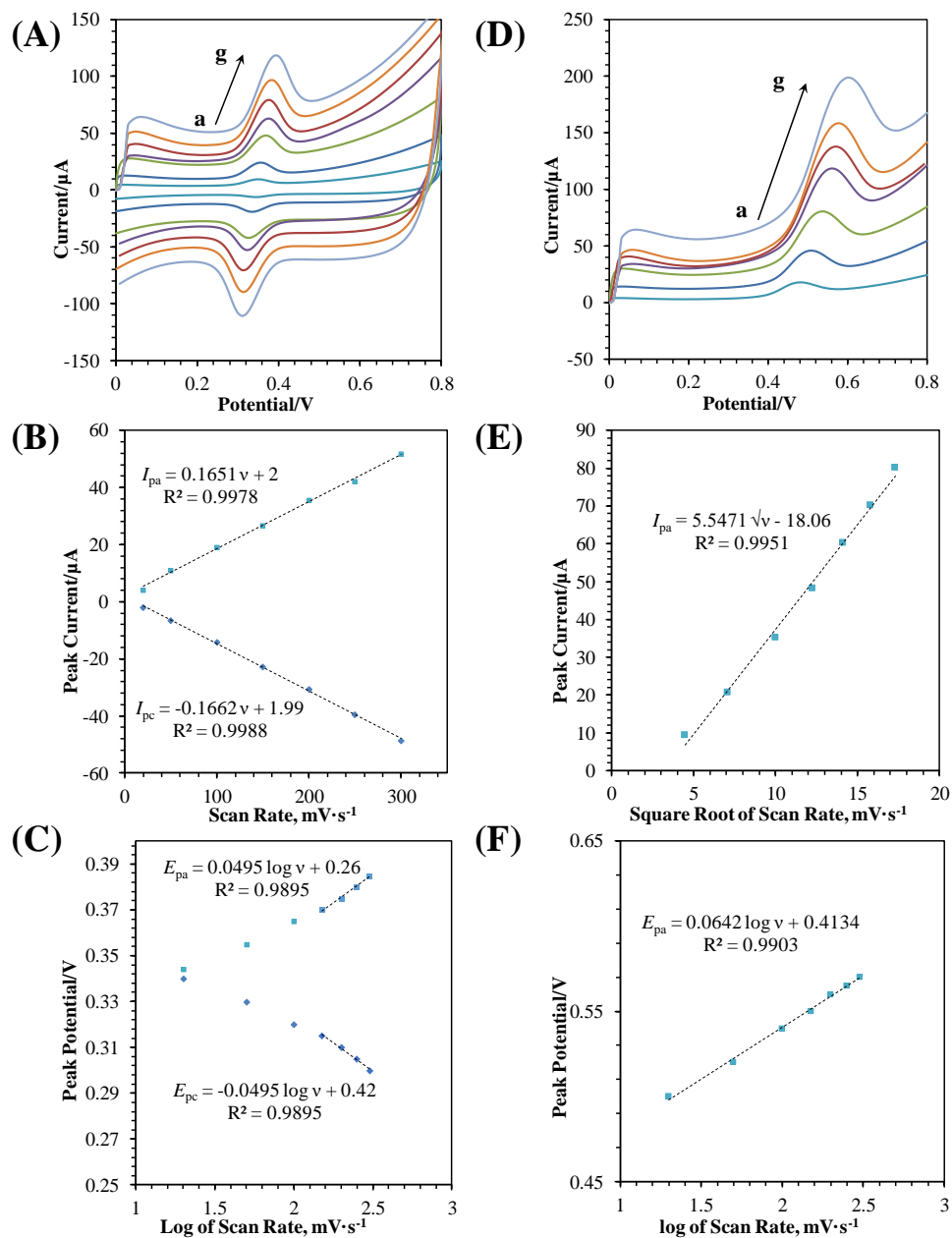
Figure A- 7: (A) Cyclic voltammetry curves of MWCNT-βCD (SE)/GCE in 0.01 M PBS (pH 7.4) with 5 µM APAP at different scan rates (20, 50, 100, 150, 200, 250, 300 mV·s^{-1}). (B) The relationship between the redox peak currents of 5 µM APAP and the scan rates. (C) The dependence of the redox peak potentials of 5 µM APAP on log of scan rate. (D) Cyclic voltammetry curves of MWCNT-βCD (SE)/GCE in 0.01 M PBS (pH 7.4) with 5 µM E2 at different scan rates (20, 50, 100, 150, 200, 250, 300 mV·s^{-1}). (E) The relationship between the redox peak currents of 5 µM E2 and the scan rates. (F) The dependence of the redox peak potentials of 5 µM E2 on log of scan rate. All the experiments were done with an open circuit potential of 300 seconds under magnetic stirring before measurements.

pH dependent sensing performance of the modified electrodes
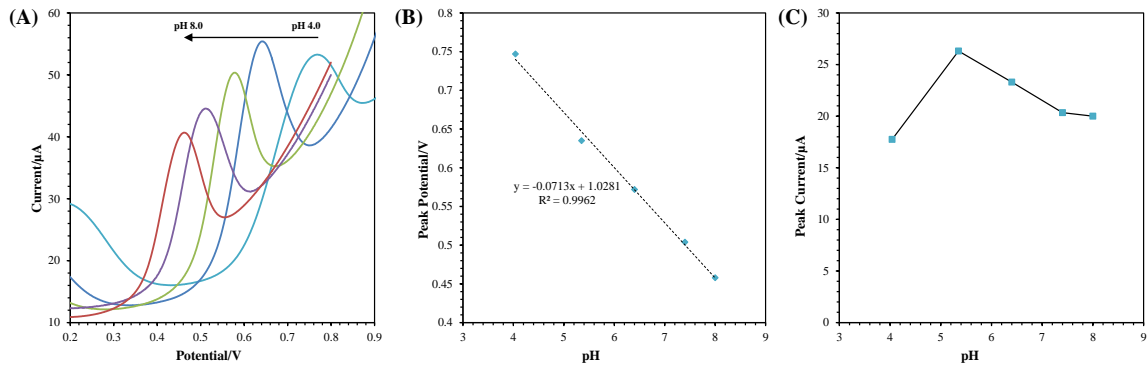
Figure A- 8: (A) Cyclic voltammetry curves of MWCNT-βCD (SE)/GCE in 0.01 M PBS with different pH values (4.0, 5.0, 6.0, 7.4 and 8.0) in the presence of 5 µM E2 at a scan rate of 50 mV·s^{-1}. (b) Plots of the anodic peak currents of E2 against the pH values. (c) Plots of the peak potentials of E2 against the pH values.

Calibration curve and linearity for detection of APAP and E2

(A) APAP

(B) E2
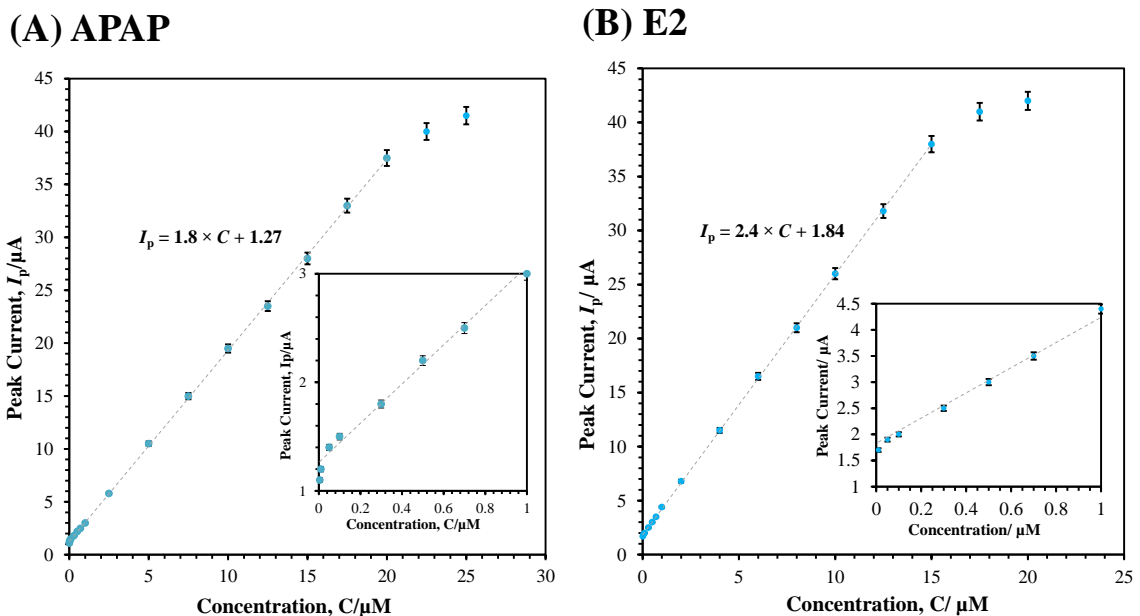
Figure A- 9: (A) Calibration curve (i.e., peak current vs APAP concentration) for MWCNT-βCD (SE)/GCE. (B) Calibration curve (i.e., peak current vs E2 concentration) for MWCNT-βCD (SE)/GCE. All the experiments were done with an open circuit potential of 300 seconds under magnetic stirring before measurements.

Electrochemical sensing performance of MWCNT-βCD(CC)

(A) APAP(5 μM)

(B) E2 (5 μM)
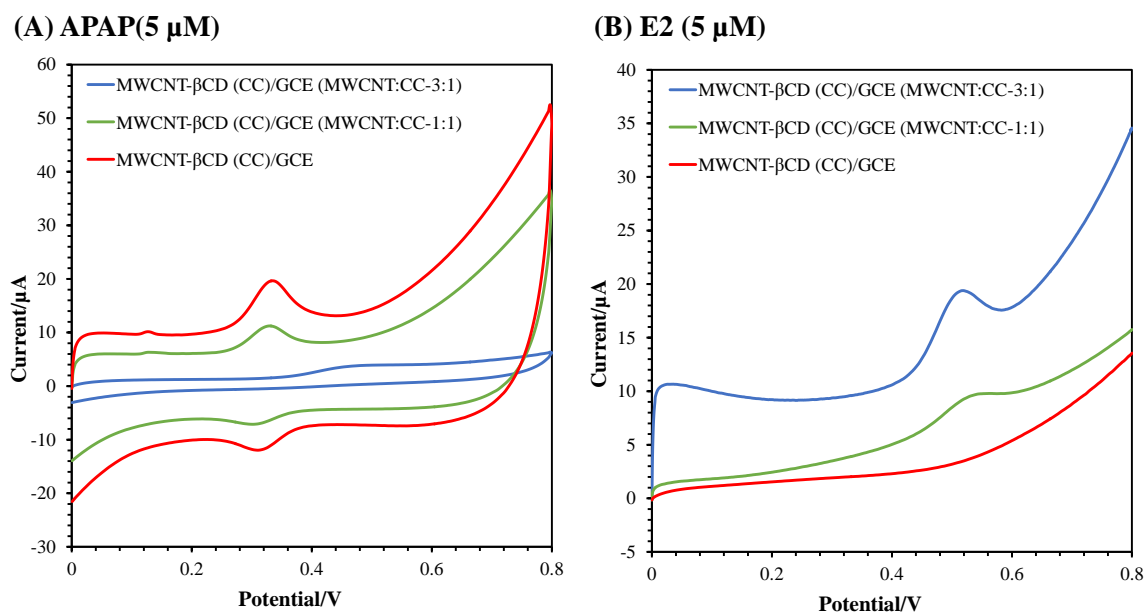
Figure A- 10: (A) Cyclic voltammetry curves of MWCNT-βCD (CC)/GCE recorded in 0.01 M PBS (pH 7.4) in the presence of 5 μM APAP at a scan rate of 50 mV·s^{-1} with mixing of pure MWCNT (at 1:1 and 3:1 weight ratio) and without mixing. (B) Cyclic voltammetry curves of MWCNT-βCD (CC)/GCE recorded in 0.01 M PBS (pH 7.4) in the presence of 5 μM E2 at a scan rate of 50 mV·s^{-1} with mixing of pure MWCNT (at 1:1 and 3:1 weight ratio) and without mixing. All the experiments were done with an open circuit potential of 300 seconds under magnetic stirring before measurements.

Appendix B

Supporting Information for Chapter 6

Characterization of the silicon and PEDOT:PSS based thermistors

❑ **Silicon: (+ve) TCR**
  ❑ **1 cm × 10 cm Si with metal contacts on two ends**
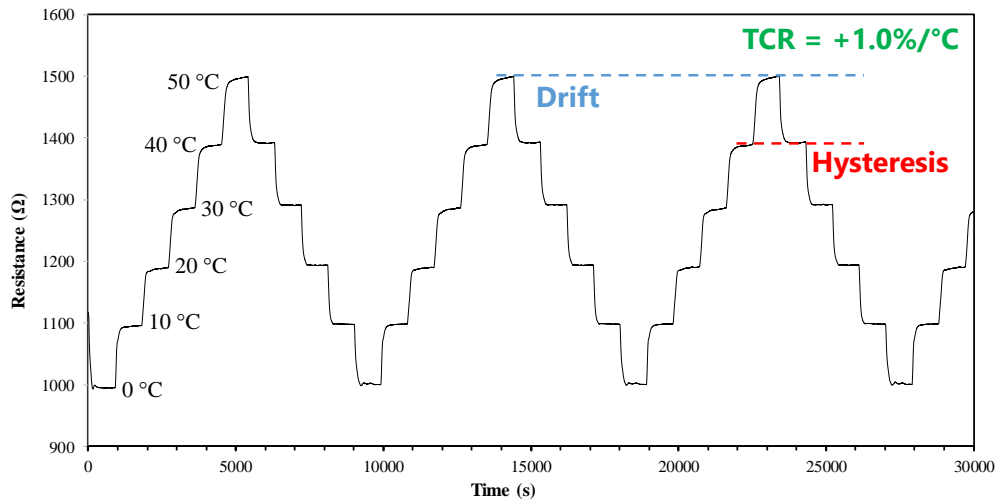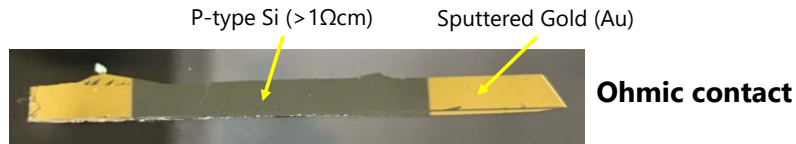
Figure B- 1: Temporal response of the temperature dependent resistance of p-type silicon for temperatures between 0 and 50 °C.

❑ **PEDOT:PSS: (-ve) TCR**
   ❑ **2 µl of PEDOT:PSS (2 wt% in water) drop-casted and dried on glass**
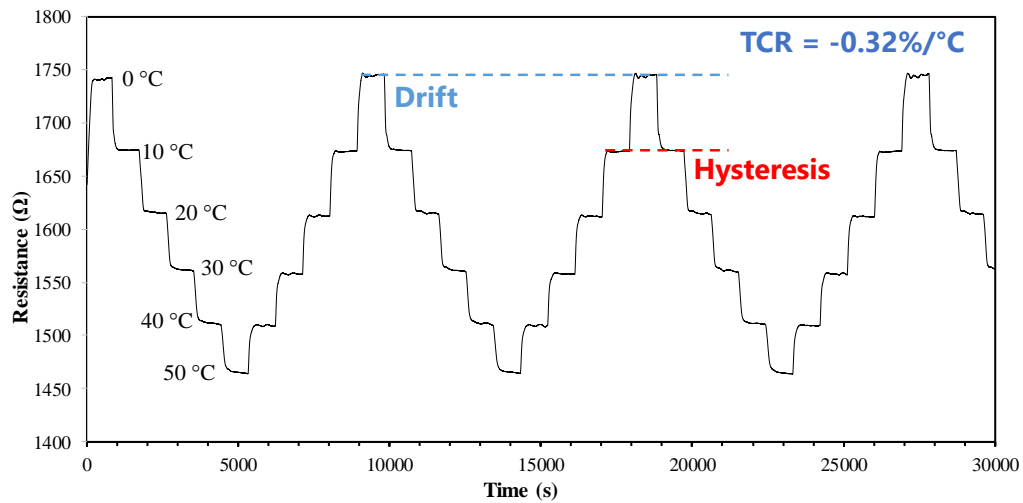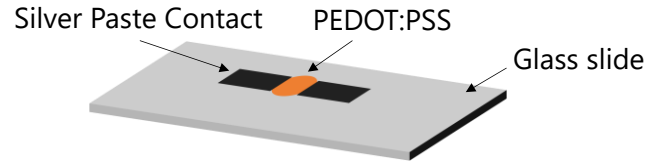
Figure B- 2: Temporal response of the temperature dependent resistance of PEDOT:PSS for temperatures between 0 and 50 °C.

Circuit schematic of the potentiostat shield

Circuit schematic of the WQM shield
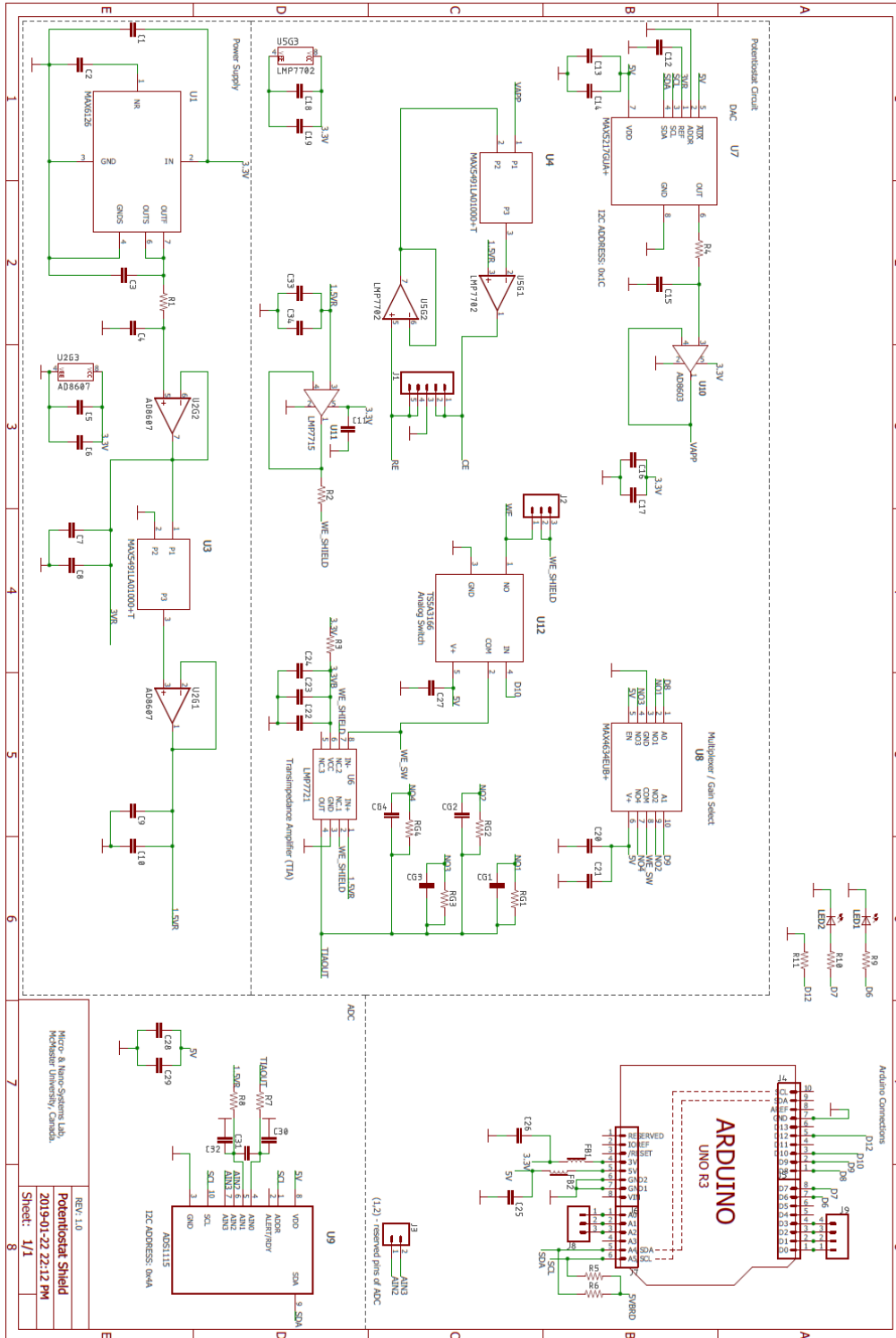
Programming code for microcontroller and Android application

Programming code may be shared through email with the Author (Arif Ul Alam)

Screenshot of the FIWQMS Android application
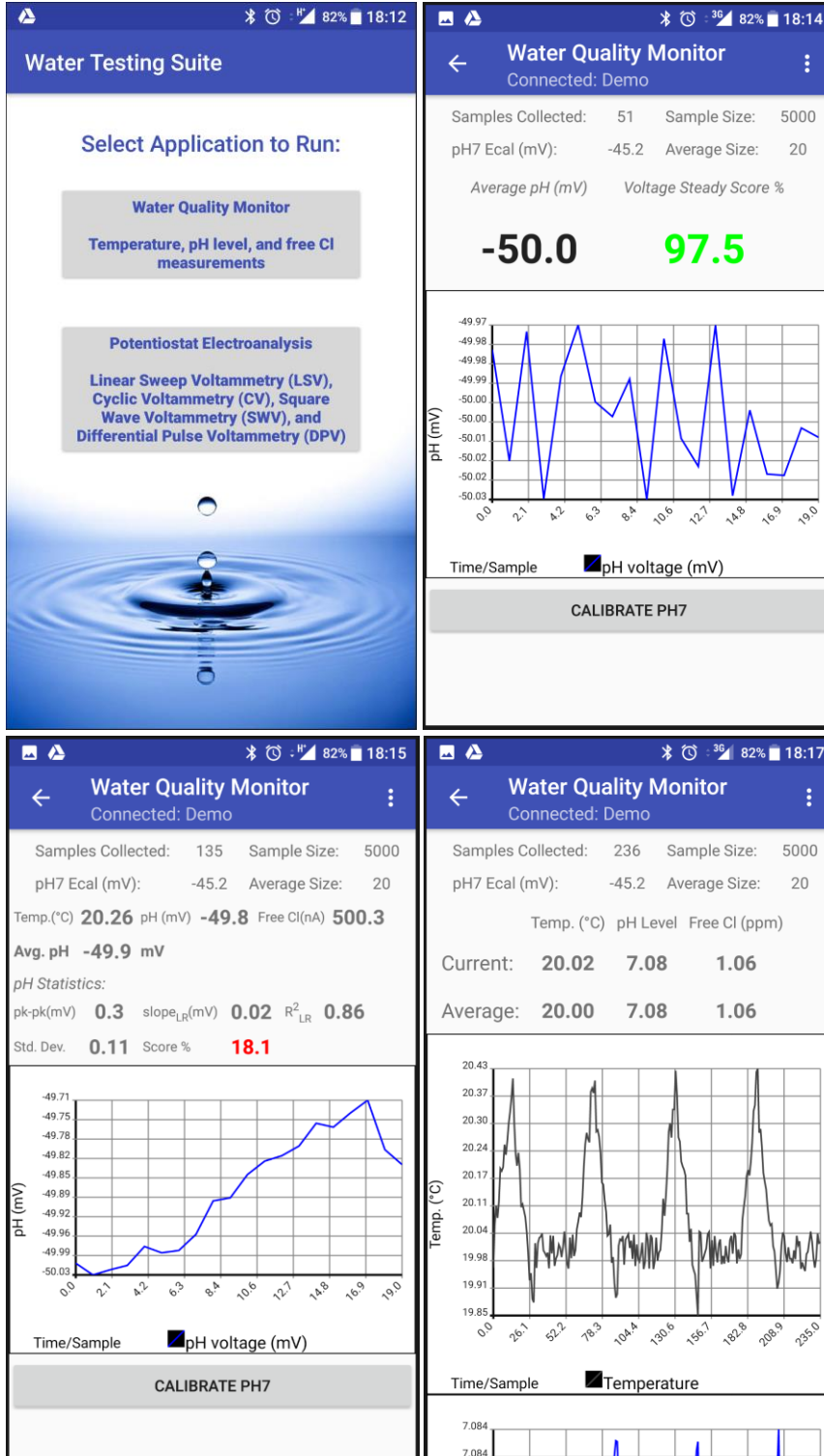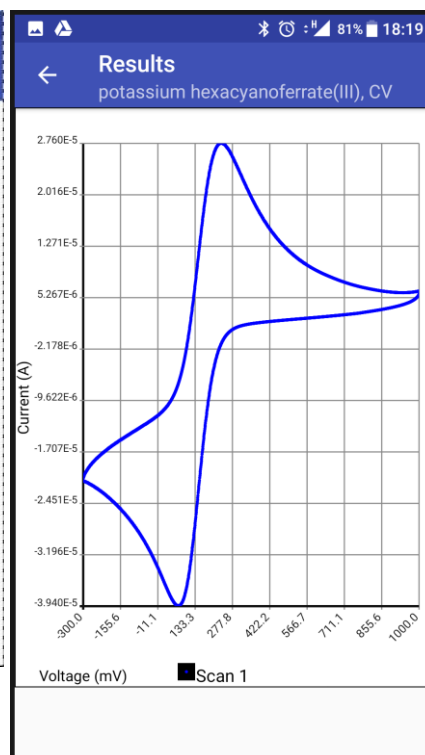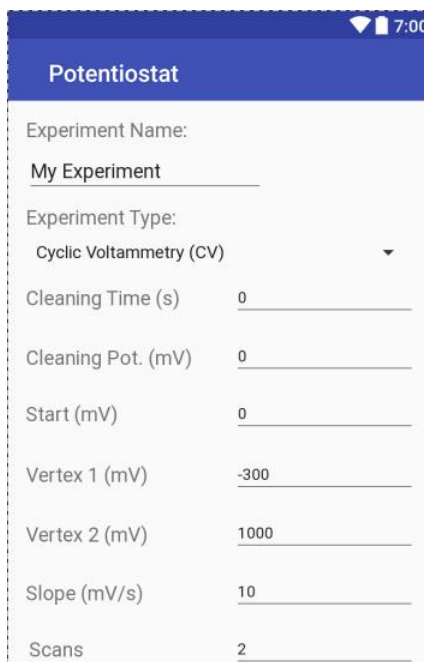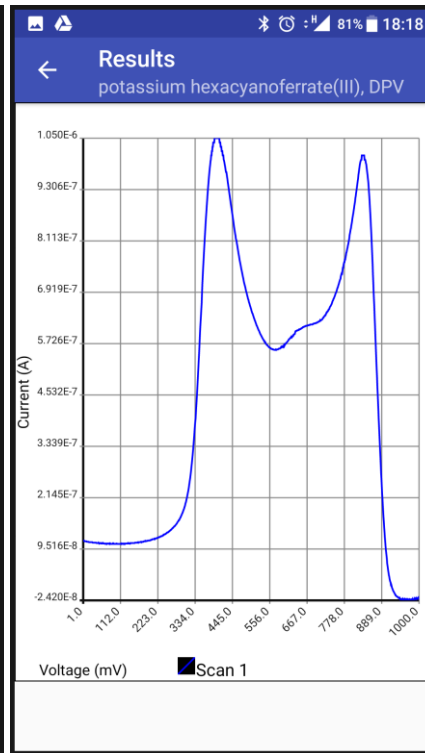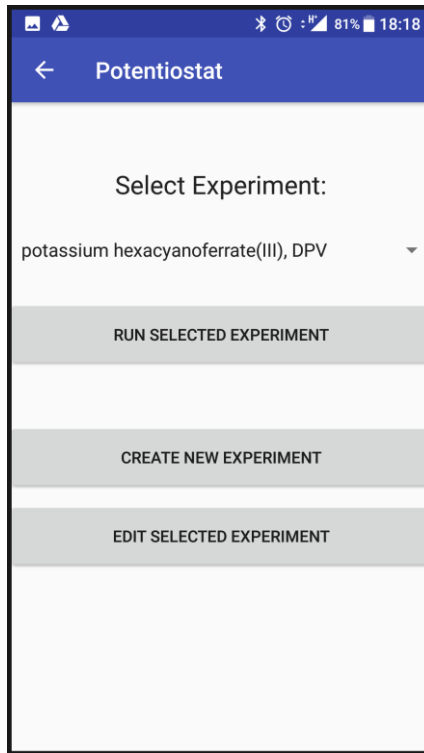
Appendix C

Copyright permissions

4/27/2019   Rightslink® by Copyright Clearance Center

Copyright Clearance Center

RightsLink®

Home | Account Info | Help | ✉

ACS Publications
Most Trusted. Most Cited. Most Read.

Title:	Tailoring MWCNTs and β-Cyclodextrin for Sensitive Detection of Acetaminophen and Estrogen
Author:	Arif Ul Alam, Yiheng Qin, Massimo Catalano, et al
Publication:	Applied Materials
Publisher:	American Chemical Society
Date:	Jun 1, 2018

Copyright © 2018, American Chemical Society

Logged in as:
Arif Ul Alam
McMaster University
Account #:
3001235103

LOGOUT

PERMISSION/LICENSE IS GRANTED FOR YOUR ORDER AT NO CHARGE

This type of permission/license, instead of the standard Terms & Conditions, is sent to you because no fee is being charged for your order. Please note the following:

- Permission is granted for your request in both print and electronic formats, and translations.
- If figures and/or tables were requested, they may be adapted or used in part.
- Please print this page for your records and send a copy of it to your publisher/graduate school.
- Appropriate credit for the requested material should be given as follows: "Reprinted (adapted) with permission from (COMPLETE REFERENCE CITATION). Copyright (YEAR) American Chemical Society." Insert appropriate information in place of the capitalized words.
- One-time permission is granted only for the use specified in your request. No additional uses are granted (such as derivative works or other editions). For any other uses, please submit a new request.

BACK | CLOSE WINDOW